Universidad de Oviedo

Programa de Doctorado en Energía y Control de Procesos

Mejora de la transferencia de calor en el intercambiador de calor Concéntrico / Eccéntrico de tubo doble horizontal mediante el uso de Nanofluido

Mohamed Abdelmagid Mohamed Abdelmagid

University of Oviedo

PhD Program in Energy and Process Control

Heat Transfer Enhancement in horizontal Double Tube Concentric/ Eccentric Heat Exchanger by Using Nanofluid

Mohamed Abdelmagid Mohamed Abdelmagid

Universidad de Oviedo

RESUMEN DEL CONTENIDO DE TESIS DOCTORAL

1.- Título de la Tesis	
Español/Otro Idioma: Mejora de la transferencia de calor en el intercambiador de calor Concéntrico / Eccéntrico de tubo doble horizontal mediante el uso de Nanofluido	Inglés: Heat Transfer Enhancement in horizontal Double Tube Concentric/ Eccentric Heat Exchanger by Using Nanofluid

2.- Autor	
Nombre: Mohamed Abdelmagid Abdelmagid	DNI/Pasaporte/NIE:
Programa de Doctorado: Energía y Control de Procesos	
Órgano responsable: Centro Internacional de Postgrado	

RESUMEN (en español)

La mejora de la eficiencia energética de los intercambiadores de calor es esencial para la reducción del consumo energético y los costes asociados. Como resultado, se han propuesto diferentes maneras en la bibliografía para mejorar la eficiencia de los intercambiadores de calor. Esta tesis se centra en la combinación de métodos activos y pasivos para aumentar la eficiencia de intercambiadores de calor de doble tubo concéntricos. El principal objetivo es desarrollar un modelo numérico para la simulación de la convección forzada en régimen de transición en un tubo concéntrico horizontal de un intercambiador de calor de tubos. Primero, se realizó una revisión bibliográfica acerca de los intercambiadores de calor, centrándose en los de doble tubo. Después, se desarrolló un modelo numérico 2D axisimétrico utilizando ANSYS FLUENT® para determinar las prestaciones de transmisión de calor en flujo convectivo forzado en transición para nanofluidos en base agua con Al_2O_3, Cu, y Cu-Al_2O_3, con concentraciones de 0 a 3 %. Después, se generó un modelo 3D para investigar el efecto de rotar el tubo interior del intercambiador de calor de 0 a 500 rpm. Ambos modelos numéricos fueron validados utilizando resultados experimentales previos. Finalmente, se desarrolló un modelo 3D para investigar posibles modificaciones geométricas del intercambiador para mejorar su eficiencia, introduciendo anillos circulares

con y sin agujeros perforados en la superficie exterior del tubo interior del intercambiador. El modelo se utilizó para analizar el efecto de cambiar la distancia entre los anillos y número de agujeros en las prestaciones del intercambiador de calor, además de los efectos de la adición de nanopartículas y rotación del tubo. Los resultados mostraron que añadir nanopartículas al agua mejora la transferencia de calor, y que concentraciones más altas de nanopartículas y velocidades de rotación elevadas contribuyen a alcanzar mayores valores de transmisión de calor. Sin embargo, la caída de presión aumenta por las alteraciones en las propiedades del fluido y el comportamiento del flujo, con movimiento rotacional y velocidades más altas. La inserción de anillos circulares en el tubo interior mejora la transmisión de calor, mientras que los agujeros en los anillos reducen la caída de presión. El efecto combinado del aumento de la velocidad de rotación con los anillos circulares perforados aumenta la turbulencia y la generación de vórtices cerca de los agujeros, mejorando la transmisión de calor. Finalmente, se presentan los principales resultados de este estudio y sus implicaciones, así como posibles líneas de investigación futuras.

RESUMEN (en Inglés)

Improving the thermal efficiency of heat exchangers is essential for reducing energy consumption and costs. As a result, several ways have been proposed in the literature for increasing the effectiveness of heat exchangers. This dissertation focuses on combined methods for increasing the efficiency of concentric double-tube heat exchangers, including both active and passive methods. The main objective of this thesis is to develop a numerical model for transitional forced convection flow simulation within a horizontal concentric tube in a tube heat exchanger. Firstly, a literature review was conducted on heat exchangers, focusing on double-tube heat exchangers. Afterwards, a 2D axisymmetric numerical model was developed using ANSYS FLUENT® to determine the heat transfer characteristics of transitional forced convection flow for water-based

Universidad de Oviedo

nanofluids based on Al_2O_3, Cu, and hybrid Cu-Al_2O_3 with concentrations ranging from 0 to 3 %. Then, a 3D numerical model was generated to investigate the effect of introducing rotation in the inner tube of the heat exchanger from 0 to 500 rpm. These numerical models were validated using previous experimental results. Finally, a 3D model was generated to investigate possible modifications of the exchanger geometry to increase its efficiency by introducing circular rings with and without perforated holes on the outer surface of the inner tube of the exchanger. The model was utilized to analyze the effect of varying the pitch ratio and number of holes on the heat transfer characteristics and heat exchanger performance, alongside the effects of nanoparticle addition and tube rotation. The results showed that adding nanoparticles to pure water improves heat transfer and that increasing nanoparticle concentration and rotational speed contribute to higher heat transfer values. However, the pressure drop increases due to alterations in the fluid properties due to the nanofluids and the flow behavior caused by swirling motion and increased velocity. Inserting circular rings on the inner tube enhances heat transfer, whereas adding perforated holes to them reduces the pressure drop. The combined effect of increasing rotational speed with the perforated circular rings increased turbulence and vortex generation near the holes, enhancing heat transfer. Finally, the main findings of this study and their implications are presented, as well as potential future research lines.

SR. PRESIDENTE DE LA COMISIÓN ACADÉMICA DEL PROGRAMA DE DOCTORADO EN ENERGÍA Y CONTROL DE PROCESOS

ACKNOWLEDGEMENTS

First of all, thanks to God the Almighty and Creator of all things that helped me in achieving this work in its final form.

I wish to express my deep gratitude and appreciation to Prof. Antonio Jose Gutierrez Trashorras, Dr. Andres Meana Fernandez and for their continuous help, valuable instruction, patience and encouragement in making this work possible. I hope one day that I can repay for all their efforts.

Special thanks are given to Prof. Eduardo Blanco Marigorta for helping me to understand CFD.

Finally, I would like to thank my wife who had believed in me and thank to my parents and family

ABSTRACT

Improving the thermal efficiency of heat exchangers is essential for reducing energy consumption and costs. As a result, several ways have been proposed in the literature for increasing the effectiveness of heat exchangers. This dissertation focuses on combined methods for increasing the efficiency of concentric double-tube heat exchangers, including both active and passive methods. The main objective of this thesis is to develop a numerical model for transitional forced convection flow simulation within a horizontal concentric tube in a tube heat exchanger. Firstly, a literature review was conducted on heat exchangers, focusing on double-tube heat exchangers. Afterwards, a 2D axisymmetric numerical model was developed using ANSYS FLUENT® to determine the heat transfer characteristics of transitional forced convection flow for water-based nanofluids based on Al_2O_3, Cu, and hybrid Cu-Al_2O_3 with concentrations ranging from 0 to 3 %. Then, a 3D numerical model was generated to investigate the effect of introducing rotation in the inner tube of the heat exchanger from 0 to 500 rpm. These numerical models were validated using previous experimental results. Finally, a 3D model was generated to investigate possible modifications of the exchanger geometry to increase its efficiency by introducing circular rings with and without perforated holes on the outer surface of the inner tube of the exchanger. The model was utilized to analyze the effect of varying the pitch ratio and number of holes on the heat transfer characteristics and heat exchanger performance, alongside the effects of nanoparticle addition and tube rotation. The results showed that adding nanoparticles to pure water improves heat transfer and that increasing nanoparticle concentration and rotational speed contribute to higher heat transfer values. However, the pressure drop increases due to alterations in the fluid properties due to the nanofluids and the flow behavior caused by swirling motion and increased velocity. Inserting circular rings on the inner tube enhances heat transfer, whereas adding perforated holes to them reduces the pressure drop. The combined effect of increasing rotational speed with the perforated circular rings increased turbulence and vortex generation near the holes, enhancing heat transfer. Finally, the main findings of this study and their implications are presented, as well as potential future research lines.

RESUMEN

La mejora de la eficiencia energética de los intercambiadores de calor es esencial para la reducción del consumo energético y los costes asociados. Como resultado, se han propuesto diferentes maneras en la bibliografía para mejorar la eficiencia de los intercambiadores de calor. Esta tesis se centra en la combinación de métodos activos y pasivos para aumentar la eficiencia de intercambiadores de calor de doble tubo concéntricos. El principal objetivo es desarrollar un modelo numérico para la simulación de la convección forzada en régimen de transición en un tubo concéntrico horizontal de un intercambiador de calor de tubos. Primero, se realizó una revisión bibliográfica acerca de los intercambiadores de calor, centrándose en los de doble tubo. Después, se desarrolló un modelo numérico 2D axisimétrico utilizando ANSYS FLUENT® para determinar las prestaciones de transmisión de calor en flujo convectivo forzado en transición para nanofluidos en base agua con Al_2O_3, Cu, y Cu-Al_2O_3, con concentraciones de 0 a 3 %. Después, se generó un modelo 3D para investigar el efecto de rotar el tubo interior del intercambiador de calor de 0 a 500 rpm. Ambos modelos numéricos fueron validados utilizando resultados experimentales previos. Finalmente, se desarrolló un modelo 3D para investigar posibles modificaciones geométricas del intercambiador para mejorar su eficiencia, introduciendo anillos circulares con y sin agujeros perforados en la superficie exterior del tubo interior del intercambiador. El modelo se utilizó para analizar el efecto de cambiar la distancia entre los anillos y número de agujeros en las prestaciones del intercambiador de calor, además de los efectos de la adición de nanopartículas y rotación del tubo. Los resultados mostraron que añadir nanopartículas al agua mejora la transferencia de calor, y que concentraciones más altas de nanopartículas y velocidades de rotación elevadas contribuyen a alcanzar mayores valores de transmisión de calor. Sin embargo, la caída de presión aumenta por las alteraciones en las propiedades del fluido y el comportamiento del flujo, con movimiento rotacional y velocidades más altas. La inserción de anillos circulares en el tubo interior mejora la transmisión de calor, mientras que los agujeros en los anillos reducen la caída de presión. El efecto combinado del aumento de la velocidad de rotación con los anillos circulares perforados aumenta la turbulencia y la

generación de vórtices cerca de los agujeros, mejorando la transmisión de calor. Finalmente, se presentan los principales resultados de este estudio y sus implicaciones, así como posibles líneas de investigación futuras.

TABLE OF CONTENTS

LIST OF TABLES

LIST OF FIGURES

LIST OF ABBREVIATIONS

A_s	Heat transfer surface area	m^2
C	Heat capacity	W/ K
C_p	Specific heat	J/kg K
D_h	Hydraulic diameter of an annulus, $D_h = D_i - d_o$	m
D_i	Inner diameter of outer tube	m
d_i	Inner diameter of inside tube	m
d_o	Outer diameter of inside tube	m
D_{ro}	Outer diameter of ring	m
D_r	Diameter of hole in ring	m
dr_i	Inner diameter of ring	m
K	Thermal conductivity	W/m.K
L	Length of concentric tube	m
$\dot{m}$	Mass flow rate	kg/s
NTU	Number of transfer unit	-
N	Number of holes for rings	-
N	Number of rings	-
P	Pitch length	m
PR	Pitch ratio (P/D_{ro})	-

Q	Heat transfer rate	W
Re	Reynolds number	-
T	Temperature	K
ΔT_{log}	Logarithmic mean temperature difference	K
t	Thickness of rings	m
u	Axial flow velocity	m/s
U	Overall heat transfer coefficient	W/m^2 K
z	Direction coordinates along the tube	m
V	Volume flow rate	m^3/s

Greek symbols

ε	Effectiveness	-
μ	Dynamic viscosity	kg/m s
ν	Kinematic viscosity	m^2/s
ϕ	Volume concentration of nanoparticles	%
ρ	Density	kg/m^3

Subscripts

avg	Average	
cf	Cold fluid	-

hf	Hot fluid	-
i	Inlet	-
o	Outlet	-
nf	Nanofluid	-
f	Fluid	-
s	Nanoparticles	-
h	Hybrid	-

CHAPTER ONE

INTRODUCTION

Chapter One - Introduction

Heat exchangers are devices that transfer heat from one fluid at a high temperature to another fluid with a lower temperature. They are an integral part of almost every thermal system and are commonly used in applications regarding electricity generation, chemical processing, air conditioning and refrigeration.

Heat transfer is the field of engineering that studies energy transfer between bodies due to temperature differences. In a heat exchanger, the heat transfer mechanisms are convection between each fluid and the wall separating them and conduction through this wall [1].

In conduction, heat transfer occurs from a high-temperature zone to a low-temperature zone via the kinetic movement of matter particles, according to Fourier's law:

$$\dot{q}_x = -k\frac{dT}{dx} \qquad (1.1)$$

where $\dot{q}_x$ is the heat flux per unit area in the x direction (W/m^2), k is the thermal conductivity of the medium (W/m·K), and $\frac{dT}{dx}$ is the temperature gradient (K/m).

In convection, heat is transferred between a surface and a moving fluid at different temperatures. There are two types of convection: natural and forced. In natural convection, the driving mechanism is the variation in temperature within the fluid, which generates a density gradient that causes convection motion due to buoyancy forces. In forced convection, the movement of the fluid is caused by an external force, such as a pump or fan, and it is the main convection mechanisms in heat exchangers.

Heat transfer by convection is determined by Newton's law of cooling:

$$\dot{q} = h(T_s - T_\infty) \qquad (1.2)$$

Where $\dot{q}$ is the convective heat flux per unit area (W/m^2), h is the heat transfer coefficient (W/m·K) and (T_s - T_∞) is the temperature difference between the wall and the fluid. The temperature difference at a position along the heat exchanger length determines the heat transfer rate between the two fluids at that position.

Heat exchangers may be classified according to the contact of the different fluids, the flow arrangement, the heat transfer mechanism, the pass arrangement and the phase change processes. ([1], [2], and [3]).

1.1. Classification based on the contact of fluids

This method of classification divides heat exchangers into two major categories: direct contact and indirect contact.

1.1.1. Heat exchangers with direct contact

In direct contact heat exchangers, two fluid streams come into direct contact for heat exchange. Direct contact exchangers are commonly used for both mass transfer and heat transfer, such as in evaporation; applications involving only sensible heat transfer are uncommon. However, the applications are restricted to situations where direct contact between two fluid streams is allowed. Some applications are:

- Heat exchangers for gas and liquids: a gas and a liquid are mixed and then separated after heat exchange. Heat is transferred with the mass transfer caused by liquid evaporation and convective heat transfer.
- Liquid-vapor heat exchangers: vapor is partially or fully condensed, using cooling water or by direct contact with steam dissipation in the heat exchanger. The outlet vapor and liquid are separated, as in open feedwater heaters.
- Immiscible fluid heat exchangers: two immiscible fluid streams (single- or multi-phase) are put in direct contact. Oil vapours are a common example, when they are condensed with water or air.

1.1.2. Heat Exchangers with Indirect Contact

In this type of heat exchangers, even though simultaneous flow of two or more fluids is required, no direct mixing occurs, as each fluid moves across its own passage. They are commonly known as regenerative heat exchangers and several configurations may be found, such as tubular, plate and surface extension heat exchangers. Heat transfers across wall that separates the different fluids, so they do not come into direct contact with each other. These exchangers may be divided into:

- Storage type: a porous solid matrix is introduced as the coupling medium between the fluids, which store or extract heat from the matrix without getting in contact.
- Fluidized bed: one side of the exchanger is immersed in a layer of split solid material, with a tube package across it. One fluid passes through the solid

material layer and the other across the tube package, exchanging heat with each other.

- Direct transfer: the hot and cold fluids flow simultaneously through the exchanger and heat is transferred across a wall separating the fluids.

1.2 Classification based on flow arrangement

There are three main flow arrangement possibilities in typical industrial heat exchangers.

1.2.1 Parallel flow

Cold and hot fluids flow from the same end and in the same direction across the heat exchanger. This arrangement is not commonly found in the industry, due to its lower efficiency. Additionally, at the inlet, there is a big difference in the temperature of the hot and cold fluids, which may lead to high thermal stress values in the heat exchanger wall.

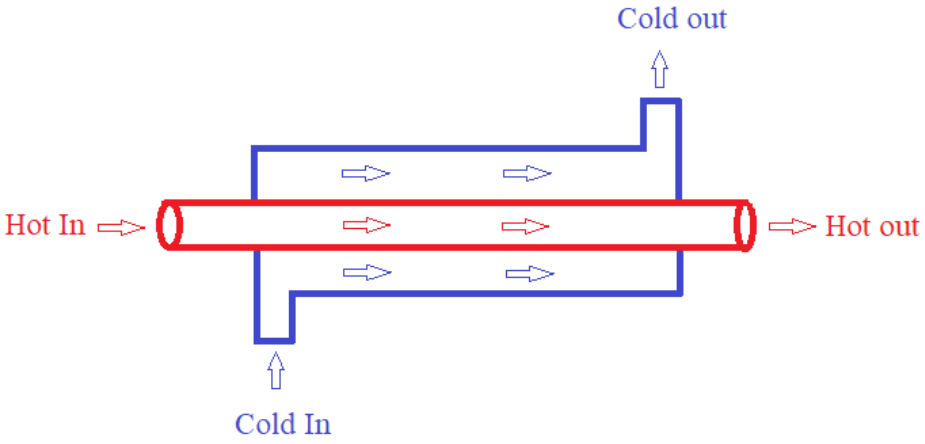

Figure 1.1: Parallel flow system.

1.2.2. Counter flow.

Cold and hot fluids enter and leave the heat exchanger at opposite ends, increasing the heat transfer efficiency, as the temperature distribution is such that the temperature difference between both fluids is maximized across the heat exchanger length.

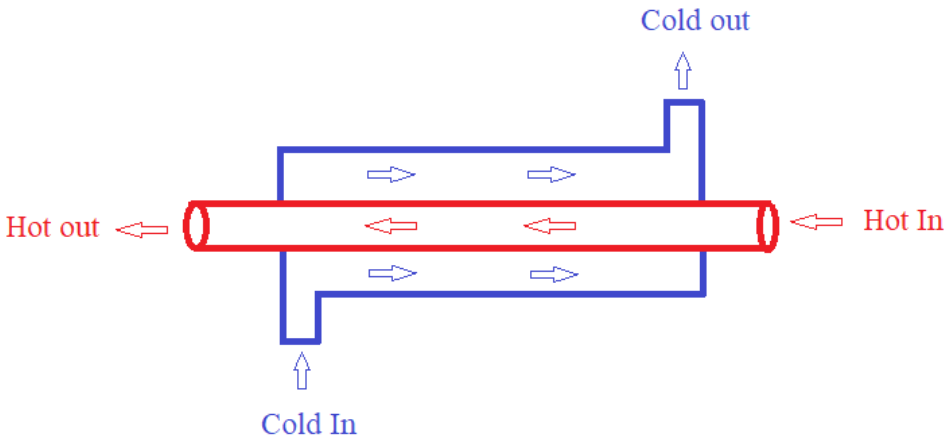

Figure 1.2: Counter flow system.

1.2.3. Cross flow

In cross flow heat exchangers, fluids move perpendicularly to each other. Mixture of fluids may occur, but it is not necessary. The effectiveness of this type of exchanger lies between the other two flow arrangement types.

1.3. Classification based on heat transfer mechanisms

The most prevalent heat transfer mechanisms are two-phase convection on both sides and a combination of convection and radiation. Convection on both sides ocurrs always, but it may be single-phase or two-phased. Every side of a two fluid heat exchanger, such as an air-conditioning evaporator, can be subjected to two-phase convection if condensation and evaporation occur on opposite sides.

1.4. Classification based on constructive features

According to constructive features, the four most prevalent heat exchanger types are plate, tubular, extended surface, and regenerative exchangers.

1.4.1 Plate type

Typically, plate type heat exchangers are built using thin plates. Plates may be flat, corrugated or smooth. In general, these exchangers cannot withstand extremely high values or changes in pressure or temperature.

- Welded plate heat exchangers: the plates are welded together on one or both fluid sides. The plate size tends to be bigger to minimize welding costs. Welding

on both sides tends to raise temperature and pressure, so care must be taken with corrosive fluids. Severall passess and more than two fluid flows can be accommodated by the welded plate heat exchanger.

- Spiral plate heat exchangers: they consist of two long metal strips, rolled up spirally together around a split, so two spiral chanells are built for two fluids. The counterflow spiral exchanger is typically used to cool liquid-to-liquid, gas-to-gas and condensing systems. The device is mounted vertically for condensation or evaporation applications, and horizontally when a fluid contains high concentrations of solids.
- Lamella heat exchangers: they comprise an outer shell of tubes that encloses an inner assembly of flat tubes, known as lamellas. They are used to keep operating pressures fixed. No obstacles are present. In order to accommodate for thermal expansion, the circular tube has one fixed end and one floating end. One fluid flows within the lamellas and the other one, between them.
- Gasketed plate heat exchangers: they are formed by a set of thin rectangular metal plates, gasketed on the sides and framed together. The structure has a fixed end with linking ports and a movable end cap. Each plate is made from stamped or engraved metal, with a wavy surface and grooves on one side of the plate.

1.4.2. Tubular Heat Exchangers

Tubular heat exchangers consist of circular, elliptic or rectangular tubes. This type of exchangers are able to handle high pressure differences betwee the fluids and the surrounding environment, and they are mainly used in thermal engineering applications involving liquid-to-liquid and condensing or evaporating liquid.

- Shell-and-tube heat exchangers: these exchangers are typically composed of a package of round tubes installed in a cylindrical shell. One fluid flows across the tubes, whereas the other one flows across the space between the tubes and the shell. Baffles may be used to direct the flow inside the exchanger.
- Double pipe heat exchangers: they are composed of two concentrical circular tubes, with a plan or finned inner tube.

- Spiral tube heat exchangers: these exchangers include one or more spirally wound coils contained within a shell. These spiral tubes have higher heat transfer rates than plain tubes, allowing for higher heat exchange surface areas, but at a cost of difficulting cleaning procedures.

1.4.3. Extended surface heat exchangers

These exchangers add fins to the main heat transfer surfaces. When one of the fluids has a lower heat transfer coefficient, finned surfaces are used to increase the heat transfer surface on its side. They are commonly used in gas-to-gas and gas-to-liquid heat exchangers to keep the design of the exchanger compact.

- Tube fin heat exchangers: typically used for gas-to-liquid heat exchangers. They are composed of tubes and fins attached to their outer sides. Heat exchangers without baffles, such as double-tube and shell-and-tube, frequently employ longitudinal fins.
- Plate fin heat exchangers: typically used in gas-to-gas processes, allowing fot the reduction of the heat exchanger size. Common applications include energy recovery in industry and refrigeration systems. Flat plates separate the fluid passages, which are sandwiched by corrugated fins.

1.5. Classification based on pass arrangements

Depending of the number of times that the fluid passes across the exchanger, they may be classified as:

- Single-pass, when the fluid passes across the exchanger once.
- Multi-pass, when the fluid is recirculated across the exchanger at least twice.

1.6. Classification based on phase change processes

1.6.1 Condensers

A condenser is a type of heat exchanger that turns vapor into liquid, with the vapor being a single component or a mixture of different components.

1.6.2 Evaporators

Evaporators absorb heat from the cold side of a refrigeration cycle by evaporating a fluid that enters as a liquid and comes out as vapor.

1.7 Research gaps

Several experimental studies on heat exchanger performance enhancement have been described in the literature as active and passive methods. Passive methods include the modification of the geometry or the working fluids, whereas active methods propose the use of energy to increase heat transfer properties. Air, water, and nanofluids with varying nanoparticle concentrations (Al_2O_3, TiO_2, CuO, MgO, Fe_3O_4, hBN, Cu-TiO_2 hybrid, Al_2O_3-MgO hybrid, Alumina–Silver hybrid, Cu-TiO_2 hybrid) have been studied as working fluids under turbulent and laminar flow. The heat exchanger geometry has been altered by incorporating fixed strips, winglets, twisted tapes, conical rings, perforated circular rings, and fins. Additionally, rotation of heat exchanger tubes has been added to increase heat transfer rates. Numerical studies of heat exchangers, based on Computational Fluid Dynamics (CFD) simulations in 2D and 3D may be found in the literature for different working fluids and single-phase and two-phase models under laminar and turbulent flow conditions, with different turbulence models.

Not so much attention has been paid to forced convection of mono and hybrid nanofluids under transitional flow with the rotation of heat exchanger tubes and the modification of their geometry.

1.8 Thesis Objective

Due to the seldom studies of transitional forced convection flow, the main focus of this thesis has been set on this topic. The main objective of this thesis is the development of a numerical model able to simulate transitional forced convection inside a horizontal heat exchanger with concentric tubes, combining both active and passive methods for heat transfer enhancement.

This main objective may be subdivided into the following specific ones:

- Understand the effects of inner tube rotation and fluid flow rate on the heat exchanger performance.
- Compare the performance of water-based nanofluids with Al_2O_3, Cu and hybrid Al_2O_3-Cu nanoparticles.

- Study the influence of varying inner tube rotational speed and nanoparticle concentration on the performance of the heat exchanger.
- Evaluate the effects of introducing typical circular rings (TCR) and perforated circular rings (PCR) with variable number of holes and pitch ratio values, when fitted on the heat exchanger inner tube.

1.9 Research Methodology

The research methodology described below was used to fulfill the research objectives:

- Firstly, a literature review on the topic, as well as the numerical and experimental methods relevant to the research, was performed.
- Then, a 2D-axisymmetric model of a concentric double tube was generated using a Computational Fluid Dynamics (CFD) approach and was validated with experimental results, evaluating different nanofluids and rotational speeds.
- Afterwards, a 3D CFD model was developed to understand spatial behavior of the heat exchanger under the same conditions as for the 2D model.
- Finally, the analysis of a concentric double tube fitted with typical and perforated circular rings was performed, using the 3D model.

1.10 Thesis outline

After Chapter 1, which is the introduction to this work, presenting the classification of heat exchangers and the main lines of the study, Chapter 2 collects the literature review, a description study and an overview of several ways for increasing the efficiency of a double tube heat exchanger including active, passive, and combined methods. Chapter 3, CFD methodology, includes details on the CFD methodology used in this thesis to analyse the two dimensional axisymmetric double tube, the three dimensional double tube with rotating inner tube, and the three dimensional double tube with fitted circular rings. Chapter 4 presents the results and discussion of the work and, finally, Chapter 5, concludes by highlighting the achievement of the research objectives, the main findings and ramifications of his work, and an overview of future research opportunities.

CHAPTER TWO

LITERATURE REVIEW

Chapter Two – Literature Review

2.1 Methods for increasing heat exchanger efficiency

Improving the thermal efficiency of heat exchangers is important to reduce energy consumption and operating costs. Several different ways to increase the efficiency of heat exchangers may be found in the literature. Focus has been set on the double-pipe heat exchanger, as it is one of the main heat exchanger types. It is composed of two concentric pipes, with the inner pipe being plain or finned carrying one of the fluids. The annulus between the inner and outer pipes carries the other fluid.

Heat transfer enhancement methods may be divided into three groups: active, passive, and combined methods. Active methods rely on an external power source to enhance heat transfer. such as a magnetic field or an assistant mechanical system, such as fluid injection or surface or fluid vibration. For example, Bezaatpour and Goharkhah [4] used a magnetic field vortex generator to increase convection heat transfer in a double tube mini heat exchanger. Passive methods, on the other hand, improve heat transfer by altering the fluid flow and the surface of the heat exchanger. For instance, rough surfaces, increase of the contact area, use of fluid additives, coiled tubes or swirl flow devices. For instance, Forooghietal. [5] added a passive insert to the flat tube heat exchanger to enhance heat transfer. Additionally, the use of nanofluids, fluids to which nano-sized solid particles have been incorporated, has shown enhancement properties in heat transfer. Finally, combined methods use both active and passive methods to reduce pump power and increase heat transfer rate.

The sections that follow discuss several existing methods for increasing the heat exchanger performance. They have been divided into experimental methodologies and numerical methodologies for double tube heat exchangers to study geometric modifications, subdivided by fluid type (water, air and nanofluid), and finally, analytical studies.

2.1.1. Experimental studies

Part of the experimental studies deal with heat exchanger geometry modifications in order to enhance their performance. Gomaa et al. [6] conducted an experiment for a double and triple concentric tube heat exchanger using water as the working fluid,

at Reynolds numbers from 1720 to 6260, finding that adding a third tube increased the heat exchanger efficiency in 53.8%. Experimental studies of air and water flows in a horizontal double-tube heat exchanger at different flow rates revealed a maximum increase in NTU of 38% and 0.35 in the effectiveness [7]. Kumar et al. [8] conducted an experiment of double concentric tubes, using water-ethylene glycol mixtures at different volume concentrations (0 - 25%) at Reynolds numbers from 800 to 18,000. The friction factor of ethylene glycol and water decreased as the Reynolds number and concentration of ethylene glycol increased. Sheikholeslami et al. [9] conducted an experiment involving a double pipe heat exchanger with an agitator insert in the inner pipe to investigate the heat transfer of air and water in turbulent flow at flow rates ranging from 120 to 200 L/h. Heat transfer enhancement decreased as the Reynolds number increased and increased with the agitator.

Regarding laminar flow for water, heat transfer improvement in the range of Reynolds numbers from 300 to 1,500 in a heat exchanger tube fitted with multiple conical strips with a varying number of conical strips with different geometrical features were experimentally studied by Liu et al. [10], finding an increase in the Nusselt number and friction factor up to 7.63 and 28.74 times respectively. Turbulent flow was addressed by the experiments of Verma et al. [11] at Reynolds numbers ranging from 5000 to 17,000 in a concentric tube heat exchanger with 4 mm pitch and 1.5 mm depth corrugated inner tubes. The Nusselt number and heat transfer coefficient increased as the rib depth and pitch decreased. Furthermore, the heat transfer rate and friction factor were evaluated for air turbulent flow in a double tube heat exchanger with a novel winglet tape insert with pitches of (30,40, and 50) mm from Reynolds numbers 6000 to 30000. The largest Nusselt number increased by 407 %, and the maximum performance was 2.69. Meanwhile, the highest friction factor increased by 846% (Thejaraju et al. [12]). Also, Chokphoemphun et al [13], determined that the average Nusselt number of air for Reynolds numbers ranging from between 5,300 and 24,000 with a winglet insert in a circular tube with different winglet widths and pitch lengths was over twice the Nusselt number of a plain tube. In addition, the thermal performance was between 1.35 and 1.59 times the original one. An experiment to examine the heat transfer characteristics and friction of

turbulent airflow with varying Reynolds numbers (6,950 - 50,050) in a circular tube fitted with a double counter twisted tape insert at varying twist ratios was conducted by Bhuiya et al. [14]. The insertion of the twisted tape significantly improved heat transfer at the cost of increasing the pressure drop. It was revealed that decreasing the twist ratio increased heat transfer, the friction coefficient, and the thermal efficiency. The Nusselt number was improved by 240 % and the friction factor increased to 286 %. The effect of perforated twisted tapes with different geometries such as triangular, square, rectangular, diamond, and circular on the thermal performance of water in the Reynolds number range (5,500 – 1,000) was studied by Vaisi et al. [15]. In terms of heat transfer and pressure drop, the results show that discontinuous turbulators perform better than continuous ones (heat transfer increased by 8.2% and pressure drop decreased by 9.8%. The shape of the perforation (circular, square, rectangular, diamond, or triangular) also seems to affect heat transfer (20.8 %, 15 %, 11 %, 8.7%, and 5 % respectively). Furthermore, the impact of different twisted tape inserts in a tube (plain, perforated, and dimpled) on transfer enhancement was studied using ethylene glycol and water subjected to turbulent flow at Reynolds numbers from 5217 to 22,754 by Dagdevir and Ozceyhan [18]. The results indicated that dimpled twisted tape outperforms perforated and plain twisted tape regarding heat transfer performance, and that twisted tape inserts significantly increase the friction factor. Pourahmad et al. [19] investigated the effects of dual twisted tape in a tube on air-to-water heat transfer in a turbulent regime at a Reynolds number of 13,600. The Nusselt number with the dual twisted tape insert in the presence of bubble injections was found to be 114% higher. Yakut and Sahin [21] studied the heat transfer characteristics and flow-induced vibration of air in a pipe with a conical ring subjected to turbulent flow with Reynolds numbers from 5,000 to 20,000. It was observed that the Nusselt number increased for all conical rings as the fluid contact with the tube wall increased. In addition, Promvonge and ard [22] evaluated the heat transfer and the friction factor of air at Reynolds numbers from 6,000 to 26,000 in a uniform heat flux tube using a combination of conical ring and twisted tape. They found that the smaller the twist ratio, the greater the heat transfer and friction factor,. The average heat transfer rates

of the conical ring and the twisted tape were 367 % higher. Moreover, Promvonge [23] examined heat transfer in air around a circular tube with various configurations of conical ring inserts, including converging, diverging, and converging-diverging conical rings with Reynolds numbers from 6,000 to 26,000. Using conical ring inserts resulted in higher heat transfer rates, with the diverging conical ring presenting the best results. Other methods for fluid excitation include insertion of rings into a tube. Kongkaitpaiboon et al. [24] investigated heat transfer enhancement of air in tubes with insert circular ring turbulators with varying diameter and pitch ratio values at Reynolds numbers from 4,000 to 20,000. An improvement of 57 to 195 % in heat transfer was observed, with maximum thermal performance at a pitch ratio of 6. Promvonge et al. [25] also studied heat transfer and friction factor characteristics of air in heat fluxed tubes with inclined vortex rings at different pitch ratio values and Reynolds numbers from 5,000 to 26,000. They discovered that the Nusselt number increased for inserted vortex rings and high pressure drop. Huang et al. [26] investigated the effects of ring-type ribs on turbulent air heat transfer in a circular tube at Reynolds numbers ranging from 3,601 to 26,025. The Nusselt number was found to increase as the rib height to tube inner diameter ratio increased. On the other hand, Singh et al. [27] investigated turbulent regimes with Reynolds numbers from 6,300 to 22,500 of air in a heat exchanger tube with several twisted tapes at different twist ratio values and solid rings with different pitch ratio values. Furthermore, an experiment on a heat exchanger fitted with a typical circular ring and a perforated circular ring at different pitch ratio values, number of holes at Reynolds numbers from 6,000 to 12,000 was performed by Sheikholeslami et al. [28]. They discovered that as the number of perforated holes increases, so does the Nusselt number, while the friction factor decreases. Finally, heat transfer in air at Reynolds numbers from 3,500 to 10,500 in a double tube heat exchanger with helical surface disc turbulators with different diameter ratio and helix angle values inside the annulus was studied by Yadav and Sahu [29]. A maximum increase in the Nusselt number of 3.28 was found with helical turbulators, with a maximum friction factor increase of 13.6. Turbulator rings in annular passages were studied by Dirker et al. [30] at Reynolds numbers from 2,000 to 7,500. The addition of turbulators

nearly doubled the local heat transfer coefficient and the average Nusselt number increased in values from 34% to 54%. Finally, natural convection of air from vertical three-dimensional finned tubes with various fin widths at a fin pitch of 2,5 mm was investigated by Ding et al. [20], finding an increase in the Nusselt number up to 207 %. Nusselt numbers increased as fin height increased, and axial fin pitch decreased.

Another option for enhancing heat exchanger performance is altering the flow with energy-activated methods. The effect of injecting air into a water flow was addressed by Moria [16], who used three twisted tapes of varying pitches in a vertical tube under turbulent flow, with different water and airflow rates. Air injection was found to increase heat transfer and pressure drop by up to 30.3% and 62 %, respectively. Chang et al. [17] studied the effects of pitching and rolling on the hydrothermal efficiency of a rectangular channel at Reynolds numbers ranging from 1,500 to 5,500 for water with twisted-tape pin-fins under laminar and turbulent flow. The combined pitching and rolling heat transfer effects reduced the effectiveness of the separate enhancements of pitching and rolling motions. It was found that the increased pressure drop when combining both pitching and rolling motions reduced hydrothermal efficiency.

Besides from these geometrical modifications, rotating exchanger tubes is another method for performance enhancement. Morris and Abadi [31] studied the effect of internal ribbing in a circular coolant channel at Reynolds numbers from 15,000 to 30,000 when the channel was rotated, finding an increase in heat transfer due to arising secondary flows. Watel et al. [32] investigated convective heat transfer in air at Reynolds numbers from 400 to 30,000 with a rotating finned tube, finding an increase in convective heat transfer. Heat transfer enhancement and pressure drop in air under turbulent regime in a plain tube and with a rotating turbine were studied by Duangthongsuk and Wongwises [33]. Average heat transfer coefficient and pressure drop were found to be much higher than that of a plain tube. Ard et al. [34] investigated the effect of the length of the rotating axes in a water heat exchanger at Reynolds numbers from 5,000 to 21,500 using twisted tapes at alternate length

ratios. As the alternate length ratio decreased, both Nusselt number and friction factor increased. The combination of fins and rotation in a heat exchanger at Reynolds numbers from 80,700 to 180,000 were studied by Abou-Ziyan et al. [35] for different rotational speeds up to 400 rpm, finding an increase in the Nusselt number up to 7.5 times the original value. A low fin spacing increased heat transfer and pressure drop of air with respect to plain static tubes. The effects of rotating turbulator inserts on forced convection heat transfer of water under turbulent conditions were examined by Goh et al. [36], finding increases in the Nusselt number up to 360% and 240%. When the distance between turbulator inserts was reduced, both Nusselt number and friction factor increased. Finally, Mohapatra et al. [37] performed an analysis of a three-fluid water heat exchanger at Reynolds numbers from 9,000 to 54,000 in a double tube heat exchanger, in which a helical coiled tube was inserted between two concentric tubes. They found that the overall heat transfer coefficient increased with the fluid mass flow rate.

The remaining actions that have been experimentally studied in the literature deal with the incorporation of nanoparticles into the working fluids, with the objective of improving heat transfer thanks to the better thermal behavior of the resulting nanofluids. Heat transfer in a concentric double tube heat exchanger for Al_2O_3 - water nanofluid at 2% and 3% concentration under laminar condition was studied by Sonawane et al. [38], finding an increase with respect to pure water. Rao et al. [39] conducted an experiment in a shell-and-tube heat exchanger to study turbulent forced convection heat transfer of Al_2O_3 nanofluid at concentrations between 0.1 and 0.4 %, finding increases in fluid viscosity, heat transfer and friction factors as the nanoparticle concentration increased. Prasad et al. [40] investigated the effect of adding Al_2O_3-Water nanofluid at concentrations of 0.01 and 0.03% combined with a trapezoidal twisted tape in a double-tube heat exchanger for Reynolds numbers from 3,000 to 30,000, finding increases in the Nusselt number up to 34.24%. TiO_2 nanofluids were studied by Duangthongsuk and Wongwises [41], who conducted an experiment to examine the convection heat transfer of a TiO_2–water nanofluid with concentrations from 0.2 to 2% in a double tube heat exchanger, finding heat transfer

coefficients 26% higher than for pure water. The pressure drop increased with the Reynolds numbers, exhibiting a marginal increase with particle concentration. Bajestan et al. [42] investigated heat transfer properties of a TiO_2-water nanofluid at concentrations from 1 to 2.3 % under laminar flow in solar heat exchangers, finding a maximum improvement of 21 %. Qi et al. [43] studied the heat transfer and flow characteristics of TiO_2-water nanofluid at concentrations of below 0.5 % in a double-tube heat exchanger with smooth and corrugated tubes at Reynolds numbers from 3,000 to 12,000, discovering an increase in heat transfer of up to 14.8% and pressure drop values of up to 6.5%. Hazbehian et al. [44] explored the heat transfer of a TiO_2-Poly Vinyl Alcohol nanofluid in a plain tube at Reynolds numbers from 800 to 30,000 with twisted tape inserts, finding increases of 30–95% in the Nusselt number just with the inserts, which rose above 100–270% higher with the nanofluid. Thianpong et al. [45] studied the heat transfer of a TiO_2-water nanofluid in a heat exchanger with loose-fit delta-wing twisted tape inserts at concentrations below 0.15% under turbulent flow conditions. They concluded that heat transfer rate and friction factor, increased as the loose-fit ratio decreased and the nanoparticle concentration increased. Cu nanoparticles were studied by Yang et al. [46] in viscoelastic fluids at Reynolds numbers ranging from 6,430 to 10,191. They found an increase rate of heat transfer performance higher than the increase rate of flow resistance. El-Maghlany et al. [47] investigated the rotational effect of an inner tube with a Cu-water nanofluid at concentrations ranging from 0% to 3% under transitional flow, revealing an increase in heat exchanger effectiveness and the pressure drop up to 30.7% and 136% respectively. Moreover, Chaurasia and Sarviya [50] investigated the thermal efficiency and friction factor of CuO-water nanofluids in a tube inserted with strip helical screw tapes with different twist ratio values, at Reynolds numbers ranging from 4,000 to 16,000. For inserted double and single strip helical screw tapes, the Nusselt number increased by 182% and 170%, respectively when the nanofluid was used. MgO–water nanofluids at 1% concentration in a circular pipe were studied by Esfe et al. [48], who concluded that the maximum enhancement of the heat transfer coefficient was approximately 36% for a nanofluid concentration of 1%. Kumar et al. [49] examined flow properties of

a Fe_3O_4 nanofluid across a pipe with strip inserts inside a double-pipe U-bend heat exchanger at concentrations below 0.06 % and a Reynolds number of 30,000. At a concentration of 0.06 %, the Nusselt number increased by 14.7% and the friction factor multiplies by 1.092. Carbon nanotube nanofluids have been studied as well by Halelfadl et al. [51] at 0.026% concentration under laminar conditions (Reynolds numbers between 500 and 2500), finding an improvement of 12% in heat transfer. Higher nanotube aspect ratio values led to higher improvements of the exchanger performance. Nitrogen-doped graphene nanofluids were studied by Goodarzi et al. [52] at concentrations below 0.06% under turbulent flow (Reynolds numbers from 5,000 to 15,000) in a counter flow double pipe heat exchanger. They observed that convective heat transfer coefficient increased by 15.86% with respect to pure water, at the cost of an increase of the friction factor and pumping power. Finally, Ilhan and Erturk [53] found an increase of 15% in heat transfer inside a circular tube exchanger at Reynolds numbers from 800 to 1,700 when adding hexagonal boron nitride-water to water at concentrations up to 1%.

To conclude with experimental research, hybrid nanofluids consisting on the addition of two different nanoparticles have been also studied in the literature. An experimental study of heat transfer characteristics in a concentric tube heat exchanger using a Cu-TiO_2 hybrid nanofluid at concentrations from 0.1% to 2% at Reynolds numbers from 4,000 to 8,000 was performed by Madhesh et al. [54]. Convective heat transfer and pressure drop were found to increase by 68% and 14.9% respectively. Hormozi et al. [55] investigated the effects of surfactants on the thermal efficiency of Alumina–Silver hybrid nanofluids in helical coil heat exchangers under laminar flow, using ionic Sodium Dodecyl Sulfate and nonionic Poly Vinyl Pyrrolidone at weight concentrations ranging from 0.1 to 0.4%. They concluded that the maximum thermal efficiency with anionic surfactant addition was 16% greater than that of distilled water and that the maximum Nusselt number enhancement was 6.283%. The effect of combined tapered wire coils and an Al_2O_3 - MgO hybrid nanofluid with a concentration of 0.1% was studied under turbulent regime by Singh and Sarkar [56], finding increase values in the Nusselt number up

to 84 %. In addition, Singh and Sarkar [57] studied the hydrothermal behaviour of an Al_2O_3 and multi-walled carbon nanotubes hybrid nanofluid at 0.01 % volume concentration in a double-tube heat exchanger with different twisted tape and wire coil inserts in the Reynolds number range from 8,000 to 40,000.The pressure drop was greater for tapered wire coils than for V-cut twisted tapes, and the heat transfer coefficient increased as the twist ratio decreased.

2.1.2. Numerical studies

Numerical methods have been applied as well to the study of heat transfer enhancement in heat exchangers. Abishek et al. [58] used the SST k-ω turbulence model with a second-order upwind discretization to simulate two-phase flow characteristics of a double pipe evaporative heat exchanger at Reynolds numbers between 7,630 and 16,350. Their results showed an increase in the local heat transfer coefficient with the flow advancement, which was later altered due to the high vapor fraction. Zanchini and Jahanbin [59] investigated numerically a double U-tube borehole heat exchanger with water and an annular heat transfer fluid. The thermal resistance of the borehole heat exchanger cross section was found to be determined by ground thermal conductivity, rather than the bulk temperature difference between the sets of tubes.

Different geometries have been studied using numerical simulations. Double tube shell-and-tube heat exchangers with a rectangular header were investigated by Shao et al. [60], using water as the working fluid at a Reynolds number of 43,500. Using the SST k-ω turbulence model, they concluded that the flow distribution of the traditional header was uniform enough for practical applications, but it presented problems at the initial tube pass A circular tube with separated inclined grooves was studied by Zheng et al. [61]. The SST k-ω model, along with the SIMPLE algorithm for velocity pressure coupling and the second-order upwind discretization scheme were used. In comparison to smooth tubes, inclined grooved tubes seemed to increase heat transfer and friction factor by a factor of 2.17 and 3.75, respectively.

Al-Obaidi [62] found an improvement of almost 27% in heat transfer in circular corrugated tubes with respect to smooth pipes at Reynolds numbers from 1,500 to

24,000 using the k-ε turbulence model. Wu et al. [63] analysed the flow and heat transfer in a double heat exchanger with inner corrugated tubes using the Spalart-Allmaras model in turbulent regime and the SIMPLE algorithm to handle the velocity-pressure coupling. Vortices generated at the corrugations led to higher turbulence values, higher heat transfer rates and higher pumping requirements.

Fins of different geometries in heat exchangers were studied by Dastmalchi et al. [69] at Reynolds numbers from 3,000 to 100,000 in a double pipe heat exchanger with the k-ε turbulence model and a second-order discretization scheme. As the inner diameter of the tube increase, optimal helix angle and fin height increased as well. Results indicate that as the inner diameter of the tube increases, the optimal helix angle and micro-fin height increase for all Reynolds numbers considered. Maakoul et al. [77] examined the thermohydraulic performance of a double-pipe heat exchanger with helical and longitudinal fins with different fin spacing ranges at Reynolds number from 12,700 to 17,000 with the realizable k- ε turbulence model, the SIMPLE algorithm, and a second order upwind scheme. Helical fins showed a better performance that longitudinal fins. Anvari et al. [79] studied the heat transfer characteristics and pressure drop in a round tube with converging and diverging conical ring inserts under a turbulent regime. They observed that diverging conical rings outperformed converging ones.

Twisted tapes have been also addressed via numerical simulations. Aliabadi and Feizabadi [64] simulated heat transfer and fluid flow inside tube heat exchangers with twisted-tape inserts and twisted tubes under laminar flow, using the SIMPLE algorithm and the second-order upwind scheme. The twisted tape was found to increase the heat transfer coefficient by 216.5%. Yu et al. [65] performed numerical simulations of heat transfer in twisted tubes with twisted tapes with the standard k–ω model and SIMPLE algorithm at Reynolds numbers from 5,000 to 53,000, finding an increase of around 25% in the Nusselt number in the best case. Harish and Manjunath [66] investigated the flow and heat transfer characteristics of water inside a circular pipe with twisted-tape inserts under laminar condtions, finding an improvement of 24% with respect to a plain tube. Kalateh et al. [67], on the other

hand, reported improvements higher than 46% in the Nusselt number with twisted tapes Bucak and Yilmaz [68] investigated the heat transfer enhancement in a pipe with a twisted tape insert and periodically spherical dimple-protrusion patterned walls at Reynolds numbers between 3,000 and 27,000 with the realizable k-ε turbulence model. Their resutls outperformed conventional twisted tapes and plain tubes.

Winglet inserts have been studied by Liang et al. [74] at different inclination angles under turbulent conditions and the SST k-ω turbulence model. Nusselt numbers were found to increase with the length of the inserts and to decrease with the inclination angle. Skullong et al. [75] simulated the effects of curved winglet inserts with different sizes and pitch values on the thermal and flow behavior of tubes at Reynolds numbers from 4,150 to 25,400 with the realizable k-ε turbulence model. The thermal enhancement factor of the curved winglet was approximately 1.62 and it was found that perforating the winglet resulted in lower pressure drop values. Different V-winglet tapes were studied by Promvonge et al. [76], finding that the V-down configuration was more effective than the V-up (2%).

Regarding the use of conical geometries, Chen et al. [70] used the k-ε model with enhanced wall treatment, finding that the Nusselt number of a flat tube heat exchanger with dual modified conical turbulators was up to 33 % higher than that of a plain tube heat exchanger. Sheikholeslami et al. [80] evaluated heat transfer and friction factor characteristics in a double pipe heat exchanger fitted with circular rings, perforated circular rings, and perforated conical rings at Reynolds numbers from 6,000 to 12,000 using the RNG k-ε model. The Nusselt number was found to increase with the number of perforated holes, whereas the friction factor decreased. Thermal performance improved with the cone angle, while the opposite trend was found for reverse conical ring arrays. V-shaped hexagonal conical rings were studied by Sripattanapipat et al. [81] at Reynolds numbers between 3000 and 20,000 with a realizable k–ε turbulence model. The hexagonal conical ring was found to improve heat transfer by 2.3–3.7 times. Perforated conical rings were also studied Nakhchi and Esfahani [82] at Reynolds numbers between 4,000 and 14,000 with the RNG k-

ε model. With 4 holes, the thermal performance increased in 24.63; while with 10 holes, it increased in 40.17 %. The friction factor was reduced in 88.06% with 10 holes. Ibrahim et al. [83] studied the enhancement of heat transfer with conical ring inserts with different pitch ratios at Renyolds numbers from 6,000 to 25,000 in air. Using the RNG k-ε turbulence model with enhanced wall treatment, they found that the average Nusselt up to 765% with respect to a plain tube. Conical perforated rings were also studied by Uniyal et al. [84] with the standard k-ε turbulence model at Reynolds numbers from 4,000 to 20,000. The increase in the Reynolds number decreased the friction factor, and the conical perforated rings increased heat transfer substantially.

Other particular geometries have been studied in the literature. CFD simulations of the thermal properties of a circular tube heat exchanger incorporated circular ring with different mesh inserts were performed by Bartwa et al. [85] at Reynolds numbers from 5,000 to 40,000. The RNG k-ε turbulence model was used, and the SIMPLE and second-order upwind schemes were applied. The Nusselt number was found to increase by 354% with the metal wire mesh, compared to a plain tube. Moreover, Chamoli et al. [86] studied the turbulent flow heat transfer and flow characteristics in a circular tube equipped with tori. The standard k-ε model was used, along with the SIMPLE algorithm and second-order upwind schemes. The Nusselt number increased 1.93 to 3.36 times over the plain tube, while the friction factor increased 4.76 to 29.05 times.

Free convection heat transfer has been addressed with CFD methods as well. Nada and Said [78] simulated a horizontal annulus with and without annular and longitudinal rectangular fins under laminar conditions, using the standard laminar viscous flow model and a second-order upwind discretization scheme. They observed that heat transfer increased with the number of fins and annular thickness, and that longitudinal fins performed better than annular fins.

CFD simulations have been also applied to analyze the performance of rotating tubes. Ali et al. [71] studied a double pipe heat exchanger with a rotating inner pipe

(0 – 500 rpm) with variable eccentricity values. Rotation increased the Nusselt number by 491 % at low velocity and 120 % at high velocity compared to static tubes. In addition, the pressure drop increased by 178 % at low Reynolds numbers, but by only 12 % at high Reynolds numbers. Song et al. [72] investigated the effects of rotating twisted tapes on heat transfer and fluid flow in an elliptical channel under laminar conditons. Their findings showed that twisted tapes increased average Nusselt number by 24 to 179%, at the cost of increasing pumping requirements by 50 to 250%. Dang and Wang [73] investigated the enhancement of convective heat transfer in a circular tube with a twined coil insert at Reynolds numbers between 400 and 1,800, finding that the twined coil insert resulted in better performances than smooth inserts.

The following studies used CFD simulation to address the behavior of nanofluids for heat exchange purposes. Shirvan et al. [87] studied convection heat transfer in a double-pipe heat exchanger with Al_2O_3 nanofluid concentrations ranging from 0.01 to 0.05 in the laminar regime. A mixture model was used to simulate the two-phase behavior, with the second order upwind scheme and the SIMPLE algorithm. The addition of nanoparticles improved the performance of the exchanger. Albojamal and Vafai [88] investigated the differences in hydrodynamic and thermal properties between single-phase, mixture, and Lagrangian-Eulerian models for Al_2O_3 nanofluid transport in tubes at low concentration values under laminar flow. The maximum deviation between the single-phase and Lagrangian-Eulerian models was 5.9%, whereas the two-phase mixture model could not predict accurately the results. Hence, a single-phase model may be a quick and inexpensive option for the analysis of nanofluids.

2D-axisymmetric simulations offer a less expensive modeling of the heat exchanger behavior. Siadaty and Kazazi [89] investigated, using such simulations of an annular tube, the heat transfer characteristics of Al_2O_3 and Cu nanofluids with concentrations up to 0.5%. They used the realizable k-ε turbulence model, a second-order upwind scheme, and the SIMPLE algorithm. The Nusselt number and entropy generation could be accurately predicted by a single-phase model. Cu-water increased the average Nusselt number by 141.18 % compared to Al_2O_3-water. Mohamed et al.

[91] also used a 2D axisymmetric model of a double tube heat exchanger to compare the behavior of Al_2O_3 and Cu–water nanofluids at concentrations ranging from 0% to 3%, with the RNG k-ε model with enhanced wall treatment, single phase, second order upwind discretizations and the SIMPLE algorithm. They found that Cu–water nanofluid outperformed Al_2O_3 and water by 13%.

A numerical investigation of the heat transfer and turbulent flow characteristics of Al_2O_3-water nanofluid at a volume concentration range from 0 to 10 % in parallel and counter flow double tube heat exchangers using the standard k-ε model and single phase for nanofluid was performed by Bahmani et al. [90], revealing that the addition of nanoparticles to water increased maximum thermal efficiency and average Nusselt number by 30% and 32.7 %, respectively. Darzi et al. [92] also studied an Al_2O_3-water nanofluid at 2 % and 4% concentrations in a helical corrugated tube at Reynolds numbers between 10,000 and 40,000. The standard k–ε and two–phase models were chosen. Heat transfer in the corrugated tube was increased in a factor of 1.58 with the addition of nanoparticles. Karimi et al. [93] used the same nanofluid combined with twisted tape inserts with different pitch ratio values in a double-tube heat exchanger. The SST k-ω turbulence model and the two phase mixture model were used. The Nusselt number increased with the nanofluid concentration and decreased as the pitch ratio fell. Moreover, the addition of twisted tapes to a pipe increased heat transfer and pressure drop.

Not only Al_2O_3-based nanofluids have been studied. Fattahi [109] modelled an Al_2O_3-CuO-water nanofluid at concentrations of 0.02 and 0.04 in a cylindrical pipe with twisted tapes using the RNG k- ε and single-phase models. At concentrations of 0.02 and 0.04, the Nusselt number increased by 23 and 20 %, respectively, with a maximum performance increase of 23 % at 0.02 concentration. Saedodin et al. [94] examined water with SiO_2, TiO_2, Al_2O_3, and CuO nanoparticles at concentrations from 0.5 to 2 % in a circular tube with a twisted turbulator under turbulent conditions. The k-ω and single-phase models were applied in the simulation, discovering that the use of turbulators increased heat transfer, and CuO had the best performance enhancemet of 1.063. Mohammed et al. [95] analyzed turbulent two-phase forced convection of Al_2O_3, CuO, SiO_2, and ZnO nanofluids in circular tubes

with inserted convergent and divergent conical rings with the k-ε model. Heat transfer increment and pressure drop were higher for divergent conical ring inserts than for convergent ones. The insertion of rings increased the Nusselt number by up to 365 % for divergent conical ring configurations and up to 280 % for convergent conical ring configurations. SiO_2, Al_2O_3, ZnO, and CuO in that order, achieved the best performances. Karuppasamy et al. [96] developed a 3D model to study the effect of a cone-shaped insert in a double-tube heat exchanger with Al_2O_3 and CuO-water nanofluids at 1% volume concentration under turbulent regime, applying a single-phase model. It was revealed that the cone-shaped inserts increased heat transfer rate and that Al_2O_3 - water nanofluid performed better than CuO. Demir et al. [97] used a 2D–axisymmetric numerical model of turbulent forced convection flows in a double-tube heat exchanger with 1.4 % TiO_2 concentrations. A single-phase model was used, finding that higher nanoparticle concentrations improved heat transfer at the cost of higher pressure drop values. Using RNG k-ε and single phase models, Ard and Kiatkittipong, [98] developed a three-dimensional numerical model to investigate the effect of multiple twisted tapes with different arrangements and a TiO_2 nanofluid at concentrations of 0.07%, 0.14, and 0.21 under turbulent regime. They observed that the Nusselt number, friction factor, and thermal performance factor increased as the number of tapes increased. The greatest increase in Nusselt number was 10.29 times that of the plain tube. In addition, the addition of TiO_2 nanoparticles to water significantly enhanced thermal performance. A CuO-water nanofluid was studied by Cruz et al. [99] with the realizable k-ε and single-phase models. The highest nanoparticle concentration resulted in a maximum improvement in heat transfer of 48%, but at the expense of a pressure drop twice as big as the original one. Nakhchi and Esfahani [100] studied the turbulent flow behavior of a CuO-water nanofluid at concentrations ranging from 0% to 2% in a heat exchanger pipe with a perforated louvered strip insert using RNG k-ε and two-phase models at Reynold numbers between 5,000 and 14,000. Using perforated louvered strip vortex generators, they were able to enhance the performance of the exchanger. Nakhchi and Esfahani [102] investigated the properties of a Cu-water nanofluid with a concentration of 0 to 1.5% in a heat exchanger tube with perforated

conical rings (PCR) and a number of holes up to 10 under a turbulent regime with a Reynold number between 5000 and 14,000. The single-phase and RNG k-ε models were selected. Their findings indicate that heat transfer rate and frictional loss increased with increasing nanoparticle concentration and number of holes, and the maximum Nusselt number increased by 278.2% compared to a plain tube. Moayedi [103] used Open FOAM to develop a single-phase 2D model of double rotating cylinders in a vented cavity filled with Cu-water nanofluid under laminar flow. Heat transfer was found to increase when both cylinders rotated in opposite directions, with the Nusselt number increasing by more than 330% of its initial value. Furthermore, Murali et al. [104] examined the effect of a trapezoidal twisted tape at a twist ratio of 4.4 with Fe_3O_4 nanofluid at a volume concentration of 0.06 % in a circular tube at Reynold number ranging from 2000 to 12000, observing a 78.6% increase in heat transfer rate compared to a plain tube. Wang et al. [105] developed a numerical model to investigate heat transfer characteristics of SiO_2-water nanofluids in tubes with porous twisted tapes under turbulent regime, using the RNG k-ε and single-phase models. They found that increasing the amount of porous twisted tape increased the Nusselt number. Holes on the twisted tape could improve performance, with the temperature in the tube decreasing as the distance between holes increased. In addition, the combined use of porous twisted tape, nanofluids, and triangular tubes could substantially improve heat transfer efficiency. Jasim et al. [110] conducted a 2D numerical simulation of Al_2O_3-Cu- water hybrid nanofluid at concentrations ranging from 0 to 0.02% inside a vented cavity with a rotating cylinder under laminar regime. An increase in the Reynolds number enhanced heat transfer, while simultaneously increasing pressure drop. The maximum improvement in heat transfer over pure water was 10.6%.

Carbon nanotubes (CNT) may serve as well as fluid additives. Saeedan et al. [101] developed a CFD model to investigate them, as well as Cu and CuO nanoparticles in a double pipe helically baffled heat exchanger with fined tubes at volume concentrations ranging from 1% to 5% under turbulent regime, using the RNG k-ε and single-phase models. The Nusselt number improved with CuO and Cu increasing concentrations, but not with the CNTs. Chandrasekar [106], on the other

hand, investigated the performance of Multi-Walled Carbon Nanotubes (MWCNT) nanofluids at 0.2%, 0.4%, and 0.6% concentrations in a double helically coiled tube heat exchanger under turbulent flow conditions with the k-ε and the single-phase models. Nusselt numbers increased by up to 30% for concentration values of 0.6% with a pressure drop increase of 10%. A biological graphene nanofluid up to 0.1% concentration, combined with double twisted tapes and rotation rates from 0 to 900 rpm, was studied by Bahiraei et al. [107]. The single-phase and the RNG k-ε with enhanced wall treatment models were used. Heat transfer coefficient was found to increase by 34% at a twist ratio of 3 and 900 rpm. Due to the higher rotational speeds and flow disturbances, the fluid particles followed a longer path, resulting in an increase in particle residence time and pumping power. A hybrid nanofluid of graphene nanoplatelets and platinum at concentrations up to 0.1% in a triple tube heat exchanger with inserted ribs was studied by Bahiraei et al. [108] with the same numerical approach. By increasing nanoparticle concentration and rib height, heat transfer characteristics were improved.

2.1.3. Analytical studies

Analytical methodologies have been also applied to the study of heat exchangers. Chen and Hsu [111] used both the finite difference method and the least-squares method to calculate the average heat transfer coefficient on the fin of annular finned tube heat exchangers with different fin spacing. The results showed that, as fin spacing increases, average heat transfer coefficient also increases.

An analysis of the effects of rotating inner and outer tubes on incompressible turbulent flow and heat transfer in an annulus was conducted by Pfitzer and Beer [112]. The Nusselt number increased with the inner tube rotation, with the additional rotation of the outer tube proving a marginal improvement of heat transfer. Shi and Dong [113] studied laminar forced convective flow in a rotating helical tube heat exchanger, finding a decrease in entropy generation due to heat transfer, but a significant increase in flow friction as the rotational speed increased. Bahiraei et al. [114] used an Artificial Neural Network to investigate the thermodynamic properties of a nanofluid based on graphene nanoplatelets in heat exchangers enhanced with

rotating coaxial double twisted tape inserts and rotational speeds up to 900 rpm, using the results from CFD simulations for the neural network model. The ratio of the Nusselt number to the rotational speed increased as the rotational speed increased, while it decreased as the Reynolds number increased.

A theoretical investigation into the thermal conductivities and viscosities of ethylene glycol-based nanofluids containing TiO_2 nanoparticles at volume concentrations ranging from 0 to 7 % was performed by Khedkar et al. [115]. The addition of nanoparticles to base fluids increased both thermal conductivity and viscosity of the resulting fluids.

Finally, Yang et al. [116] examined forced convection heat transfer in a concentric annulu, comparing the performance of Al_2O_3 and TiO_2-water at different concentrations in a laminar flow regime. The Nusselt number was discovered to reach an optimal value for the Al_2O_3 nanofluid, but no maximum was found for the TiO_2 nanofluid.

2.2 Summary

Experimental and computational fluid dynamics (2D and 3D) simulation studies on the improvement of heat exchanger performance have been reviewed. Different working fluids have been used in the literature , such as air, water, and nanofluids at different concentrations (Al_2O_3, TiO_2, CuO, MgO, ZnO, Fe_3O_4, hBN, CNT, Cu-TiO_2 hybrid, Al_2O_3-MgO hybrid, Alumina–Silver hybrid, Cu-TiO_2 hybrid) under turbulent and laminar flow. As the nanoparticle concentration increased, heat transfer improved, but the friction increased. Geometrical modifications, such as the addition of different fixed strips, winglets, twisted tapes, conical rings, perforated circular rings, and fins have been tried to increase the heat exchanger performance. Rotation of the heat exchanger tubes also seems to increase heat transfer. Considering numerical simulations, the single-phase model for analyzing nanofluids has shown to be faster and less computationally expensive than the two-phase mixture model.

Numerical simulation of forced convection of mono- and hybrid nanofluids under transitional flow is seldom found in the literature. Adding rotational effects, as well as performing geometrical modifications under these flow conditions, is even scarcer. Hence, the main objective of this thesis is the development of 2D and 3D numerical models of forced convection under transitional flow inside a horizontal concentric tube-in-tube heat exchanger. The performance of water-based nanofluids with Al_2O_3, Cu, and hybrid Cu-Al_2O_3 nanofluids at different concentrations, as well as the addition of perforated circular rings, will be addressed, in addition to the effect of rotating the exchanger inner tube.

CHAPTER THREE

NUMERICAL METHODOLOGY

Chapter Three – Numerical methodology

The main focus of this chapter is set on Computational Fluid Dynamic (CFD) models, detailing all the aspects of the methodology applied in this work. Firstly, the experiments performed by El-Maghlany et al. [47] that were used to validate the models developed in this thesis are presented.

A 2D axisymmetric model is then introduced, as well as the 3D model for the study of the original heat exchanger. Finally, the 3D model with the geometrical modifications proposed, circular rings with and without holes, is presented. The commercial software ANSYS FLUENT® 15.0. was used to develop the models and run the simulations in this work. Figure 3.1 shows a scheme of the CFD methodology followed in this study.

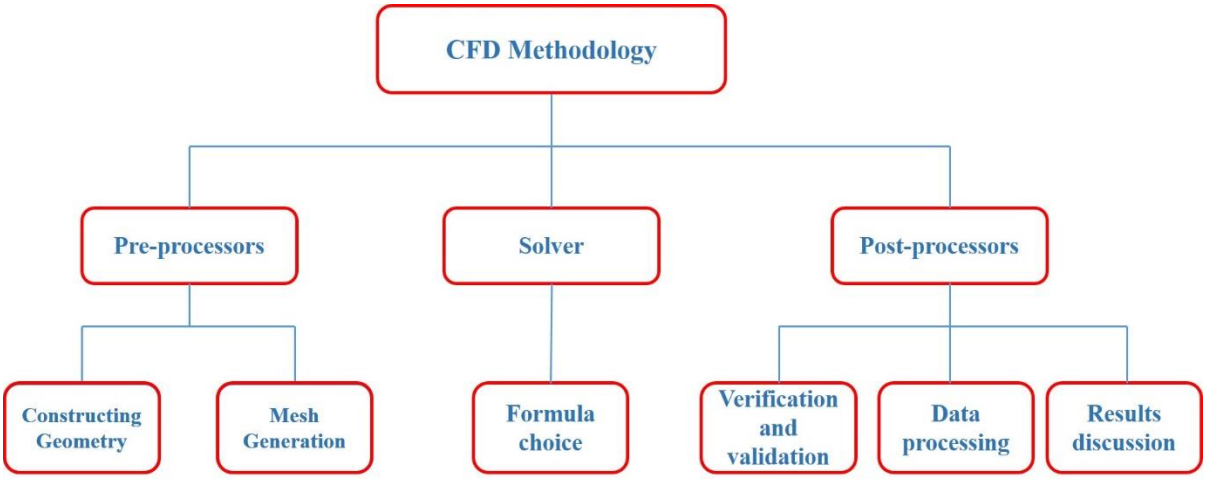

Figure 3.1 CFD methodology sequence.

The evaluation of technological flows using CFD tools must include simplifications in order to simulate the desired physical effects. These simplifications include:

- Phyiscal simulation: in reality, complex flows are developed, with transitional and turbulent regions, multiphase and three-dimensional flows with unsteady behaviors, etc. CFD models use a turbulence model to account for these effects with respect to the bulk fluid characteristics.

- Discretization: although reality is continuous, numerical models require discrete domains to perform the calculations. Hence, the formulae that describe the physical phenomena must be discretized into finite elements conforming a mesh. In the case of CFD solvers, the finite volume method is the most common formulation.
- Boundary conditions: as the simulation domain must be limited in space, boundary conditions must be imposed at the domain limits, modelling the relevant phenomena that occur in physical reality. These boundary conditions may affect the results.
- Convergence issues: CFD methods solve the equations by iteration, so a residual between each iteration is calculated. Convergence is reached when the residual values drop below a certain threshold. However, in some cases, convergence may be hindered by the solver programming, the mesh definition, or the boundary conditions applied.

3.1 Experimental reference test

The experimental reference test that was used to validate the models developed in this thesis was conducted by El-Maghlany et al. [47] as shown in Figure 3.2.

The device consists of two concentric pipe heat exchangers in a horizontal counter-flow position. Water was used as the hot fluid, whereas a Cu-water nanofluid was used as the cold fluid. Two closed loops were used for the circulation of the working fluids, equipped with the necessary measurement instruments. The main test section consists of two pipes, with the inner tube having a 25.4 mm diameter, 2 mm thickness and made of copper; and the outer tube having a 76.2 mm diameter, 5 mm thickness and made of transparent Plexiglas. The total tube length is 1.2 m for both tubes. Two tanks store the two working fluids, which are pumped by two centrifugal pumps. An AC bolt electric heated is used to set the desired inlet temperature of the pure water. There is a refrigeration unit attached to the storage tank in the nanofluid loop, which serves to cool the nanofluid down back to initial conditions. Four T-type thermocouples are attached to the inlet and outlet of the exchanger tubes, to measure the temperature of the fluids. The inlet temperatures of the nanofluid and

the hot water are set to 301 and 333 K respectively. Additionally, pressure transducers are used to estimate the pressure drop in the heat exchanger, by measuring inlet and outlet pressures in both fluid loops. A 1 HP motor drives the exchanger inner tube with a belt-pulley system, and a frequency inverter has been installed to control rotational speed up to 500 rpm. Fiberglass insulation is used to reduce heat losses from the exchanger to the surroundings. The experiments were conducted at 2,473, 3,092.7, 3,713, 4,331 and 4,946 Reynolds numbers for the nanofluid, while the Reynolds number for the hot water was kept constant at 9,780.

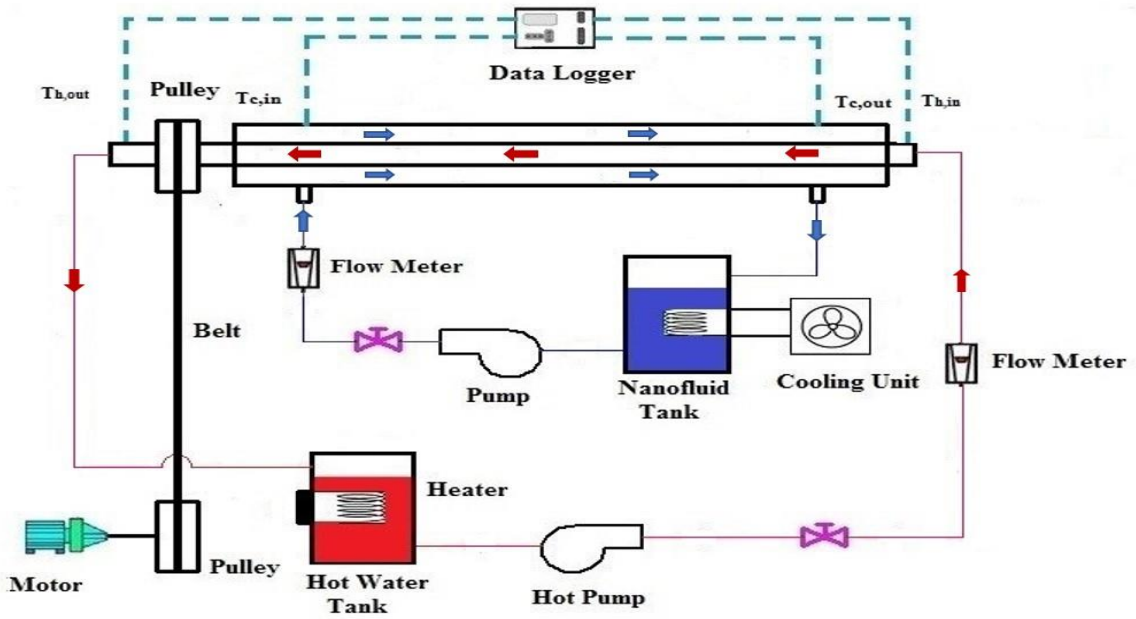

Figure 3.2 Schematic diagram of experimental test.

3.2 Heat transfer equations

In these sections, the formulation used to analyze the heat exchanger is explained. As heat exchangers typically operate for extended periods of time at almost constant operating conditions, they may be studied as steady flow devices. This means that the fluid mass flow rates remain constant, as well as fluid properties. There are two main approaches for heat exchanger analysis: the The Log Mean Temperature Difference (LMTD) and the Number of Transfer Units (NTU) methods. The outer

surface of the heat exchanger is assumed to be perfectly insulated, so that there are no heat losses to the surroundings.

High values of effectiveness (ε) correspond to small temperature differences between the hot and cold fluids, whereas larger temperature differences result in higher heat transfer rates. To achieve both high heat transfer values and high effectiveness, the size of the exchanger or the fluid velocity must be increased.

The main equations for the analysis of the heat exchanger are the following:

Heat lost from the hot fluid.

$$Q_{hf} = \dot{m}_{hf} C_{p,hf} \, (T_{hf,i} - T_{hf,o}) \tag{3.1}$$

Heat absorbed by the cold fluid

$$Q_{cf} = \dot{m}_{cf} C_{p,cf} \, (T_{cf,o} - T_{cf,i}) \tag{3.2}$$

Average heat transfer rate

$$Q_{avg} = \frac{Q_{hf} + Q_{cf}}{2} \tag{3.3}$$

Overall heat transfer coefficient

$$U = \frac{Q_{avg}}{A_s \, \Delta T_{log}} \tag{3.4}$$

where ΔT_{log} is the logarithmic mean temperature difference, obtained as:

$$\Delta T_{log} = \frac{(T_{hf,o} - T_{cf,i}) - (T_{hf,i} - T_{cf,o})}{ln \frac{(T_{hf,o} - T_{cf,i})}{(T_{hf,i} - T_{cf,o})}} \tag{3.5}$$

Number of transfer units (NTU)

$$NTU = \frac{U \, A_s}{C_{min}} = \frac{Q_{avg}}{\Delta T_{log} \, C_{min}} \tag{3.6}$$

where C_{min} is the smallest fluid heat capacity value.

$$C_{min} = \min(C_h, C_f) \qquad C_h = \dot{m}_{hf} C_{p,hf} \qquad C_c = \dot{m}_{cf} C_{p,cf} \tag{3.7}$$

Heat exchanger effectiveness

$$\varepsilon = \frac{1 - \exp\left[\left(-NTU\left(1 - \frac{C_{min}}{C_{max}}\right)\right]\right.}{1 - \frac{C_{min}}{C_{max}} \exp\left[\left(-NTU\left(1 - \frac{C_{min}}{C_{max}}\right)\right]\right.} \tag{3.8}$$

Hot and cold fluid Reynolds numbers

$$\mathrm{Re_{hf}} = \frac{\rho_{hf} u_{hfi} d_i}{\mu_{hf}} \qquad \mathrm{Re_{cf}} = \frac{\rho_{cf} u_{cfi} D_h}{\mu_{cf}} \tag{3.9}$$

Pumping power required for the exchanger [107]

$$W = \left(\dot{V}\, \Delta P\right)_{cf} + \left(\dot{V}\, \Delta P\right)_{hf} \tag{3.10}$$

where ΔP (Pa) is the pressure drop, and $\dot{V}$ is the volumetric flow rate (m^3/s).

3.4 Material Properties

Material properties must be correctly modeled to perform the simulations. The exchanger outer tube is made of transparent Plexiglas, while the inner tube is made of copper.

Regarding the working fluids, several researchers in the literature have measured physical properties of nanofluids. The effective properties of the nanofluids may be calculated with the following equations:

Effective density [47]

$$\rho_{nf} = (1 - \phi)\rho_f + \phi\rho_s \tag{3.11}$$

Specific heat [108]

$$\left(\rho C_p\right)_{nf} = (1 - \phi)\left(\rho C_p\right)_f + \phi\left(\rho C_p\right)_s \tag{3.12}$$

Thermal conductivity [117]

$$k_{nf} = k_f \left[\frac{k_s + 2k_f + 2\phi\left(k_s - k_f\right)}{k_s + 2k_f - \phi\left(k_s - k_f\right)}\right] \tag{3.13}$$

Dynamic viscosity for $\phi \leq 5\%$

$$\mu_{nf} = (1 + 2.5\phi)\mu_f \tag{3.14}$$

For hybrid nanofluids, the equations are modified:

Effective density for two mixture nanoparticles [89]

$$\rho_{hnf} = \phi_{s1}\rho_{s1} + \phi_{s2}\rho_{s2} + (1 - \phi_h)\rho_f \tag{3.15}$$

where the volume concentration for hybrid nanofluids [118] is

$$\phi_h = \phi_{s1} + \phi_{s2} \tag{3.16}$$

Heat capacity of hybrid nanofluids [118]

$$(\rho C_p)_{hnf} = \phi_{s1}\rho_{s1}C_{p,s1} + \phi_{s2}\rho_{s2}C_{p,s2} + (1-\phi_h)\rho_f C_{p,f} \quad (3.17)$$

Dynamic viscosity of hybrid nanofluids [118]

$$\mu_{hnf} = (1 + 2.5\phi_h + 6.2\phi_h^2)\mu_f \quad (3.18)$$

Thermal conductivity of hybrid nanofluids (modified Maxwell model) [118]

$$k_{hnf} = k_f \left[\frac{\frac{\phi_{s1}k_{s1} + \phi_{s2}k_{s2}}{\phi_{hnf}} + 2k_f + 2(\phi_{s1}k_{s1} + \phi_{s2}k_{s2}) - 2\phi_{hnf}k_f}{\frac{\phi_{s1}k_{s1} + \phi_{s2}k_{s2}}{\phi_{hnf}} + 2k_f - (\phi_{s1}k_{s1} + \phi_{s2}k_{s2}) + \phi_{hnf}k_f} \right] \quad (3.19)$$

The thermo-physical properties of copper, Plexiglas, water, Cu and Al_2O_3 are shown in Table 3.1.

Table 3.1. Thermo-physical properties of pure water, nanoparticles and nanofluids.

Material	Density (ρ) Kg/m^3	Specific Heat (CP) J/kg .k	Thermal Conductivity (k) W/m .k	Viscosity (μ) *Pa*. s
Copper	8978	381	387.6	-
Plexiglas	1180	1465	0.19	-
Water [47]	997.1	4179	0.6	0.001
Cu [47]	8933	385	385	-
Al_2O_3 [89]	3970	765	36	-

3.5. 2D Axisymmetric Model

3.5.1 Mesh Generation

The mesh was generated in ANSYS ® 15.0 with quadrilateral grids, as shown in Figure 3.3. The discretization was verified for water at the Reynolds number Re_{cf}= 2473, testing four different grids as shown in figure 3.4 and using the Number of Transfer Units (NTU) as the verification parameters. It may be observed that the NTU remains stable when the total number of cells reaches 152,750 cells. Hence, the mesh with 152,750 cells was chosen, as it provided the best accuracy to computational cost ratio.

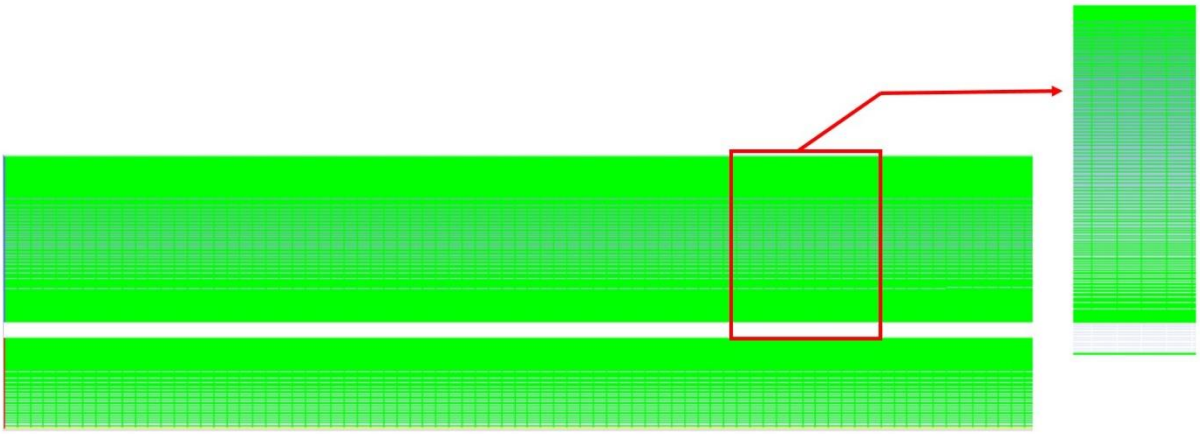

Figure 3.3 2-D Axisymmetric mesh (152,750 cells).

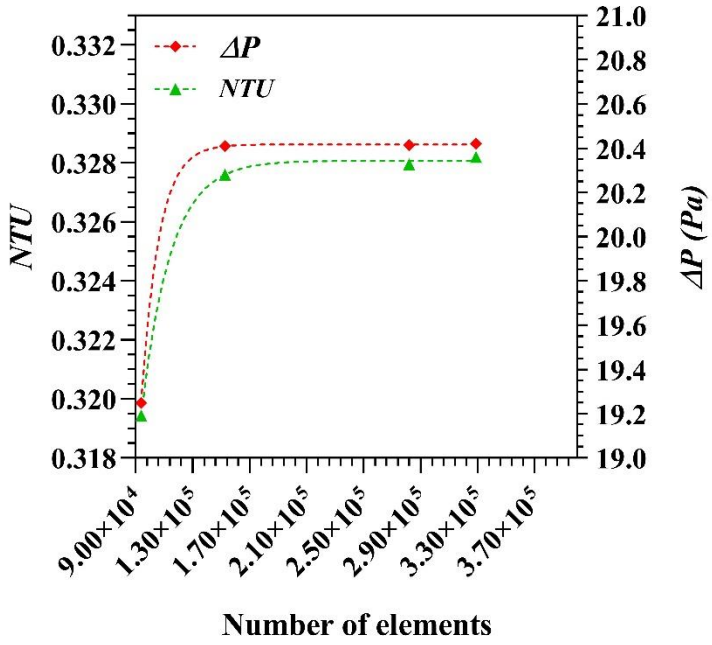

Figure 3.4 Grid independence study at Re_{cf} = 2473

3.5.2 Numerical solver

A pressure-based solver was chosen for solving the Navier-Stokes equations that govern the fluid flow and energy transport, due to the less amount of memory required

and the higher flexibility in the solving process. The governing equations were solved iteratively until reaching convergence.

3.5.2.1 Boundary conditions

The boundary conditions applied to the simulation domain are shown in Figure 3.5. A velocity inlet condition has been set at the domain inlet, with values calculated from the required Reynolds number for each simulation case (2,473 – 4,946).

$$u = \frac{Re\ \mu}{\rho\ D} \tag{3.20}$$

The inlet temperatures of the cold fluid and the hot water were fixed at 301 K and 333 K, corresponding to the experimental tests. A pressure outlet condition equal to atmospheric pressure has been set at the domain outlet. In addition, the no-slip wall condition is applied to the tube walls.

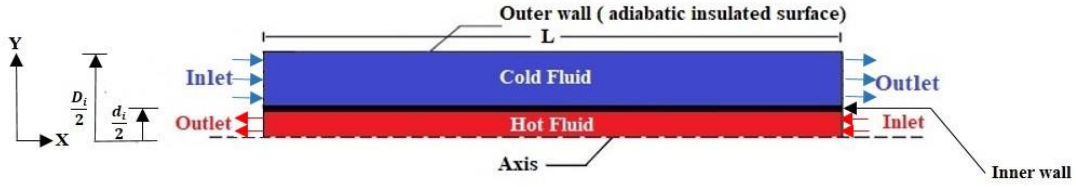

Figure 3.5 Geometric schematic of 2D axisymmetric double tube.

3.5.2.2 Turbulence and phase modeling

The turbulence closure of the discretized Navier-Stokes equations was addressed with the Renormalized Group (RNG) k-ε turbulence model, one of the most widely known and validated turbulence models. This model has proven to be accurate and dependable for a wide range of flows with low Reynolds numbers, as it is the case in this study. It is also able to account for rotation and swirl flow motion [101,105,107,108]:

$$\nabla.(\rho k\,\bar{V}) = \nabla.\left((\alpha_k \mu)\ \nabla(k)\right) + G_k - \rho\varepsilon \tag{3.21}$$

$$\frac{\partial}{\partial t}(\rho\varepsilon) + \frac{\partial}{\partial x_i}(\rho\varepsilon u_i) = \frac{\partial}{\partial x_j}\left(\alpha_\varepsilon \mu_{eff}\frac{\partial \varepsilon}{\partial x_j}\right) + C_{1\varepsilon}\frac{\varepsilon}{k}(G_k + C_{3\varepsilon}G_b) - C_2\rho\frac{\varepsilon^2}{k} - R_\varepsilon + S_\varepsilon \tag{3.22}$$

where α_k and α_ε are the inverse effective Prandtl numbers for k and ε, respectively, and G_k is the production of turbulence kinetic energy rate, calculated from:

$$G_k = \nabla.\left(-\rho\overline{V'V'}\right) \quad (3.23)$$

A single-phase methodology for the nanofluid description has been selected, as the literature has confirmed the suitability of this approach [50, 101,105,107,108].
The Navier -Stokes equations have been solved in forced convection in steady-state flow of an incompressible and newtonian fluid using ANSYS-FLUENT 15.0 software:

Continuity equation:

$$\nabla.(\rho\bar{V}) = 0 \quad (3.24)$$

Momentum equation:

$$\nabla.(\rho\overline{VV}) = -\nabla\bar{P} + \mu\nabla^2\bar{V} \quad (3.25)$$

Energy equation:

$$\nabla.\left(\rho c_p \bar{V} T\right) = \nabla.(K\nabla T) \quad (3.26)$$

3.5.2.3 Discretization scheme

The Semi-Implicit Method for Pressure Linked Equation (SIMPLE) algorithm was chosen for this study, as it is strong stable and provides good results with structured meshes. The least squares cell-based discretization was used as spatial discretization of the gradients of solution variables, due to its better accuracy-cost ratio than the node-based gradient method. The remaining discretization schemes (pressure, momentum, turbulent kinetic energy, turbulent dissipation rate, and energy) were chosen as second-order upwind, as they allow a higher-order accuracy at cell faces for the calculation of the solution variables.

3.5.2.4 Convergence

The convergence criteria was set as obtaining a decrease of three orders of magnitude in the residuals from the simulation. A criterion of 10^{-5} for the continuity and momentum equations, and 10^{-6} for the energy equation were used.

3.5.3 Experimental validation

The CFD model was validated using the experimental results from El-Maghlany et al. [47]. The comparison between the results from both studies may be observed in Figure 3.6, where it may be appreciated that the results from the model developed in this work agree consistently with the experimental results. Maximum deviations of 3.88% for the NTU and of 4.05% for the pressure drop were observed, so the numerical model may be considered as valid for the purposes of this work.

Figure 3.7. summarizes the main steps followed for the development of the 2D numerical model.

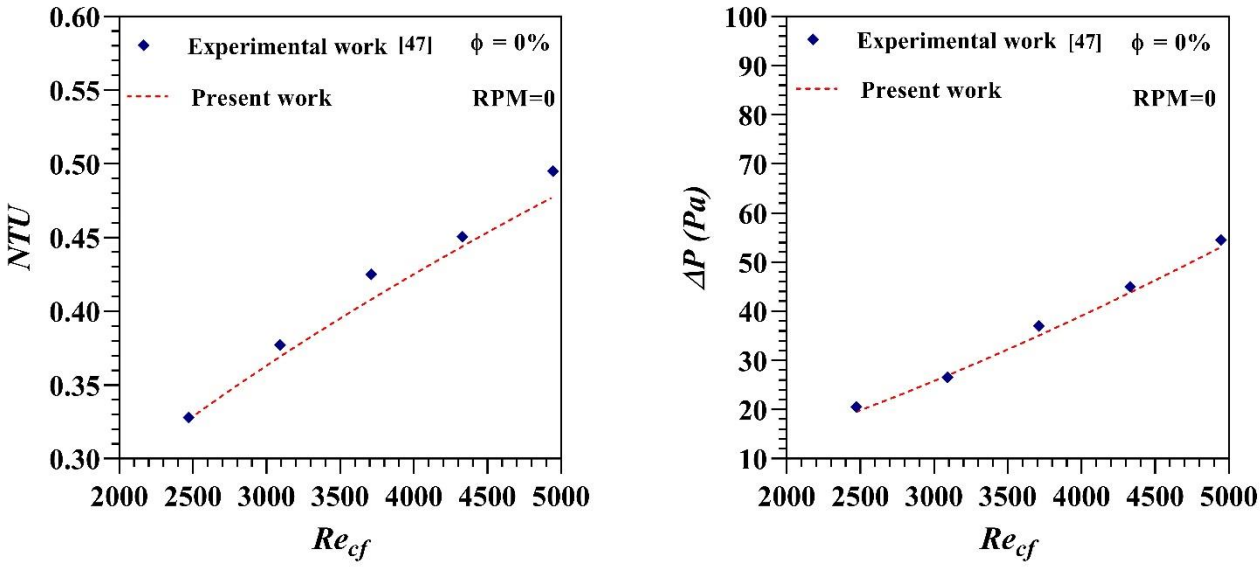

Figure 3.6 Validation with experimental data.

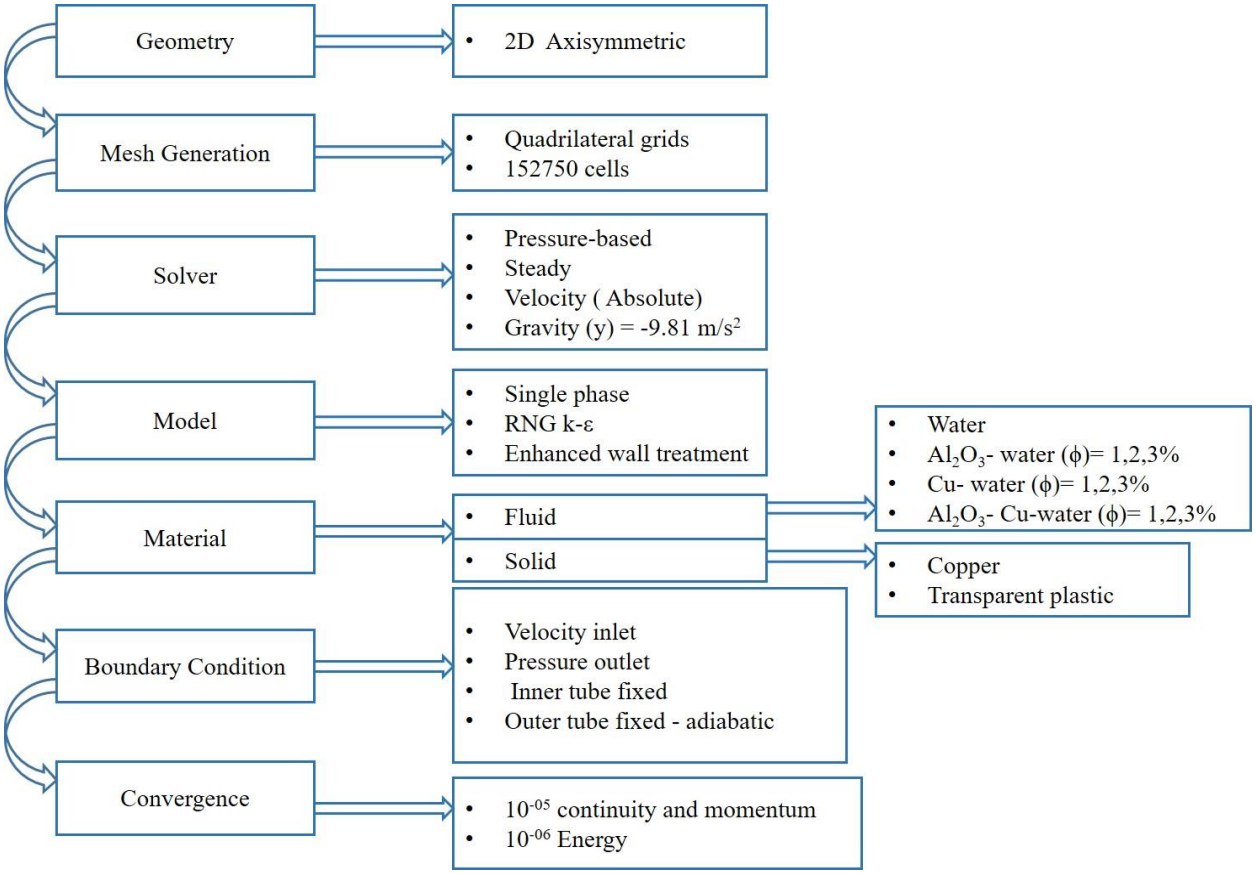

Figure 3.7 Steps of numerical simulation for 2D Asymmetric.

3.6. 3D numerical model of the double-tube heat exchanger

After observing the results from the 2D model, a complete 3D model of a double-tube counter-flow heat exchanger, as depicted in Figure 3.8, was developed.

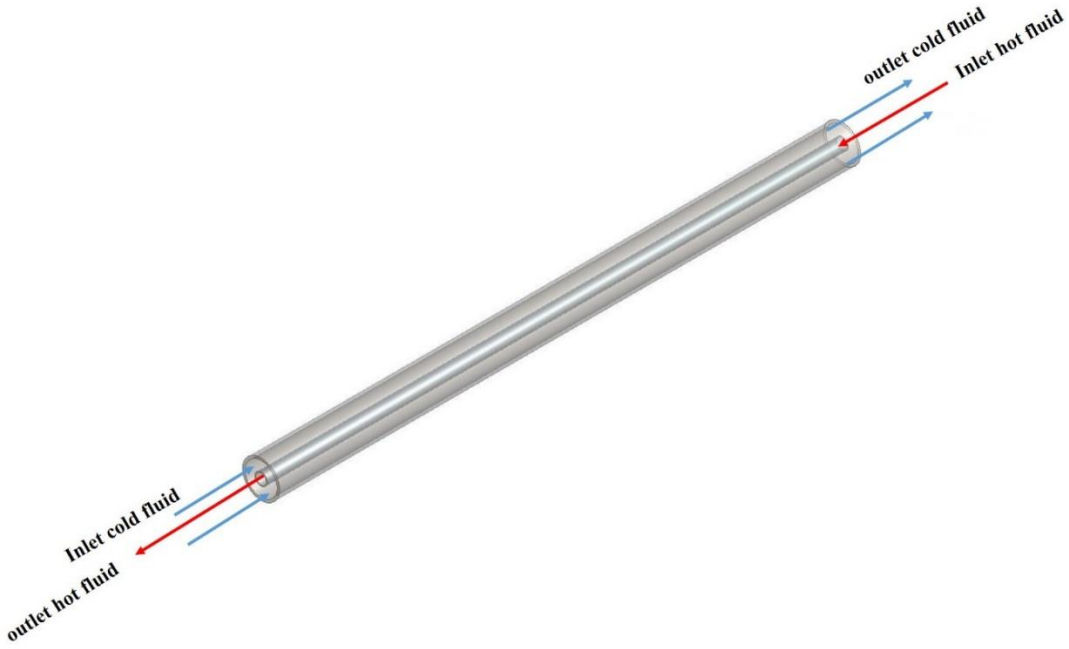

Figure 3.8 Schematic of 3D double tube heat exchanger.

3.6.1 Mesh Generation

The 3D model was generated with a combination of hexahedral and tetrahedral cells, as shown in figure 3.9. Verification of the model was performed at the Reynolds number Re_{cf}= 2473, as with the previous model. Four different mesh sizes were tested, as shown in figure 3.10. It may be appreciated that the grid with 1,835,524 cells, with an error around 0.81 % for the NTU, is suitable for the purposes of this study.

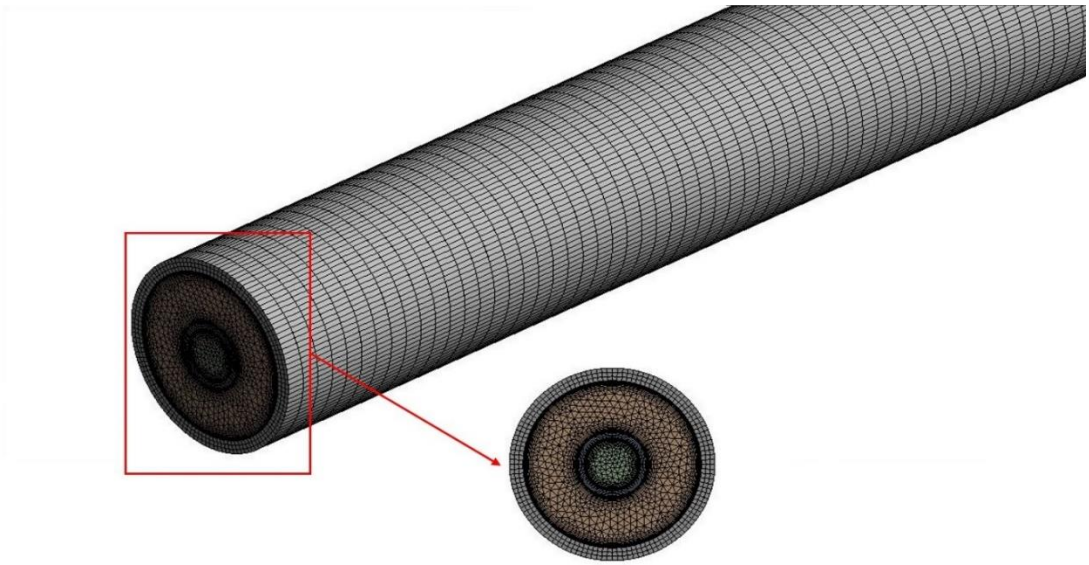

Figure 3.9. Mesh configuration of the double tube heat exchanger.

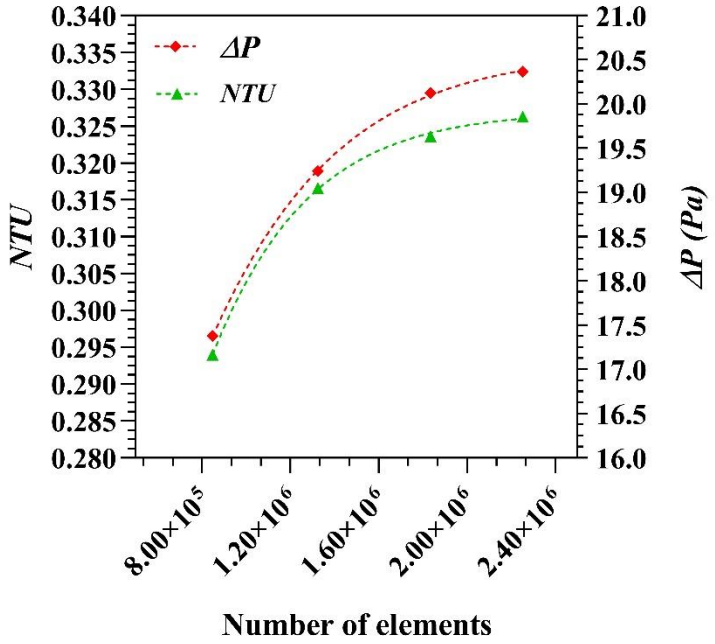

Figure 3.10. Verification study at Re_{cf} = 2473

3.6.2 Numerical solver

The same pressure-based numerical solver as from the previous case was chosen.

3.6.2.1 Boundary conditions

The same boundary conditions shown in Figure 3.8 were applied to the 3D numerical domain. The velocity inlet conditions set at the domain inlets were calculated from Equation 3-20, parting from the Reynolds number values (2473 – 4946). Inlet temperatures of the cold fluid and the hot water were fixed at 301 K and 333 K respectively. At the domain outlet, a pressure outlet condition equal to atmospheric pressure has been set. The wall no-slip condition was also applied to the tube walls. Rotation of the inner tube was applied, with different rotational speeds ranging from 0 to 500 rpm in 100 rpm increments.

3.6.2.2 Turbulence Model

The Renormalized Group (RNG) *k*- ε turbulence model with enhanced wall treatment has ben chosen, as it has shown to be suitable for the description of low Reynolds numbers with swirl flow [6,101,105,107,108]. A single-phase approach for modeling the behavior of nanofluids has been selected, as it reduced simulation time while keeping enough accuracy when compared to the two-phase approach [50, 101,105,107,108].

The 3D Navier-Stokes equations were then discretized and solved:

Continuity equation:

$$\frac{\partial \rho u_i}{\partial x_i} = 0 \qquad (3.27)$$

where x_i is each Cartesian coordinate, u_i is the component of velocity in the i-direction and ρ is the fluid density.

Momentum equation:

$$\frac{\partial(\rho u_i u_j)}{\partial x_i} = -\frac{\partial p}{\partial x_i} + \frac{\partial}{\partial x_j}\left[\mu\left(\frac{\partial u_i}{\partial x_j} + \frac{\partial u_j}{\partial x_i} - \frac{2}{3}\delta_{ij}\frac{\partial u_l}{\partial x_l}\right)\right] + \frac{\partial}{\partial x_j}\left(-\rho\,\overline{u_i' u_j'}\right) \qquad (3.28)$$

where $-\rho\,\overline{u_\iota\, \acute{u_j}}$ are Reynolds stresses, ρ is the fluid density, p is the pressure and μ is the dynamic viscosity

Energy equation:

$$\nabla \cdot \left(\vec{v}(\rho E + p)\right) = \nabla \cdot \left(k_{eff} \nabla T - \sum_j h_j \vec{J}_j + \left(\bar{\bar{\tau}}_{eff} \cdot \vec{v}\right) \right) \quad (3.29)$$

Where k_{eff} is the effective conductivity ($k + k_t$, where k_t is the turbulent thermal conductivity) and $\vec{J}_j$ is the diffusion flux of species j. Energy at every control volume is calculated as:

$$E = h - \frac{p}{\rho} + \frac{v^2}{2} \quad (3.30)$$

where h is the fluid enthalpy

Turbulent viscosity μ_t is calculated as:

$$\mu_t = \rho \, C_\mu \, \frac{k^2}{\varepsilon} \quad (3.31)$$

, leading to the turbulent kinetic energy equation (k):

$$\frac{\partial(\rho u_i k)}{\partial x_i} = \frac{\partial}{\partial x_j}\left(\alpha_k \, \mu_{eff} \frac{\partial k}{\partial x_i}\right) G_k - \rho\varepsilon \quad (3.32)$$

and the turbulent energy dissipation equation (ε):

$$\frac{\partial(\rho \varepsilon u_i)}{\partial x_i} = \frac{\partial}{\partial x_j}\left(\alpha_\varepsilon \, \mu_{eff} \frac{\partial \varepsilon}{\partial x_j}\right) + C_{1\varepsilon} \frac{\varepsilon}{k} G_k - C_{2\varepsilon} \rho \frac{\varepsilon^2}{k} - R_\varepsilon \quad (3.33)$$

where G_k is the generation rate of turbulent kinetic energy due to the mean velocity gradients and is obtained from

$$G_k = -\rho \, \overline{u_i' u_j'} \frac{\partial u_j}{\partial x_i} \quad (3.34)$$

The effective turbulent viscosity μ_{eff} is calculated as

$$\mu_{eff} = \mu + \mu_t \quad (3.35)$$

The model constants used in the above equations were selected as:

$\alpha_k = 1.393$, $\alpha_\varepsilon = 1.393$, $C_\mu = 0.0845$, $C_{1\varepsilon} = 1.42$, $C_{2\varepsilon} = 1.68$

where α_k and α_ε are the inverse effective turbulent Prandtl numbers for k and ε.

3.6.2.3 Discretization scheme

The SIMPLE algorithm was chosen for the coupling of velocity and pressure fields, and second-order upwind discretization schemes were selected for the spatial discretization of pressure, momentum, turbulent kinetic energy, turbulent dissipation rate, and energy equations.

3.6.2.4 Convergence criteria

Convergence was addressed by monitoring the residuals of the simulation and setting 10^{-5} as the threshold value for the continuity and momentum residuals, and 10^{-6} for the energy residuals.

3.6.3 Validation

A comparison of the numerical simulations and the experimental results from El-Maghlany et al. [47] was performed to validate the numerical model. The NTU and pressure drop for water and the Cu –water nanofluid at ϕ=3% were used as validation variables.

Figure 3.11 shows a good agreement between numerical and experimental results, with a maximum deviation of 4.3 % and 4.88 % in the NTU values for water and the Cu –water nanofluid respectively, and a maximum deviation in pressure drop values of 4 % and 3.62 % for water and the Cu –water nanofluid. Hence, it may be considered that the numerical model is valid for the purposes of this work.

Figure 3.12. shows a scheme with the main steps followed to develop the 3D numerical model.

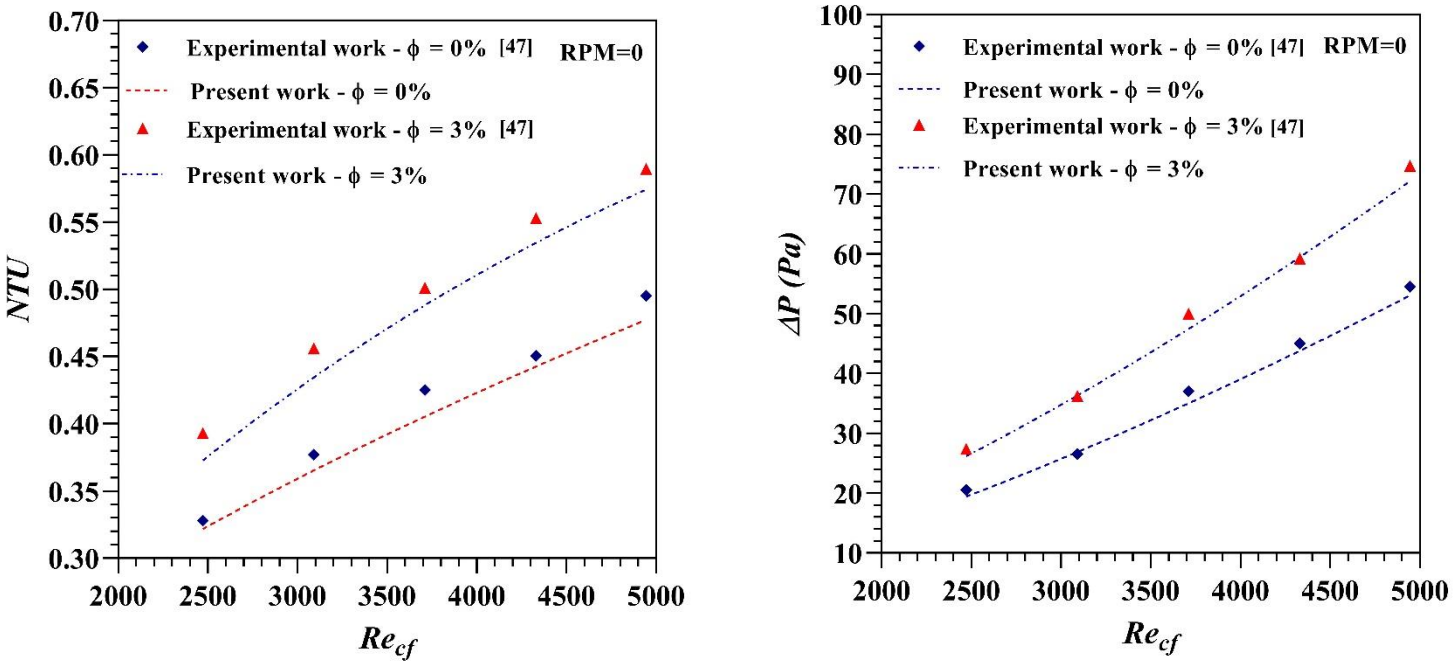

Figure 3.11 Validation with experimental data for water and Cu- water at ϕ=3%.

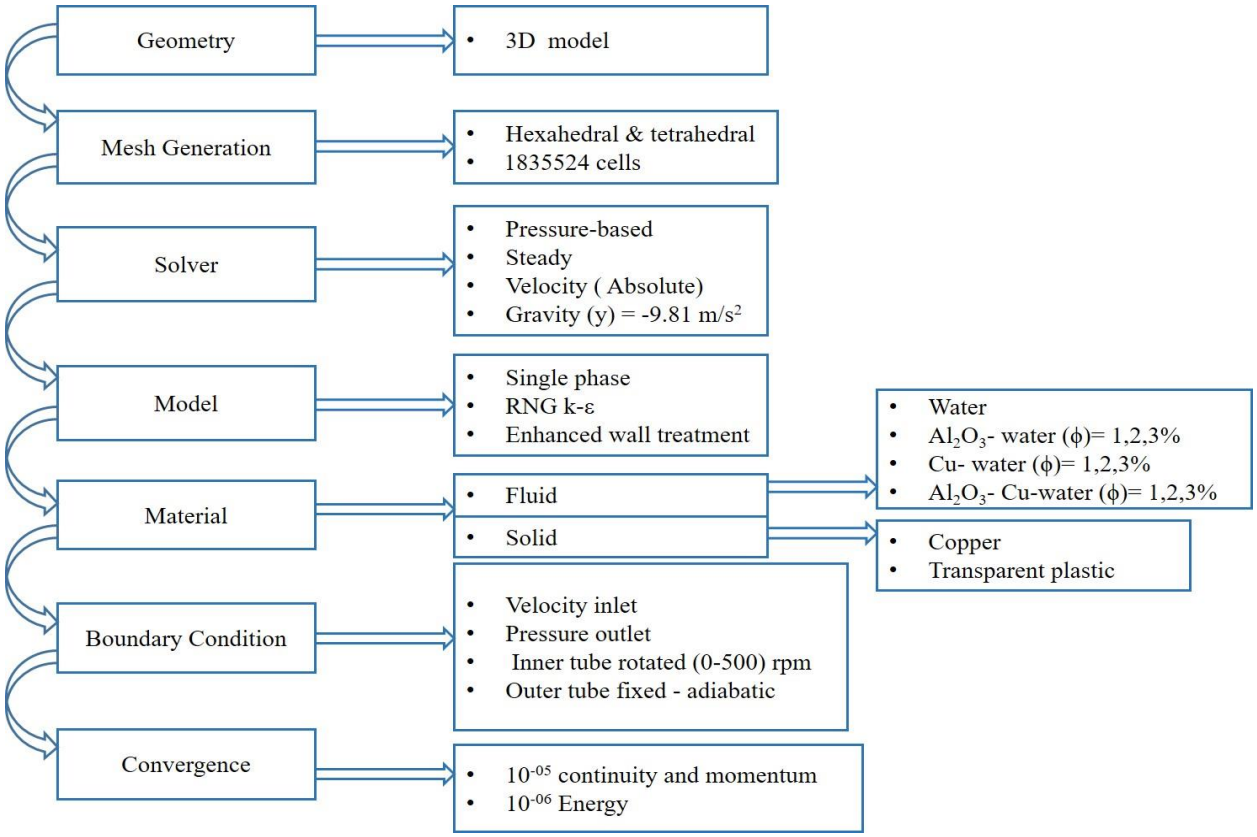

Figure 3.12 Steps of numerical simulation for 3D model.

3.7. 3D numerical model of the double tube heat exchanger fitted with perforated circular rings (PCR)

3.7.1 Geometry

After the results with the 3D numerical model of the heat exchanger were obtained, the insertion of typical (TCR) and perforated (PCR) circular rings in the inner tube was addressed. Different numbers of holes were tested (N=0, 4, and 8), with similar values as the ones found in the literature [28,82,102]. The heat exchanger length remains as 1.2 m, with the inner (d_i) and outer (D_i) tube diameters being 25.4 and 76.2 mm, respectively. The thickness of the inner tube is 2 mm. Figure 3.13 shows the geometry of the proposed modification with circular rings perforated with 8 holes.

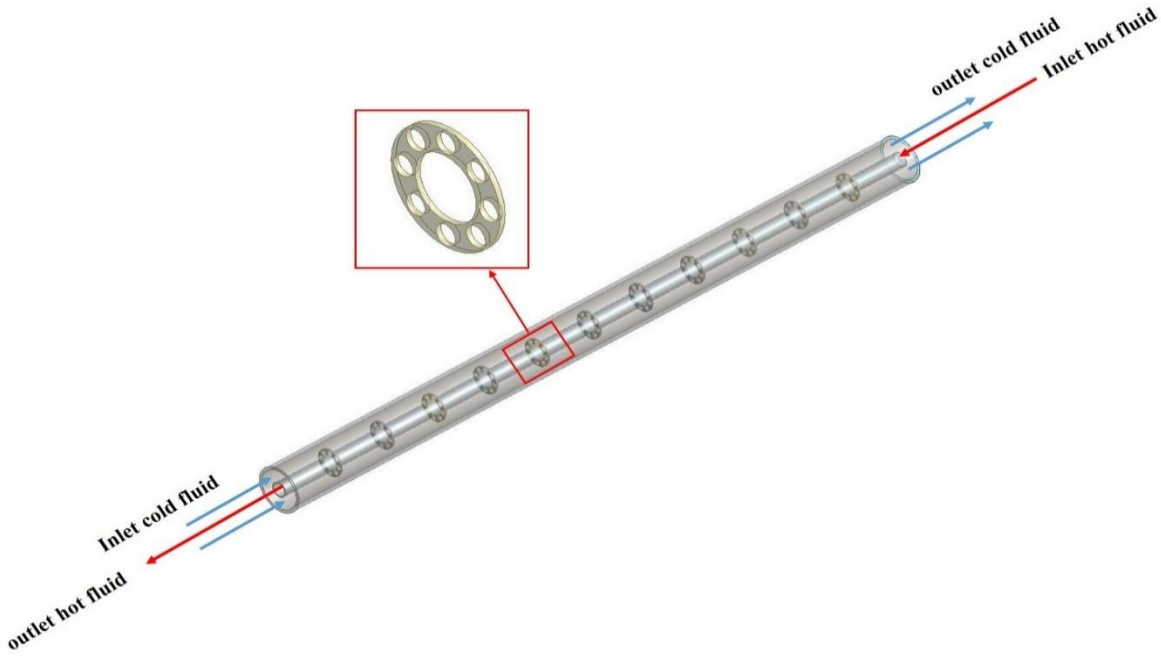

Figure 3.13 3D model of double tube heat exchanger with PCR inserts.

The rings are made of copper and have a thickness t=2 mm, an inner diameter dr_i=25.4 mm and an outer diameter Dr_o that varies between 35.4, 45.4, and 55.4 mm. The pitch length (P) vales studied are 100 and 200 mm, and the pitch ratio (PR) values change from 2.82, 2.2 and 1.8 when the number of rings (n) is 11 to

5.64, 4.4 and 3.61 when the number of rings is 5. Figure 3.14 shows a depiction of typical circular rings fitted on the inner tube

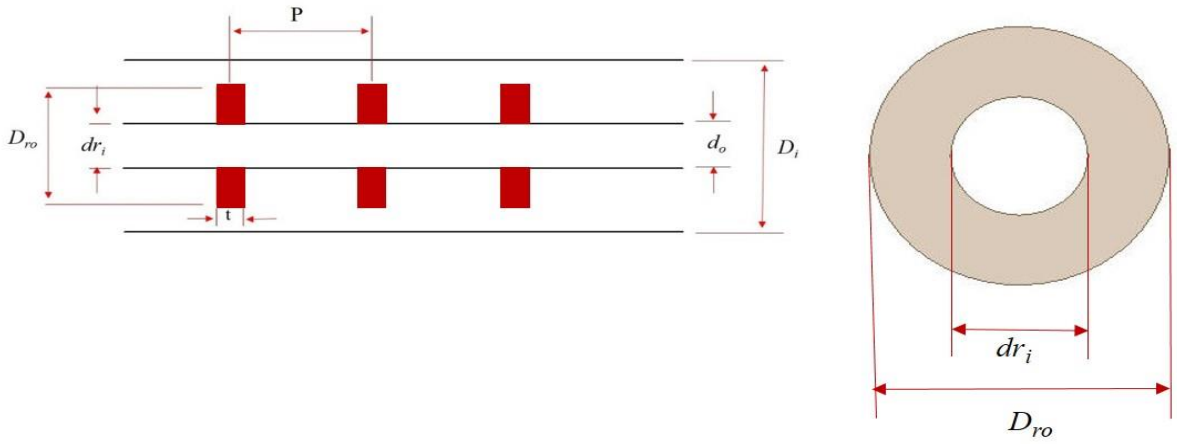

Figure 3.14 Schematic of typical circular ring (TCR).

For addressing the effect of the number of holes in the perforated rings, the configuration with a pitch ratio equal 2.2 and 11 rings was chosen to be perforated with N = 4 and 8 holes of a diameter D_r=6mm, as shown in figure 3.15.

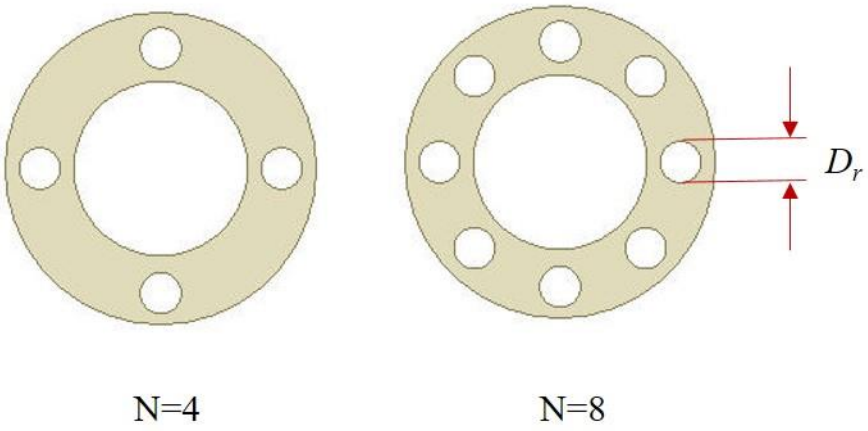

Figure 3.15 Effect of number of hole.

3.7.2 Mesh Generation

The mesh was generated using a combination of hexahedral and tetrahedral cells, as shown in figure 3.16. Mesh sensitivity tests were performed using water as the working fluid at a Reynolds number Re_{cf} = 2473, with no rotation of the inner tube and without circular rings. The number of transfer units (NTU) and pressure drop

were used as the parameters for verifying grid independence. The grid with 3,604,873 cells, with a deviation of around 0.98 % for the NTU, was estimated to be accurate enough for the purposes of this study. The results from the grid independence study are shown in Figure 3.17.

The simulation setup and parameters are the same as for the previous 3D model; hence, for the sake of brevity, they will not be repeated here. Figure 3.18 shows the methodology followed to develop this final 3D model.

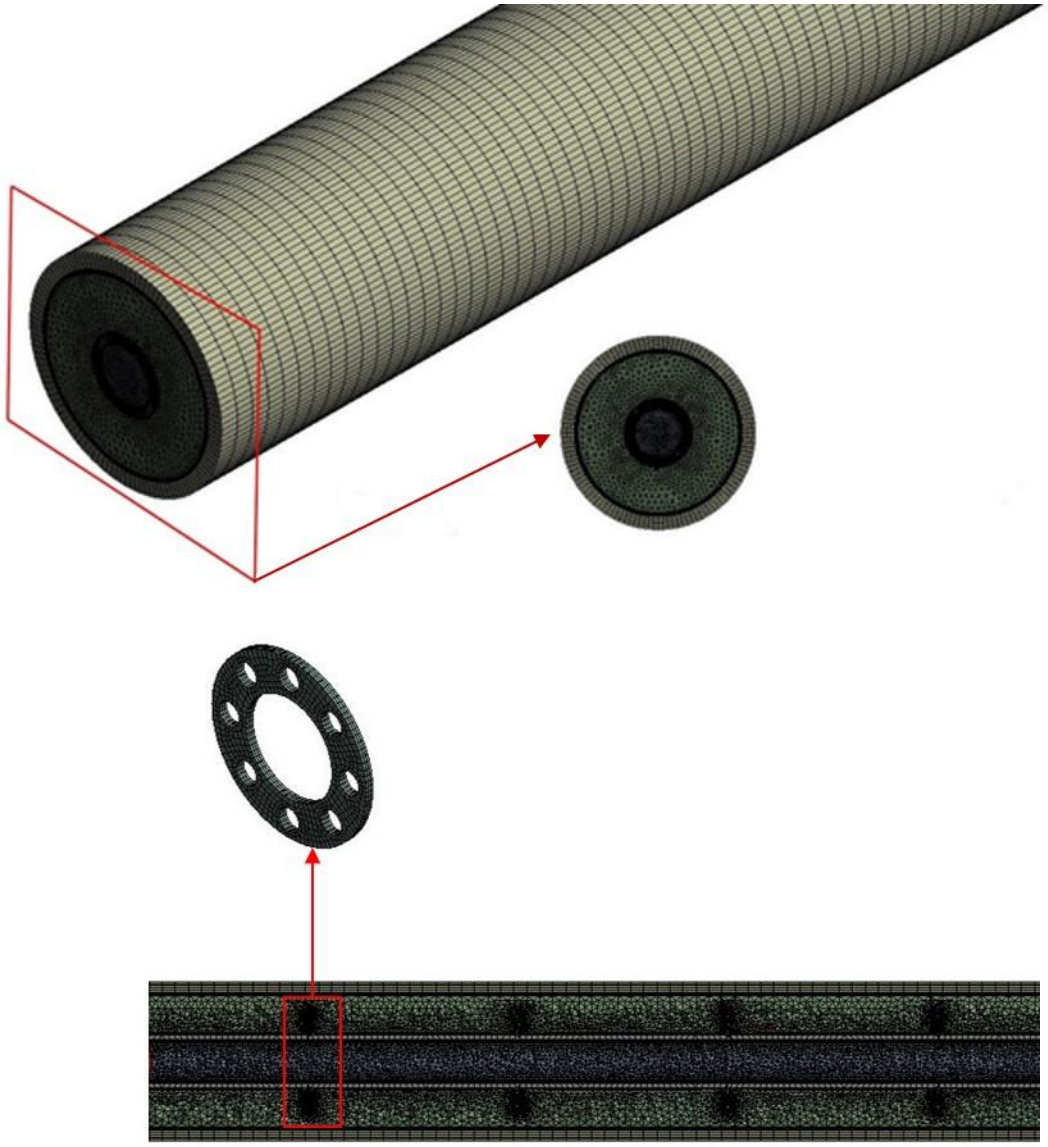

Figure 3.16 Grids for the computation domain of double tube with PCR inserts.

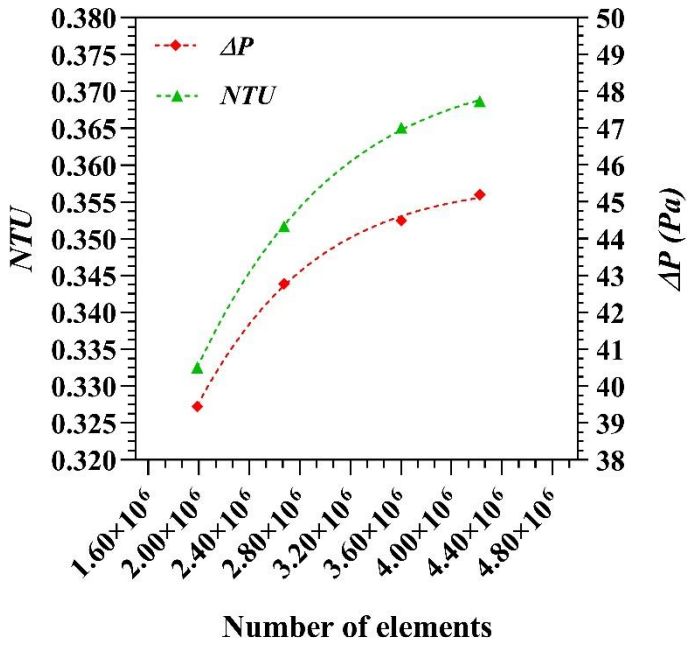

Figure 3.17 Number of cells study at Re_{cf} = 2473

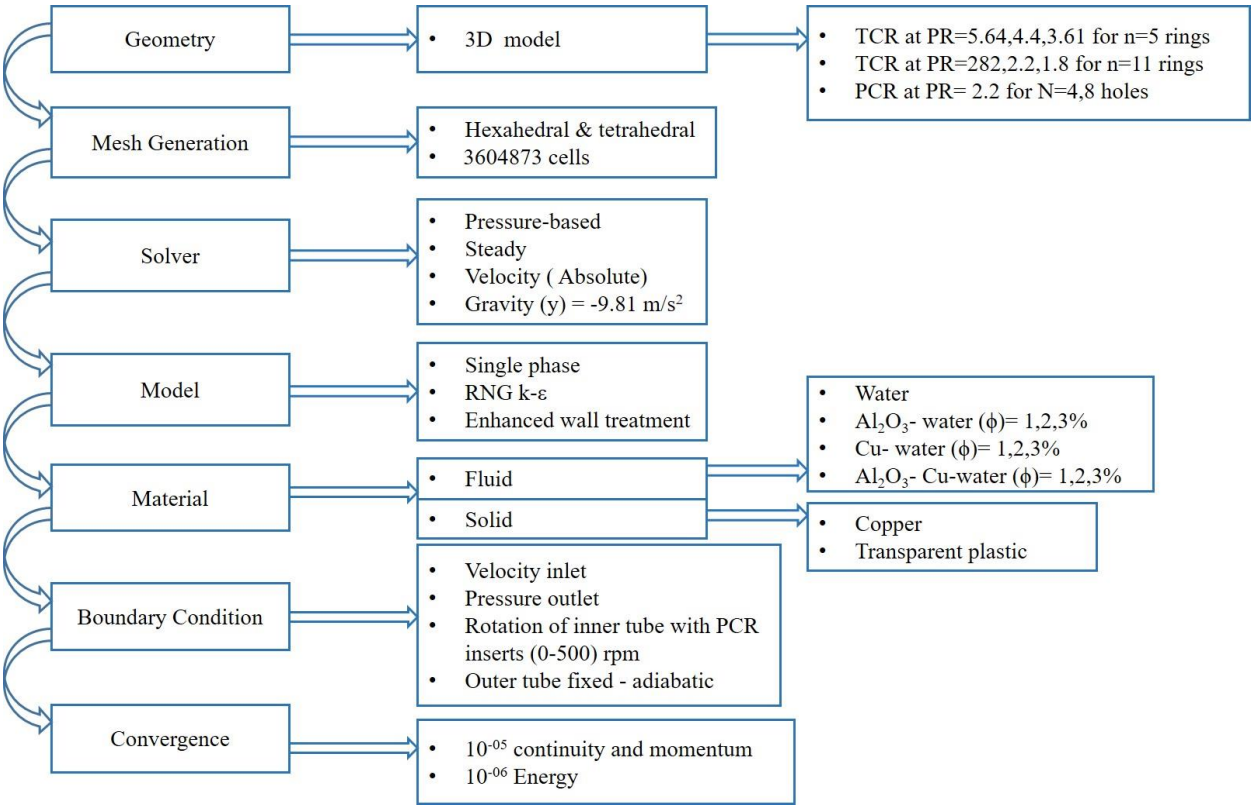

Figure 3.18 Steps of numerical simulation for 3D model with PCR inserts.

CHAPTER FOUR

RESULTS AND DISCUSSION

Chapter Four - Results and Discussion

4.1 2D axisymmetric numerical model

The 2D axisymmetric numerical model was used to study the behavior of the exchanger at the following cold fluid Reynolds numbers: 2473, 3092, 3712, 4331, and 4946. These numbers were estimated from the properties of water and the different Cu-water, Al_2O_3-water, and Al_2O_3-Cu-water nanofluids used at concentration values of 1, 2 and 3%. Hot water flows through the inner tube at a constant Reynolds number of 9780. These allowed to study the influence of the cold fluid Reynolds number and nanoparticle concentration in the heat exchanger performance.

4.1.1 Heat Transfer Rate

The effect of the Reynolds number and the addition of nanoparticles in the average heat transfer rate of the exchanger, calculated from Equation (3.3), may be observed in Figure 4.1. It may be appreciated that a higher Reynolds number leads to higher average heat transfer rates, due to the increased fluid convection.

The addition of nanoparticles seems to improve the thermal properties of the base fluid, as shown by its positive effect in the heat transfer rate. At Re_{cf}=2,473, for the Al_2O_3–water nanofluid, the average heat transfer rate (Q_{avg}) is improved by 1.26, 2.16 and 6.19% at 1, 2 and 3 % nanoparticle concentrations, with maximum improvements of 2.21, 3.79 and 7.6 % at Re_{cf} =4,946, as shown in Figure 4.1(a). Figure 4.1(b) depicts the results for the Al_2O_3-Cu-water nanofluid at 1, 2 and 3% nanoparticle concentrations. At Re_{cf}=2,473, heat transfer rate is improved by 1.75, 3.58 and 7.2%, whereas, at Re_{cf}=4,946, maximum improvements of 2.85, 5.63 and 10.40 % are reached. The results for Cu-water nanofluids are shown in Figure 4.1.(c). At Re_{cf} = 2,473, the addition of nanoparticles to 1,2 and 3 % concentrations increases average heat transfer rate by 2.2, 5.85 and 10.35 % respectively.

In general, in comparison to pure water, average heat transfer rate for the Al_2O_3-water, Al_2O_3-Cu-water and Al_2O_3-water nanofluids increases with increasing volume concentrations and Reynolds numbers (Re_{cf}). The Cu-water nanofluid shows the highest heat transfer rate when nanoparticles are added to 3 % concentration. The

increase in the fluid density and viscosity leads to higher pressure drops in the heat exchanger but improves substantially heat transfer.

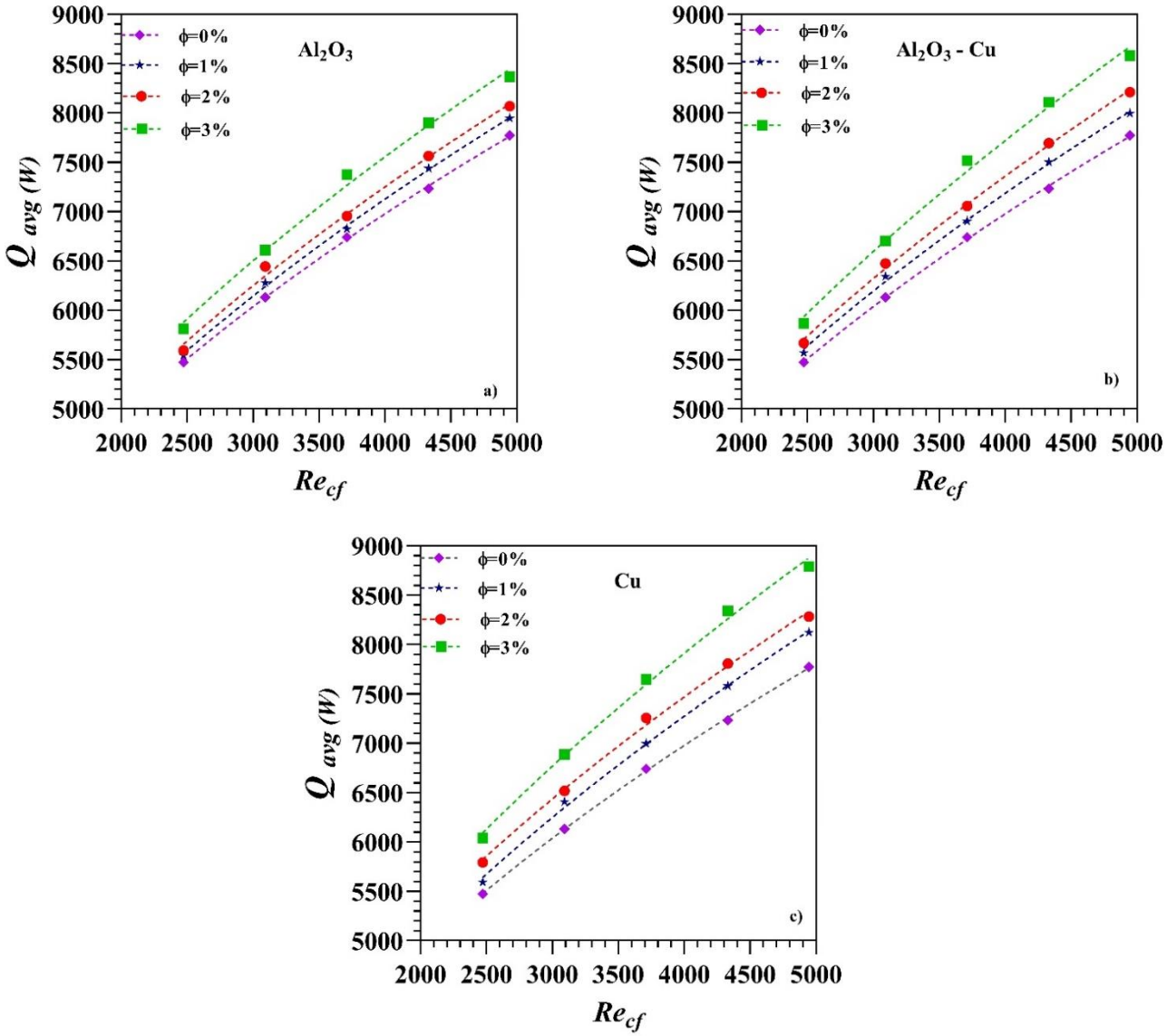

Figure 4.1 Average heat transfer rate variation for different types of nanofluids.

Figure 4.2 shows the temperature contours for water, Al_2O_3, Al_2O_3-Cu hybrid and Cu at the different concentrations studied for the cold fluid Reynolds numbers of 2,473 and 4,946. It may be observed that smoother temperature contours are related to better heat exchanger performance and higher heat transfer rates.

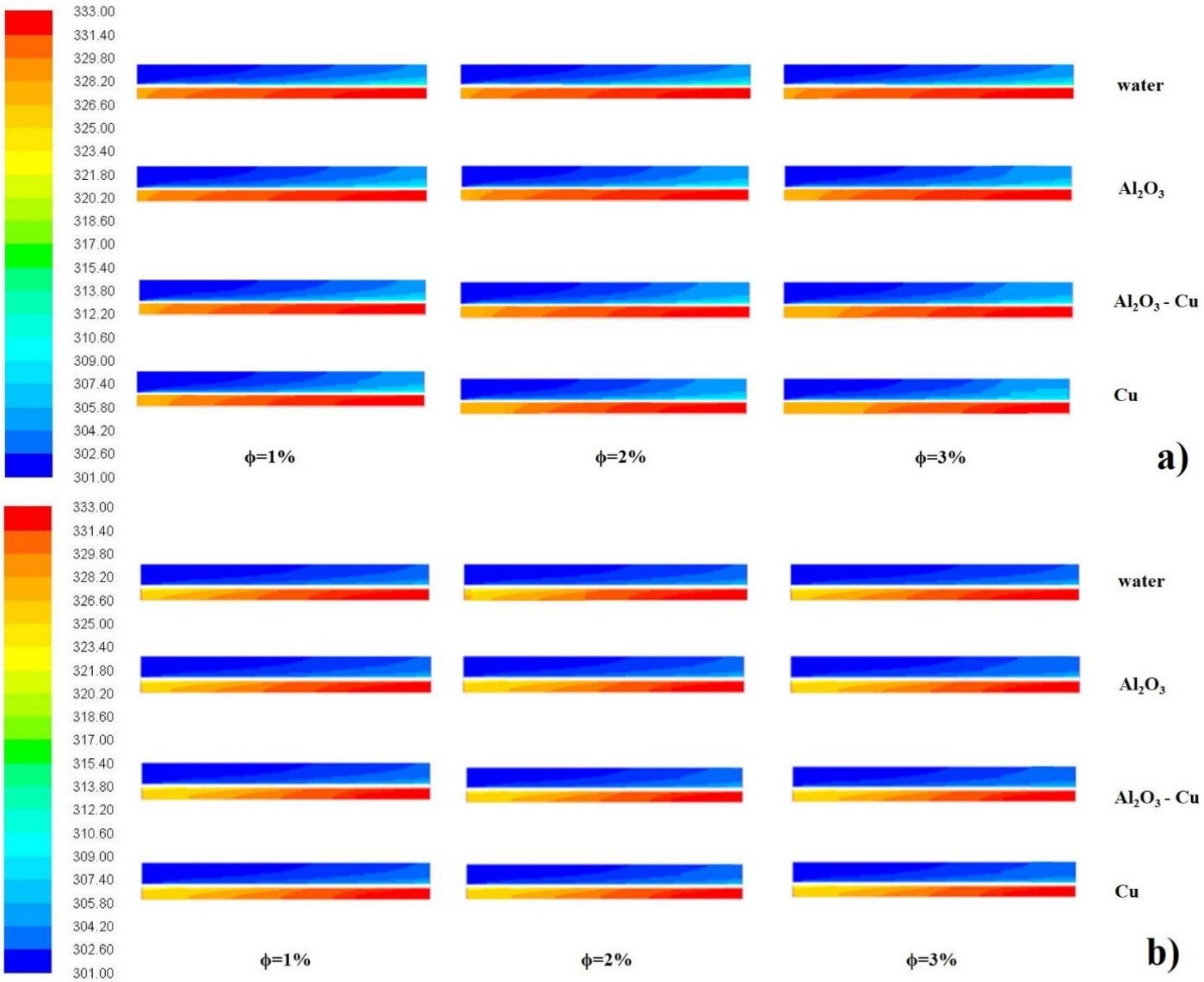

Figure 4.2 Temperature contour of 2D Axisymmetric (a) at Re_{cf} =2473, (b) at Re_{cf} =4946.

4.1.2 Number of Transfer Unit (NTU)

The number of transfer units (NTU) was calculated with the simulation results by using Equation (3.6). Figure 4.3 shows NTU values as a function of the nanofluid Reynolds number for different nanoparticle concentrations. It may be appreciated that increasing the Reynolds number improves NTU values. In addition, increasing the nanoparticle concentration leads to higher heat transfer values and a higher exchanger efficiency.

Comparing the different nanofluids, Cu-water nanofluids perform better than Al_2O_3-Cu hybrid nanofluids and Al_2O_3-water nanofluids, which has the lowest performance. In Figure 4.3 (a), the results for nanofluids at 1% concentration are shown. At Re_{cf}=2,473, NTU improves by around 1.72, 2.35 and 2.95 % for Al_2O_3-water, Al_2O_3-Cu-water and Cu-water nanofluids with respect to pure water. This improvement becomes higher at Re_{cf} = 4,946: 3.06, 3.94 and 6.2 %. At 2% concentration, as shown in Figure 4.3 (b), NTU increases at Re_{cf}=2,473 by 3, 4.84 and 7.9% for Al_2O_3-water, Al_2O_3-Cu-water and Cu-water nanofluids respectively, being these increases of 5.31, 7.78 and 9.07 % at Re_{cf} = 4946. Finally, at 3% concentration values, as depicted in Figure 4.3 (c), the NTU values increase by 8.44 %(Al_2O_3-water), 9.82 % (Al_2O_3-Cu-water) and 14.16 % (Cu-water) when compared to pure water at Re_{cf} = 2473. Maximum improvements of 10.72, 14.81, and 18.80 %, respectively, are reached at Re_{cf} = 4946.

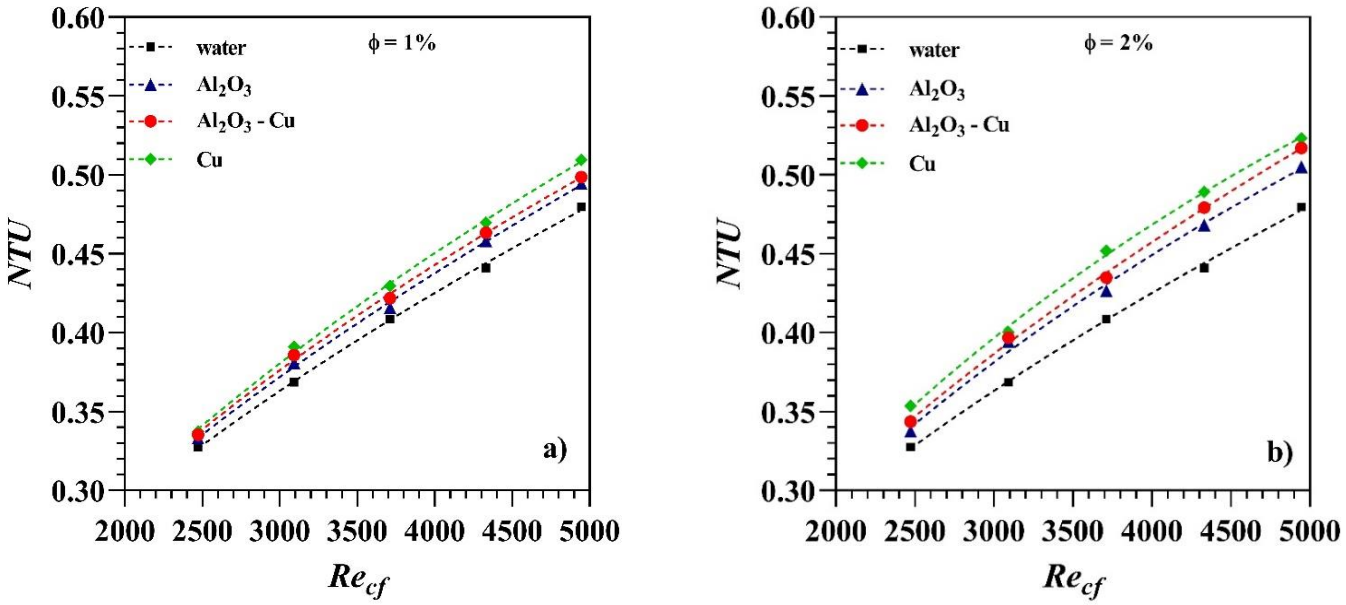

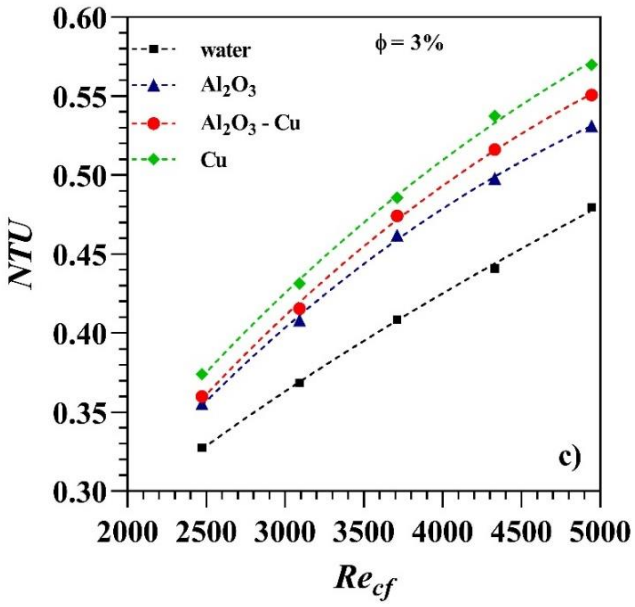

Figure 4.3 Effect of volume concentration on NTU.

4.1.3 Effectiveness (ε)

Figure 4.4 shows the heat exchanger effectiveness values as a function of the cold fluid Reynolds number, calculated with Equation (3.8). The addition of nanofluids improves effectiveness, in line with the previous results for heat transfer and NTU values. The results for 1%, 2% and 3% concentration values are shown in Figures 4.4 (a), (b) and (c) respectively. At Re_{cf}=2,473, effectiveness is increased by 1.26, 1.75 and 2.2 % when adding Al_2O_3, Al_2O_3-Cu and Cu nanoparticles at 1% concentration. If the Reynolds number is increased to Re_{cf} = 4,946, the increase becomes 2.21, 2.84 and 4.46%. If the nanoparticle concentration is raised to 2%, at Re_{cf} =2473, the increase becomes 2.16, 3.58 and 5.85 %, increasing further with a Reynolds number of 4,946 by 3.79, 5.55 and 6.46 %. The maximum effectiveness values are reached with 3% nanoparticle concentrations, as shown in Figure 4.4 (c). Maximum improvements of 6.19 % for Al_2O_3-water, 7.2 % for Al_2O_3-Cu-water and 10.33 % for Cu-water are achieved at Re_{cf} = 2,473, whereas effectiveness increases by 7.57, 10.37 and 13.06 % at Re_{cf} = 4,946 with respect to pure water. Cu-water nanofluids present again the best performance in terms of effectiveness enhancement.

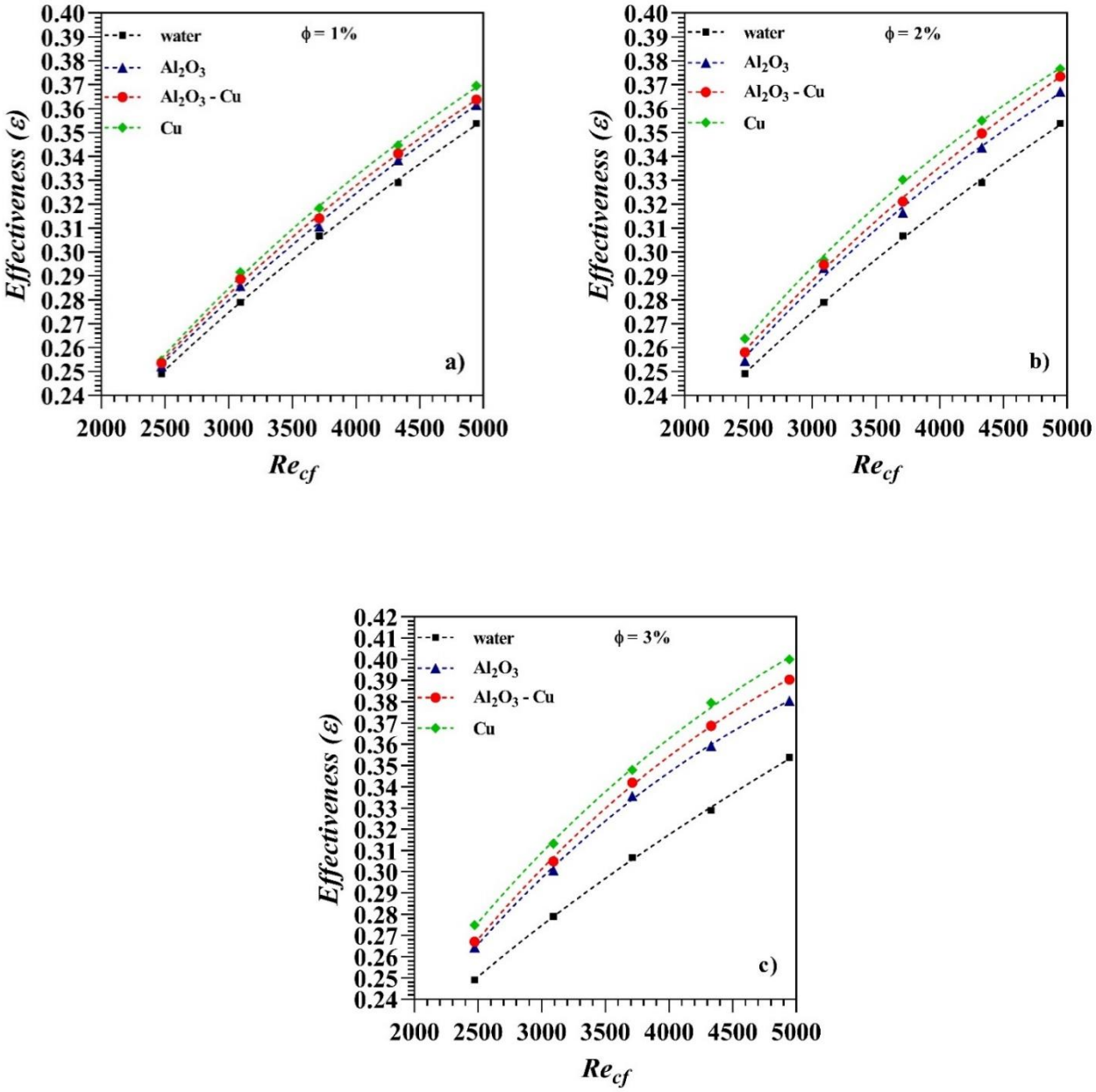

Figure 4.4 Effect of nanoparticles volume concentration on Effectiveness (ε)

4.1.4 Pressure Drop

The addition of nanoparticles generates an additional pressure drop, which should be kept as low, as it leads to higher pumping requirements. This pressure drop must be considered in heat exchanger design to minimize energy consumption by the exchanger.

Figure 4.5 depicts the pressure drop (ΔP) in the exchanger when nanoparticles are added at different concentrations and at various Reynolds numbers. The results indicate that the pressure drop increases with the Reynolds number due to the increase in fluid velocity, as well as with the concentration of nanoparticles, due to the influence of the nanofluid density and viscosity. For Al_2O_3-water nanofluids, Figure 4.5 (a) shows that the pressure drop increases by 5.45, 6.56 and 25.3 % at volume concentrations of 1, 2 and 3% and at Re_{cf} =2,473. When the Reynolds number is increased to Re_{cf} =4,946, these values increase by 3.7, 9.28 and 27.1 % at. The results for of Al_2O_3-Cu-water nanofluids are shown in Figure 4.5 (b). The pressure drop increases by 6.42, 10 and 28 % for the three different concentrations at Re_{cf} =2,473. At Re_{cf} =4,946, these increases become 4.3, 13.18 and 31.76 %. Finally, Figure 4.5 (c) depicts the maximum increases in the pressure drop of the Cu-water nanofluids. At Re_{cf} =2,473 these increases are 6.77, 14.96 and 30.75% for 1, 2 and 3% nanoparticle concentration. At a higher Reynolds number, Re_{cf} =4,946, the increases become 4.78, 18.1 and 37.26%.

To provide a picture of the pressure field inside the exchanger, Figure 4.6 shows the pressure contours for water, Al_2O_3, Al_2O_3-Cu hybrid and Cu at the three different volume concentration values studied and at two different Reynolds numbers, 2,473 and 4,946. No significant differences are evident, just a slight increase in pressure drop between the inlet and outlet with the addition of nanoparticles, so it could be assumed that the addition of nanoparticles is not going to result in much higher pumping requirements. Cu-water nanofluids show the highest increases in pressure drop, but it was commented that these fluids were the ones with the highest thermal performance, so they are still considered as the best option for improving the heat exchanger performance.

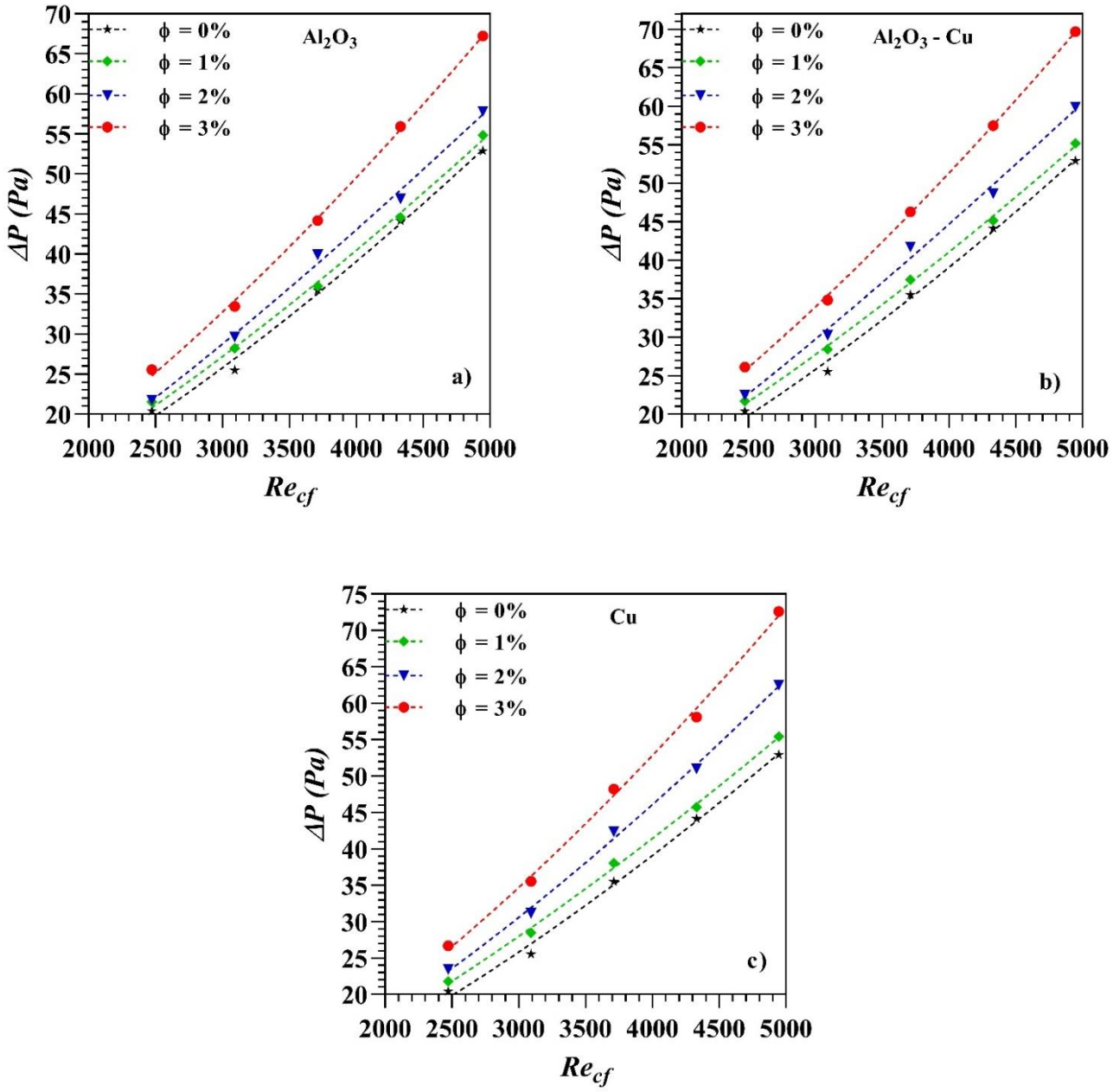

Figure 4.5 Pressure drop variation with nanofluids

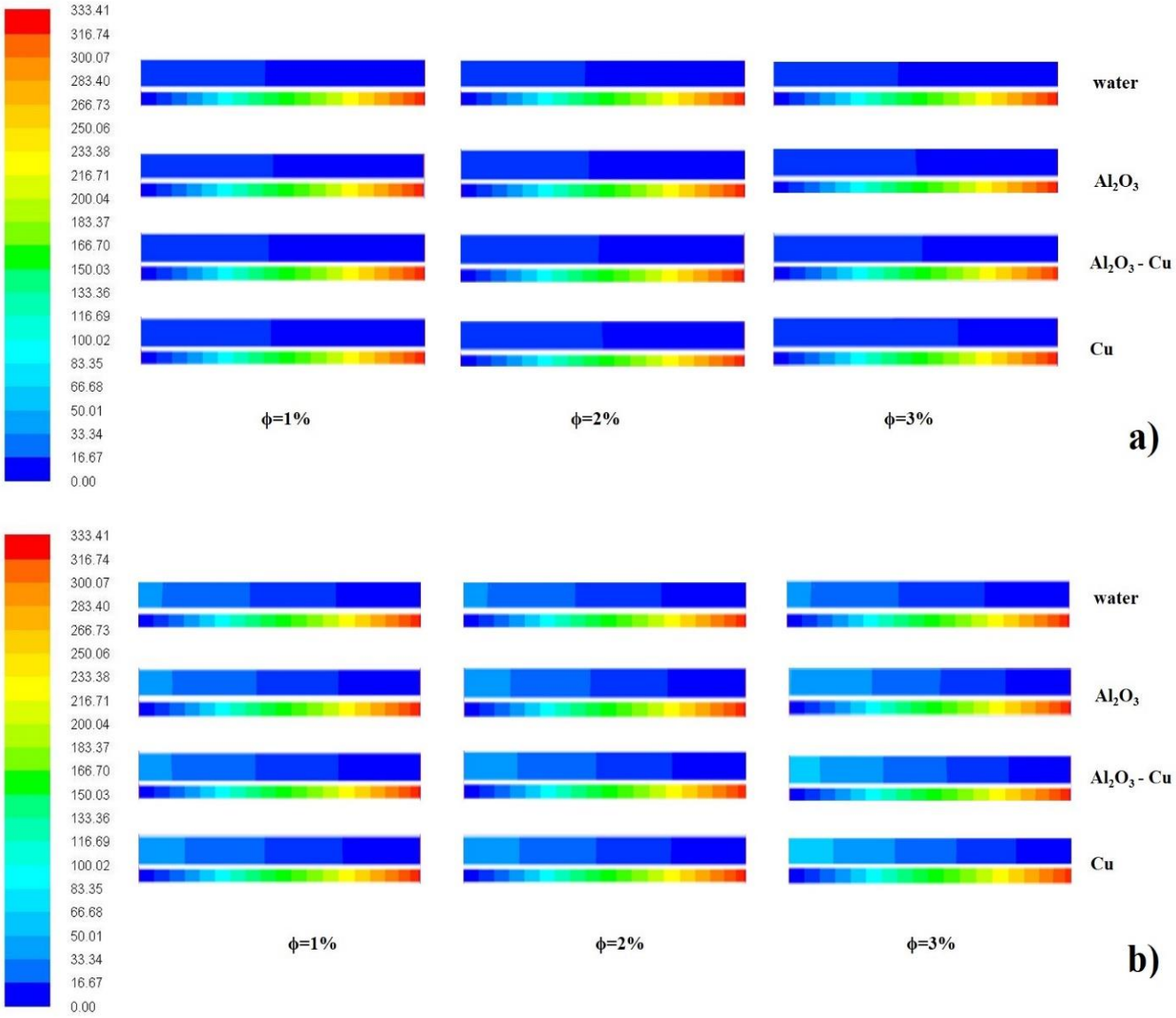

Figure 4.6 Pressure contour of 2D Axisymmetric (a) at Re_{cf} =2473, (b) at Re_{cf} =4946.

4.2. 3D numerical model of the double-tube heat exchanger

After analyzing the results from the 2D axisymmetric numerical model, the 3D model was used to study the behavior of the exchanger at the same cold fluid Reynolds

numbers: 2473, 3092, 3712, 4331, and 4946. Water and Cu-water, Al_2O_3-water, and Al_2O_3-Cu-water nanofluids were studied at nanoparticle concentration values of 1, 2 and 3%. Hot water flows through the inner tube at a constant Reynolds number of 9780. Additionally, the inner tube was rotated at speeds from 0 to 500 rpm in 100 rpm intervals to study the effect of inner tube rotation.

4.2.1 Heat transfer rate

The increase in nanoparticle concentration and rotational speed resulted in higher heat transfer values, increasing the heat exchanger efficiency for all the studied cases. There is a significant positive effect of increasing the rotational speed in convection heat transfer, which may be attributed to the swirling flow that arises and is enhanced as the rotational speed increases.

Figure 4.7 shows the effects of varying the rotational speed in the average heat transfer rate of the exchanger, as a function of the Reynolds number, for different nanofluids and nanoparticle concentrations. In Figure 4.7 (a), the results for rotating the inner tube with plain water are presented. At the lowest Reynolds number, Re_{cf} =2,473, the increase in average heat transfer ranges from 3.07% at 100 rpm to 28.47% at 500 rpm. At the highest Reynolds number, Re_{cf} =4,946, the increase becomes slightly lower, ranging from 2.91% at 100 rpm to 23.38% at 500 rpm.

Figure 4.7 (b-d) shows the results for Al_2O_3-water nanofluids. With the inner tube quiescent, increasing nanoparticle concentration to 1, 2 and 3% produces an enhancement of the heat transfer rate of 3.69, 4.58 and 8.7% respectively at a Reynolds number of Re_{cf} =4,946. When rotation is added to the nanfluid at 1% concentration at the lowest Reynolds number Re_{cf} =2,473, average heat transfer increases from 0.54% at 100 rpm to 28.72% at 500 rpm. Likewise, at Re_{cf} =4,946, the increase is from 3.68% at 100 rpm to 24% at 500 rpm. For 2% volume concentration and Re_{cf} =4,946, average heat transfer increased by 4.58% at 100 rpm and 26.64% at 500 rpm. However, maximum improvement with the Al_2O_3-water nanofluid was found at 3% volume concentration, with increase values from 8.77% at 100 rpm to 30.46% at 500 rpm.

Average heat transfer rates for Al_2O_3-Cu-water nanofluids at different concentrations and rotational speeds are shown in Figure 4.7 (e-g). At Re_{cf} =4,946, heat transfer improved in ranges between 3.96 and 27.88% for rotational speeds from 100 to 500

rpm and 1% nanoparticle volume concentration; between 5.16 and 28.42% for 2% nanoparticle concentration, and between 10.77 to 35.86% for 3% nanoparticle concentration.

Finally, average heat transfer rates for Cu-water nanofluids are depicted in Figure 4.7 (h-j). At Re_{cf} =4,946, average heat transfer rates improved between 5.21and 29.87% for 1% volume concentration; between 7.05 and 34.99 % for 2% volume concentration and between 13.44 and 41.24% for 3% volume concentration. The maximum improvement in heat transfer was found with the Cu-water nanofluid at 3% nanoparticle concentration and the inner tube rotational speed of 500 rpm.

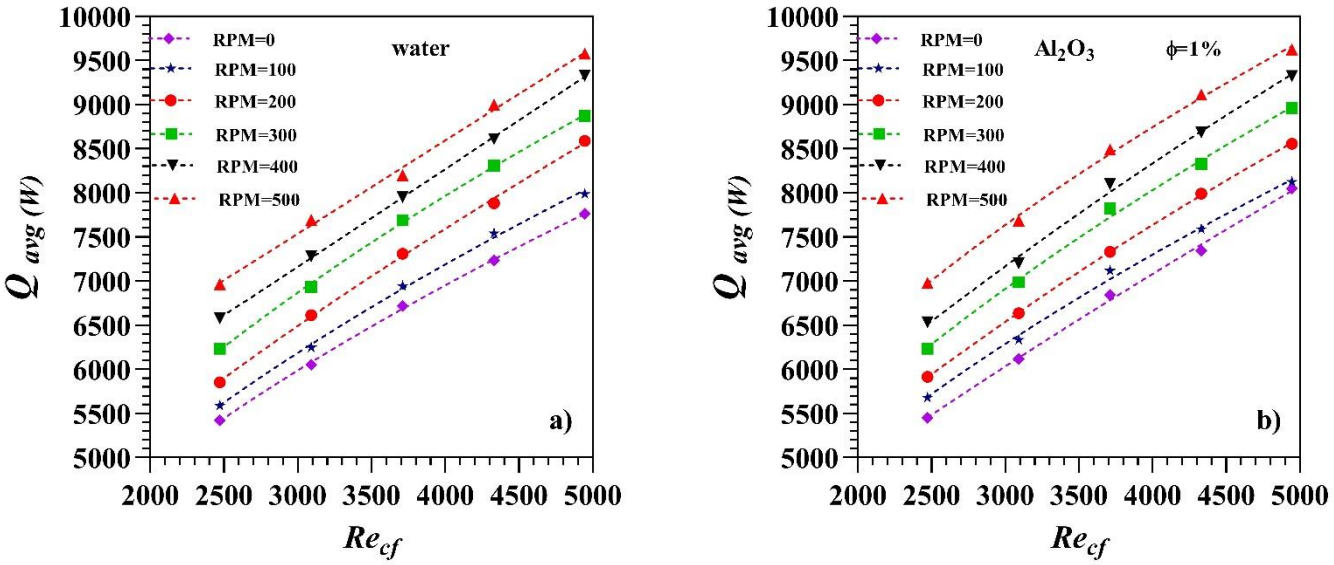

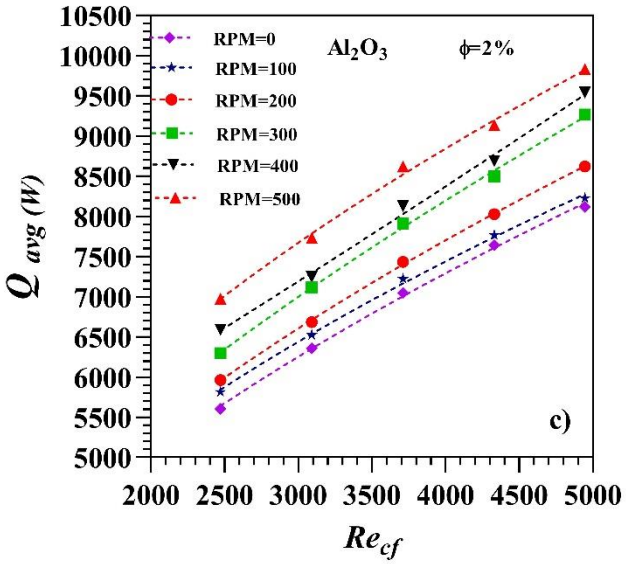
RPM=0
RPM=100
RPM=200
RPM=300
RPM=400
RPM=500
Al2O3
ϕ=2%
c)
Q avg (W)
Recf

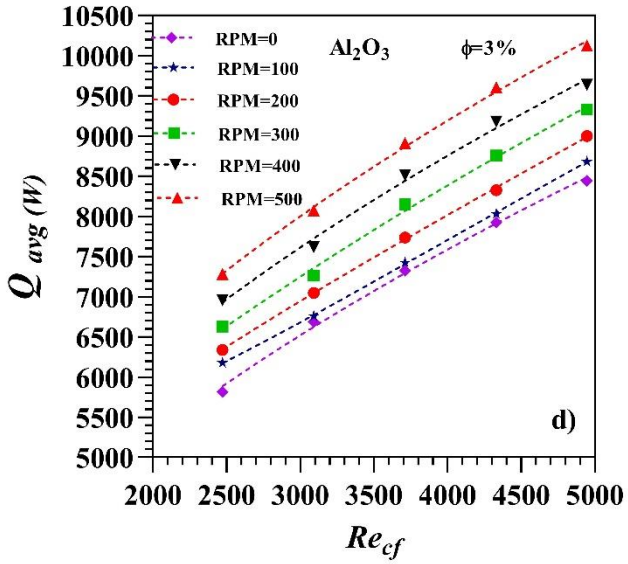
RPM=0
RPM=100
RPM=200
RPM=300
RPM=400
RPM=500
Al2O3
ϕ=3%
d)
Q avg (W)
Recf

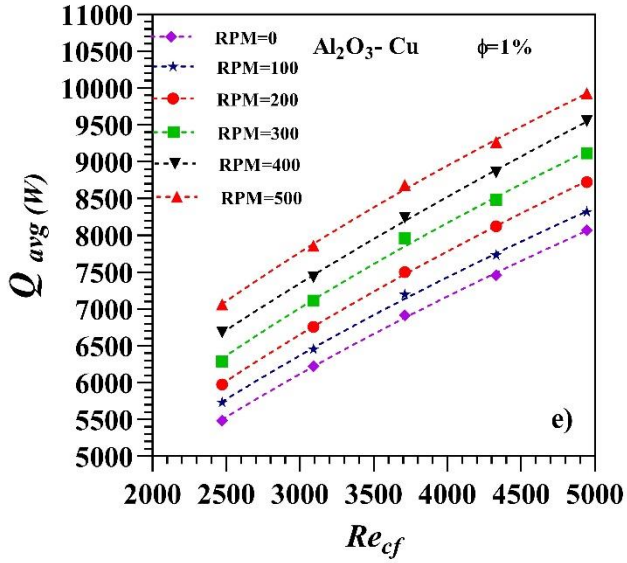
RPM=0
RPM=100
RPM=200
RPM=300
RPM=400
RPM=500
Al2O3- Cu
ϕ=1%
e)
Q avg (W)
Recf

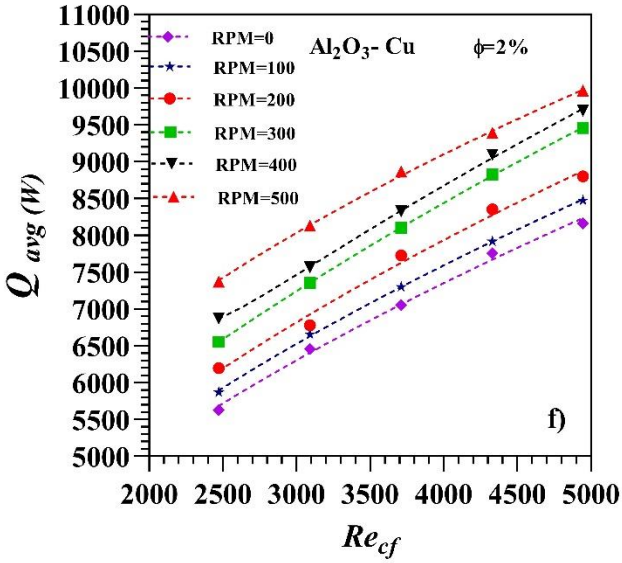
RPM=0
RPM=100
RPM=200
RPM=300
RPM=400
RPM=500
Al2O3- Cu
ϕ=2%
f)
Q avg (W)
Recf

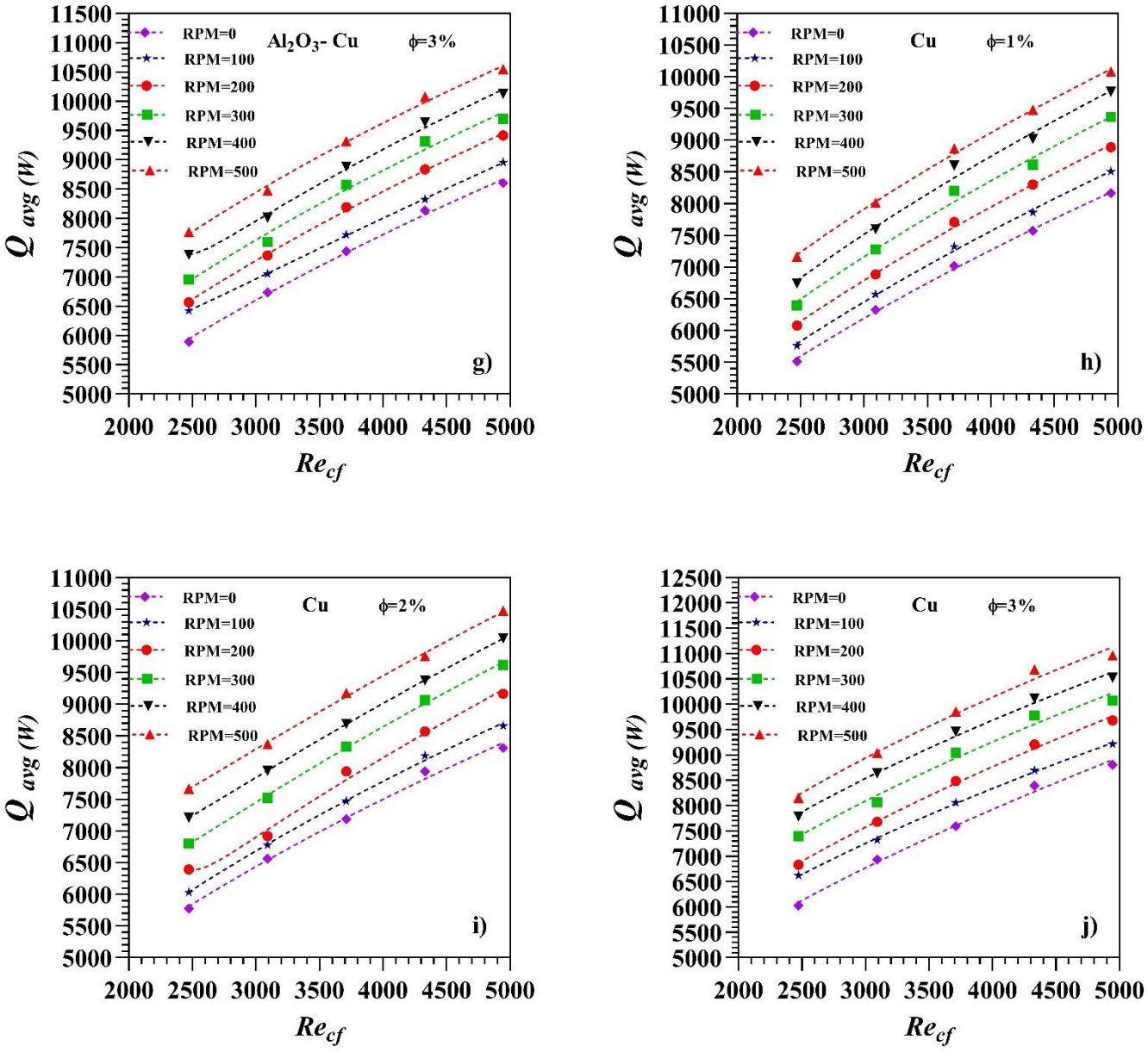

Figure 4.7 Average heat transfer rate variation with rotational speed.

The temperature contours in a plane coincident with the longitudinal axis of the exchanger are shown in Figure 4.8 for water and the studied nanofluids at different concentrations, inner tube rotational speeds and the Reynolds numbers of 2,473 and 4,946. The effect of increasing the nanoparticle concentration and the rotational speed of the inner tube becomes apparent, as the temperature contour become smoother, probably due to the higher heat transfer values.

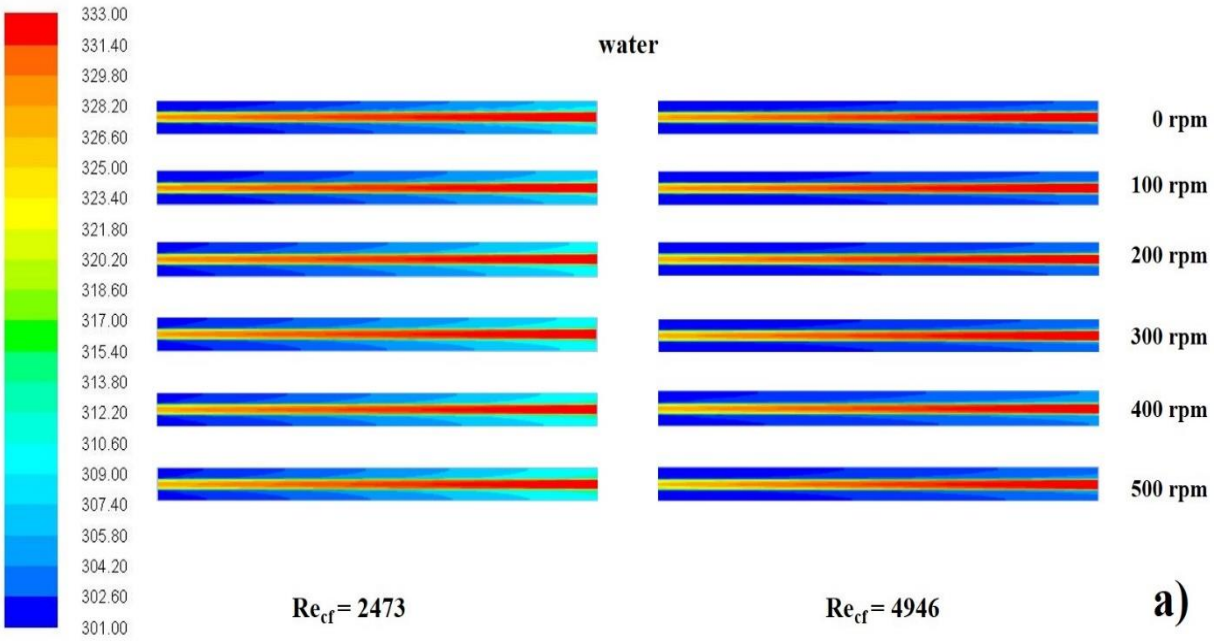
333.00
331.40
329.80
328.20
326.60
325.00
323.40
321.80
320.20
318.60
317.00
315.40
313.80
312.20
310.60
309.00
307.40
305.80
304.20
302.60
301.00
water
0 rpm
100 rpm
200 rpm
300 rpm
400 rpm
500 rpm
Re_cf = 2473
Re_cf = 4946
a)

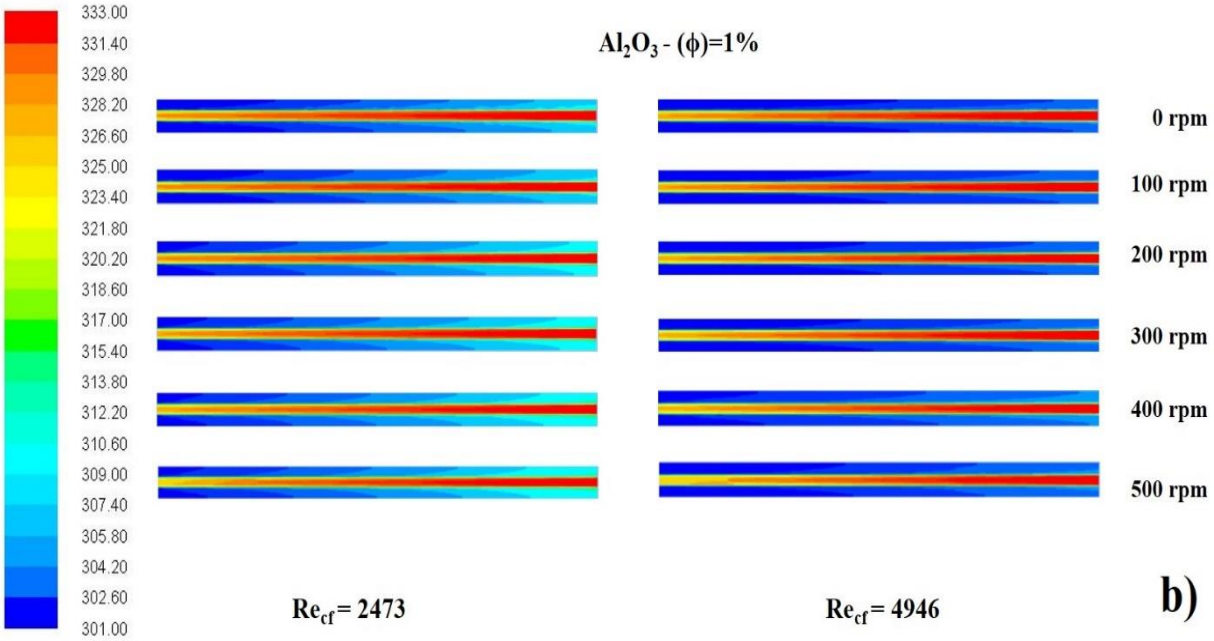
333.00
331.40
329.80
328.20
326.60
325.00
323.40
321.80
320.20
318.60
317.00
315.40
313.80
312.20
310.60
309.00
307.40
305.80
304.20
302.60
301.00
Al2O3 - (ϕ)=1%
0 rpm
100 rpm
200 rpm
300 rpm
400 rpm
500 rpm
Re_cf = 2473
Re_cf = 4946
b)

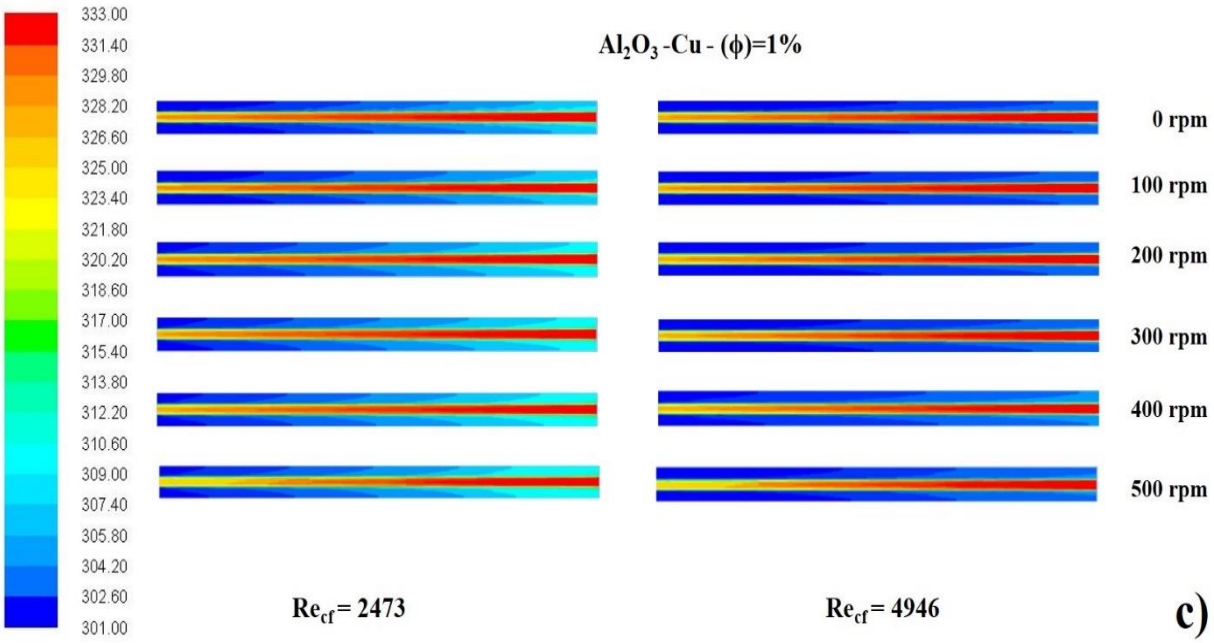
333.00
331.40
329.80
328.20
326.60
325.00
323.40
321.80
320.20
318.60
317.00
315.40
313.80
312.20
310.60
309.00
307.40
305.80
304.20
302.60
301.00
Al2O3 -Cu - (ϕ)=1%
0 rpm
100 rpm
200 rpm
300 rpm
400 rpm
500 rpm
Recf = 2473
Recf = 4946
c)

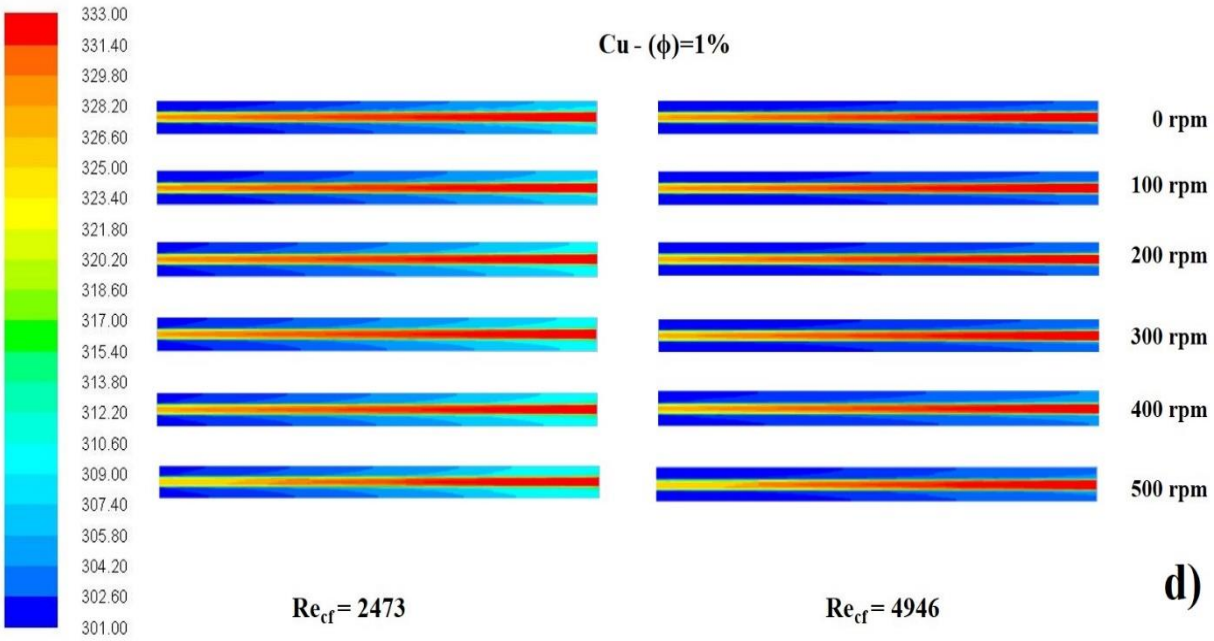
333.00
331.40
329.80
328.20
326.60
325.00
323.40
321.80
320.20
318.60
317.00
315.40
313.80
312.20
310.60
309.00
307.40
305.80
304.20
302.60
301.00
Cu - (ϕ)=1%
0 rpm
100 rpm
200 rpm
300 rpm
400 rpm
500 rpm
Recf = 2473
Recf = 4946
d)

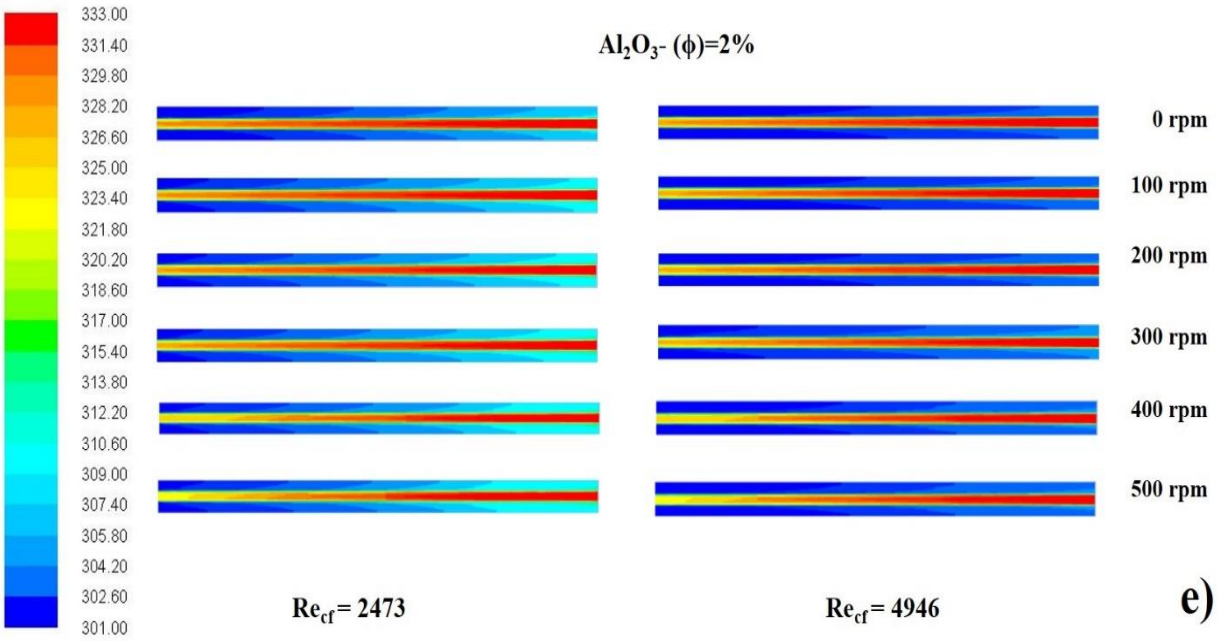
333.00
331.40
329.80
328.20
326.60
325.00
323.40
321.80
320.20
318.60
317.00
315.40
313.80
312.20
310.60
309.00
307.40
305.80
304.20
302.60
301.00
Al2O3- (ϕ)=2%
0 rpm
100 rpm
200 rpm
300 rpm
400 rpm
500 rpm
Recf= 2473
Recf= 4946
e)

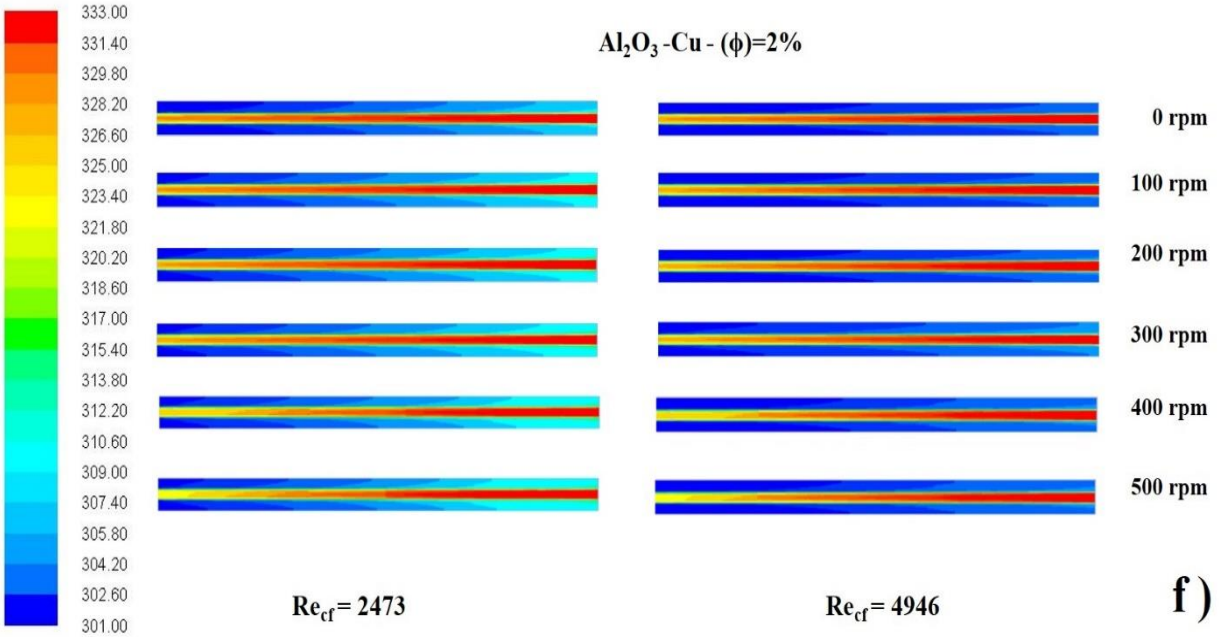
333.00
331.40
329.80
328.20
326.60
325.00
323.40
321.80
320.20
318.60
317.00
315.40
313.80
312.20
310.60
309.00
307.40
305.80
304.20
302.60
301.00
Al2O3 -Cu - (ϕ)=2%
0 rpm
100 rpm
200 rpm
300 rpm
400 rpm
500 rpm
Recf= 2473
Recf= 4946
f)

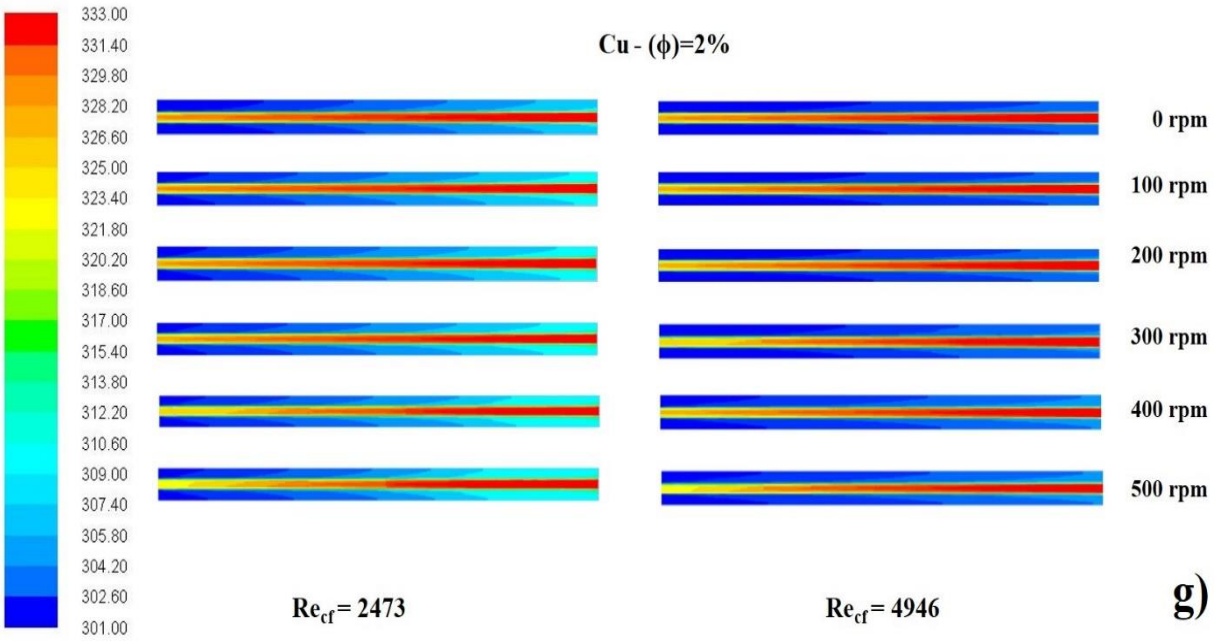
333.00
331.40
329.80
328.20
326.60
325.00
323.40
321.80
320.20
318.60
317.00
315.40
313.80
312.20
310.60
309.00
307.40
305.80
304.20
302.60
301.00
Cu - (ϕ)=2%
0 rpm
100 rpm
200 rpm
300 rpm
400 rpm
500 rpm
Re_cf = 2473
Re_cf = 4946
g)

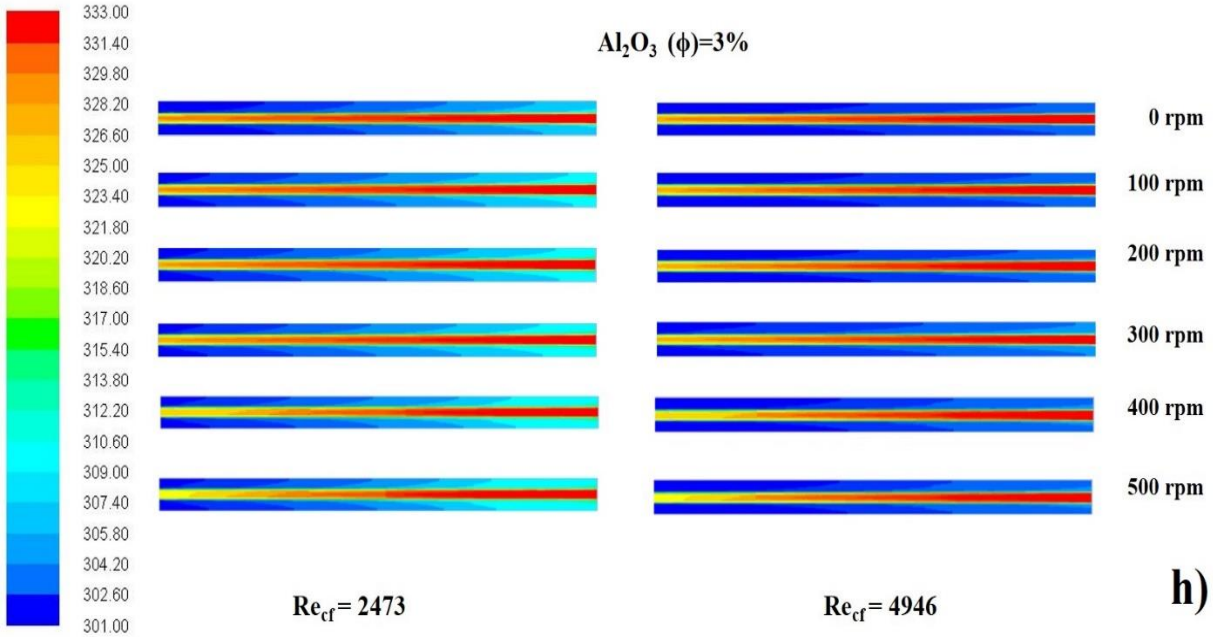
333.00
331.40
329.80
328.20
326.60
325.00
323.40
321.80
320.20
318.60
317.00
315.40
313.80
312.20
310.60
309.00
307.40
305.80
304.20
302.60
301.00
Al2O3 (ϕ)=3%
0 rpm
100 rpm
200 rpm
300 rpm
400 rpm
500 rpm
Re_cf = 2473
Re_cf = 4946
h)

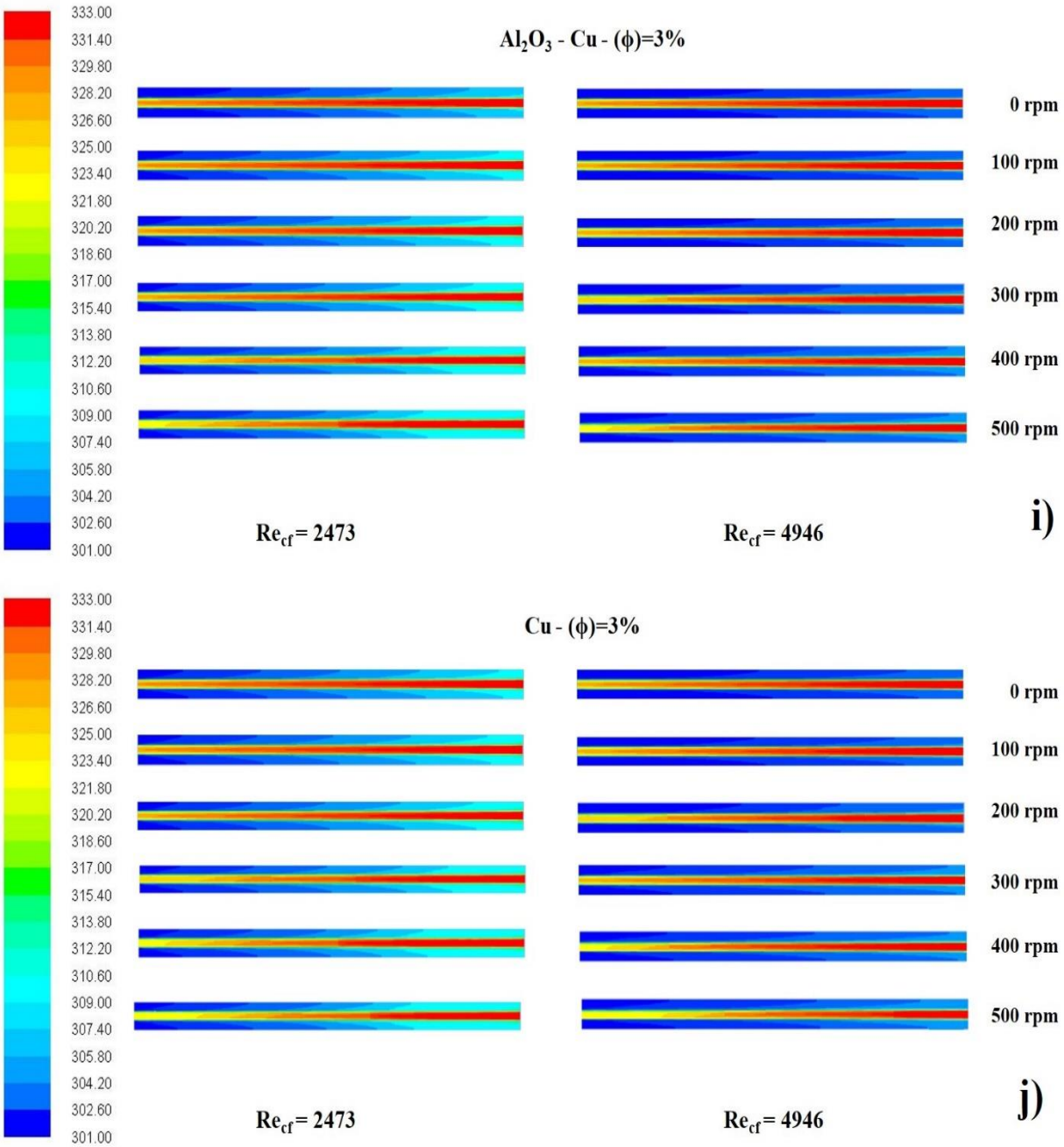

Figure 4.8 Temperature contours of 3D model (a) at Re_{cf} =2473, (b) at Re_{cf} =4946.

4.2.2 Number of Transfer Units (NTU)

Figure 4.9 depicts the number of transfer units (NTU) obtained from Equation (3.6) as a function of the Reynolds number and inner tube rotational speed for the different nanofluid types and concentrations. Higher Reynolds numbers and inner tube

rotational speed values led to an increase in the NTU values. Comparing the three nanofluid types, the Cu-water nanofluid has the best heat transfer behaviour, while the Al_2O_3-water nanofluid showed the less enhancement capability.

As shown in Figures 4.9 (a-d), at 1% volume concentration, NTU for the Al_2O_3-water nanofluid at Re_{cf}= 2,473 improved between 0.76 and 41.5% for inner tube rotational speeds from 0 to 500 rpm, when compared to pure water at 0 rpm. A similar improvement was seen at Re_{cf} = 4,946, with NTU increasing by values from 5.05 to 36 %. The behavior when adding Al_2O_3-Cu or Cu nanoparticles was analogous. For Al_2O_3-Cu-water nanofluids at 1% concentration, enhancements between 1.58 and 43.91% were found at Re_{cf}= 2,473, and between 5.45 and 42.62% at Re_{cf} = 4,946. For Cu-water nanofluids at 1% concentration, maximum improvement values from 7.25 to 46.18% were found at Re_{cf} = 4,946.

Results for nanofluids at 2% concentration are shown in Figures 4.9 (e-g). The enhancement of NTU values is apparent, obtaining improvements between 6.35 and 40.65% for Al_2O_3, between 7.22 and 43.51% for Al_2O_3-Cu, and between 9.75 and 55% for Cu, for inner tube rotational speeds from 0 to 500 rpm, when compared to pure water at 0 rpm.

Finally, Figures 4.9 (h-j) depict the results for 3% nanoparticle concentration, which provide the maximum NTU increase at Re_{cf} = 4,946. The improvement is between 12.41 to 47.31% for Al_2O_3, between 15.34 and 56.79% for Al_2O_3-Cu and between 19.33 to 66.75% for Cu, with respect to water at 0 rpm. It is confirmed again that the Cu-water nanofluid seems to have the best performance in terms of enhancing the heat transfer capability of the exchanger.

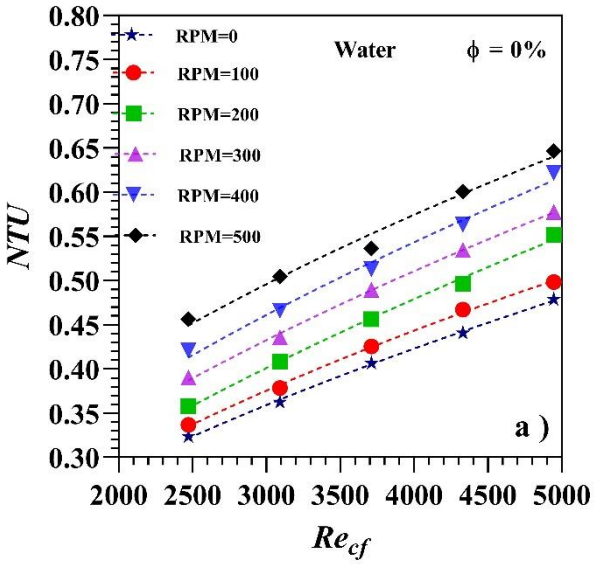
RPM=0
RPM=100
RPM=200
RPM=300
RPM=400
RPM=500
Water
ϕ = 0%
a)
NTU
Re_cf

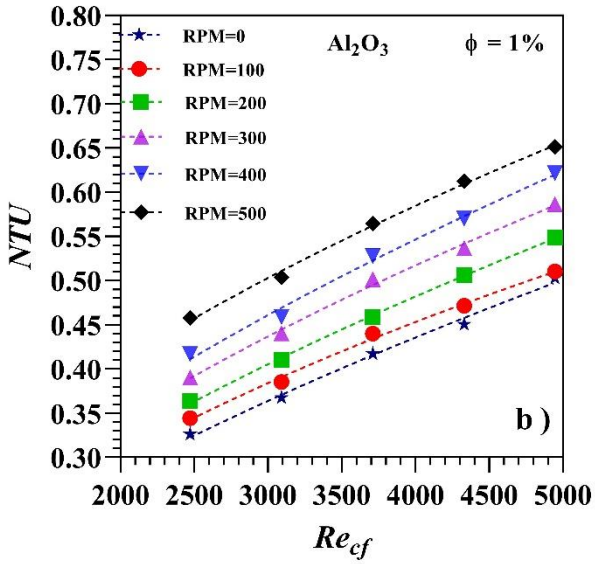
RPM=0
RPM=100
RPM=200
RPM=300
RPM=400
RPM=500
Al2O3
ϕ = 1%
b)
NTU
Re_cf

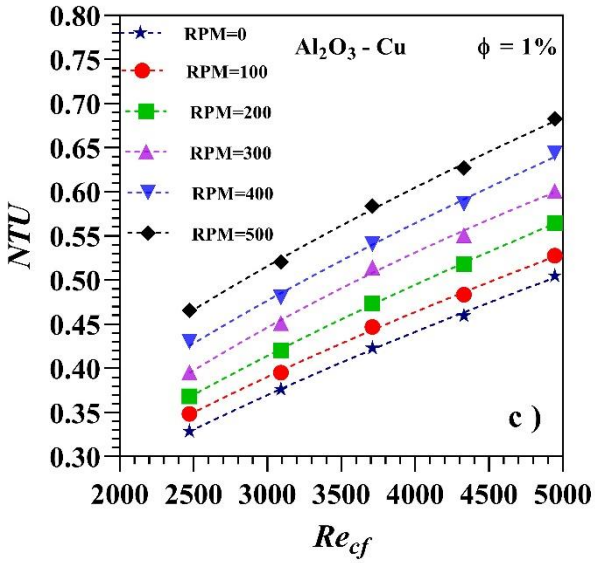
RPM=0
RPM=100
RPM=200
RPM=300
RPM=400
RPM=500
Al2O3 - Cu
ϕ = 1%
c)
NTU
Re_cf

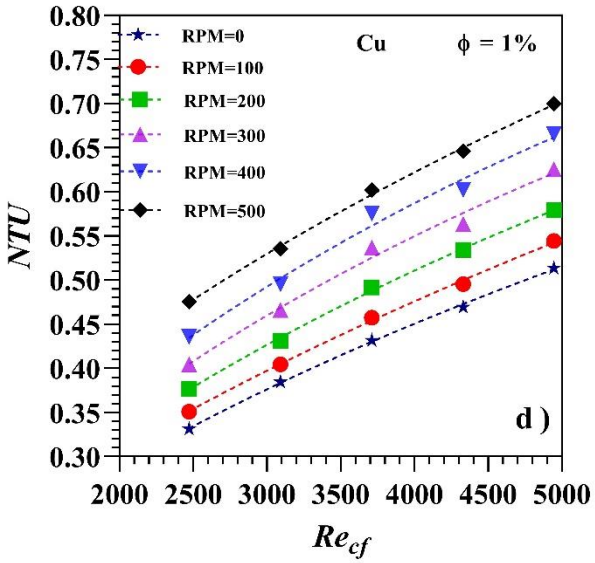
RPM=0
RPM=100
RPM=200
RPM=300
RPM=400
RPM=500
Cu
ϕ = 1%
d)
NTU
Re_cf

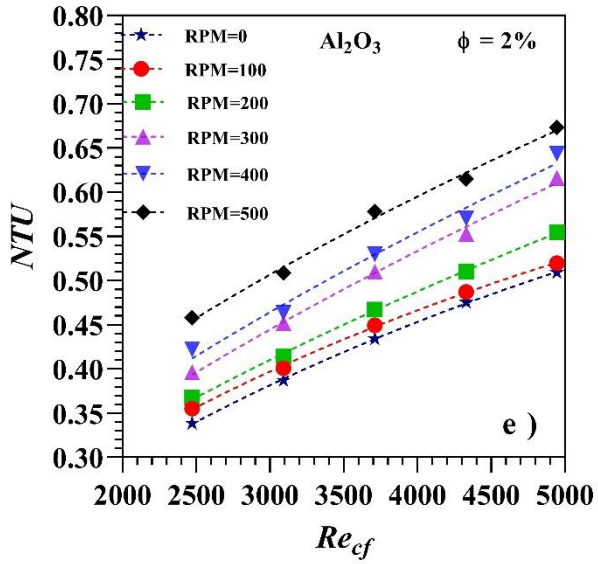
RPM=0
RPM=100
RPM=200
RPM=300
RPM=400
RPM=500
Al2O3
ϕ = 2%
e)
NTU
Recf

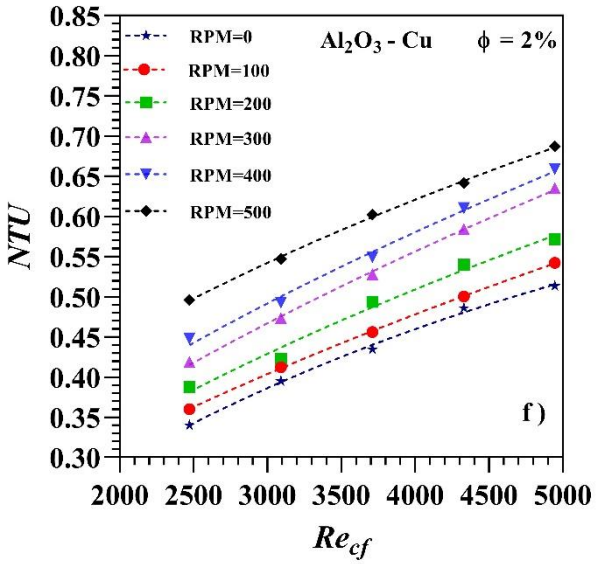
RPM=0
RPM=100
RPM=200
RPM=300
RPM=400
RPM=500
Al2O3 - Cu
ϕ = 2%
f)
NTU
Recf

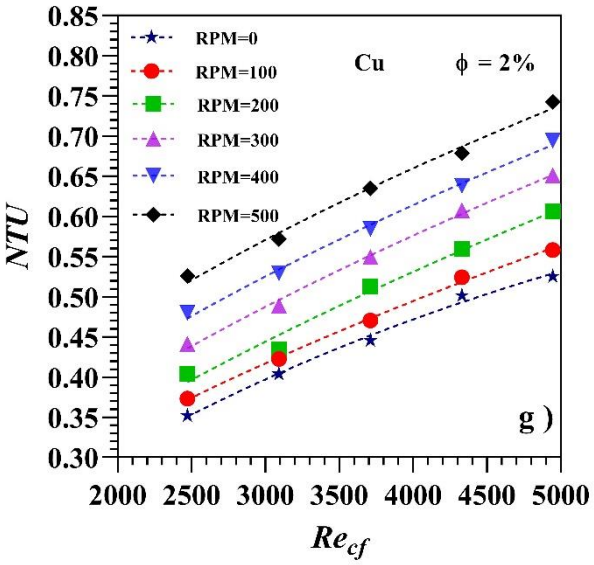
RPM=0
RPM=100
RPM=200
RPM=300
RPM=400
RPM=500
Cu
ϕ = 2%
g)
NTU
Recf

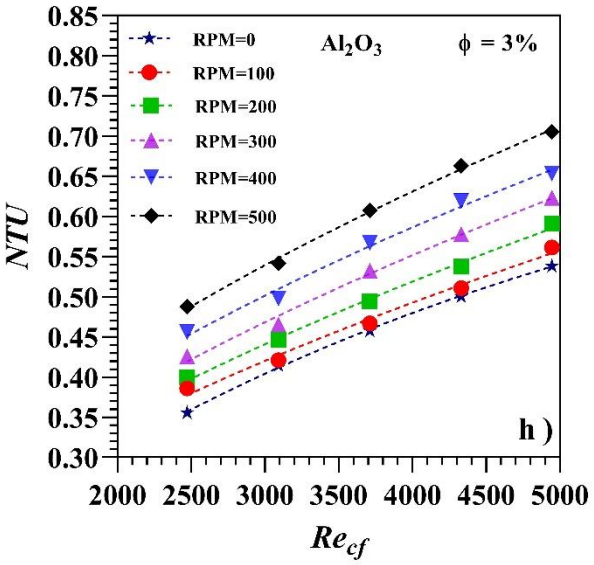
RPM=0
RPM=100
RPM=200
RPM=300
RPM=400
RPM=500
Al2O3
ϕ = 3%
h)
NTU
Recf

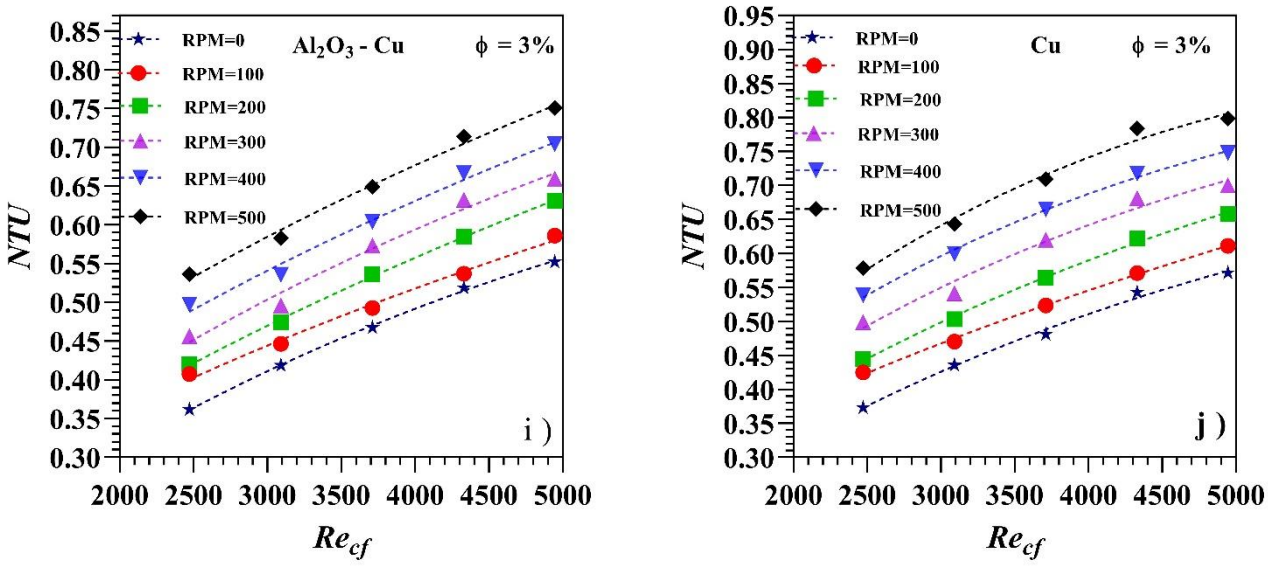

Figure 4.9 Effect of rotational speed and concentration on NTU

4.2.3 Effectiveness (ε)

Figure 4.10 shows the simulation results of the heat exchanger effectiveness (ε) as a function of the Reynolds number, obtained from Equation (3.8). The increase in effectiveness is apparent when the rotational speed and the nanoparticle concentration are increased.

As shown in Figure 4.10 (a), the effectiveness for pure water improves between 2.94 and 23.45% when the rotational speed of the inner tube is increased from 100 to 500 rpm at a Re_{cf} = 4,946.

Results for the Al_2O_3-water nanofluid are presented in Figures 4.10 (b-d),where it may be appreciated that the increase of the rotational speed improves the exchanger effectiveness. Compared to pure water at 0 rpm at Re_{cf} = 4,946, the improvement with tube rotation from 0 to 500 rpm and a 1% nanoparticle concentration ranges between 3.63 and 24%. For a 2% concentration, it lies between 4.54 and 26.77%, and for 3% concentration, it ranges between 8.7 and 30.62%.

The effects of adding the Al_2O_3-Cu-water nanofluid at 1%, 2%, and 3% concentrations with different inner tube rotational speeds are shown in Figure 4.10 (e-g). At 1% concentration, the effectiveness increases by 3.92% at 0 rpm up to by 27.97% at 500

rpm. At 2%, it increases from 5.16% to 28.46%. At 3%, it is enhanced from 10.74% to 35.94%.

However, as with previous results, maximum enhancement occurs with the Cu-water nanofluid, as shown in Figures 4.10 (h-j). For instance, at 1% concentration there are already enhancements from 5.2 to 30%. At 2% concentration, effectiveness increases from 6.94 to 35%. The best behavior is found with 3% concentration, imrproving the efficiency in the range from 13.42 to 41.3%.

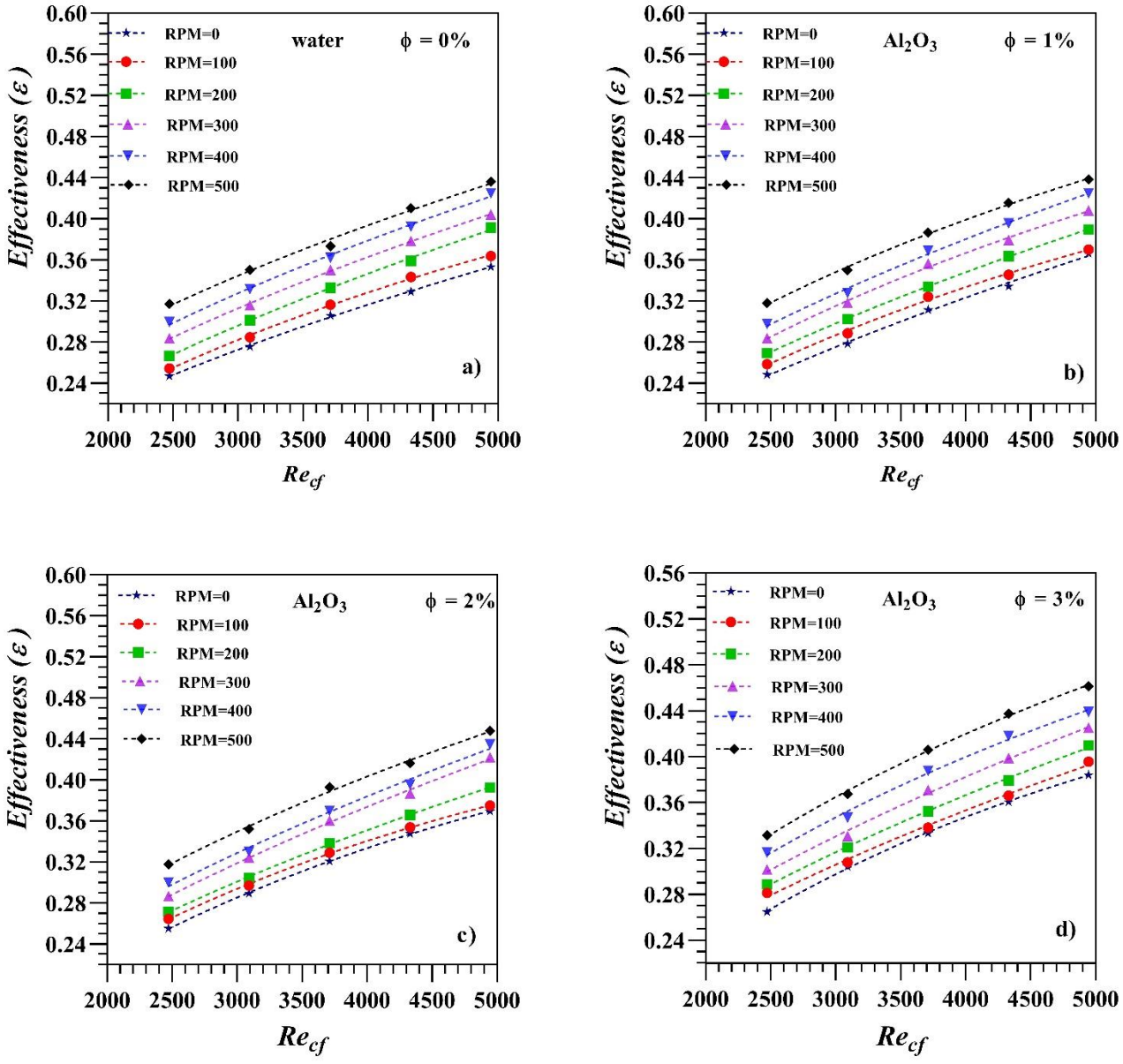

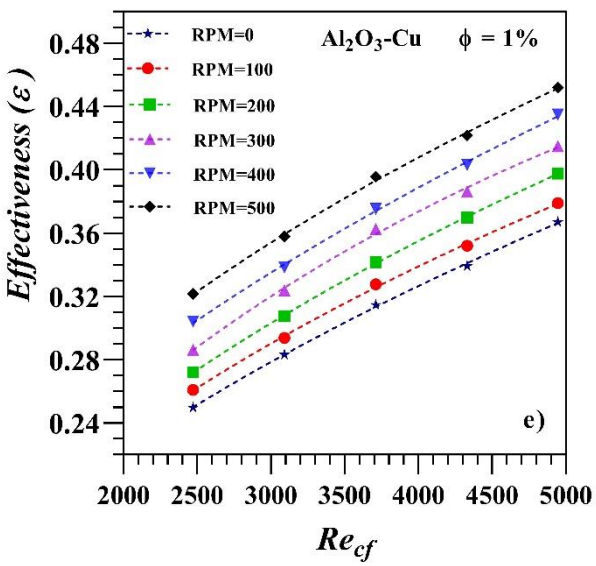
RPM=0
RPM=100
RPM=200
RPM=300
RPM=400
RPM=500
Al2O3-Cu
ϕ = 1%
e)
Effectiveness (ε)
Recf

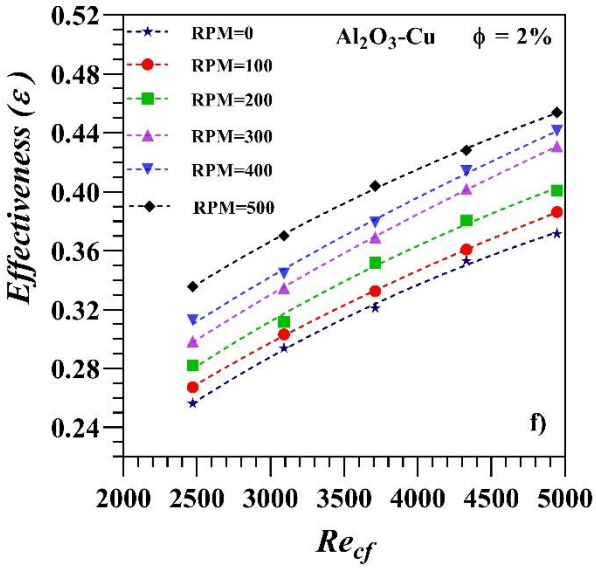
RPM=0
RPM=100
RPM=200
RPM=300
RPM=400
RPM=500
Al2O3-Cu
ϕ = 2%
f)
Effectiveness (ε)
Recf

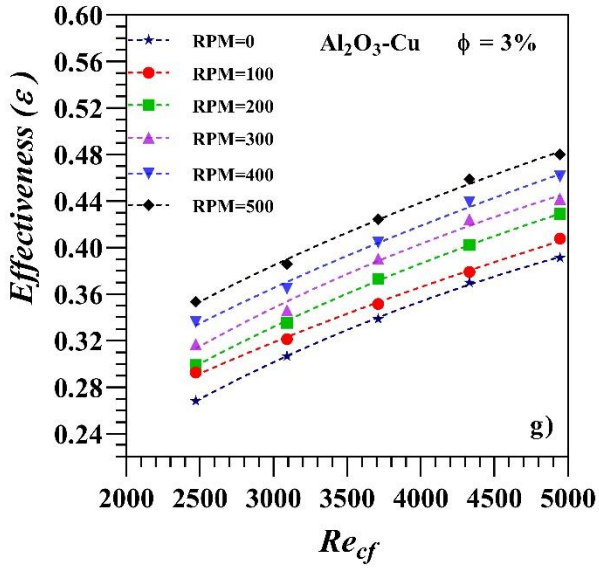
RPM=0
RPM=100
RPM=200
RPM=300
RPM=400
RPM=500
Al2O3-Cu
ϕ = 3%
g)
Effectiveness (ε)
Recf

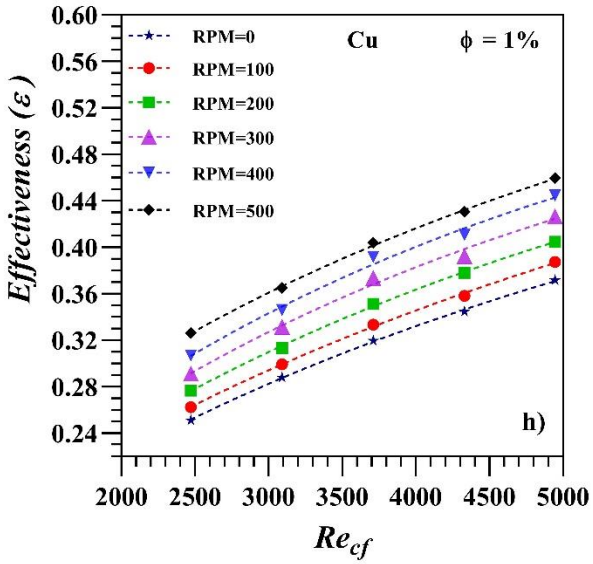
RPM=0
RPM=100
RPM=200
RPM=300
RPM=400
RPM=500
Cu
ϕ = 1%
h)
Effectiveness (ε)
Recf

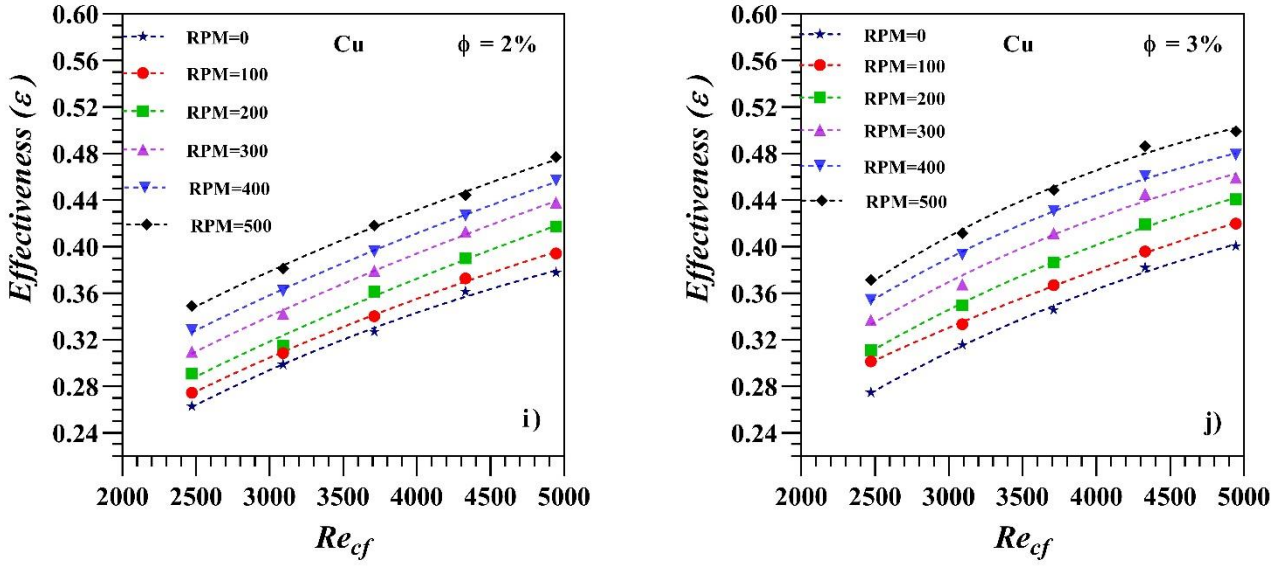

Figure 4.10 Effect of rotational speed and concentration on effectiveness

4.2.4 Local Heat Transfer Coefficients

The 3D simulation was also used to study the evolution of the inner and outer local heat transfer coefficients, as shown in Figure 4.11. The heat transfer coefficient of the hot fluid was higher than the coefficient of the cold fluid for all the studied cases. Addionally, heat transfer coefficients were higher at the hot fluid inlet, falling as the fluids traveled inside the exchanger and the hot fluid was cooled and the cold fluid was heated up.

Addition of nanoparticles was found beneficial for increasing both heat transfer coefficients, mainly as a result of the improvement of the cold fluid heat transfer related properties. The effect of inner tube rotation also appears to increase both heat transfer coefficients largely, primarily due to the turbulence caused by the swirling flow motion.

Local heat transfer coefficients increased with the concentration of nanoparticles from 0 to 3% and faster inner tube rotational speeds from 0 to 500 rpm. Again, the most beneficial results were obtained with the Cu-water nanofluid at 3% concentration at the maximum rotation rate of 500 rpm, as shown in Figure 4.11 (r).

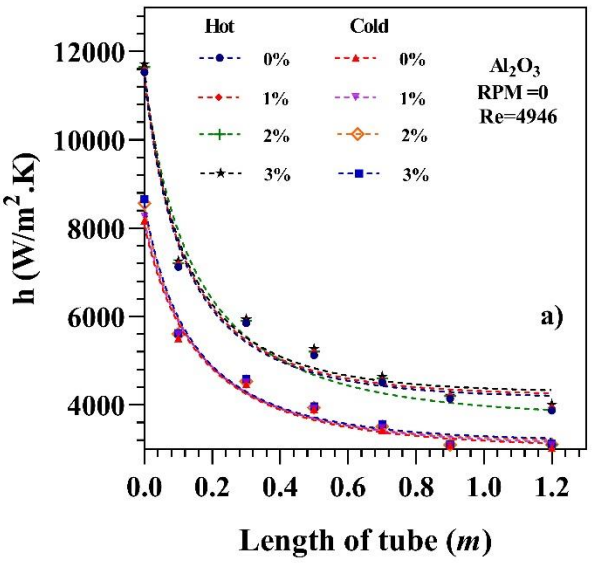
Hot
Cold
0%
1%
2%
3%
Al_2O_3
RPM =0
Re=4946
a)
h (W/m^2.K)
Length of tube (*m*)

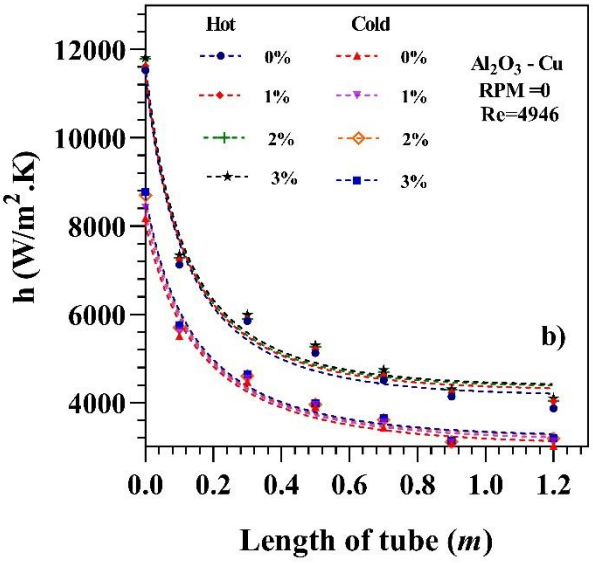
Hot
Cold
0%
1%
2%
3%
Al_2O_3 - Cu
RPM =0
Re=4946
b)
h (W/m^2.K)
Length of tube (*m*)

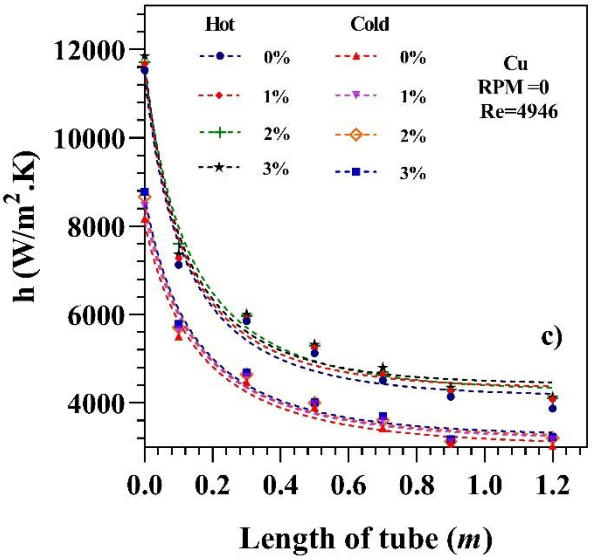
Hot
Cold
0%
1%
2%
3%
Cu
RPM =0
Re=4946
c)
h (W/m^2.K)
Length of tube (*m*)

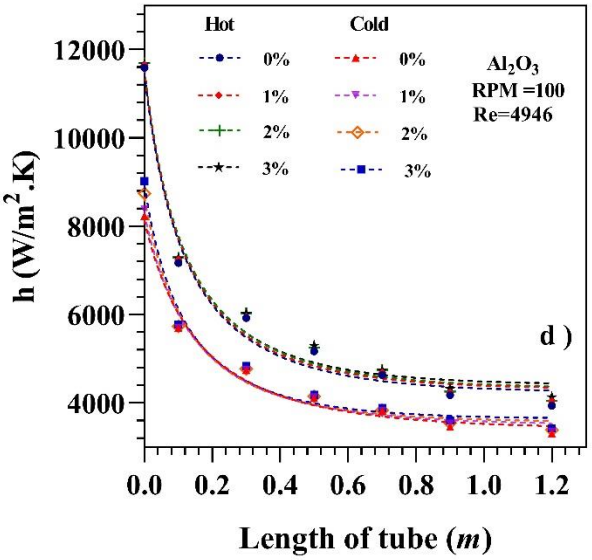
Hot
Cold
0%
1%
2%
3%
Al_2O_3
RPM =100
Re=4946
d)
h (W/m^2.K)
Length of tube (*m*)

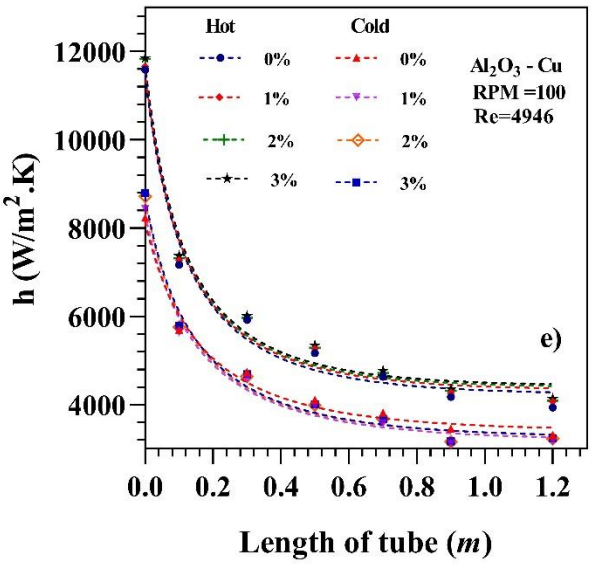
Hot
Cold
0%
1%
2%
3%
Al_2O_3 - Cu
RPM =100
Re=4946
e)
h (W/m^2.K)
Length of tube (*m*)

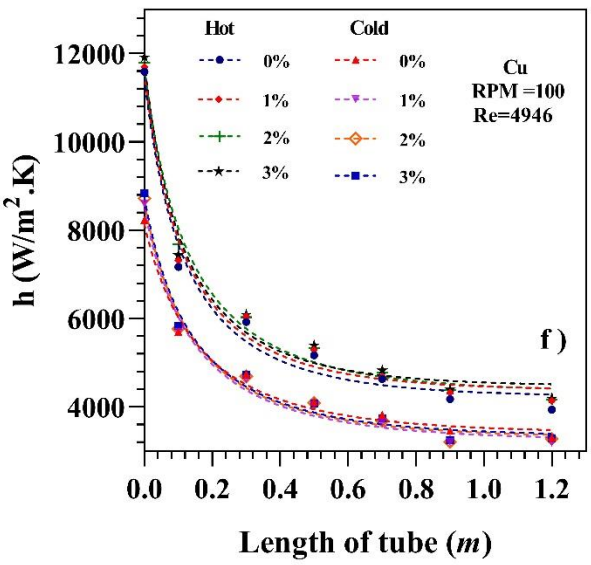
Hot
Cold
0%
1%
2%
3%
Cu
RPM =100
Re=4946
f)
h (W/m^2.K)
Length of tube (*m*)

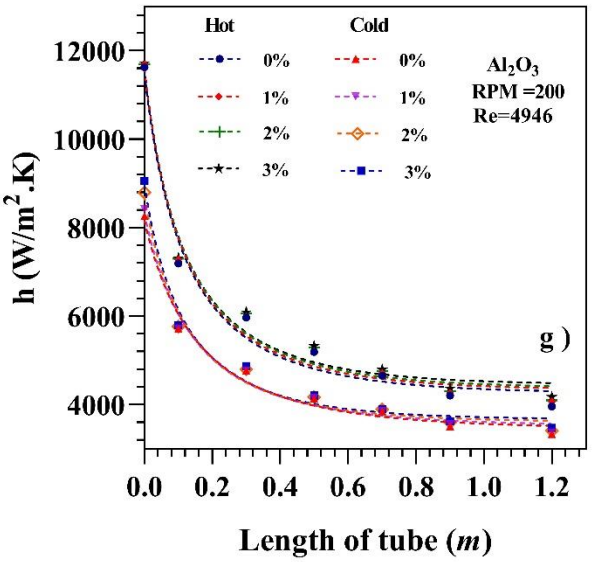
Hot
Cold
0%
1%
2%
3%
Al_2O_3
RPM =200
Re=4946
g)
h (W/m^2.K)
Length of tube (*m*)

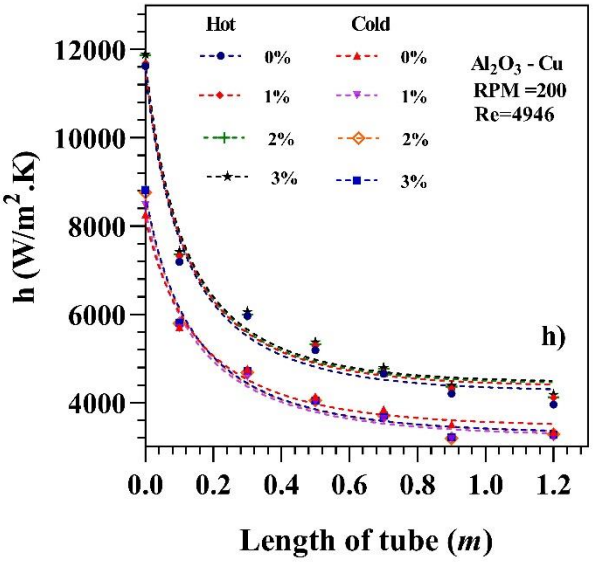
Hot
Cold
0%
1%
2%
3%
Al_2O_3 - Cu
RPM =200
Re=4946
h)
h (W/m^2.K)
Length of tube (*m*)

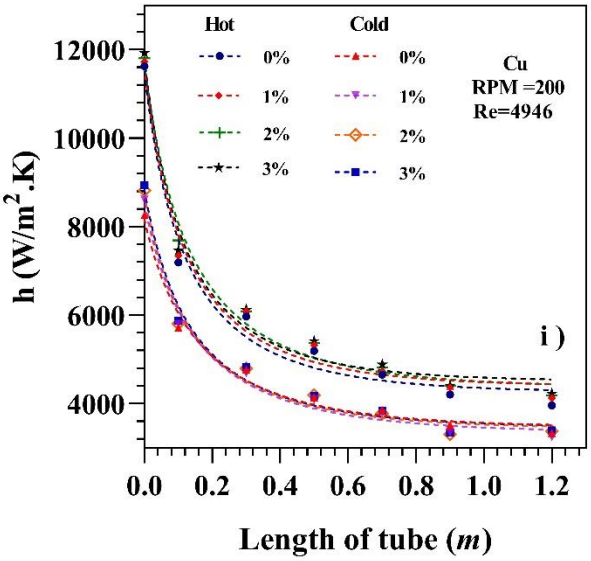
Hot
Cold
0%
1%
2%
3%
Cu
RPM =200
Re=4946
i)
h (W/m^2.K)
Length of tube (*m*)

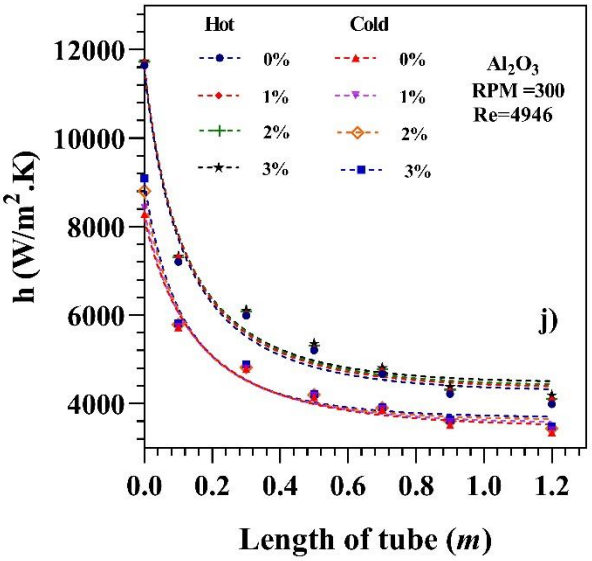
Hot
Cold
0%
1%
2%
3%
Al_2O_3
RPM =300
Re=4946
j)
h (W/m^2.K)
Length of tube (*m*)

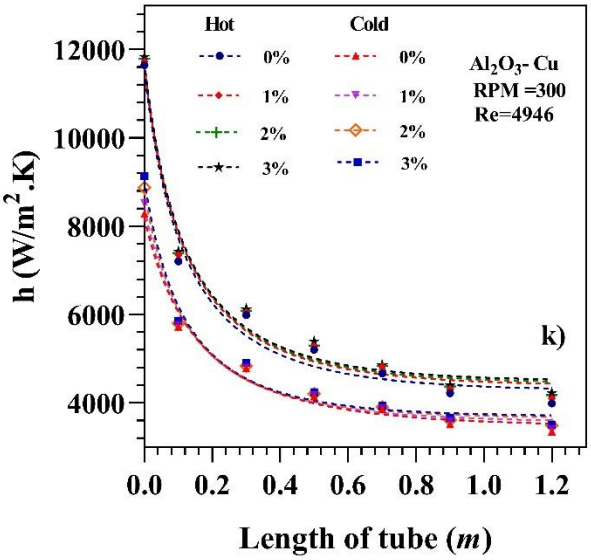
Hot
Cold
0%
1%
2%
3%
Al_2O_3- Cu
RPM =300
Re=4946
k)
h (W/m^2.K)
Length of tube (*m*)

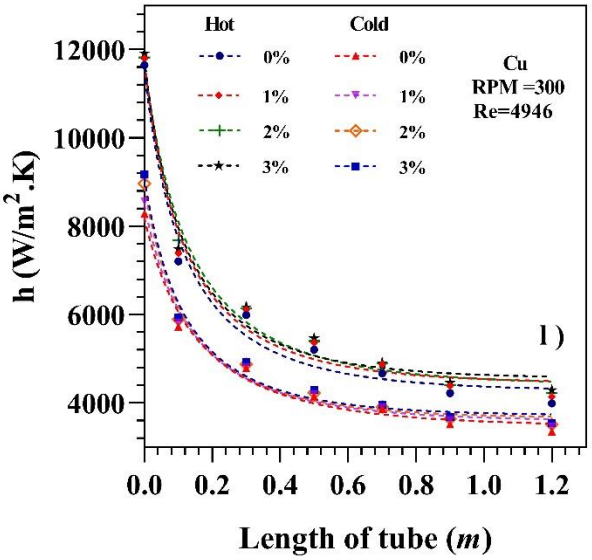
Hot
Cold
0%
1%
2%
3%
Cu
RPM =300
Re=4946
l)
h (W/m^2.K)
Length of tube (*m*)

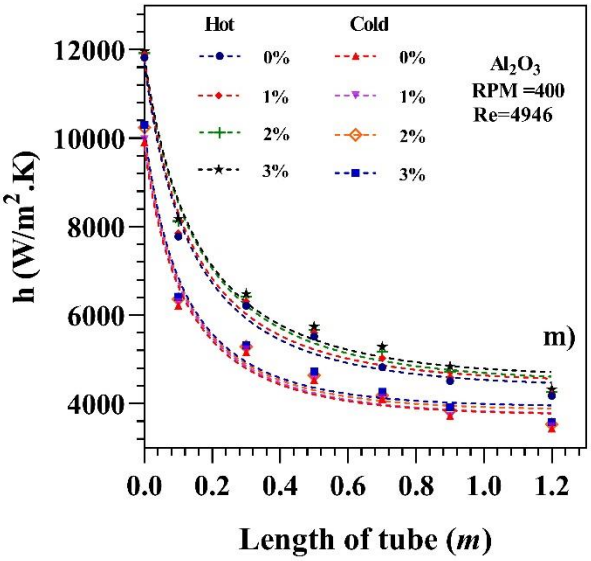
Hot
Cold
0%
1%
2%
3%
Al_2O_3
RPM =400
Re=4946
m)
h (W/m^2.K)
Length of tube (*m*)

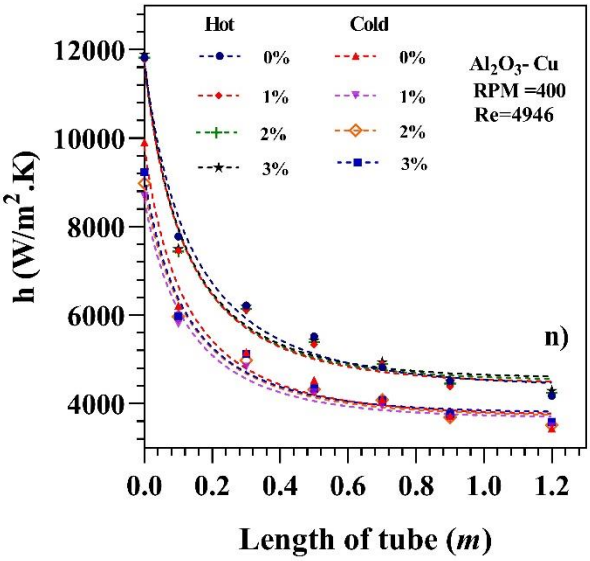
Hot
Cold
0%
1%
2%
3%
Al_2O_3- Cu
RPM =400
Re=4946
n)
h (W/m^2.K)
Length of tube (*m*)

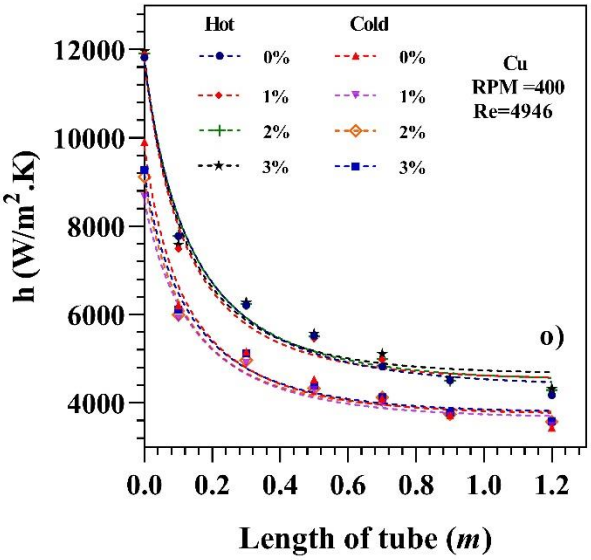
Hot
Cold
0%
1%
2%
3%
Cu
RPM =400
Re=4946
o)
h (W/m^2.K)
Length of tube (*m*)

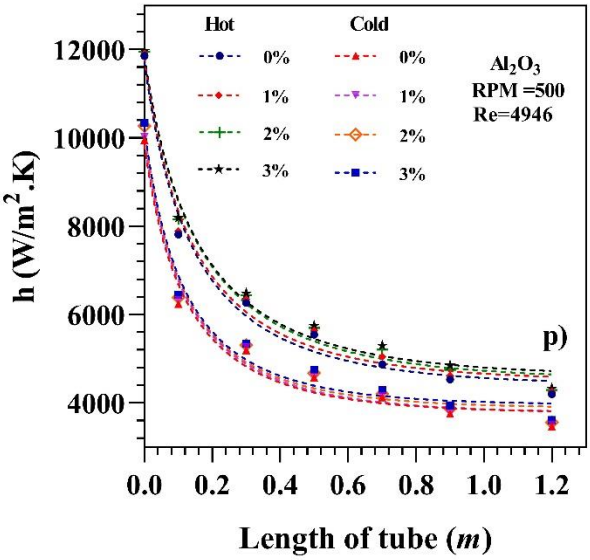
Hot
Cold
0%
1%
2%
3%
Al_2O_3
RPM =500
Re=4946
p)
h (W/m^2.K)
Length of tube (*m*)

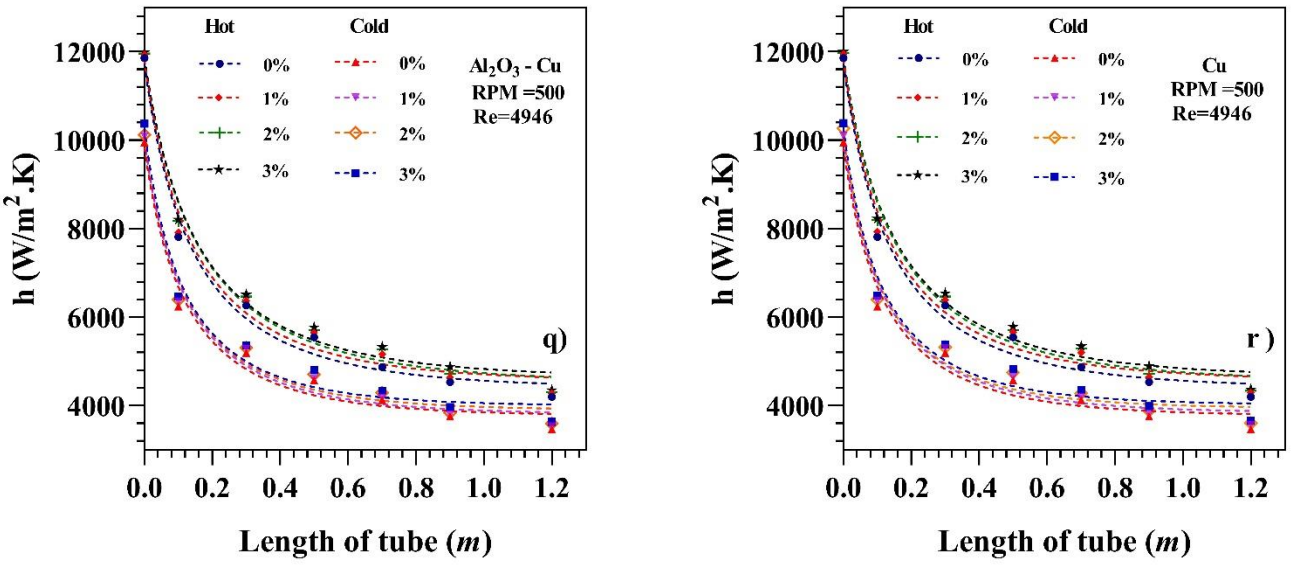

Figure 4.11 local heat transfer coefficients of inner and outer fluids

4.2.5 Pressure Drop

As previously commented, the pressure drop introduced by the addition of nanofluids must be addressed to reduce energy consumption and propose efficient heat exchanger designs. Rotation of the inner tube introduces an additional pressure drop.

Figure 4.12 shows the pressure drop in the heat exchanger, which increases with the volume concentration of nanofluids, due to the changes in density and viscosity that promote flow friction. Furthermore, increasing the inner tube rotational speed results in an increase in the pressure drop, due to the higher fluid velocities.

Figure 4.12 (a) depicts the pressure drop of pure water with the increase in the inner tube rotational speed from 0 to 500 rpm at Re_{cf} = 4,946. The pressure drop increases between 4.85 and 87% from 100 to 500 rpm when compared to the static inner tube value.

Concerning the Al_2O_3-water nanofluid, presented in Figure 4.12 (b-d), the pressure drop increased as the concentration and rotational speed increased. Increases from 4.93 to 80.42% were found for 1% volume concentration when the inner tube rotational speed was increased from 0 to 500 rpm. The increase ranged from 12.96 to

88.57% for 2% volume concentration; and from 24.2 to 104.77% for 3% concentration, all with respect to pure water at 0 rpm.

For the Al_2O_3-Cu-water nanofluid, as shown in Figure 4.12 (e-g), the pressure drop increased between 5.84 and 89.81% for 1% volume concentration, between 14.37 and 94.12% for 2% volume concentration and between 33.8 and 124.6% for 3% volume concentration when compared to pure water at 0 rpm.

The maximum pressure drop values were found for the Cu-water nanofluid, as depicted in Figure 4.12 (h-j). The pressure drop increased between 6.03 and 91.67% for 1% volume concentration, between 18.33 and 116.22% for 2% volume concentration, and between 38.45 and 156.31% for 3% volume concentration when compared to pure water at 0 rpm.

Figure 4.13 shows the pressure contours in a longitudinal plane of the heat exchanger for the different fluids under study and the different rotational speeds at the cold fluid Reynolds numbers 2,473 and 4,946. The effect of the rotational speed is much more relevant that the addition of nanoparticles to water in terms of increasing the pressure drop across the exchanger. Nevertheless, maximum pressure drop is below 140 Pa, so the beneficial effects in terms of heat exchanger efficiency may be more significant that the additional required pumping power.

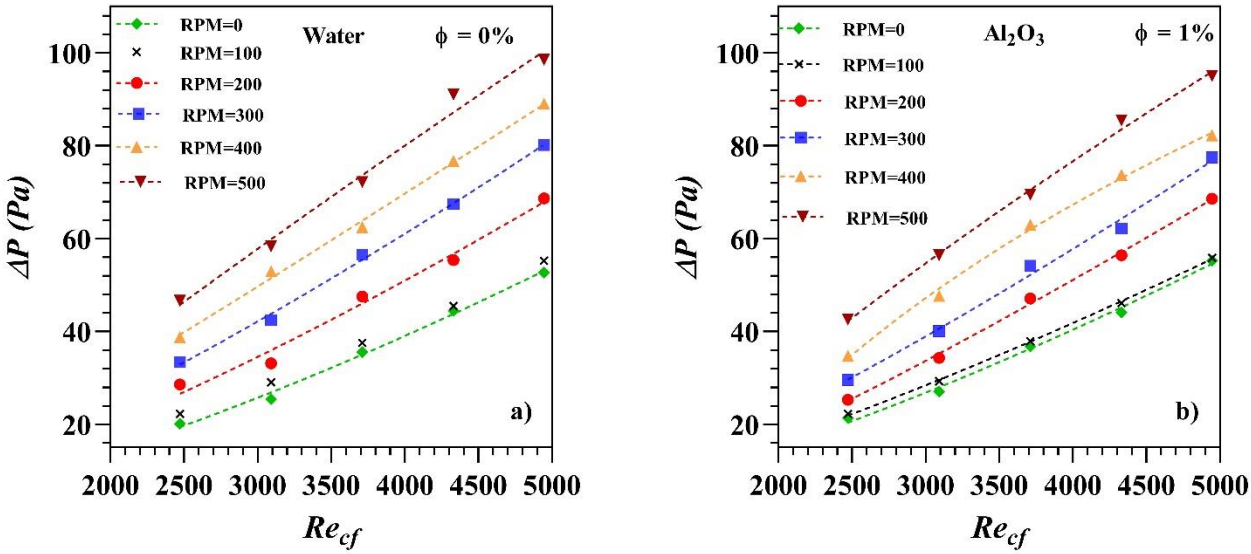

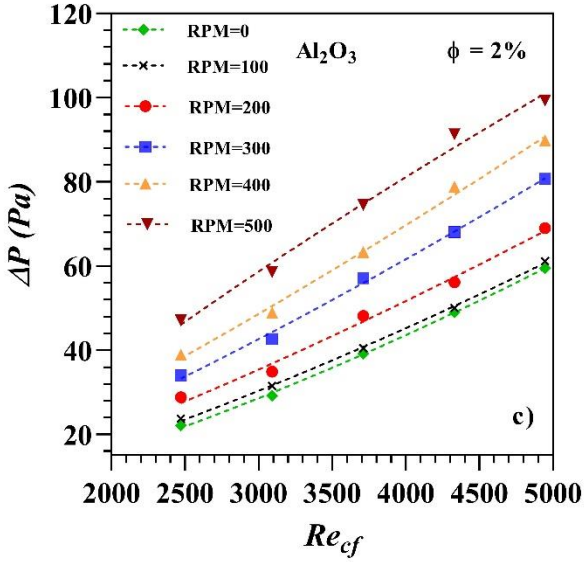
RPM=0
RPM=100
RPM=200
RPM=300
RPM=400
RPM=500
Al2O3
ϕ = 2%
c)
ΔP (Pa)
Recf
120
100
80
60
40
20
2000 2500 3000 3500 4000 4500 5000

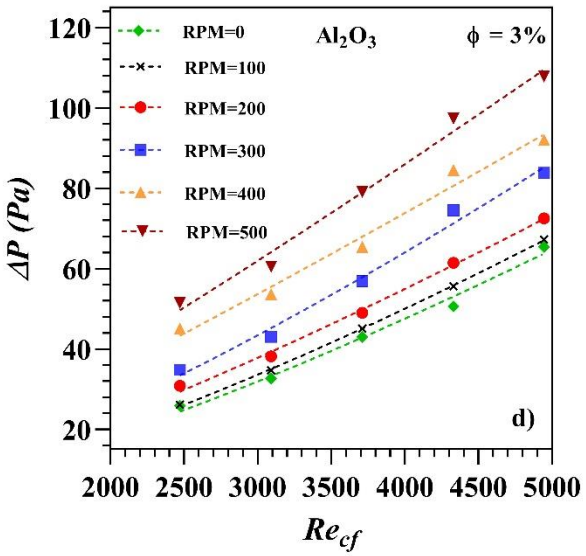
RPM=0
RPM=100
RPM=200
RPM=300
RPM=400
RPM=500
Al2O3
ϕ = 3%
d)
ΔP (Pa)
Recf
120
100
80
60
40
20
2000 2500 3000 3500 4000 4500 5000

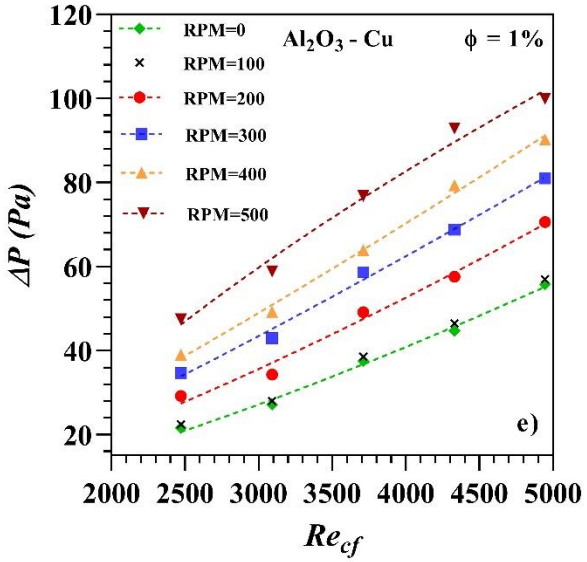
RPM=0
RPM=100
RPM=200
RPM=300
RPM=400
RPM=500
Al2O3 - Cu
ϕ = 1%
e)
ΔP (Pa)
Recf
120
100
80
60
40
20
2000 2500 3000 3500 4000 4500 5000

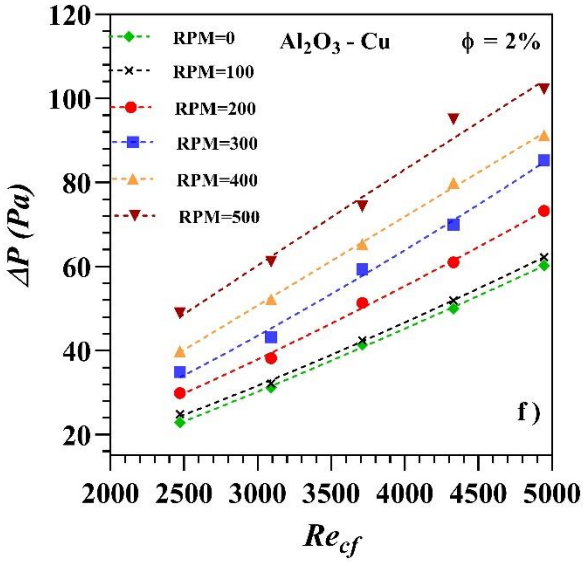
RPM=0
RPM=100
RPM=200
RPM=300
RPM=400
RPM=500
Al2O3 - Cu
ϕ = 2%
f)
ΔP (Pa)
Recf
120
100
80
60
40
20
2000 2500 3000 3500 4000 4500 5000

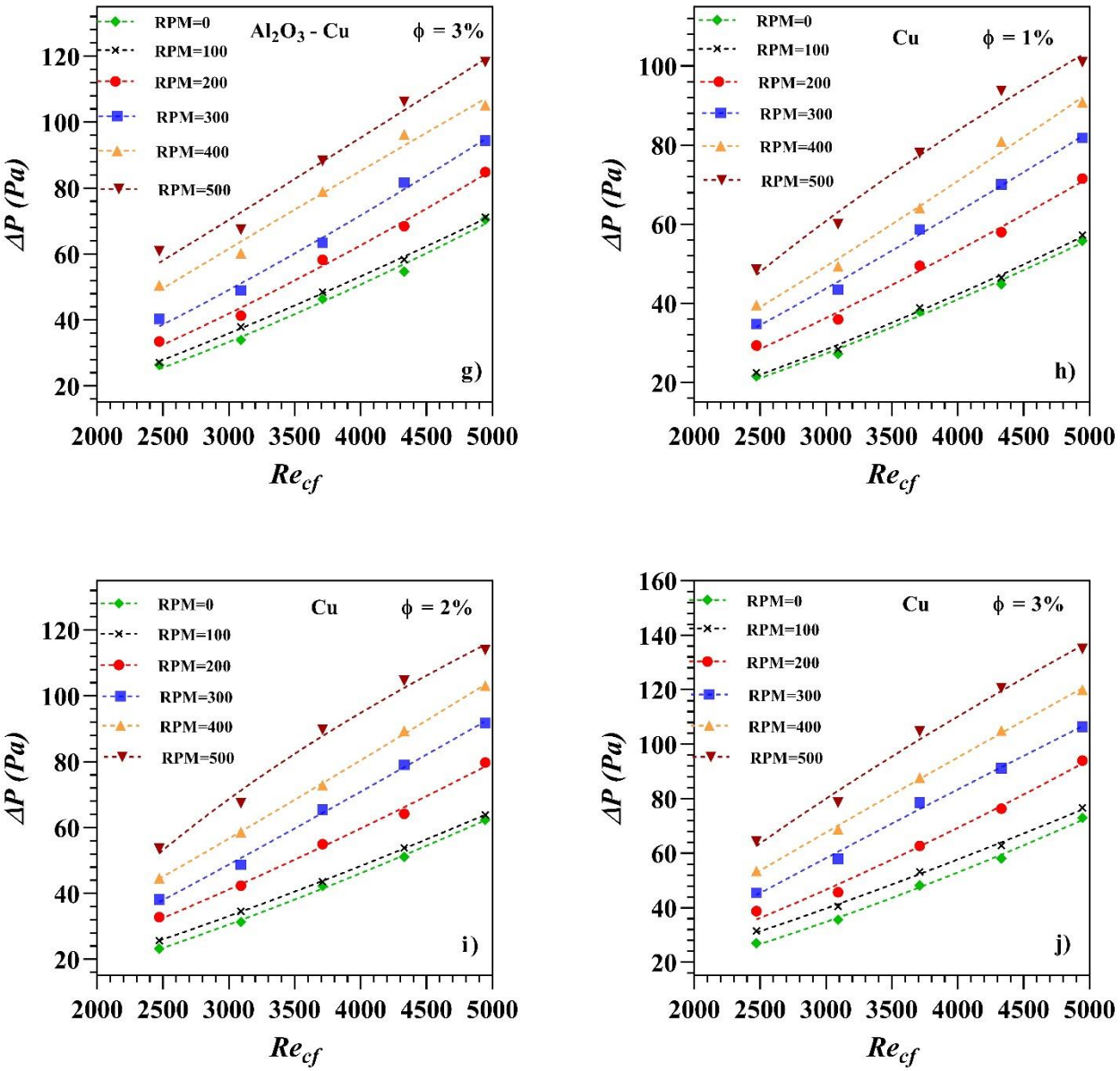

Figure. 4.12 Effect of concentration and rotational speeds on pressure drop.

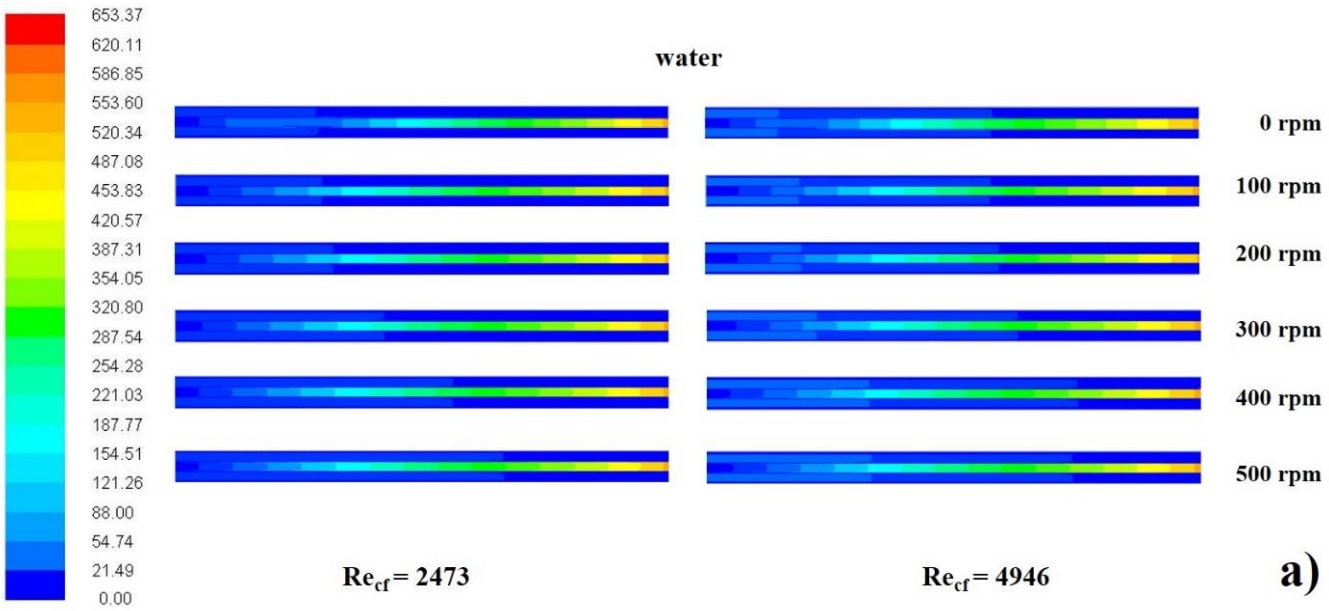
653.37
620.11
586.85
553.60
520.34
487.08
453.83
420.57
387.31
354.05
320.80
287.54
254.28
221.03
187.77
154.51
121.26
88.00
54.74
21.49
0.00
water
0 rpm
100 rpm
200 rpm
300 rpm
400 rpm
500 rpm
Re_cf = 2473
Re_cf = 4946
a)

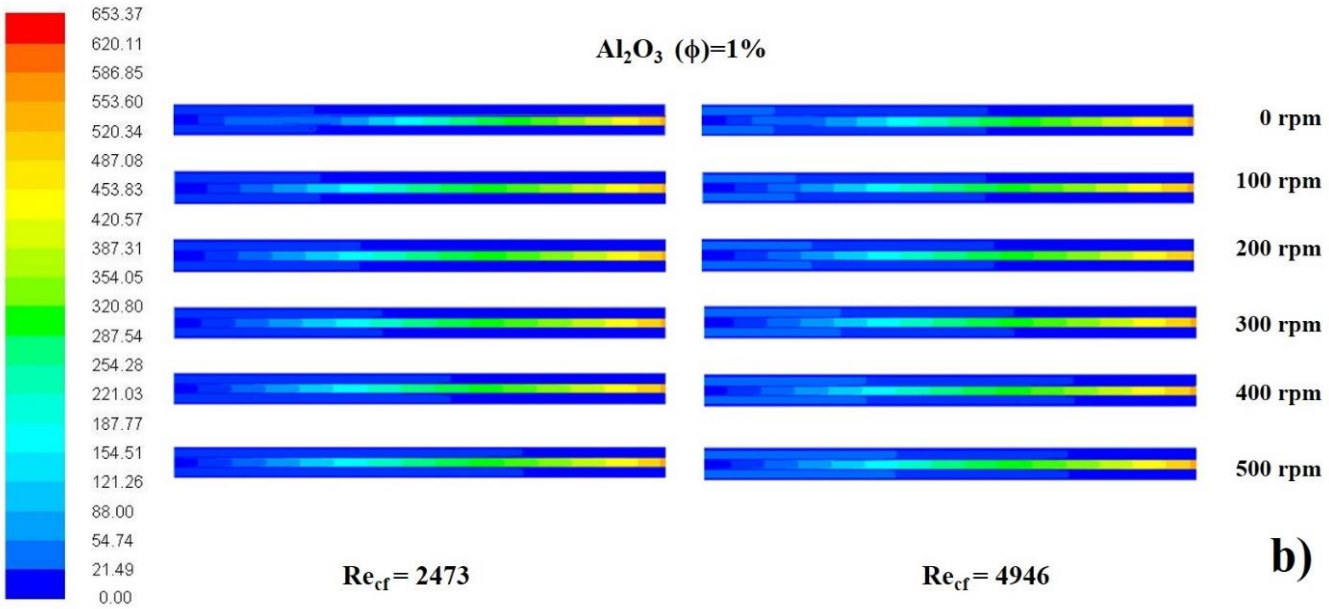
653.37
620.11
586.85
553.60
520.34
487.08
453.83
420.57
387.31
354.05
320.80
287.54
254.28
221.03
187.77
154.51
121.26
88.00
54.74
21.49
0.00
Al2O3 (ϕ)=1%
0 rpm
100 rpm
200 rpm
300 rpm
400 rpm
500 rpm
Re_cf = 2473
Re_cf = 4946
b)

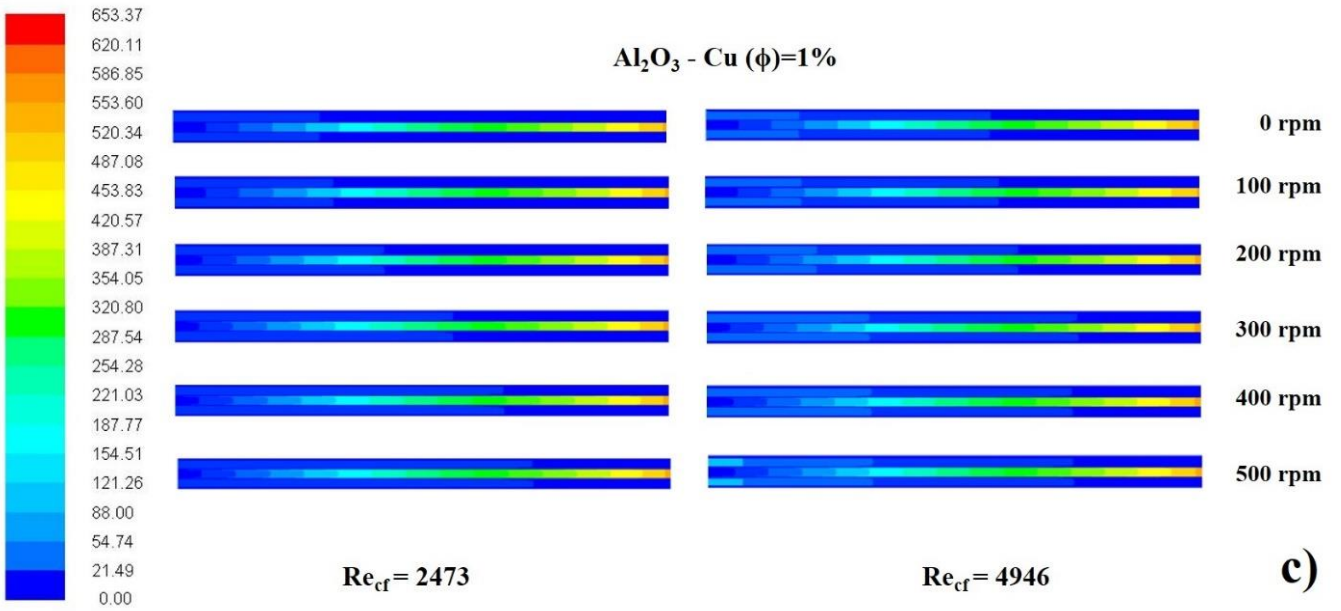
653.37
620.11
586.85
553.60
520.34
487.08
453.83
420.57
387.31
354.05
320.80
287.54
254.28
221.03
187.77
154.51
121.26
88.00
54.74
21.49
0.00
Al2O3 - Cu (ϕ)=1%
0 rpm
100 rpm
200 rpm
300 rpm
400 rpm
500 rpm
Recf = 2473
Recf = 4946
c)

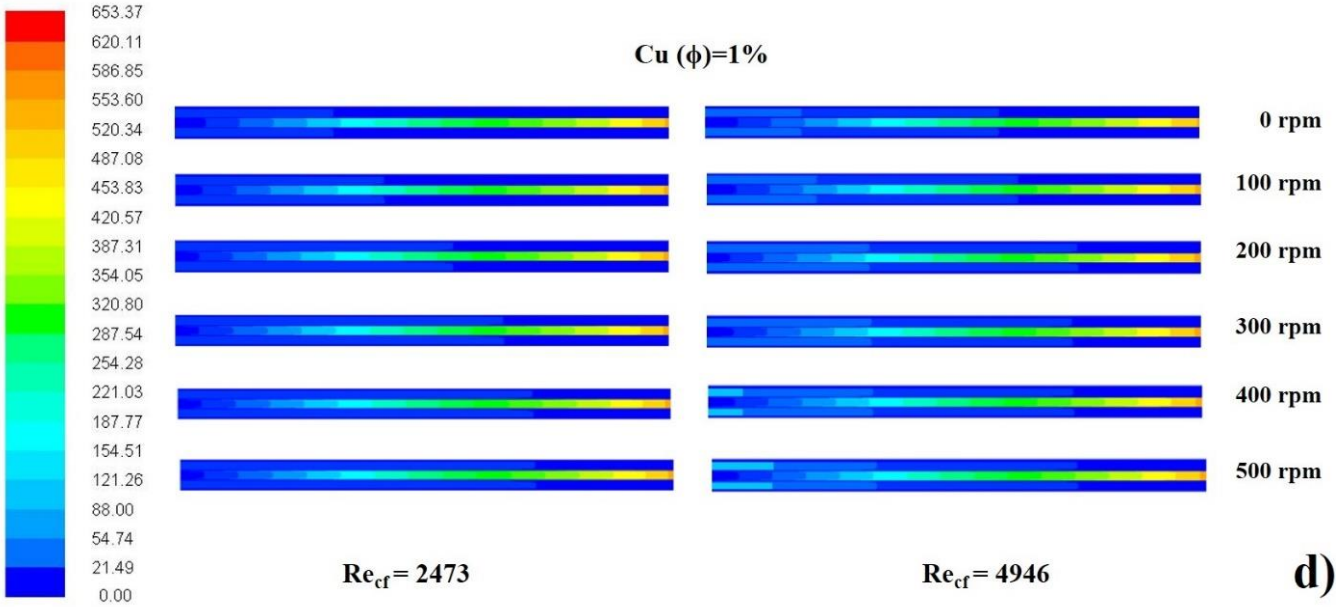
653.37
620.11
586.85
553.60
520.34
487.08
453.83
420.57
387.31
354.05
320.80
287.54
254.28
221.03
187.77
154.51
121.26
88.00
54.74
21.49
0.00
Cu (ϕ)=1%
0 rpm
100 rpm
200 rpm
300 rpm
400 rpm
500 rpm
Recf = 2473
Recf = 4946
d)

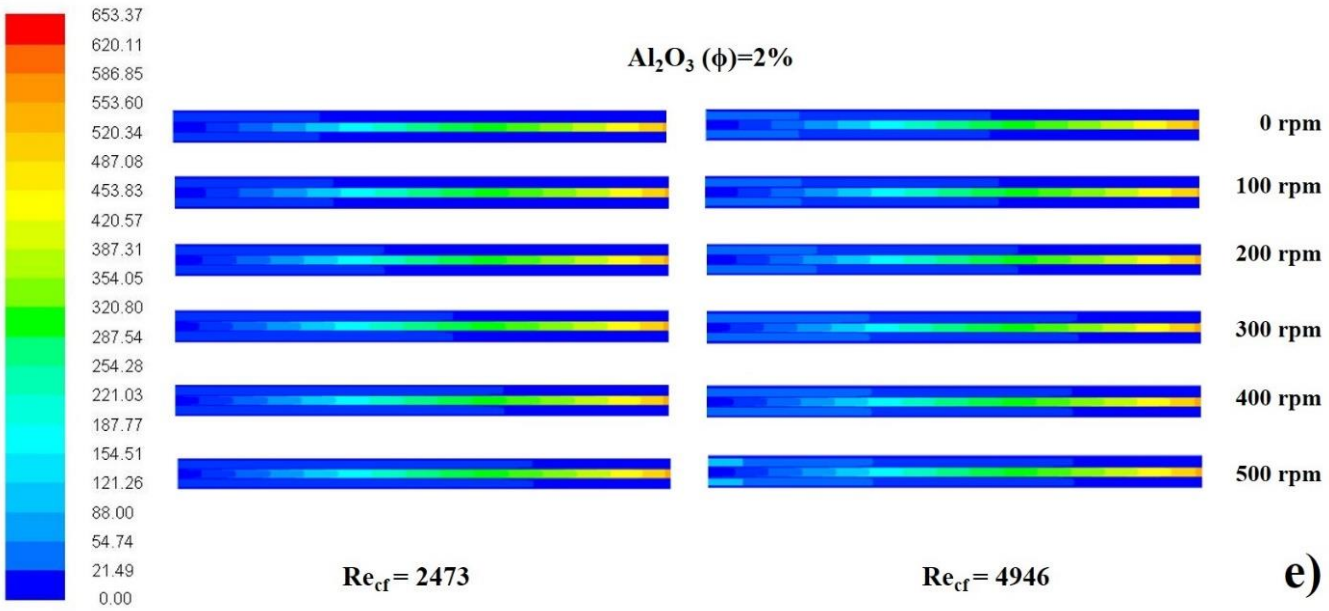
653.37
620.11
586.85
553.60
520.34
487.08
453.83
420.57
387.31
354.05
320.80
287.54
254.28
221.03
187.77
154.51
121.26
88.00
54.74
21.49
0.00
Al_2O_3 (ϕ)=2%
0 rpm
100 rpm
200 rpm
300 rpm
400 rpm
500 rpm
Re_{cf} = 2473
Re_{cf} = 4946
e)

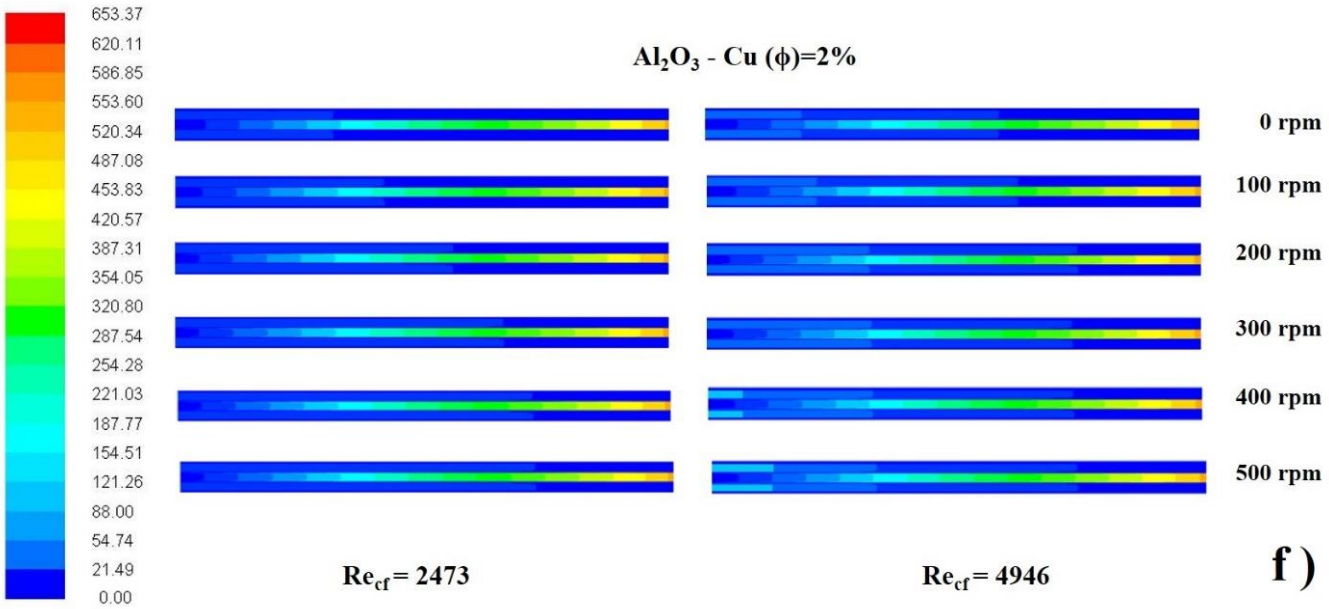
653.37
620.11
586.85
553.60
520.34
487.08
453.83
420.57
387.31
354.05
320.80
287.54
254.28
221.03
187.77
154.51
121.26
88.00
54.74
21.49
0.00
Al_2O_3 - Cu (ϕ)=2%
0 rpm
100 rpm
200 rpm
300 rpm
400 rpm
500 rpm
Re_{cf} = 2473
Re_{cf} = 4946
f)

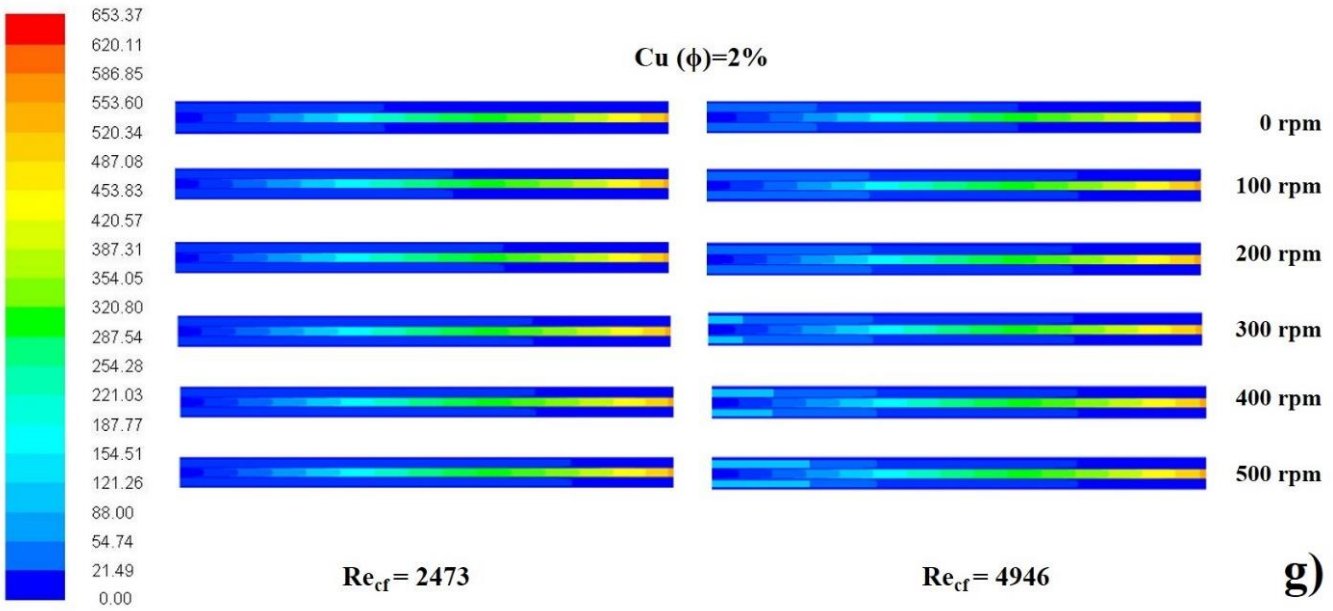
653.37
620.11
586.85
553.60
520.34
487.08
453.83
420.57
387.31
354.05
320.80
287.54
254.28
221.03
187.77
154.51
121.26
88.00
54.74
21.49
0.00
Cu (ϕ)=2%
0 rpm
100 rpm
200 rpm
300 rpm
400 rpm
500 rpm
Re_cf = 2473
Re_cf = 4946
g)

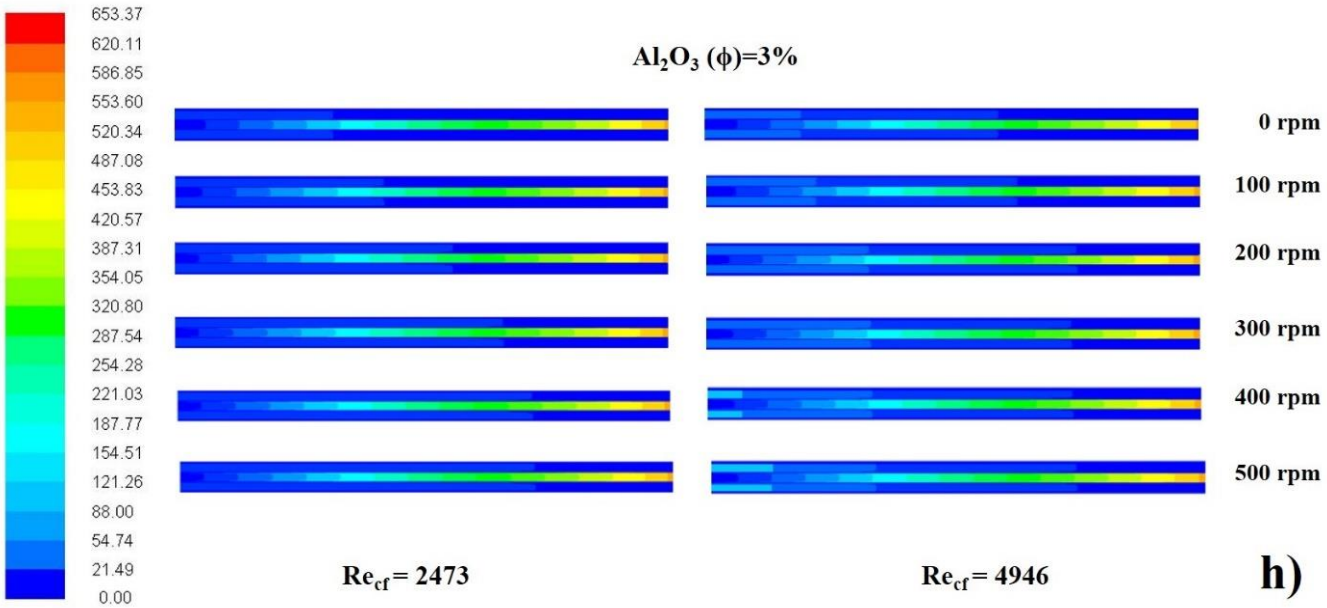
653.37
620.11
586.85
553.60
520.34
487.08
453.83
420.57
387.31
354.05
320.80
287.54
254.28
221.03
187.77
154.51
121.26
88.00
54.74
21.49
0.00
Al2O3 (ϕ)=3%
0 rpm
100 rpm
200 rpm
300 rpm
400 rpm
500 rpm
Re_cf = 2473
Re_cf = 4946
h)

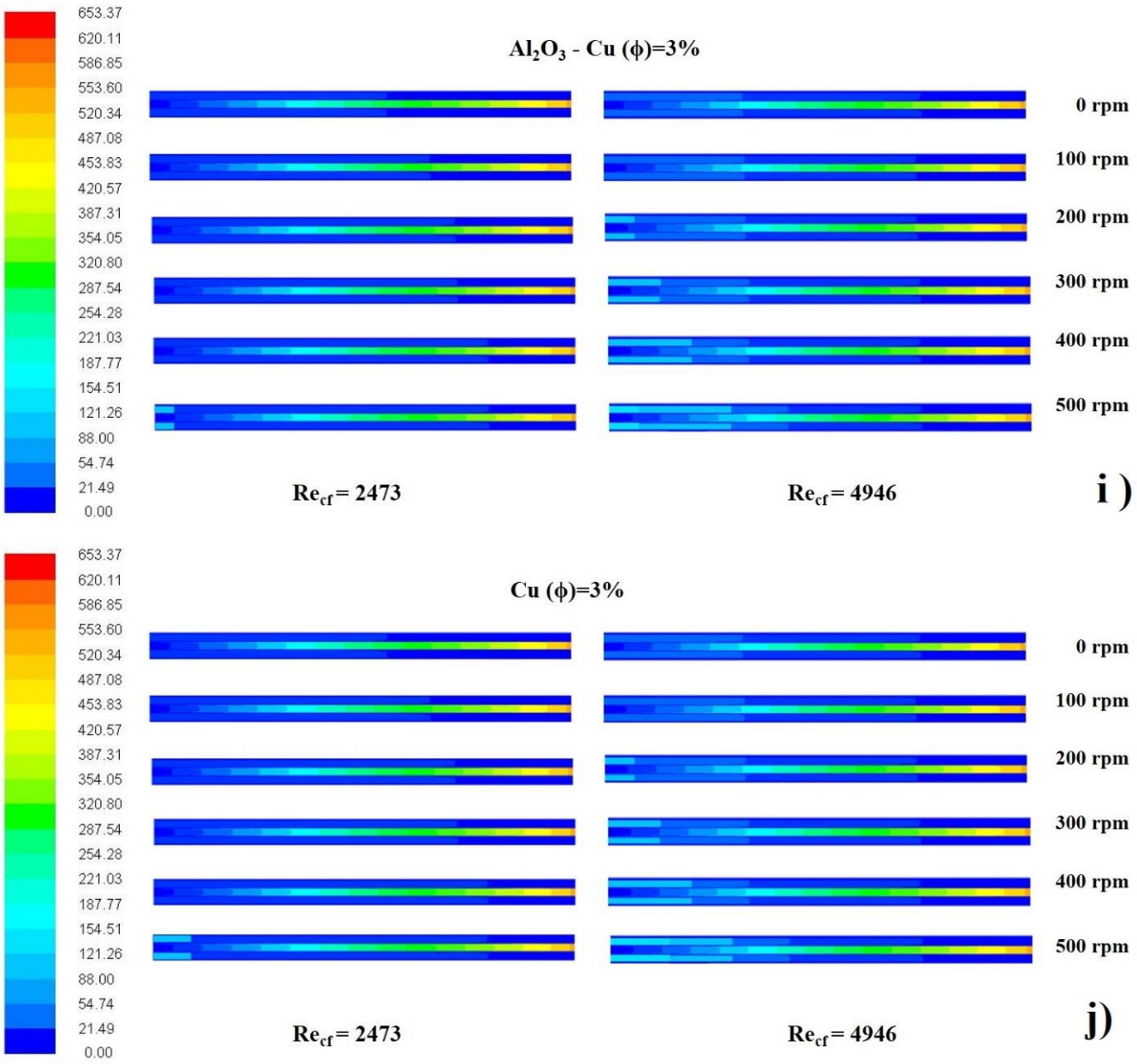

Figure 4.13 Pressure contour of 3D model (a) at Re_{cf} =2473, (b) at Re_{cf} =4946.

4.2.6 Flow Structure

The 3D numerical model allowed to study the flow structure along the exchanger. Figure 4.14 depicts the streamlines for water at different inner tube rotational speeds

and colored by velocity magnitude at the cold fluid Reynolds numbers 2,473 and 4,946.

The flow is mainly axial, with smooth velocity streamlines at 0 RPM. Nevertheless, as the rotational speed increases, the rotational component of the flow starts gaining presence. The continuous disturbance of the boundary layer, as well as the generation of a swirling flow pattern, may be the reasons behind the improvement of convective heat transfer and the increase of the pressure drop. Additionally, larger rotational speeds change the main flow direction strongly, forcing the flow to rotate perpendicularly to the tube and resulting in longer paths and residence times inside the exchanger. The additional turbulence generation and flow disruption is a fact known to enhance heat transfer.

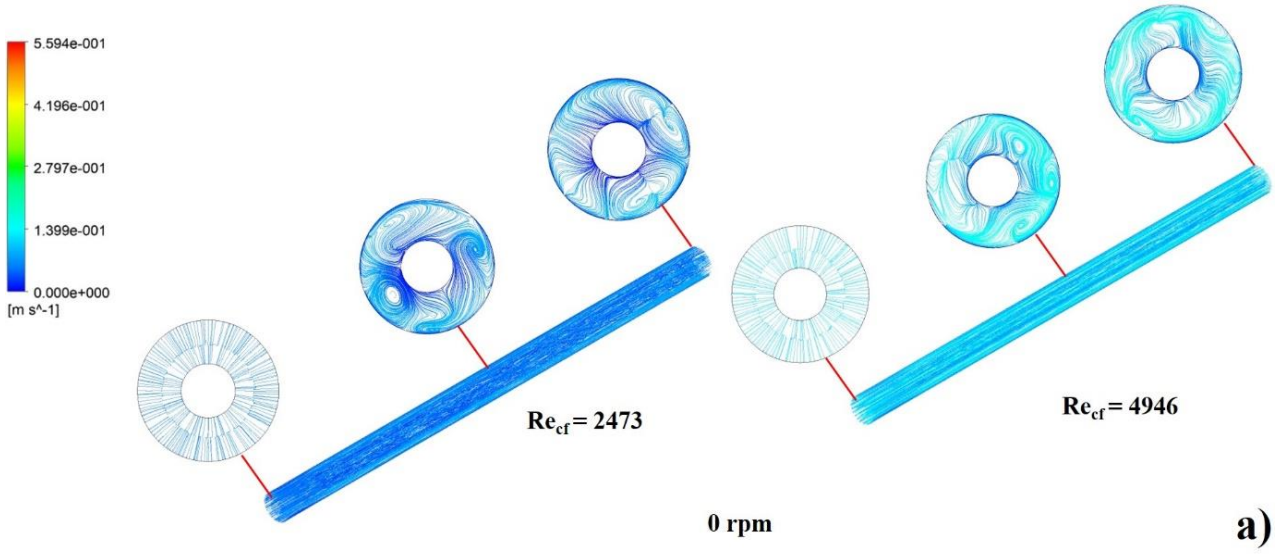

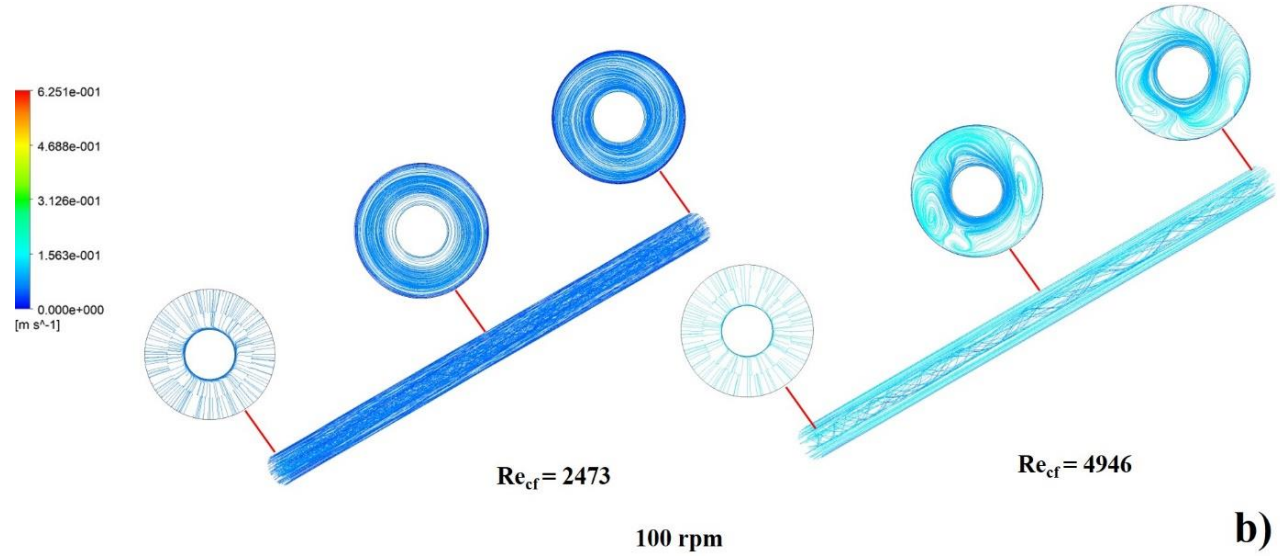

100 rpm **b)**

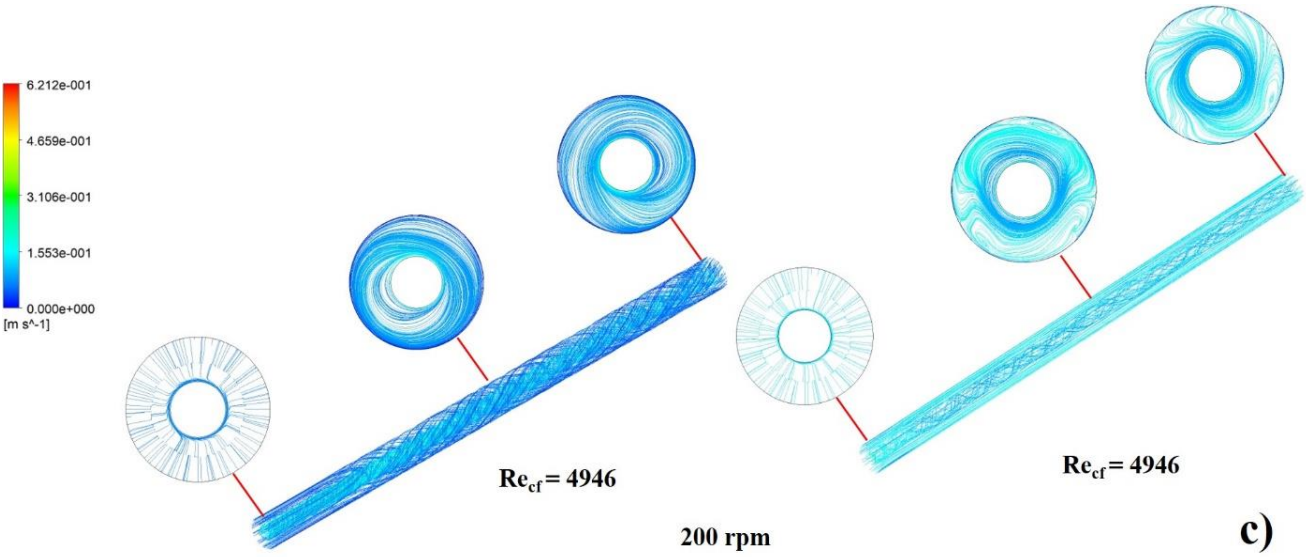

200 rpm **c)**

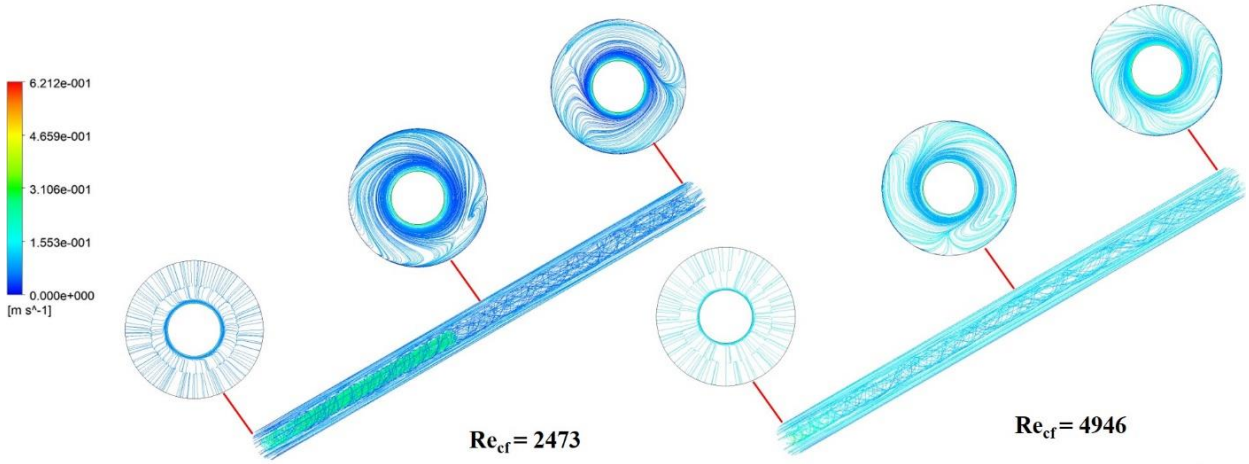

300 rpm **d)**

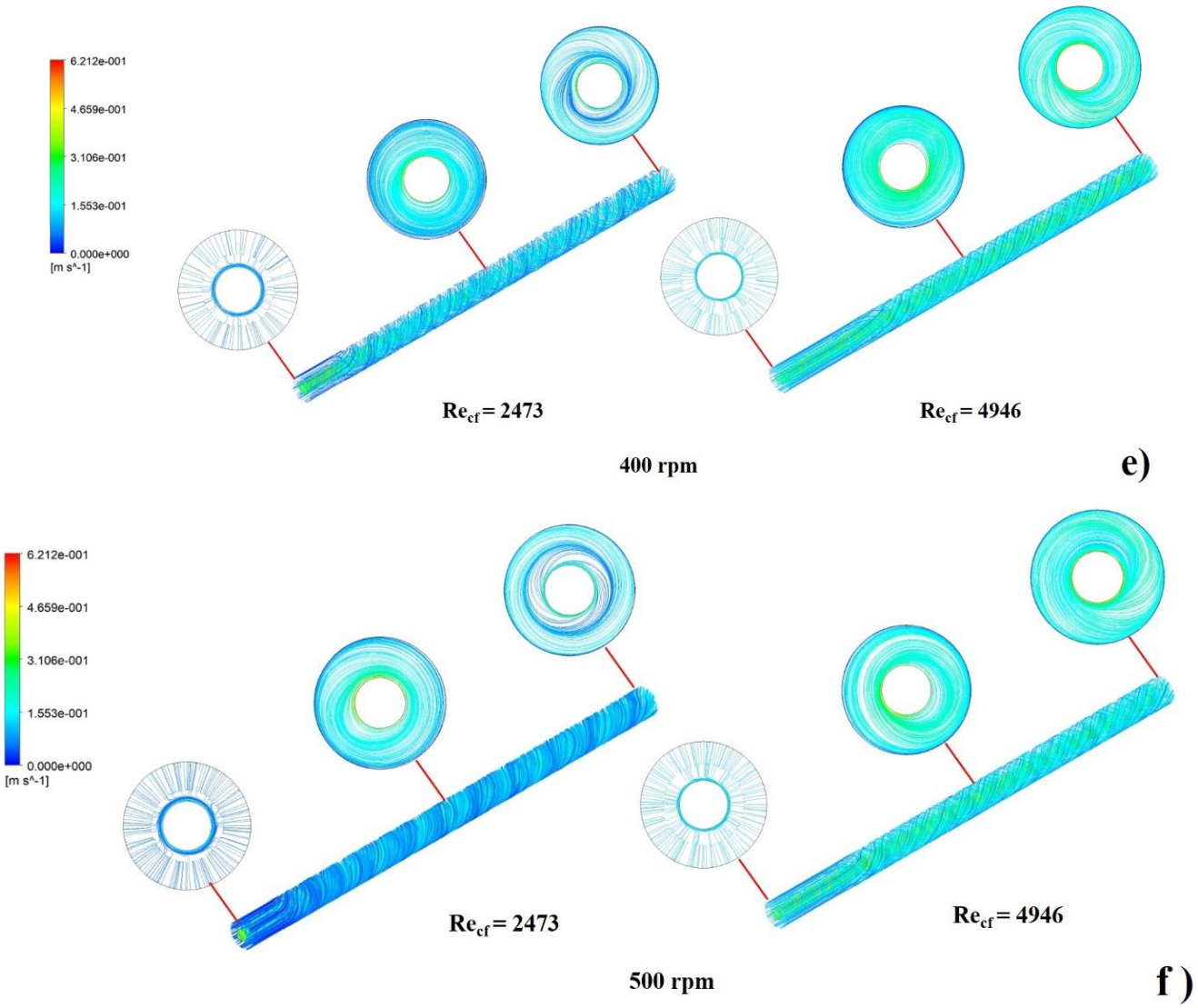

Figure 4.14 3D streamlines in double tube at different rotational speeds.

4.2.7 Pumping Power

The increasing pressure drop across the heat exchanger leads to higher pumping power requirements. The required external power has been calculated using Equation (3.10). Figure 4.15 shows the results of the pumping power required by the heat exchanger, as a function of nanofluid volume concentration and inner tube rotational speed for the three studied nanofluids.

The increase in nanoparticle concentrations, which increase fluid density, have the direct effect of increasing the pumping power. The rotational speed causes an increase in the pumping power as well, as shown in Figure 4.15. At Re_{cf} = 4,946, an inner tube rotational speed of 500 rpm and a nanoparticle concentration of 3%, the pumping

power increases by 20.3% (Al_2O_3), 22.91% (Al_2O_3-Cu) and 24.36% (Cu) compared to 0 rpm and 1% volume concentration.

Figure 4.16 depicts the ratio of average heat transfer to pumping power, in order to visualize better the enhancement of the heat transfer performance of the exchanger with respect to the additional required pumping cost. It may be appreciated how the Cu-nanofluid has the highest heat transfer values per unit pumping power among all the studied nanofluids. Additionally, the heat transfer to pumping power ratio increases with the nanoparticle concentration.

On the other hand, an excessive increase of the rotational speed may not be useful to optimize the heat exchanger performance. The increase of the rotational speed only benefits the heat transfer per unit pumping power at low rotational speeds, suggesting that speeds above the maximum one (500 rpm) may not be appropriate for operation of the heat exchanger.

Although the increase of the pumping power needs to be considered; in this case, the maximum pumping power is 0.1W, which should not cause any issues with the same operating pump as for the original heat exchanger.

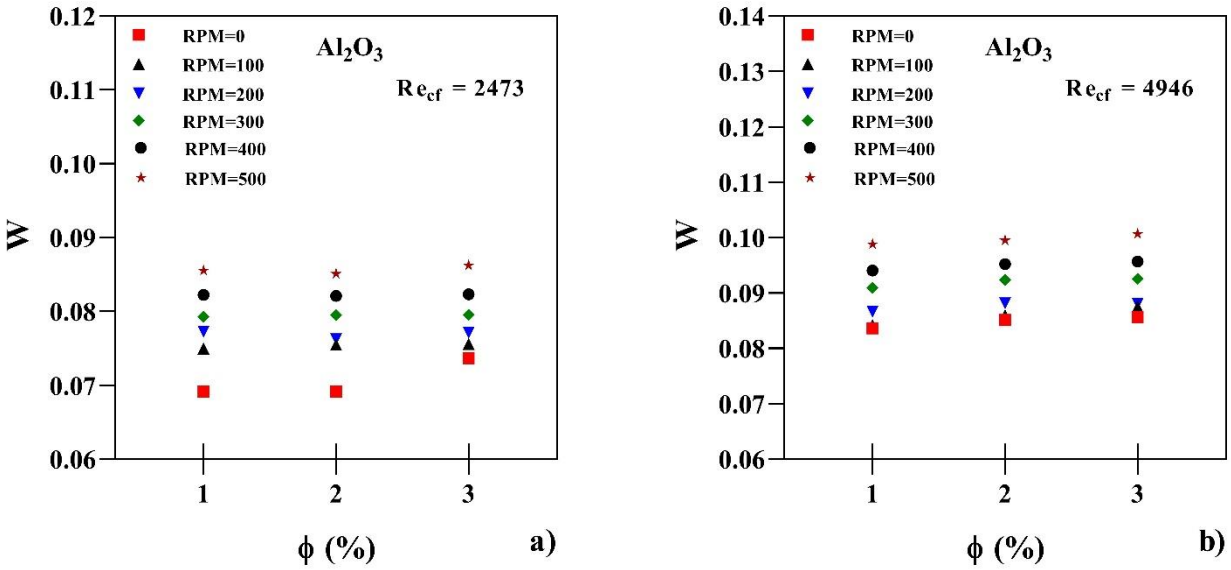

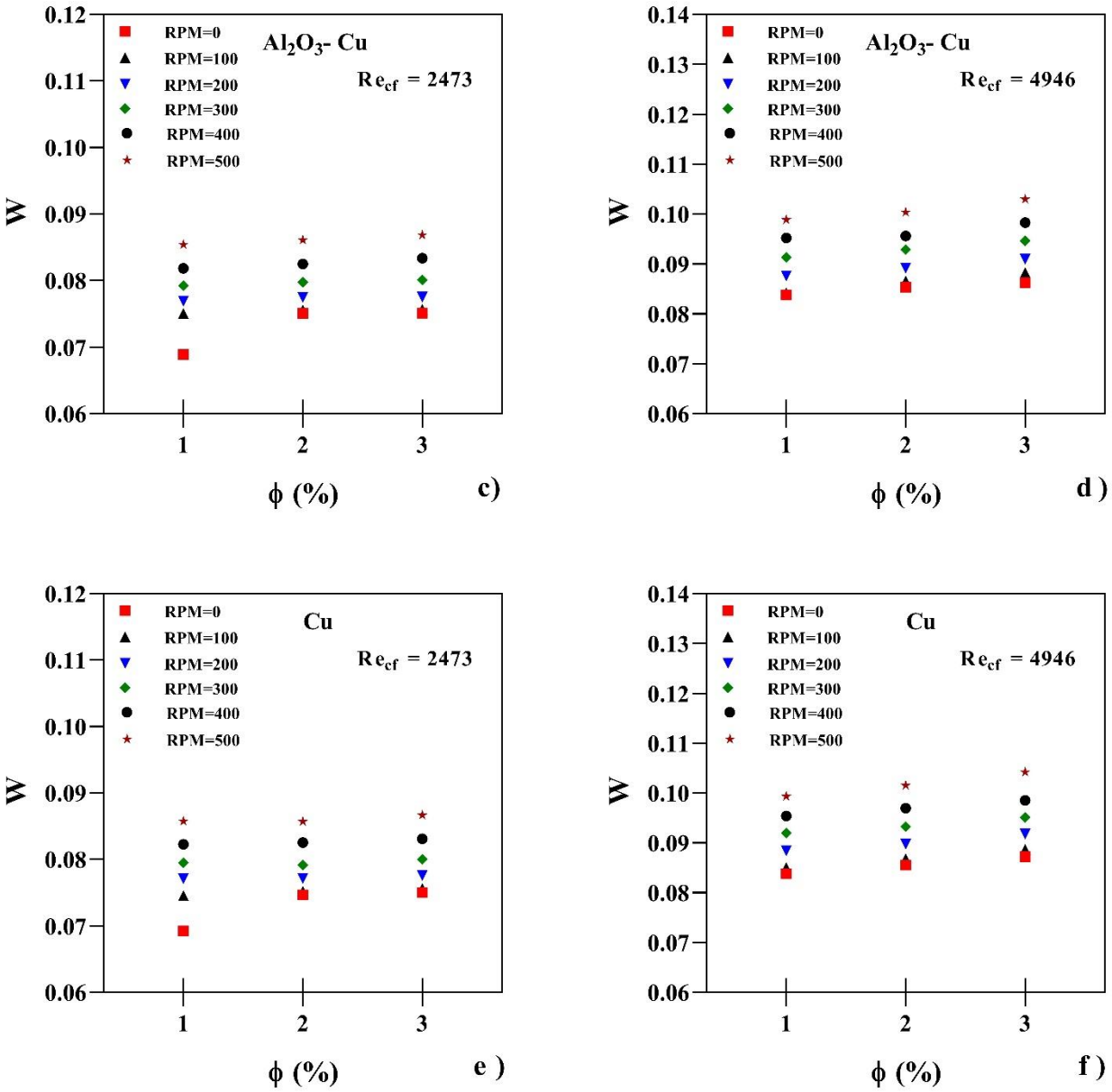

Figure 4.15 Effect of rotational speed and concentration on pumping power

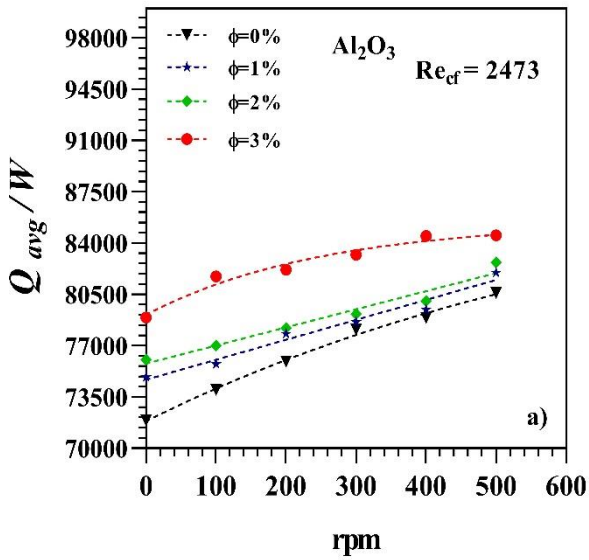
ϕ=0%
ϕ=1%
ϕ=2%
ϕ=3%
Al2O3
Recf = 2473
Q avg / W
rpm
a)

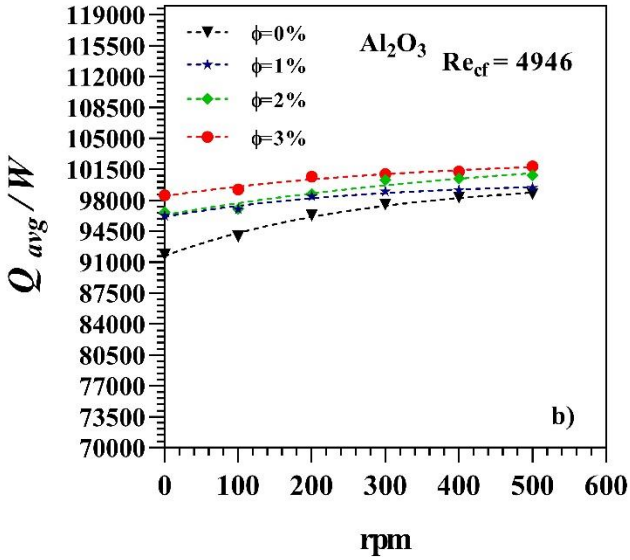
ϕ=0%
ϕ=1%
ϕ=2%
ϕ=3%
Al2O3
Recf = 4946
Q avg / W
rpm
b)

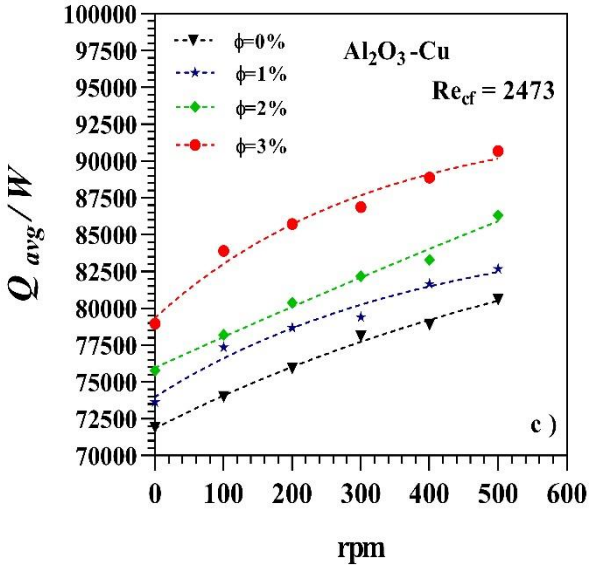
ϕ=0%
ϕ=1%
ϕ=2%
ϕ=3%
Al2O3 -Cu
Recf = 2473
Q avg / W
rpm
c)

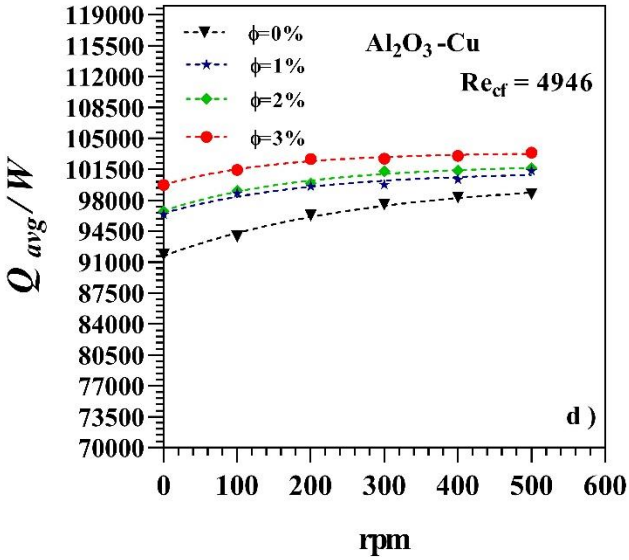
ϕ=0%
ϕ=1%
ϕ=2%
ϕ=3%
Al2O3 -Cu
Recf = 4946
Q avg / W
rpm
d)

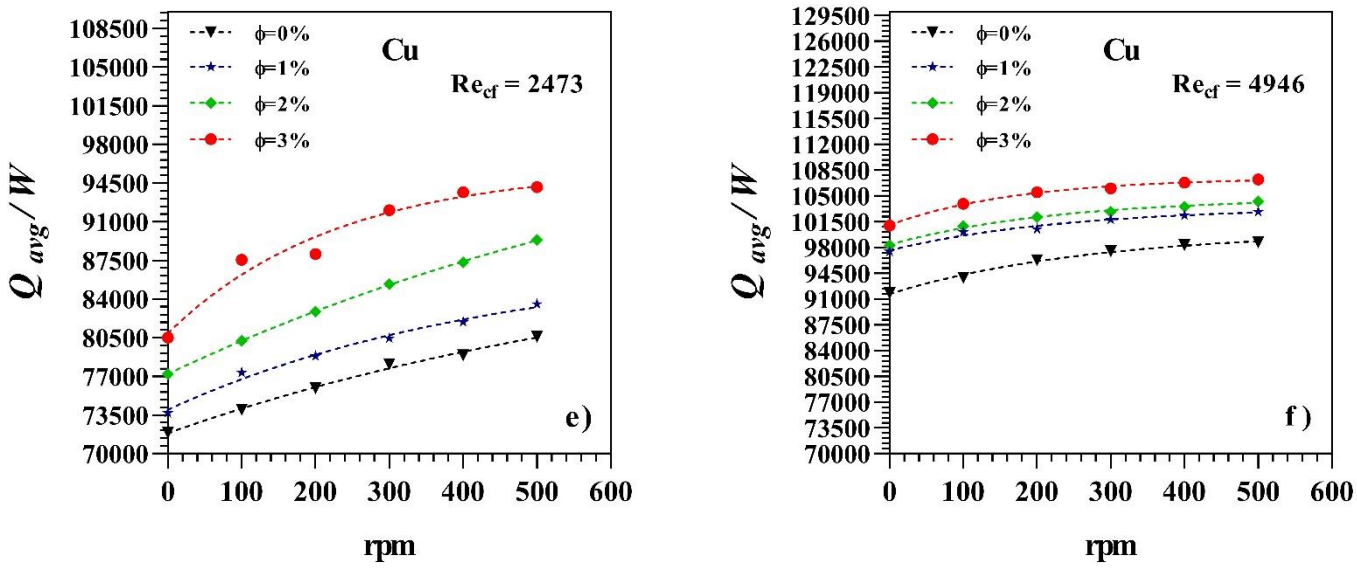

Figure 4.16 Ratio of average heat transfer and pumping power with rotational speed.

4.3. 3D numerical model of the double tube heat exchanger fitted with perforated circular rings (PCR).

After completing the analysis of the original geometry of the heat exchanger with different nanofluids and inner tube rotational speeds, modifications in the geometry were proposed to enhance the exchanger performance. Firstly, the use of fitted circular rings was addressed. Then, perforated circular rings were proposed to increase the heat exchanger efficiency. An optimized configuration for the heat exchanger was found, and then the analysis of the different nanofluids and inner tube rotational speeds was performed.

4.3.1 Addition of typical circular rings (TCR)

This first subsection discusses the effects of adding circular rings fitted in the inner tube of the heat exchanger, with different configurations.

4.3.1.1 Effect of ring pitch ratio (PR)

The NTU and pressure drop as a function of the Reynolds number for different Typical Circular Rings (TCR) and a plain tube are presented in Figure 4.17.

Figure 4.17 (a) shows the results for a tube with 5 rings and a pitch length of 200 mm, with different pitch ratio values (5.64, 4.4 and 3.61) compared with the plain tube. Firstly, an increase in the NTU with the Reynolds number is apparent, as a consequence of the higher convection rates. In addition, the TCR inserts contribute to enhance heat transfer with respect to the plain tube. The higher turbulence levels generated by the TCR inserts may be the explanation behind this behavior. At Re_{cf} = 4,946, NTU improves by 5.5, 8.8 and 10.11% for PR values of 5.64, 4.4 and 3.61 when compared to a plain tube.

Regarding the pressure drop caused by the TCR inserts, Figure 4.17(b) depicts the corresponding results for the same configurations as Figure 4.17(a). The pressure drop increases with the inserts by 28, 85 and 670% for PR values of 3.61, 4.4 and 5.64 when compared to the plain tube. The odd behavior at PR=3.61 should be investigated with further detail. In any case, the maximum difference in the NTU values with PR=4.4. and 3.61 is 1.2%. Hence, TCR inserts at PR=4.4 could be the most adequate option for enhancing heat transfer in the exchanger with a low pressure drop increase.

The results for a tube with 11 rings with a pitch length of 100 mm and PR values of 2.82, 2.2 and 1.8 are shown in Figure 4.18 at Re_{cf} = 4,946. Enhancements of 8, 12.6 and 14.86% for PR values of 2.82, 2.2 and 1.8 were found when compared to the plain tube. The pressure drop increased by 44.26, 168.72 and 838.8% respectively. In this case, the PR=2.2 would be selected as the most adequate option, as the maximum difference between the NTU with the PR=1.8 is 2%. Hence, 11 TCR inserts at PR=2.2 would be the best option for optimizing the heat transfer performance and pressure drop of the exchanger.

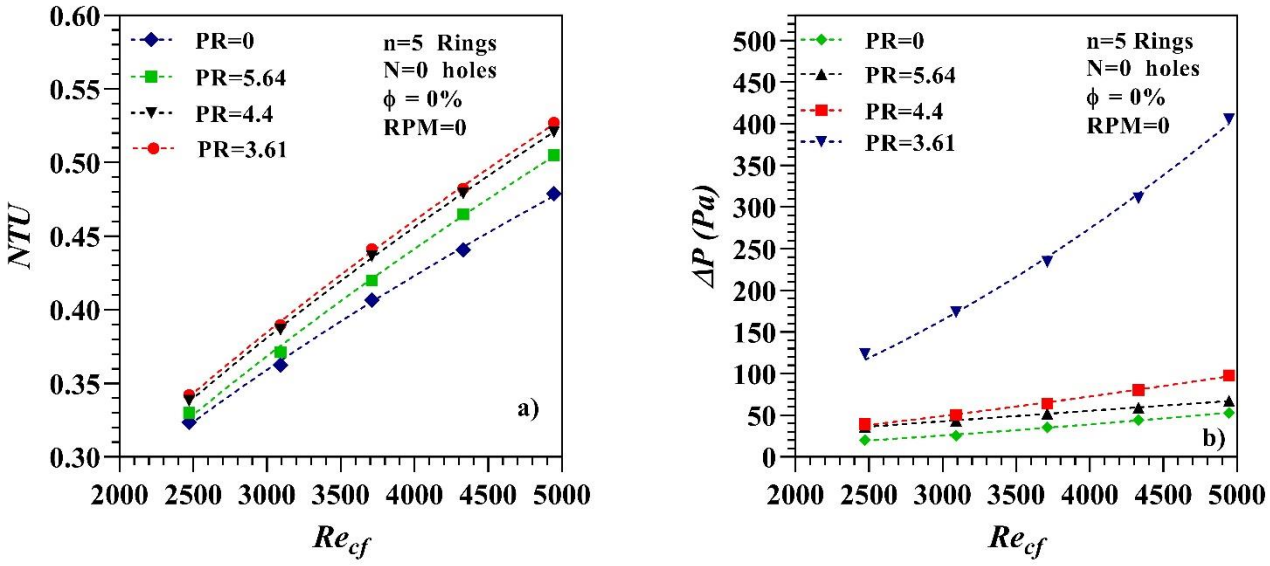

Figure 4.17 Different pitch ratio at n=5 and N=0.

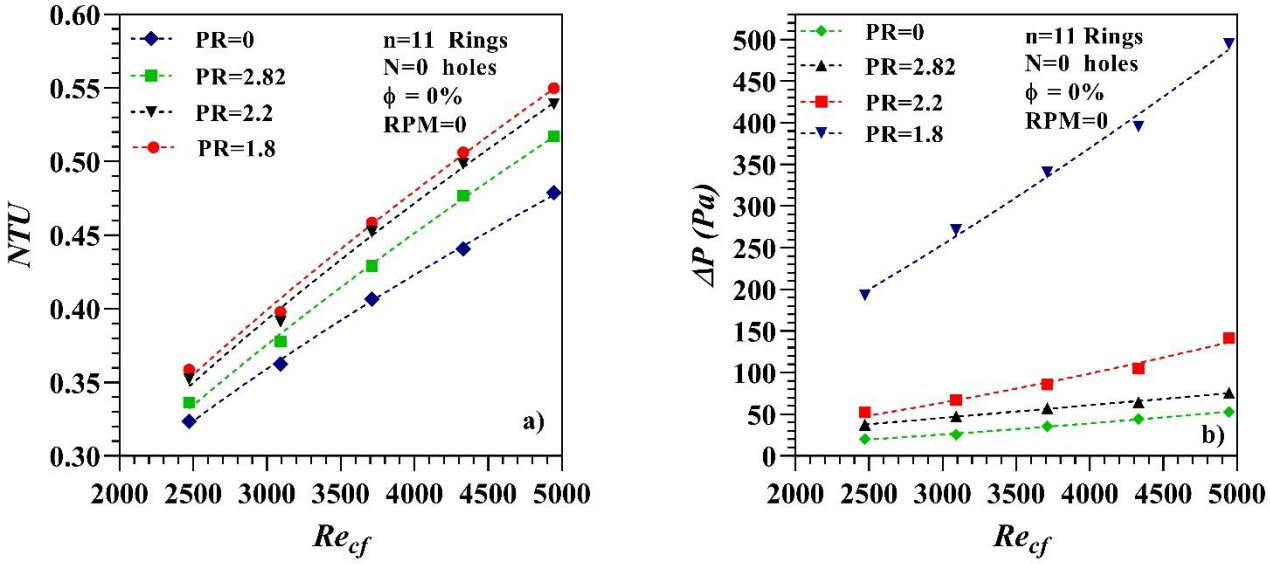

Figure 4.18 Different pitch ratio at n=11 and N=0.

4.3.2 Addition of perforated circular rings (PCR)

After finding the optimum number and pitch ratio of the circular rings for fitting the inner tube of the heat exchanger, the effect of including perforated holes in the rings

was addressed with the 3D model.

4.3.2.1. Effect of the number of perforated holes

Figure 4.19 shows the effects of adding perforated holes to the circular ring inserts as a function of Reynolds number in the NTU and pressure drop. Starting with the 11 circular rings fitted into the tube at a pitch ratio PR=2.2, the addition of N=4 and 8 holes was evaluated.

The results show the NTU of a heat exchanger with perforated circular rings (PCR) is higher than with typical circular rings (TCR), as well as the plain tube. With 4 and 8 holes respectively, the NTU is 1.26 and 6% higher than without holes at PR=2.2 and Re_{cf} = 4,946. Additionally, the pressure drop decreases with the addition of holes, which is a beneficial effect. For 4 and 8 holes, pressure drop decreases by 6.54 and 16.67% when compared to the same situation without holes. Summarizing all the results, the perforated circular rings with PR=2.2 and 8 holes seem to be the best option for optimizing the heat exchanger in terms of heat transfer maximization and pressure drop reduction.

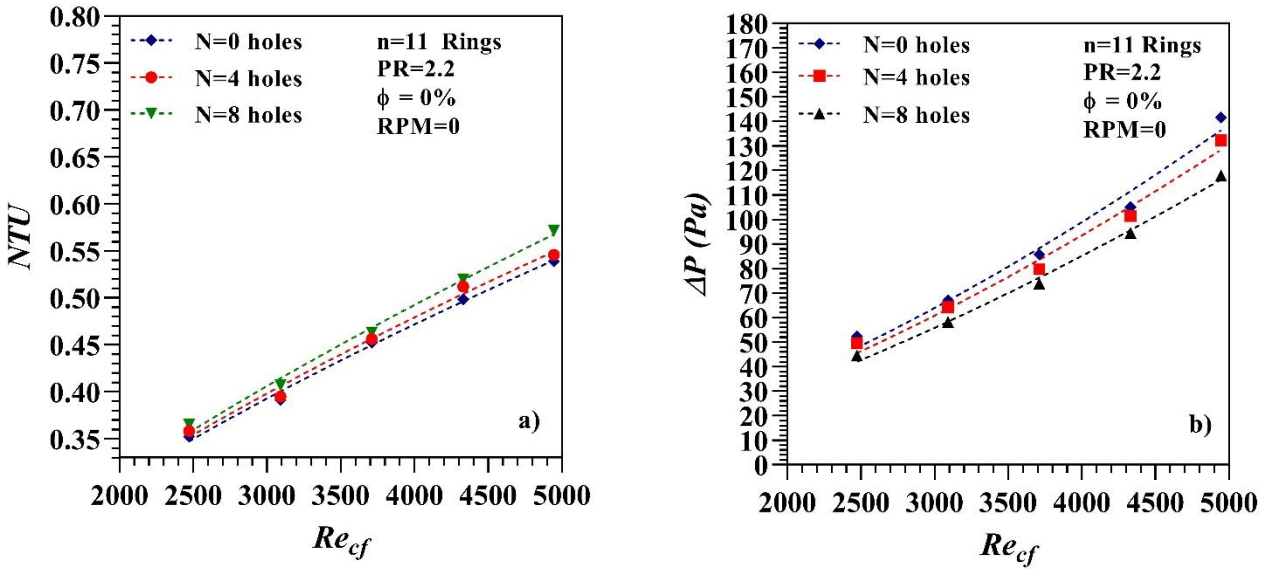

Figure 4.19 Comparison between number of holes.

Once an optimal configuration for the heat exchanger was found, the analysis of the different nanofluids at concentrations from 0 to 3% and inner tube rotational speeds from 0 to 500 rpm was performed, as done with the original heat exchanger. The optimal configuration has perforated circular ring inserts at a PR=2.2 with 8 holes.

4.3.3. Heat Transfer Rate

Figure 4.20 presents the results for the heat transfer rate of the proposed heat exchanger configuration with different nanofluids and inner tube rotational speeds. As already observed in the previous simulations, average heat transfer rate increases with the rotational speed. At Re_{cf}=2,473, the increase lies between 1.47 and 17.45 for rotational speeds from 100 to 500 rpm, when compared to the static tube (Figure 4.20 (a)). At Re_{cf}=4,946, this increase is between 3.7 and 16%.

Concerning the addition of nanoparticles to the working fluid, heat transfer rate of the Al_2O_3-water nanofluid increased by 1.59, 3.54 and 4.32% at Re_{cf}=4,946 with respect to pure water when nanoparticles were added to 1, 2 and 3% concentration values, as shown in Figure 4.20 (b-d). At 1% concentration, including inner tube rotation from 0 to 500 rpm increased heat transfer by 1.25 to 18.22% at Re_{cf}=2,473 with respect to pure water. At Re_{cf}=4,946, the increase lied between 1.59 and 19.1%. A similar effect was observed at 2% concentration, where heat transfer was increased by 3.54 to 29.13% at Re_{cf}=4,946; as well as at 3% concentration, where these values lied between 4.32 and 32.33%.

Figure 4.20 (e-g) shows the average heat transfer rate for the Al_2O_3-Cu-water nanofluid at different rotational speeds. Improvements between 2.94 and 22.7% were found for 1% concentration when increasing the rotational speed between 0 and 500 rpm, between 3.87 and 31.37% for 2% concentration, and between7.45 and 33.94% for 3% concentration.

Again, the maximum average heat transfer rate was found for the Cu-water nanofluid at the highest rotational speed and nanoparticle concentration. The results, depicted in Figure 4.20 (h-j), showed improvements between 4.48 and 24% for 1% concentration when increasing the rotational speed from 0 to 500 rpm, between 6.9 and 33% for 2% concentration, and between 8.27 and 34.52% for 3% concentration.

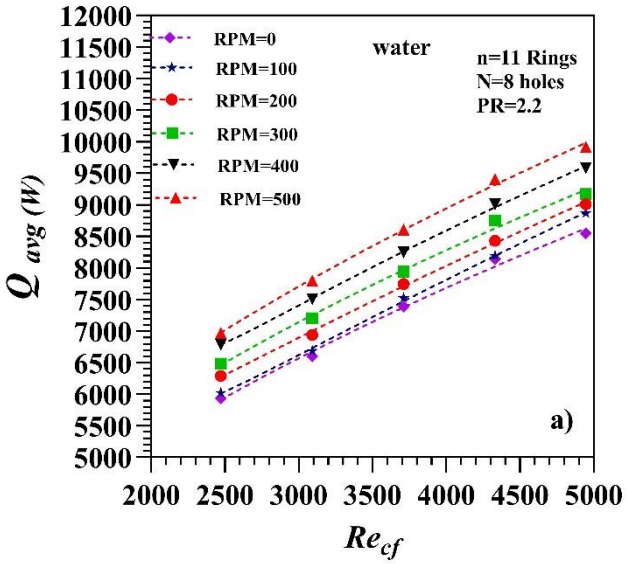
RPM=0
RPM=100
RPM=200
RPM=300
RPM=400
RPM=500
water
n=11 Rings
N=8 holes
PR=2.2
a)
Q_{avg} (W)
Re_{cf}

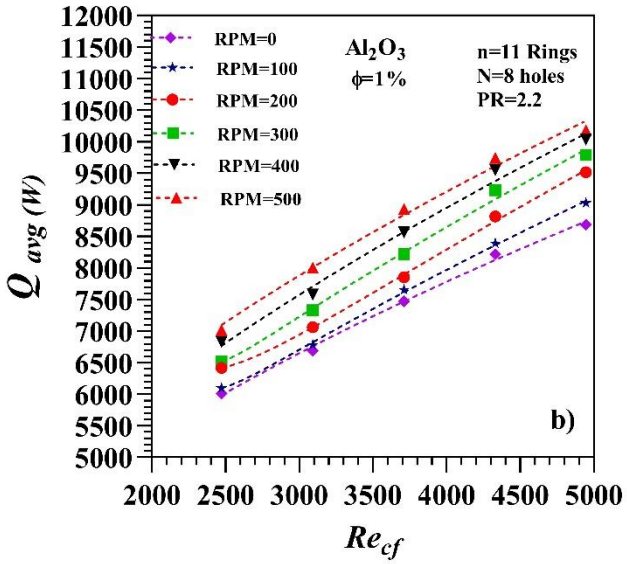
RPM=0
RPM=100
RPM=200
RPM=300
RPM=400
RPM=500
Al_2O_3
ϕ=1%
n=11 Rings
N=8 holes
PR=2.2
b)
Q_{avg} (W)
Re_{cf}

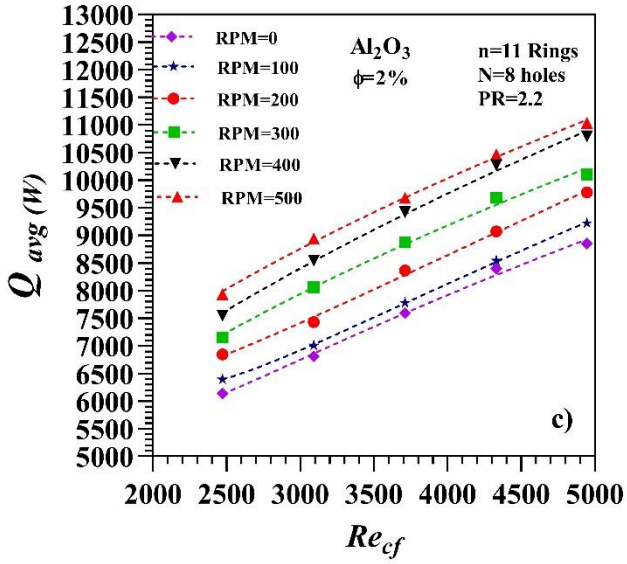
RPM=0
RPM=100
RPM=200
RPM=300
RPM=400
RPM=500
Al_2O_3
ϕ=2%
n=11 Rings
N=8 holes
PR=2.2
c)
Q_{avg} (W)
Re_{cf}

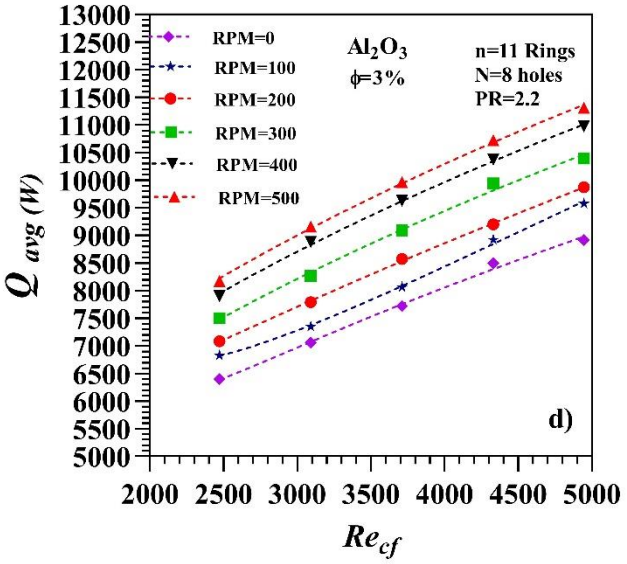
RPM=0
RPM=100
RPM=200
RPM=300
RPM=400
RPM=500
Al_2O_3
ϕ=3%
n=11 Rings
N=8 holes
PR=2.2
d)
Q_{avg} (W)
Re_{cf}

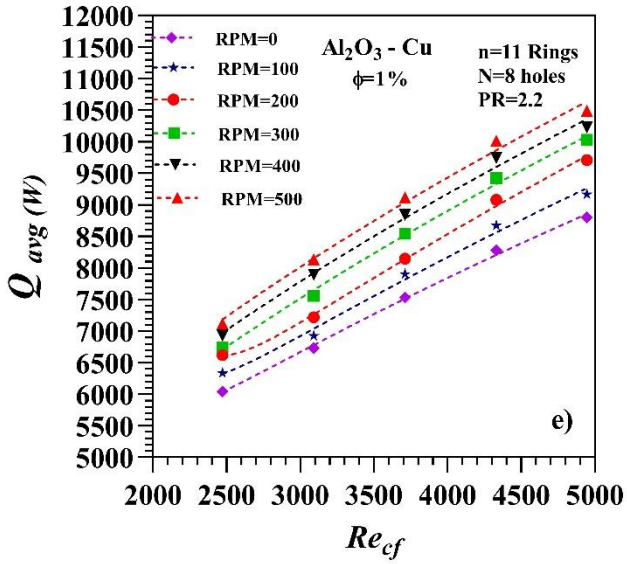
RPM=0
RPM=100
RPM=200
RPM=300
RPM=400
RPM=500
Al2O3 - Cu
ϕ=1%
n=11 Rings
N=8 holes
PR=2.2
e)
Q avg (W)
Recf

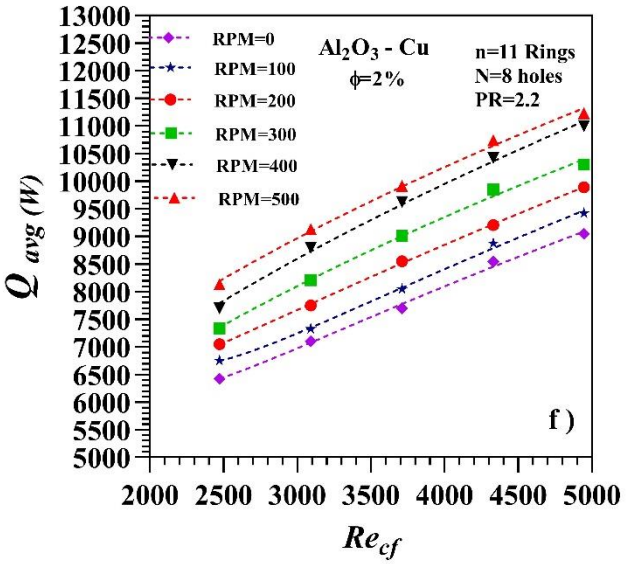
RPM=0
RPM=100
RPM=200
RPM=300
RPM=400
RPM=500
Al2O3 - Cu
ϕ=2%
n=11 Rings
N=8 holes
PR=2.2
f)
Q avg (W)
Recf

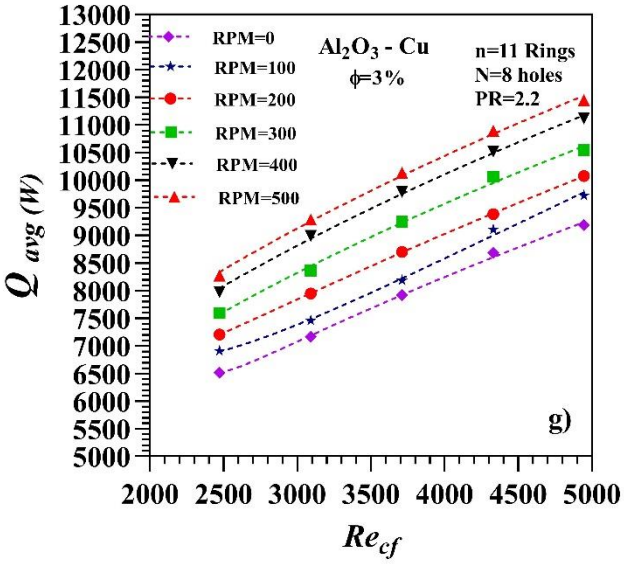
RPM=0
RPM=100
RPM=200
RPM=300
RPM=400
RPM=500
Al2O3 - Cu
ϕ=3%
n=11 Rings
N=8 holes
PR=2.2
g)
Q avg (W)
Recf

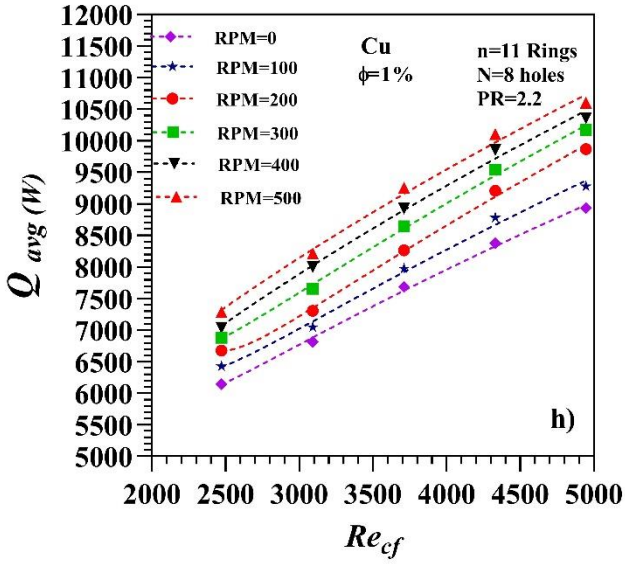
RPM=0
RPM=100
RPM=200
RPM=300
RPM=400
RPM=500
Cu
ϕ=1%
n=11 Rings
N=8 holes
PR=2.2
h)
Q avg (W)
Recf

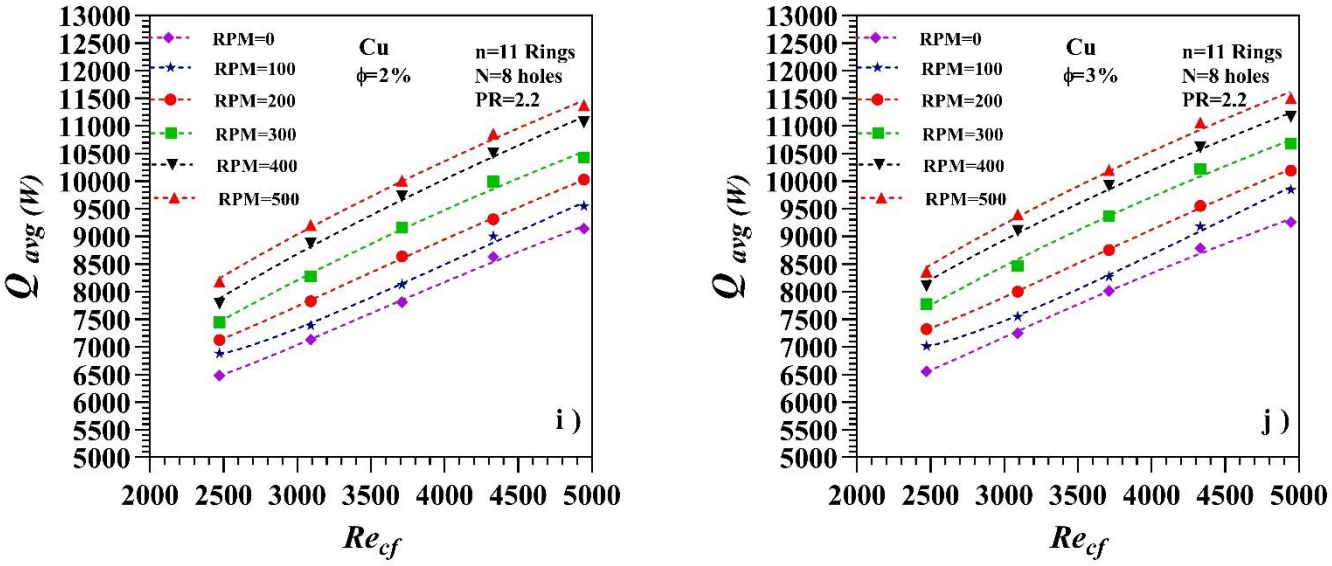

Figure 4.20 Average heat transfer rate variation with rotational speed

In order to provide a visual depiction of the temperature evolution inside the tube, Figure 4.21 shows the temperature contours at different cross sections of the concentric tube for the Cu- water nanofluid at 3% volume concentration for different inner tube rotational speeds and at Re_{cf} of 2,473 and 4,946. The circular rings with holes help to distribute thermal energy, as it is visible in the temperature contours. The increase of the rotational speed also contributes to temperature uniformity. It may be appreciated as well how the hot fluid has been cooled down at z=0.1 and how the cold fluid has been heated up at z=0.9.

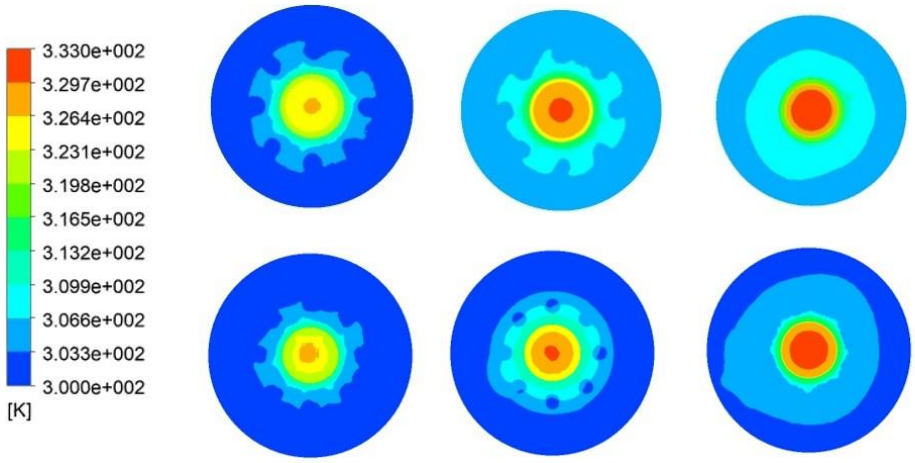

a)

0 rpm

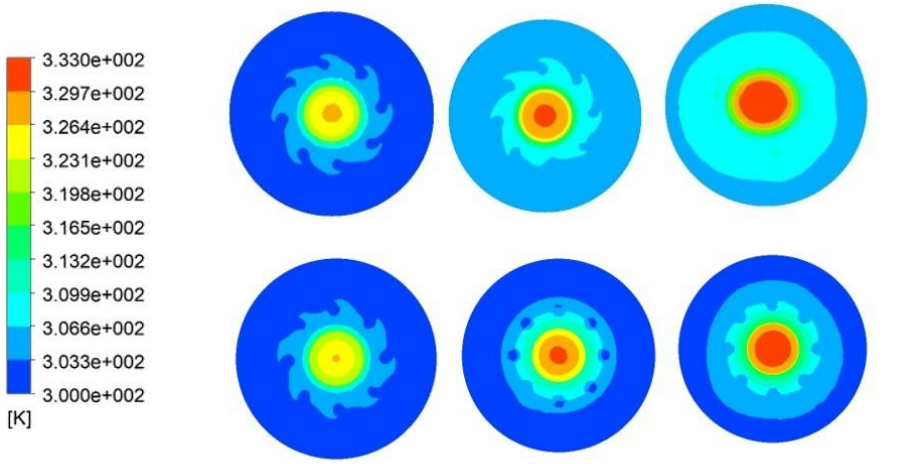

b)

100 rpm

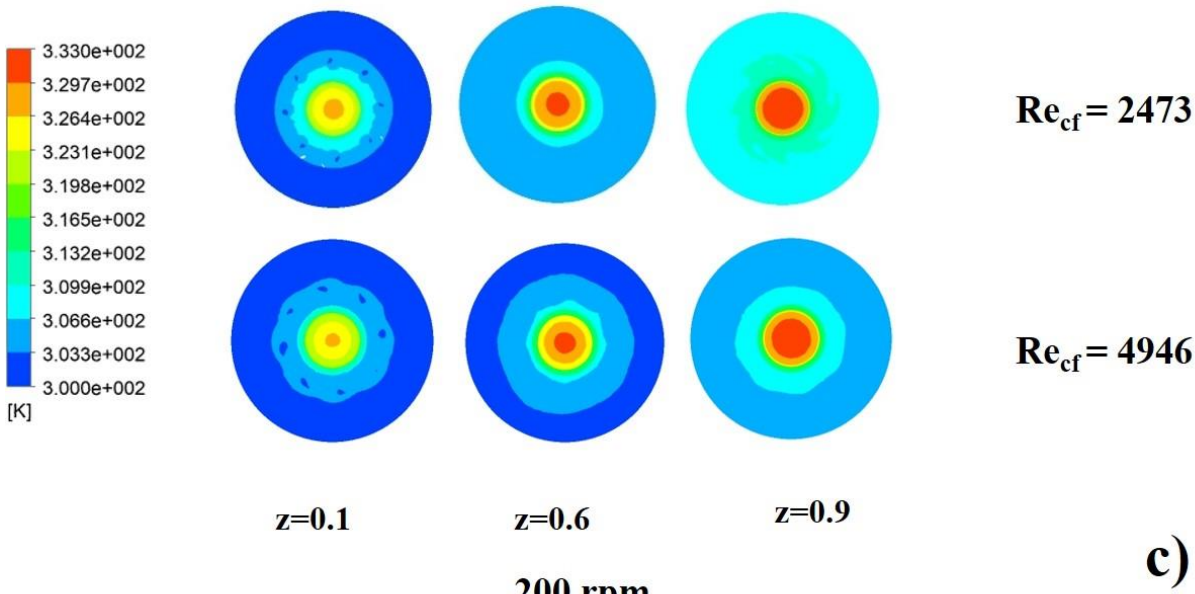

c)

200 rpm

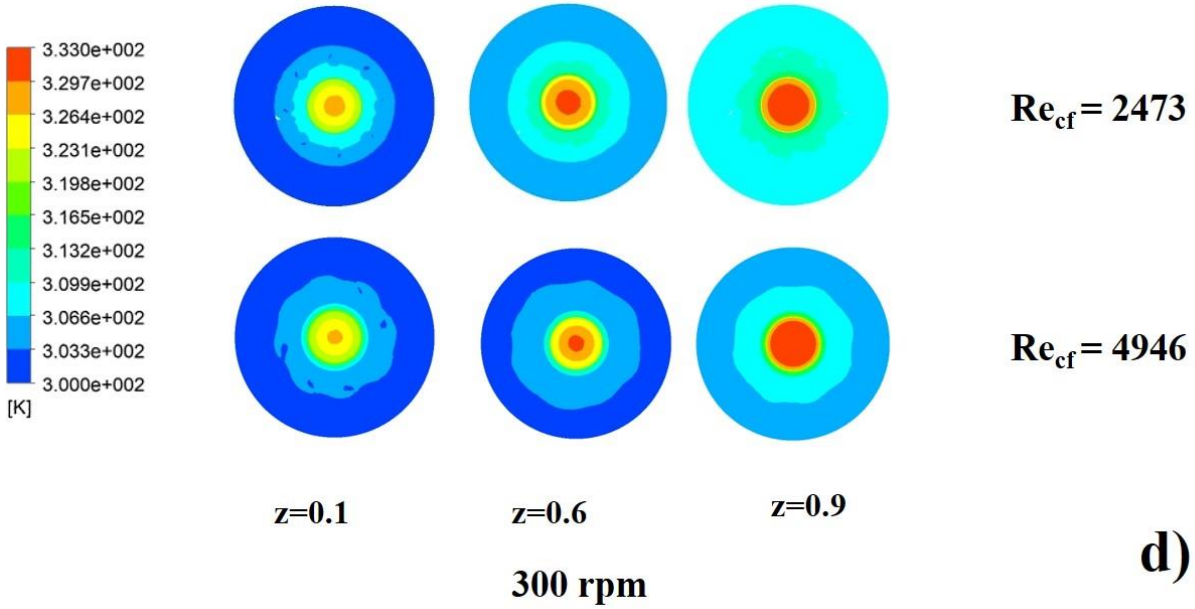

d)

300 rpm

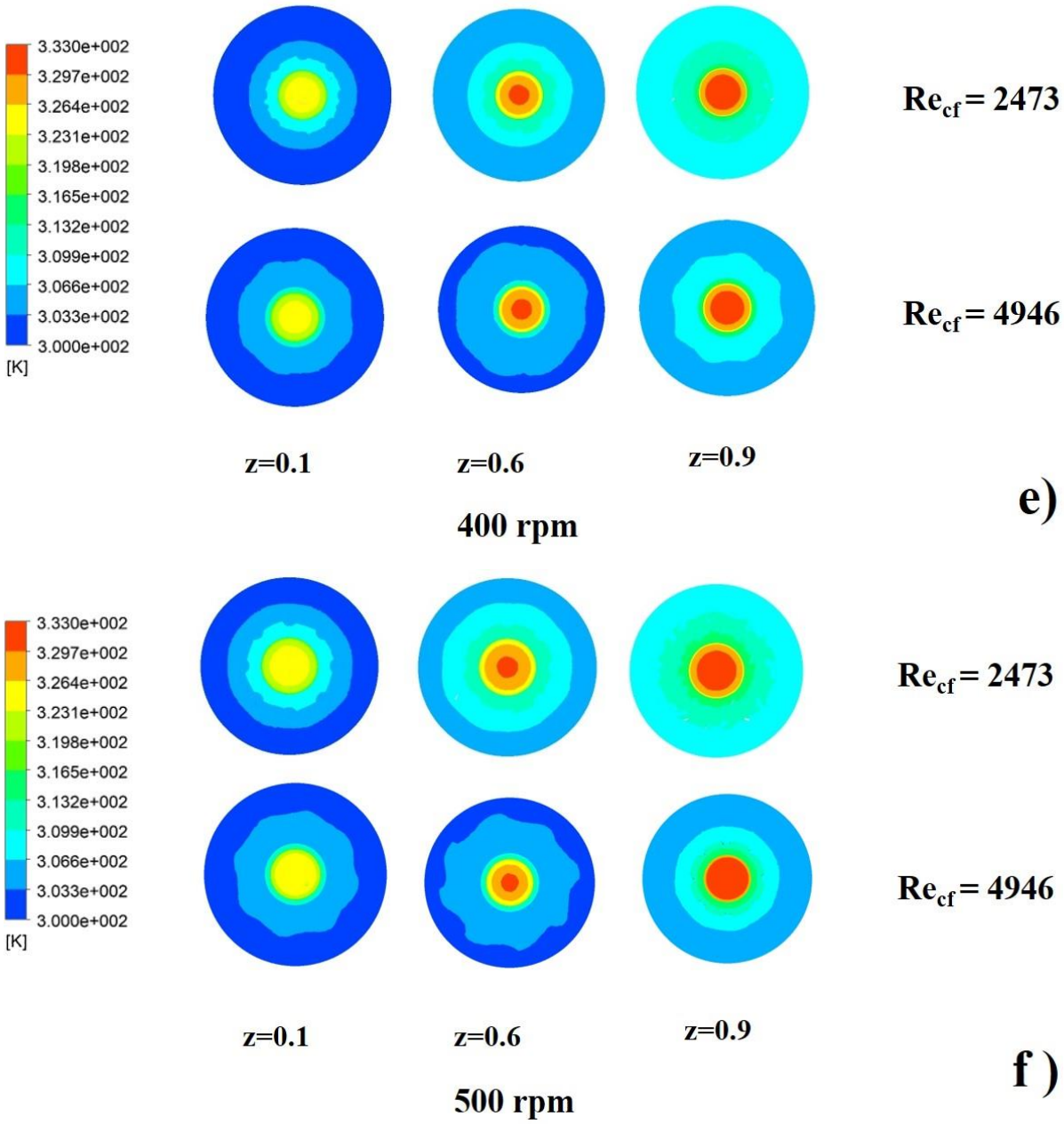

Figure 4.21 Temperature contour at cross section plane of 3D model (a) at Re_{cf} =2473, (b) at Re_{cf} =4946.

4.3.3 Number of Transfer Units (NTU)

Figure 4.22 shows the number of transfer units (NTU) as a function of nanoparticle concentration for the different nanofluids, cold fluid Reynolds number and inner tube

rotational speeds. Again, the increase in the Reynolds number and the inner tube rotational speed lead to an increase in the NTU.

The various plots also show the effect of the nanoparticle type and volume concentration. According to the results obtained, increasing the concentration of nanoparticles from 0 to 3% and the rotation speed from 0 to 500 rpm increases the heat transfer value and improves the efficiency of heat exchangers for all types of nanoparticles. The effect of rotational speed on convective heat transfer coefficient may be attributed to the swirling flow, which becomes stronger with increasing speeds. Furthermore, comparing the results obtained with different nanofluids and water, the advantage of nanoparticles is obvious, as the NTU increases significantly.

Figures 4.22 (a-d) depict NTU at 1% volume concentration. It may be observed that the Cu-water nanofluid has the highest performance, the Al_2O_3-Cu hybrid nanofluid the second one, and the Al_2O_3-water nanofluid the lowest one. At 500 rpm and Re_{cf}= 2,473, the NTU is enhanced by 33.5, 29 and 26.4% respectively for the Cu-water nanofluid, the Al_2O_3-Cu hybrid nanofluid, and the Al_2O_3-water nanofluid when compared to pure water at 0 rpm. A similar effect is observed at Re_{cf} = 4,946, where the NTU is enhanced by 37.63% for Cu-water, 35.5%for Al_2O_3-Cu and 29.8 % for Al_2O_3-water.

At 2% volume concentration, the NTU enhancement is of 59.12% for Cu-water, 57.8% for Al_2O_3-Cu-water and 51.96% for Al_2O_3-water at Re_{cf} = 2,473 and 500 rpm when compared to pure water at 0 rpm (Figures 4.22 (e-g)). Similarly, at Re_{cf} = 4,946, the maximum enhancement of NTU is 54.14 % for Cu-water, 51.1 % for Al_2O_3-Cu and 47.32 % for Al_2O_3-water.

As shown in Figures 4.22 (h-j), at 3% volume concentration, an inner tube rotational speed of 500 rpm and Re_{cf}= 2,473, the NTU is enhanced by 64.83 % for Cu-water, 62% for Al_2O_3-Cu and 59.15% for Al_2O_3-water when compared to pure water at 0 rpm. Likewise, at Re_{cf} = 4,946, maximum NTU enhancement is 57.35 % for Cu-water, 56.29 % for Al_2O_3-Cu and 53.13 % for Al_2O_3-water. Therefore, the Cu-water nanofluid seems to be the most efficient in terms of improving the performance of the exchanger.

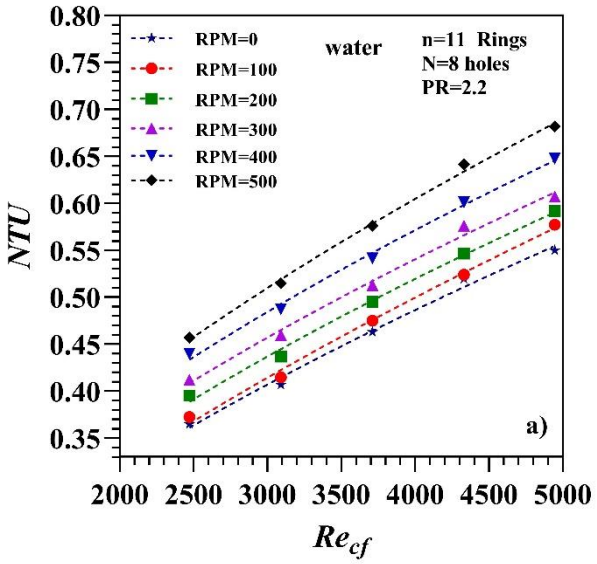
RPM=0
RPM=100
RPM=200
RPM=300
RPM=400
RPM=500
water
n=11 Rings
N=8 holes
PR=2.2
a)
NTU
Re_{cf}

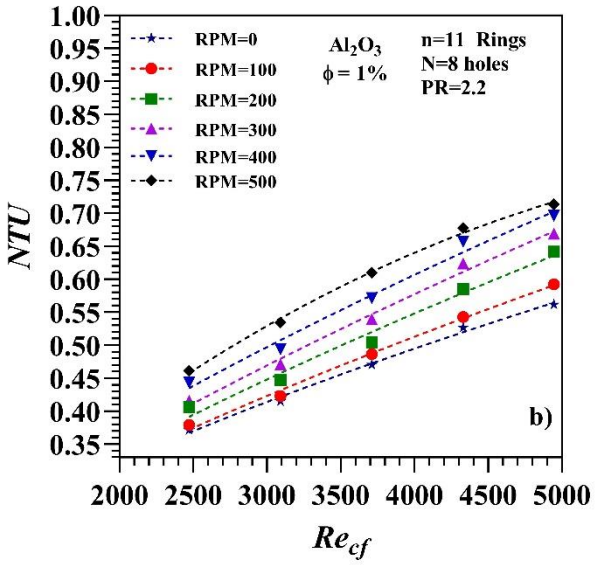
RPM=0
RPM=100
RPM=200
RPM=300
RPM=400
RPM=500
Al_2O_3
ϕ = 1%
n=11 Rings
N=8 holes
PR=2.2
b)
NTU
Re_{cf}

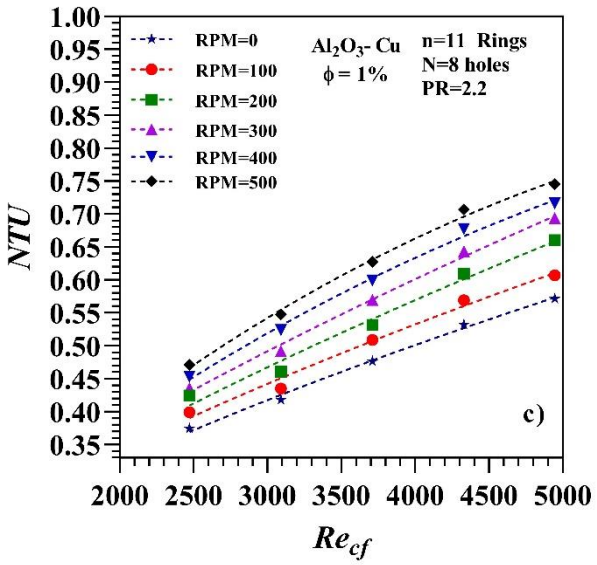
RPM=0
RPM=100
RPM=200
RPM=300
RPM=400
RPM=500
Al_2O_3- Cu
ϕ = 1%
n=11 Rings
N=8 holes
PR=2.2
c)
NTU
Re_{cf}

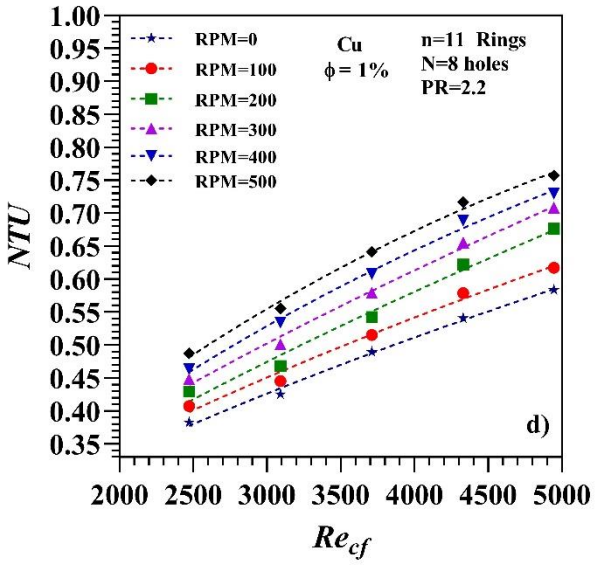
RPM=0
RPM=100
RPM=200
RPM=300
RPM=400
RPM=500
Cu
ϕ = 1%
n=11 Rings
N=8 holes
PR=2.2
d)
NTU
Re_{cf}

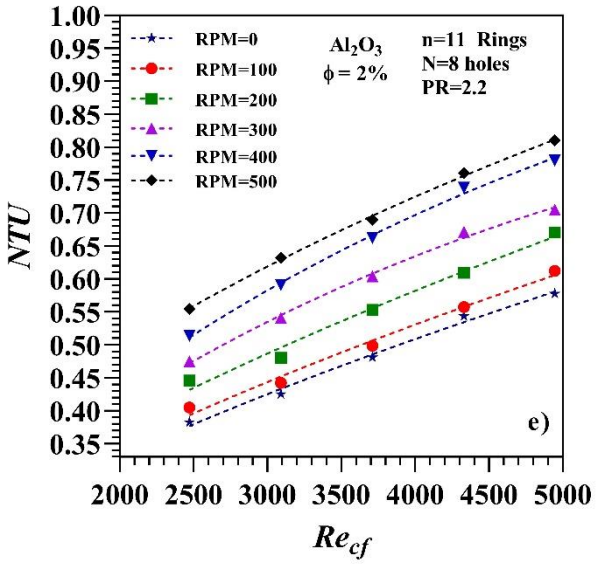
RPM=0
RPM=100
RPM=200
RPM=300
RPM=400
RPM=500
Al_2O_3
ϕ = 2%
n=11 Rings
N=8 holes
PR=2.2
e)
NTU
Re_{cf}

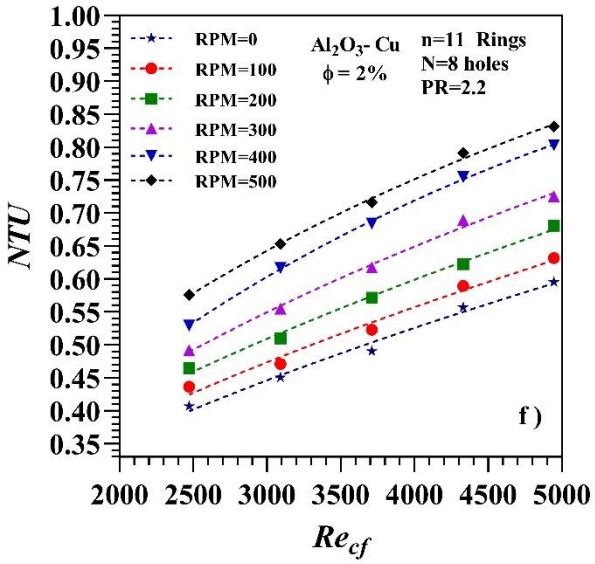
RPM=0
RPM=100
RPM=200
RPM=300
RPM=400
RPM=500
Al_2O_3- Cu
ϕ = 2%
n=11 Rings
N=8 holes
PR=2.2
f)
NTU
Re_{cf}

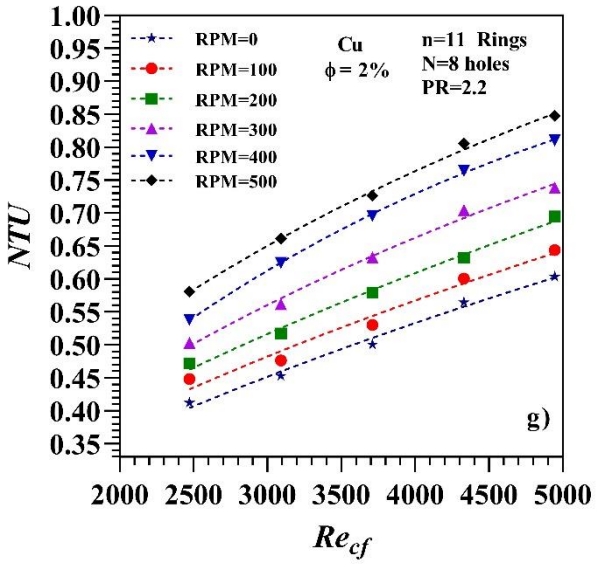
RPM=0
RPM=100
RPM=200
RPM=300
RPM=400
RPM=500
Cu
ϕ = 2%
n=11 Rings
N=8 holes
PR=2.2
g)
NTU
Re_{cf}

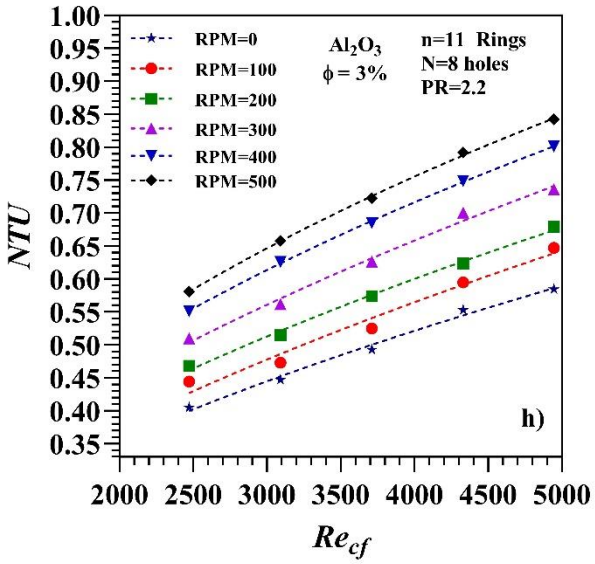
RPM=0
RPM=100
RPM=200
RPM=300
RPM=400
RPM=500
Al_2O_3
ϕ = 3%
n=11 Rings
N=8 holes
PR=2.2
h)
NTU
Re_{cf}

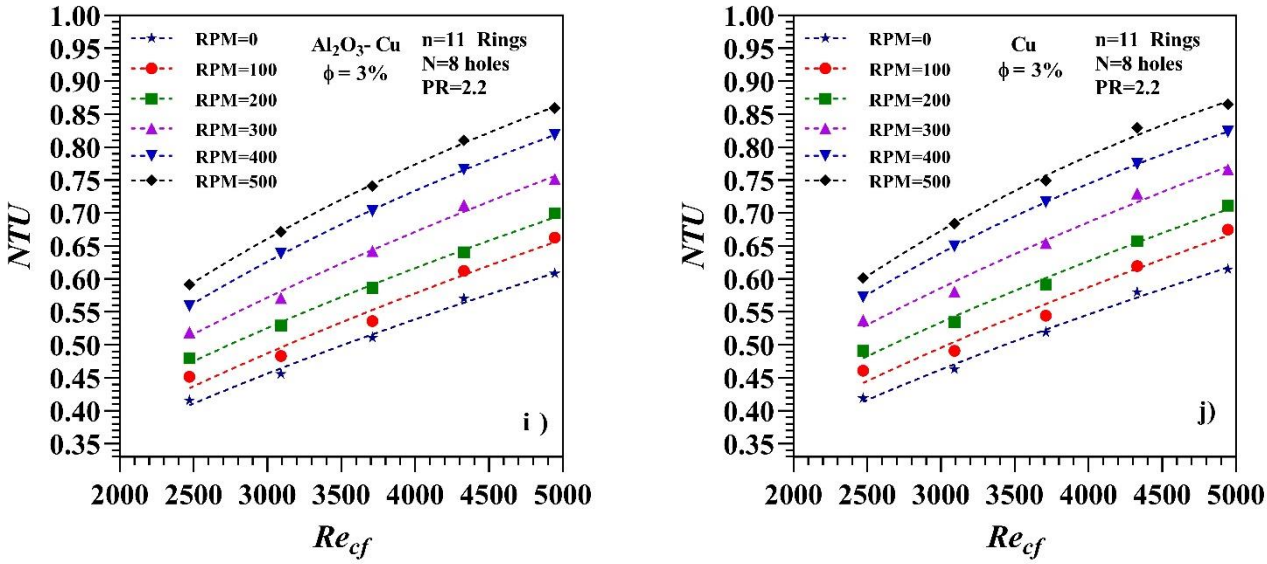

Figure 4.22 Effect of rotational speed, PCR and concentration on NTU.

4.3.4 Effectiveness (ε)

Heat exchanger effectiveness values shows a similar trend as the NTU. Figure 4.23 shows the effect of nanofluid volume concentration and cold fluid Reynolds number in the heat exchanger effectiveness for inner tube rotational speeds form 0 to 500 rpm. The results for 1% volume concentration are presented in Figures 4.23 (a-d). It may be observed that the Cu-water has the best performance, followed by the Al_2O_3-Cu hybrid nanofluid and the Al_2O_3-water nanofluid. At Re_{cf}= 4,946 and 500 rpm, the effectiveness is enhanced by 23.75, 22.55 and 19.2% respectively for them when compared to pure water at 0 rpm. Similarly, at 2% concentration and the same cold fluid Reynolds number, the maximum enhancement of effectiveness is 32.65 % for Cu-water, 31 % for Al_2O_3-Cu and 29 % for Al_2O_3-water, as shown in Figures 4.23 (e-g). Maximum enhancement of effectiveness occurs at 3% concentration and 500 rpm, being 34.27% for Cu-water, 33.7 % for Al_2O_3-Cu and 32 % for Al_2O_3-water, when compared to pure water at 0 rpm (Figures 4.23 (h-j)).

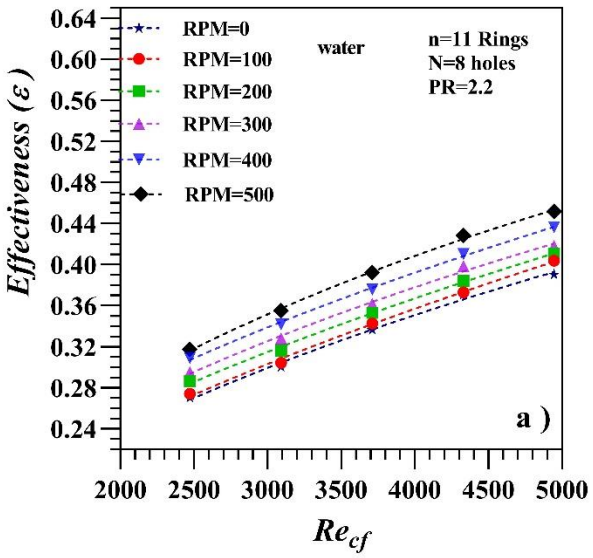
RPM=0
RPM=100
RPM=200
RPM=300
RPM=400
RPM=500
water
n=11 Rings
N=8 holes
PR=2.2
a)
Effectiveness (ε)
Re_cf

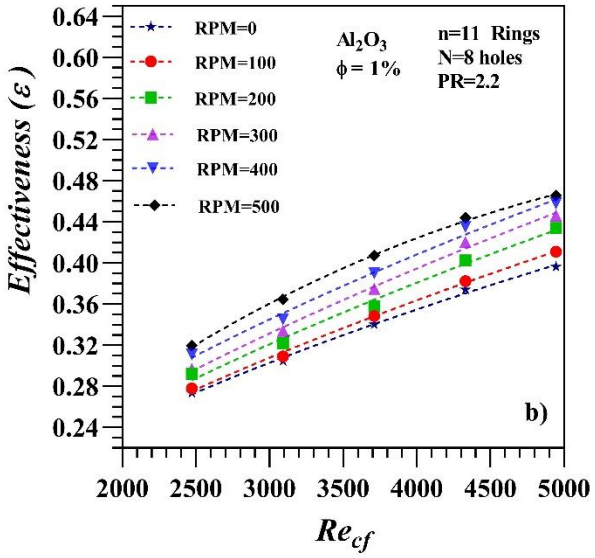
RPM=0
RPM=100
RPM=200
RPM=300
RPM=400
RPM=500
Al2O3
ϕ = 1%
n=11 Rings
N=8 holes
PR=2.2
b)
Effectiveness (ε)
Re_cf

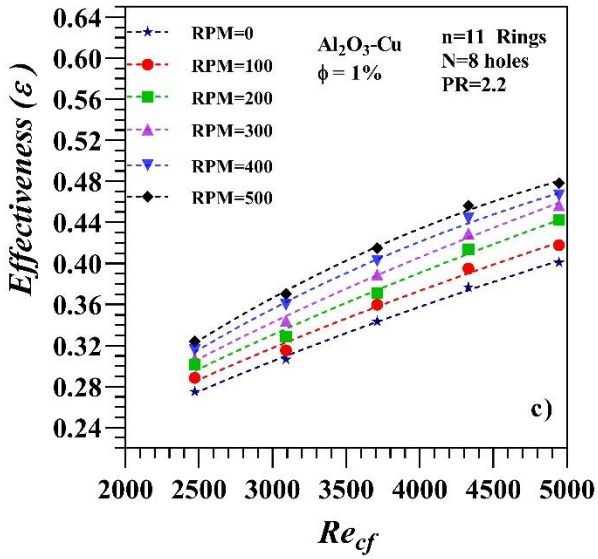
RPM=0
RPM=100
RPM=200
RPM=300
RPM=400
RPM=500
Al2O3-Cu
ϕ = 1%
n=11 Rings
N=8 holes
PR=2.2
c)
Effectiveness (ε)
Re_cf

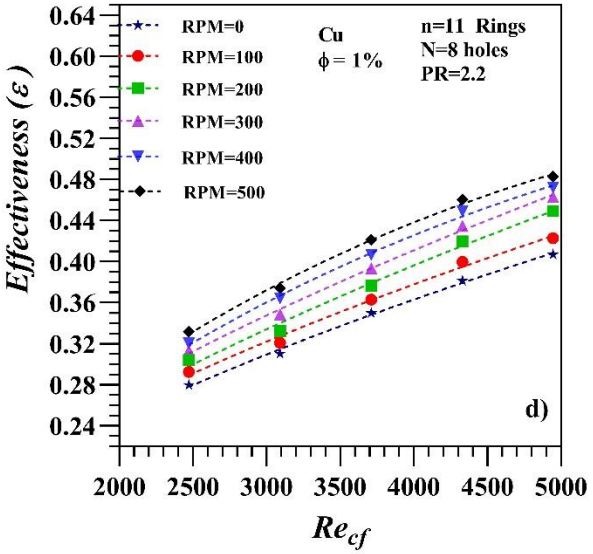
RPM=0
RPM=100
RPM=200
RPM=300
RPM=400
RPM=500
Cu
ϕ = 1%
n=11 Rings
N=8 holes
PR=2.2
d)
Effectiveness (ε)
Re_cf

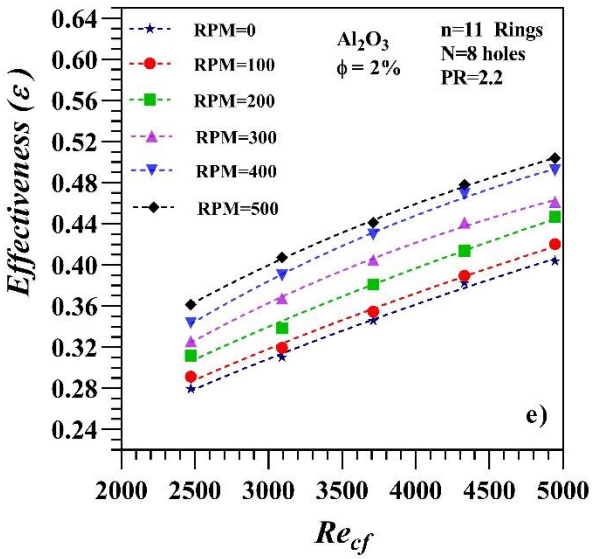
RPM=0
RPM=100
RPM=200
RPM=300
RPM=400
RPM=500
Al_2O_3
ϕ = 2%
n=11 Rings
N=8 holes
PR=2.2
e)
Effectiveness (ε)
Re_{cf}

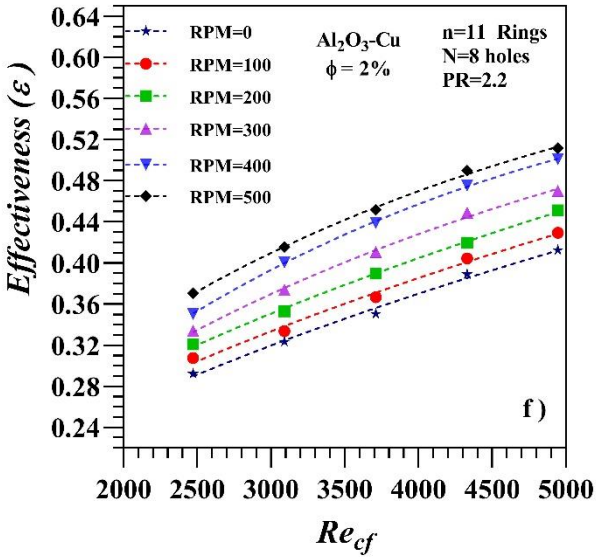
RPM=0
RPM=100
RPM=200
RPM=300
RPM=400
RPM=500
Al_2O_3-Cu
ϕ = 2%
n=11 Rings
N=8 holes
PR=2.2
f)
Effectiveness (ε)
Re_{cf}

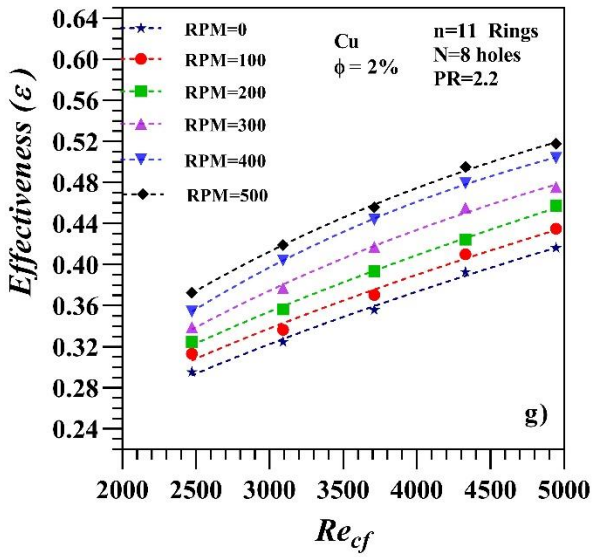
RPM=0
RPM=100
RPM=200
RPM=300
RPM=400
RPM=500
Cu
ϕ = 2%
n=11 Rings
N=8 holes
PR=2.2
g)
Effectiveness (ε)
Re_{cf}

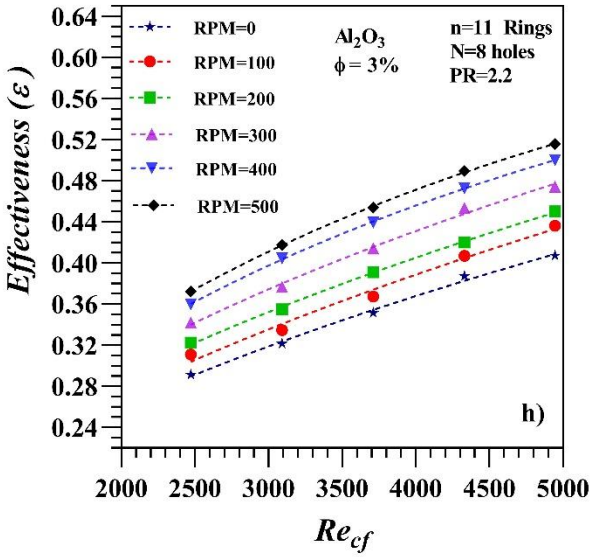
RPM=0
RPM=100
RPM=200
RPM=300
RPM=400
RPM=500
Al_2O_3
ϕ = 3%
n=11 Rings
N=8 holes
PR=2.2
h)
Effectiveness (ε)
Re_{cf}

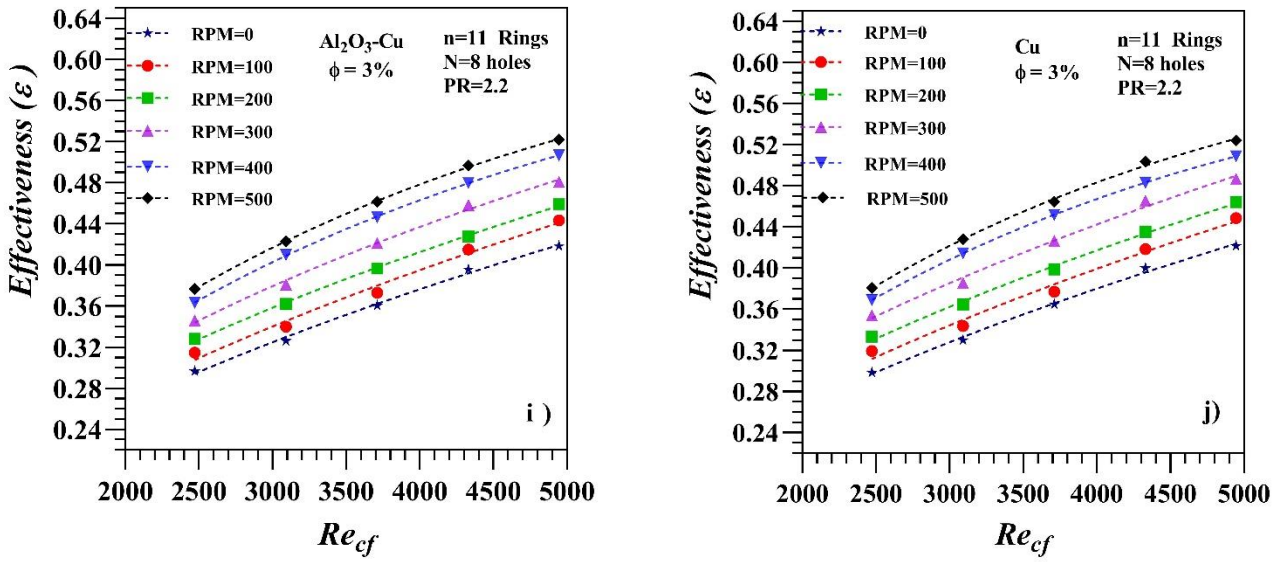

Figure 4.23 Effect of rotational speed, PCR and concentration on effectiveness.

4.3.5 Local Heat Transfer Coefficients

The inner and outer fluid local heat transfer coefficients are depicted in Figure 4.24. For all the studied cases, the heat transfer coefficient of the hot fluid was found to be higher than the coefficient of the cold fluid. The highest coefficients are found at the hot fluid inlet, falling as the hot fluid is cooled down and the cold fluid is heated up. Due to the change in the working fluid properties, the addition of nanoparticles increases both heat transfer coefficients. Additionally, the turbulence caused by the fluid swirl motion, the inner tube rotation and the PCRs seems to increase heat transfer coefficients.

The local heat transfer coefficient has been found to increase with the concentration of nanoparticles from 0 to 3% and the inner tube rotational speed from 0 to 500 rpm. Again, the best performance has been observed with the Cu-water nanofluid.

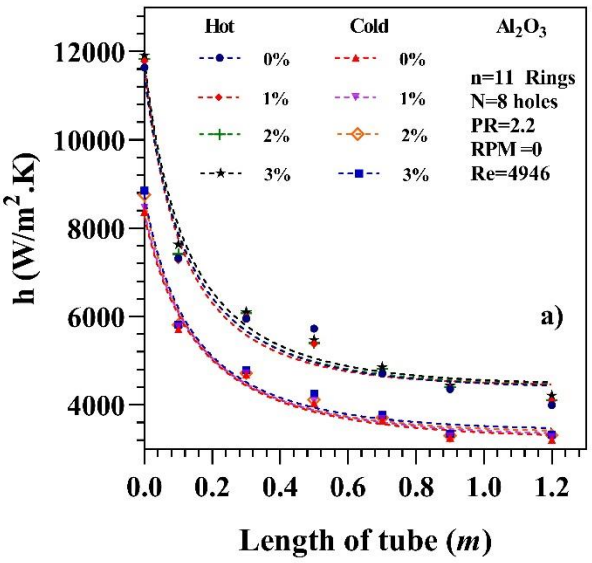
Hot
Cold
Al_2O_3
0%
1%
2%
3%
n=11 Rings
N=8 holes
PR=2.2
RPM =0
Re=4946
a)
h (W/m^2.K)
Length of tube (*m*)

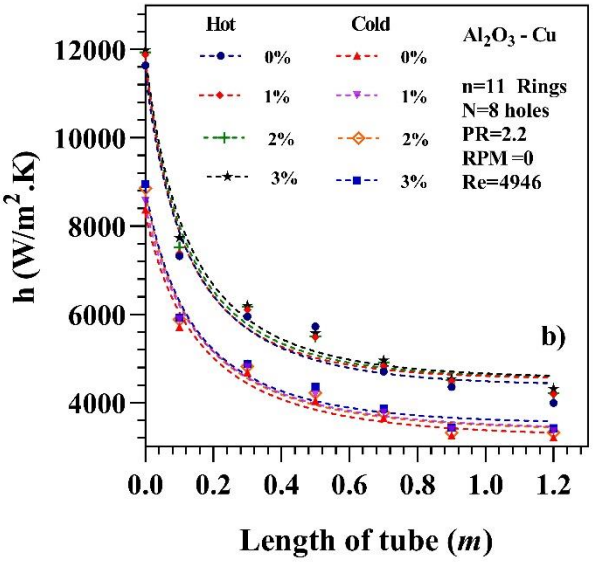
Hot
Cold
Al_2O_3 - Cu
0%
1%
2%
3%
n=11 Rings
N=8 holes
PR=2.2
RPM =0
Re=4946
b)
h (W/m^2.K)
Length of tube (*m*)

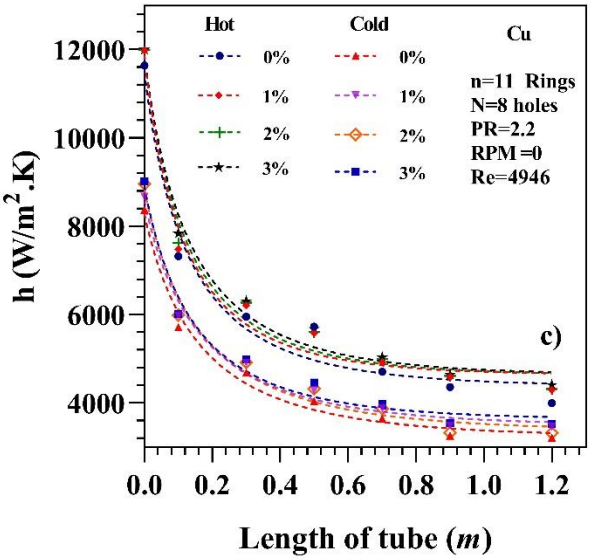
Hot
Cold
Cu
0%
1%
2%
3%
n=11 Rings
N=8 holes
PR=2.2
RPM =0
Re=4946
c)
h (W/m^2.K)
Length of tube (*m*)

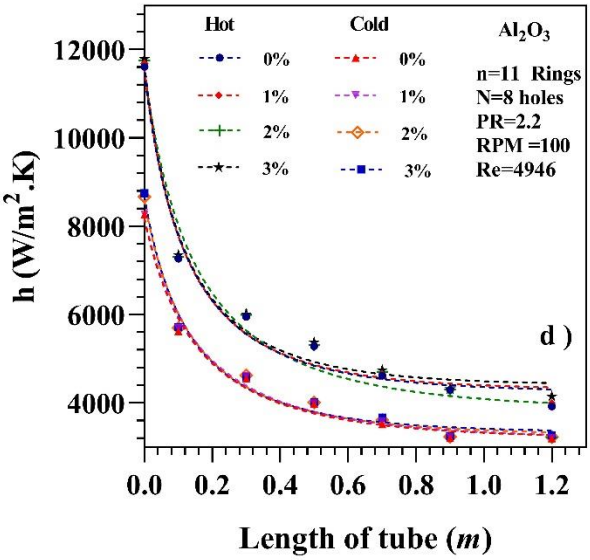
Hot
Cold
Al_2O_3
0%
1%
2%
3%
n=11 Rings
N=8 holes
PR=2.2
RPM =100
Re=4946
d)
h (W/m^2.K)
Length of tube (*m*)

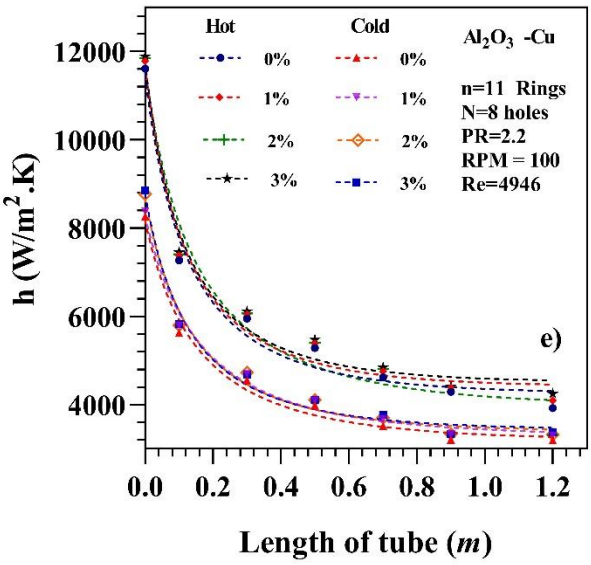
Hot
Cold
Al_2O_3 -Cu
0%
1%
2%
3%
n=11 Rings
N=8 holes
PR=2.2
RPM = 100
Re=4946
e)
h (W/m^2.K)
Length of tube (*m*)

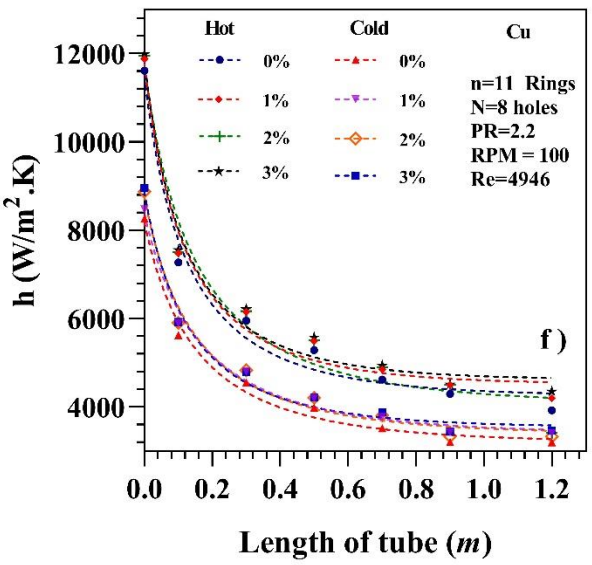
Hot
Cold
Cu
0%
1%
2%
3%
n=11 Rings
N=8 holes
PR=2.2
RPM = 100
Re=4946
f)
h (W/m^2.K)
Length of tube (*m*)

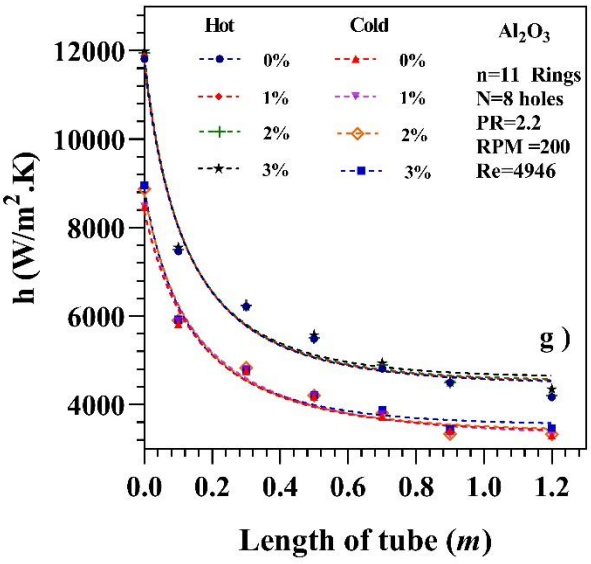
Hot
Cold
Al_2O_3
0%
1%
2%
3%
n=11 Rings
N=8 holes
PR=2.2
RPM =200
Re=4946
g)
h (W/m^2.K)
Length of tube (*m*)

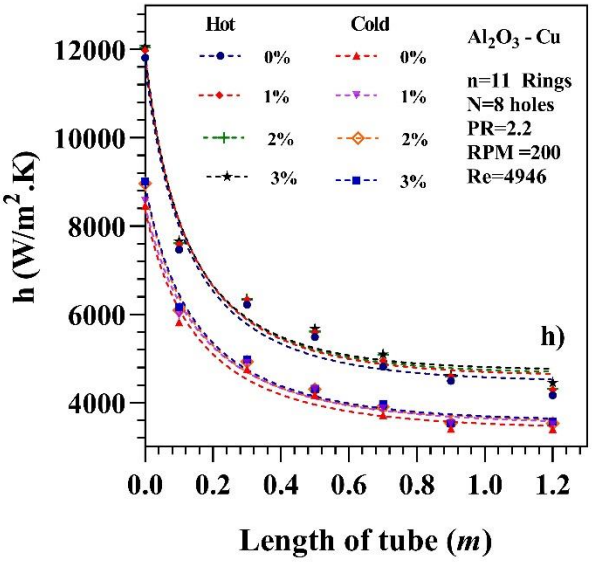
Hot
Cold
Al_2O_3 - Cu
0%
1%
2%
3%
n=11 Rings
N=8 holes
PR=2.2
RPM =200
Re=4946
h)
h (W/m^2.K)
Length of tube (*m*)

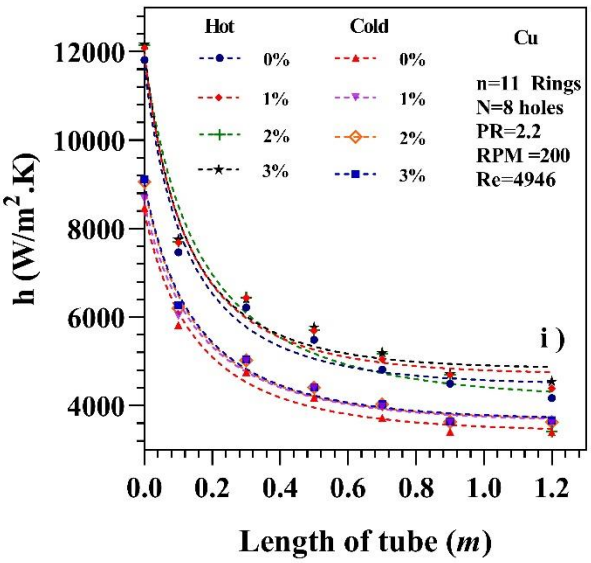
Hot
Cold
Cu
0%
1%
2%
3%
n=11 Rings
N=8 holes
PR=2.2
RPM =200
Re=4946
i)
h (W/m^2.K)
Length of tube (*m*)

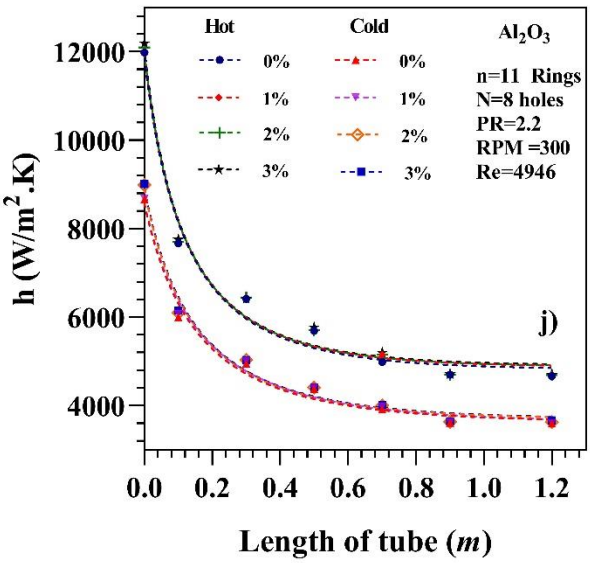
Hot
Cold
Al_2O_3
0%
1%
2%
3%
n=11 Rings
N=8 holes
PR=2.2
RPM =300
Re=4946
j)
h (W/m^2.K)
Length of tube (*m*)

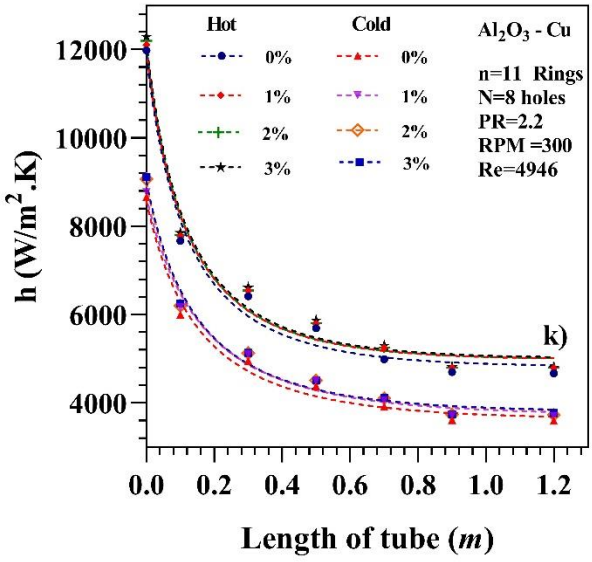
Hot
Cold
Al_2O_3 - Cu
0%
1%
2%
3%
n=11 Rings
N=8 holes
PR=2.2
RPM =300
Re=4946
k)
h (W/m^2.K)
Length of tube (*m*)

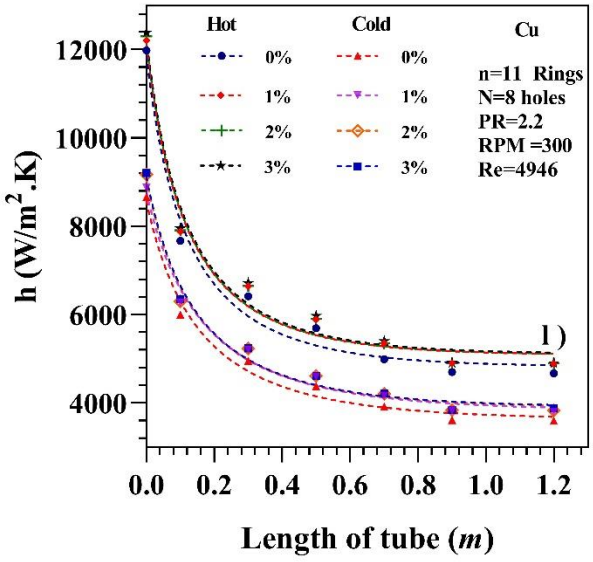
Hot
Cold
Cu
0%
1%
2%
3%
n=11 Rings
N=8 holes
PR=2.2
RPM =300
Re=4946
l)
h (W/m^2.K)
Length of tube (*m*)

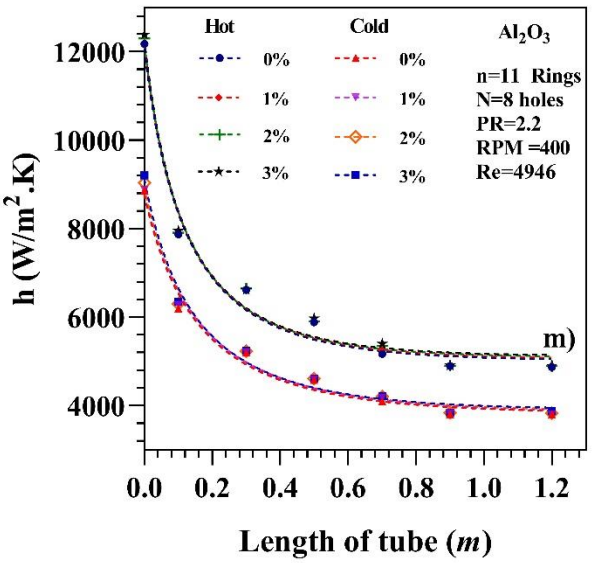
Hot
Cold
Al_2O_3
0%
1%
2%
3%
n=11 Rings
N=8 holes
PR=2.2
RPM =400
Re=4946
m)
h (W/m^2.K)
Length of tube (*m*)

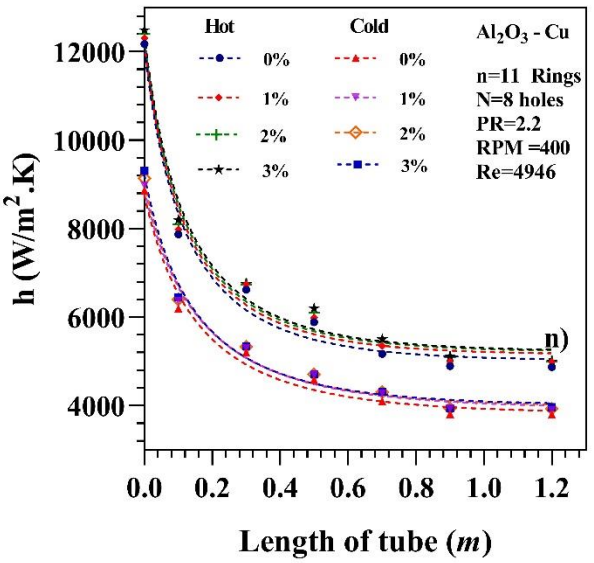
Hot
Cold
Al_2O_3 - Cu
0%
1%
2%
3%
n=11 Rings
N=8 holes
PR=2.2
RPM =400
Re=4946
n)
h (W/m^2.K)
Length of tube (*m*)

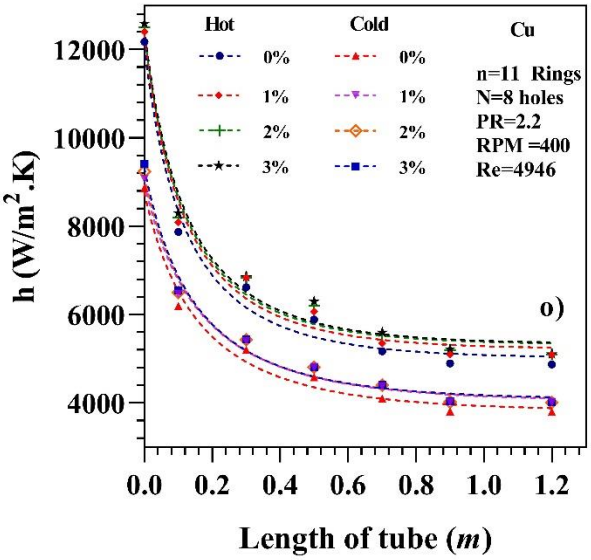
Hot
Cold
Cu
0%
1%
2%
3%
n=11 Rings
N=8 holes
PR=2.2
RPM =400
Re=4946
o)
h (W/m^2.K)
Length of tube (*m*)

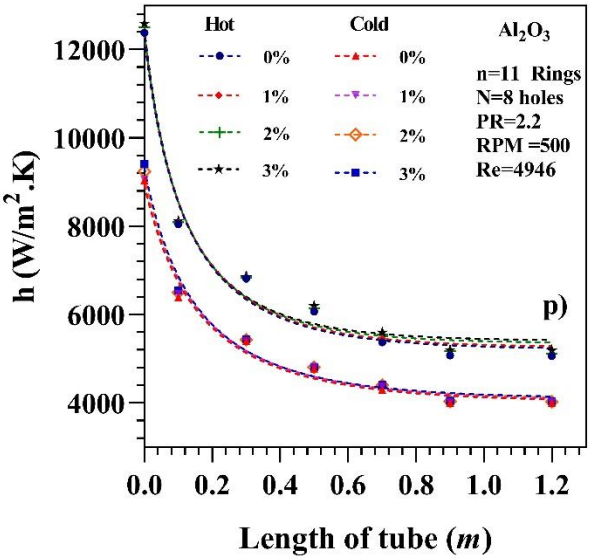
Hot
Cold
Al_2O_3
0%
1%
2%
3%
n=11 Rings
N=8 holes
PR=2.2
RPM =500
Re=4946
p)
h (W/m^2.K)
Length of tube (*m*)

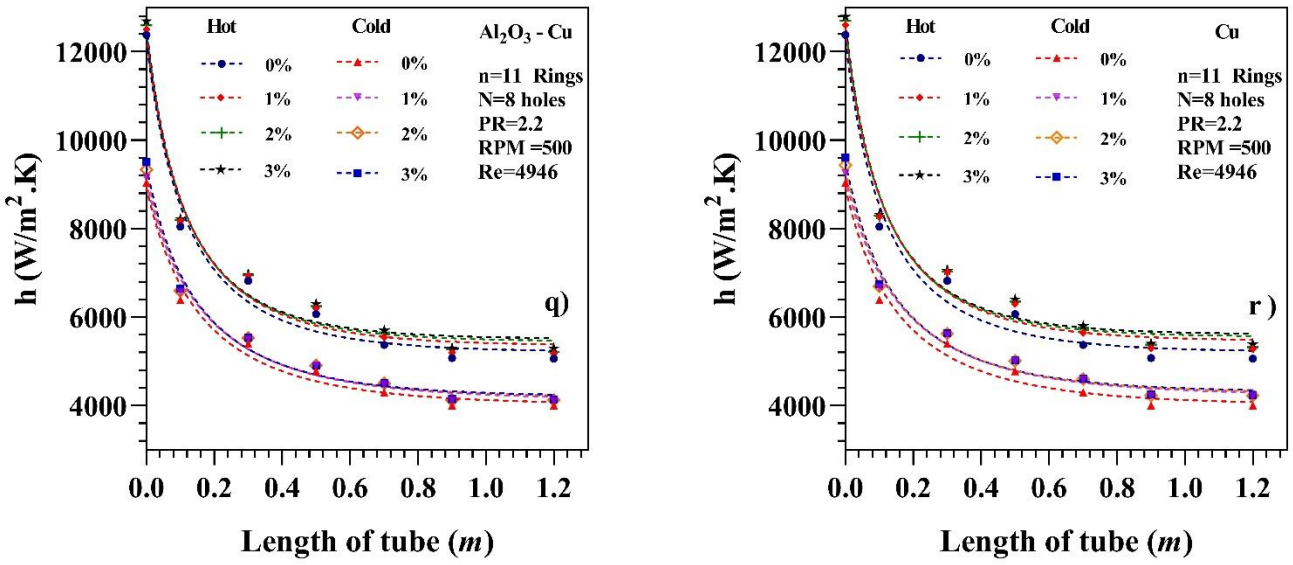

Figure 4.24 local heat transfer coefficients of inner and outer fluids with PCR inserts

4.3.6 Pressure Drop

Figure 4.25 shows the pressure drop of the double tube heat exchanger fitted with PCR at pitch ratio (PR) of 2.2, N=8 holes, n=11 PCR. This pressure drop increases with the volume concentration of the nanofluids and the inner tube rotational speed. Increasing the nanoparticle concentration leads to an increase in the density and viscosity of the nanofluid, which leads to an increase in friction. Additionally, the rotation of the tube with fitted PCRs lead to an increase of the pressure drop, due to the increased fluid velocity and turbulence. The pressure drop of the Al_2O_3-water nanofluid increased up to 67.95, 68.26 and 79.91% for 1, 2 and 3% volume concentrations at Re_{cf}= 4,946 and 500 rpm when compared to pure water at 0 rpm, as shown in Figures 4.25 (a-d). Similarly, for the Al_2O_3-Cu hybrid nanofluid, the pressure drop increased up to 76.86, 84.29 and 95.28% for 1, 2 and 3% volume concentrations, as shown in figures 4.25 (e-g). Figures 4.25 (h-j) depict the maximum pressure drop values, which were found for the Cu-water nanofluid and are 79.96, 90.4 and 98% for 1, 2 and 3% volume concentrations.

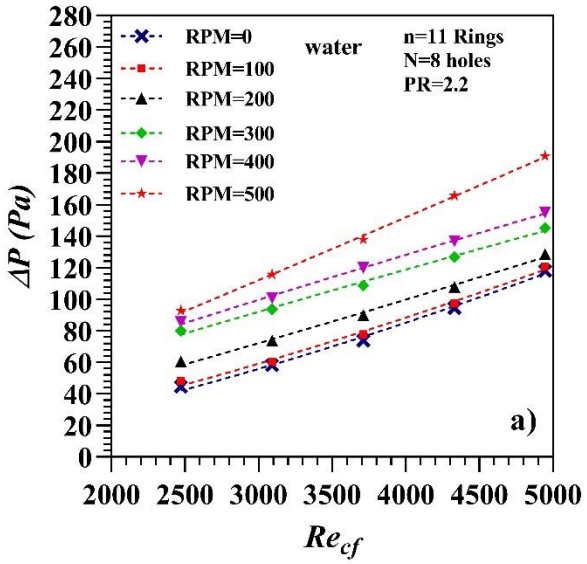
RPM=0
RPM=100
RPM=200
RPM=300
RPM=400
RPM=500
water
n=11 Rings
N=8 holes
PR=2.2
a)
ΔP (Pa)
Re_cf

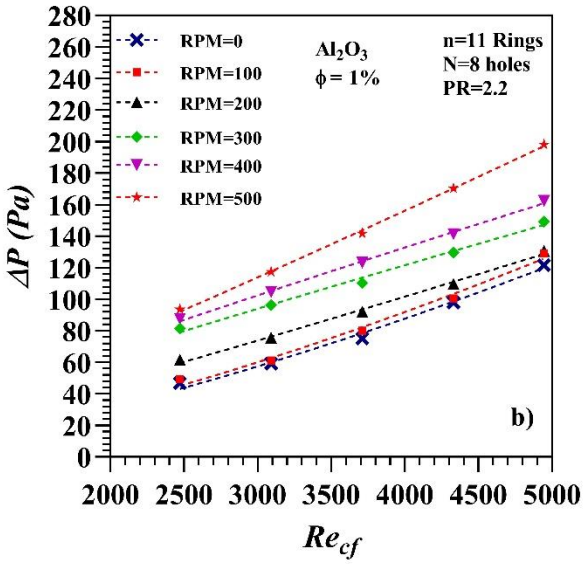
RPM=0
RPM=100
RPM=200
RPM=300
RPM=400
RPM=500
Al2O3
ϕ = 1%
n=11 Rings
N=8 holes
PR=2.2
b)
ΔP (Pa)
Re_cf

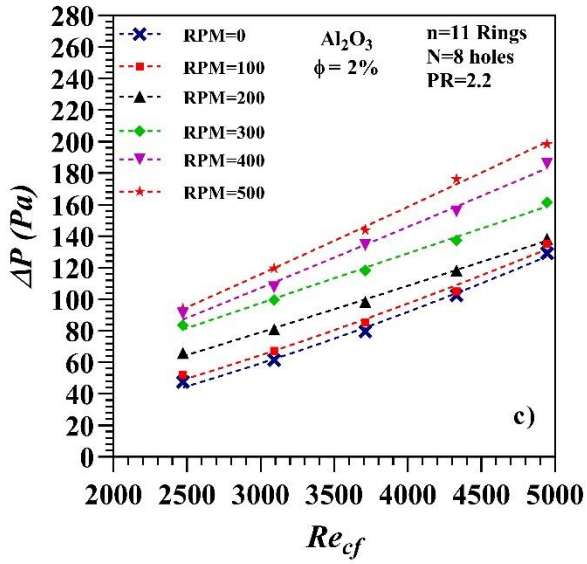
RPM=0
RPM=100
RPM=200
RPM=300
RPM=400
RPM=500
Al2O3
ϕ = 2%
n=11 Rings
N=8 holes
PR=2.2
c)
ΔP (Pa)
Re_cf

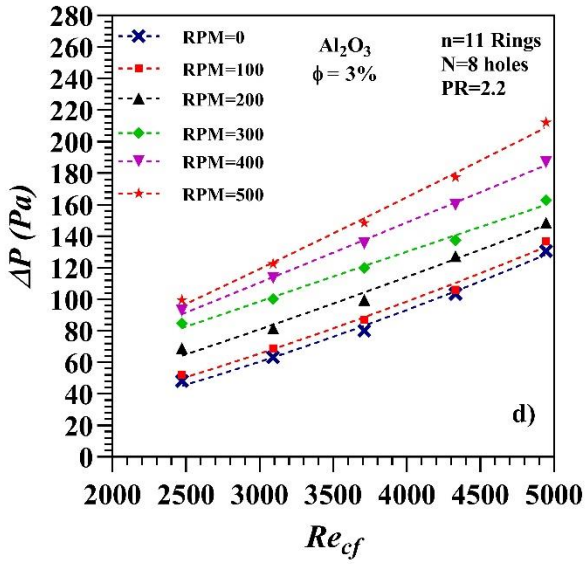
RPM=0
RPM=100
RPM=200
RPM=300
RPM=400
RPM=500
Al2O3
ϕ = 3%
n=11 Rings
N=8 holes
PR=2.2
d)
ΔP (Pa)
Re_cf

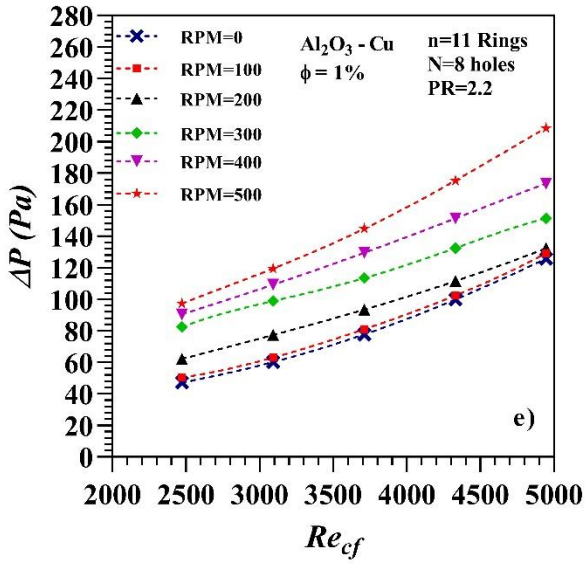
RPM=0
RPM=100
RPM=200
RPM=300
RPM=400
RPM=500
Al2O3 - Cu
ϕ = 1%
n=11 Rings
N=8 holes
PR=2.2
e)
ΔP (Pa)
Recf

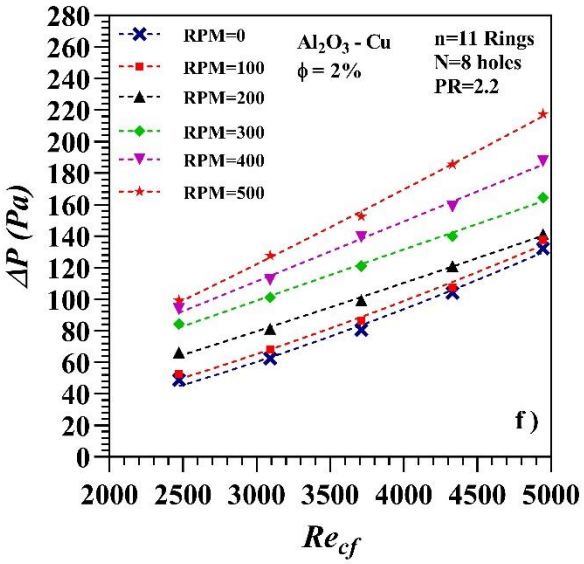
RPM=0
RPM=100
RPM=200
RPM=300
RPM=400
RPM=500
Al2O3 - Cu
ϕ = 2%
n=11 Rings
N=8 holes
PR=2.2
f)
ΔP (Pa)
Recf

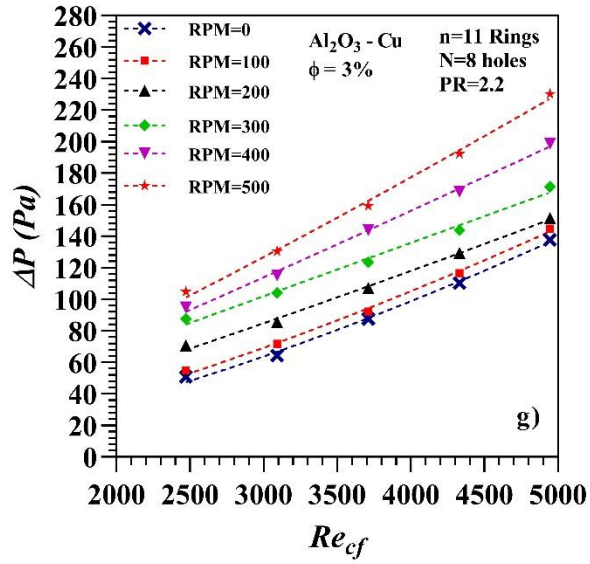
RPM=0
RPM=100
RPM=200
RPM=300
RPM=400
RPM=500
Al2O3 - Cu
ϕ = 3%
n=11 Rings
N=8 holes
PR=2.2
g)
ΔP (Pa)
Recf

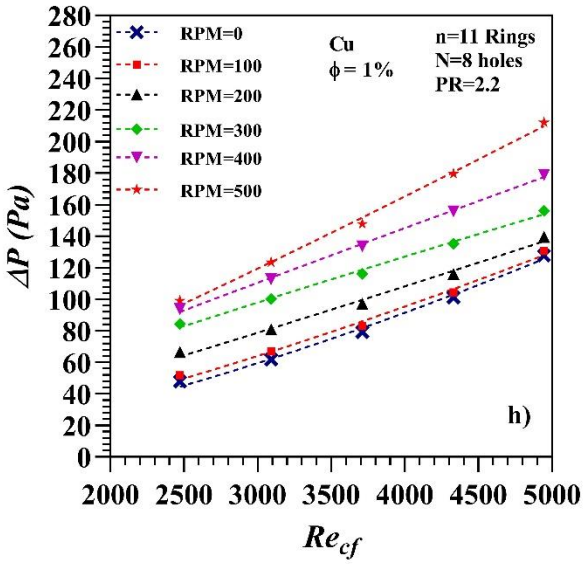
RPM=0
RPM=100
RPM=200
RPM=300
RPM=400
RPM=500
Cu
ϕ = 1%
n=11 Rings
N=8 holes
PR=2.2
h)
ΔP (Pa)
Recf

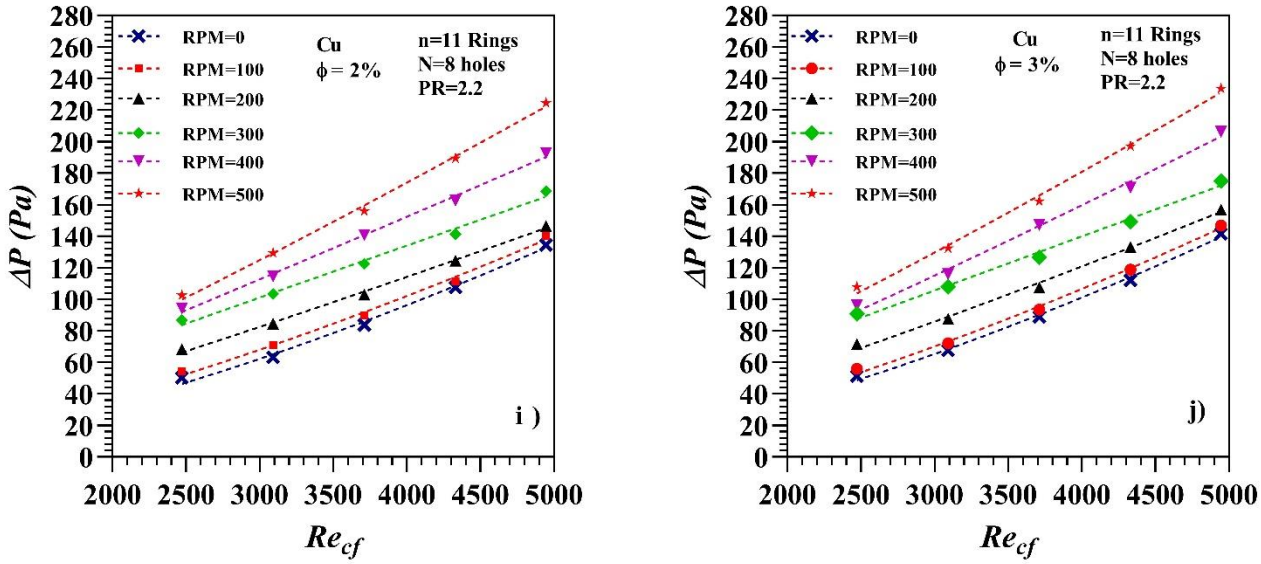

Figure. 4.25 Effect of concentration, PCR and rotational speeds on pressure drop.

4.3.7 Flow Structure

Figure 4.26 was added to obtain insight into the flow structure generated by the perforated circular rings. It shows the flow streamlines in the heat exchanger for Re_{cf} of 2,473 and 4,946 and different inner tube rotational speeds from 0 to 500 rpm for the Cu-water nanofluid at a 3% concentration.

The first noticeable effect is the generation of vortices near the rings and the ring holes. These vortices disrupt the flow, improving heat transfer at the cost of increasing the pressure drop. At 0 rpm, the flow is mainly axial, with smooth velocity streamlines. As the rotational speed increases, the flow develops a rotational component. These patterns are thought to improve convective heat transfer, due to the turbulence generation and the vortex structures in the boundary layers. At the higher rotational speeds, near 500 rpm, the flow arrangement changes and causes the fluid to go round the tube, resulting in longer fluid paths and residence times inside the exchanger. Moreover, the presence of holes combined with the rotational speed leads to higher turbulence levels and more vortex generation near the holes, improving heat transfer.

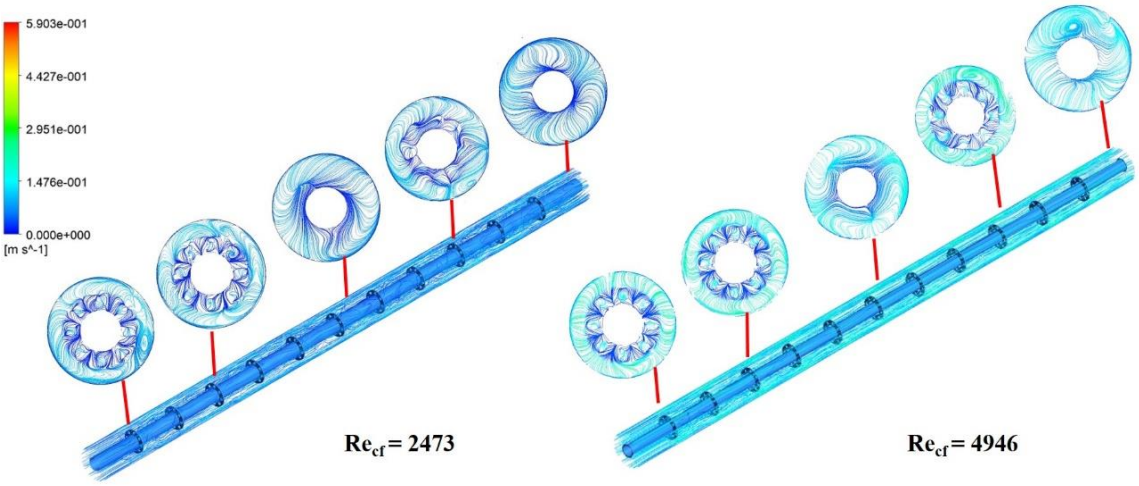

0 rpm **a)**

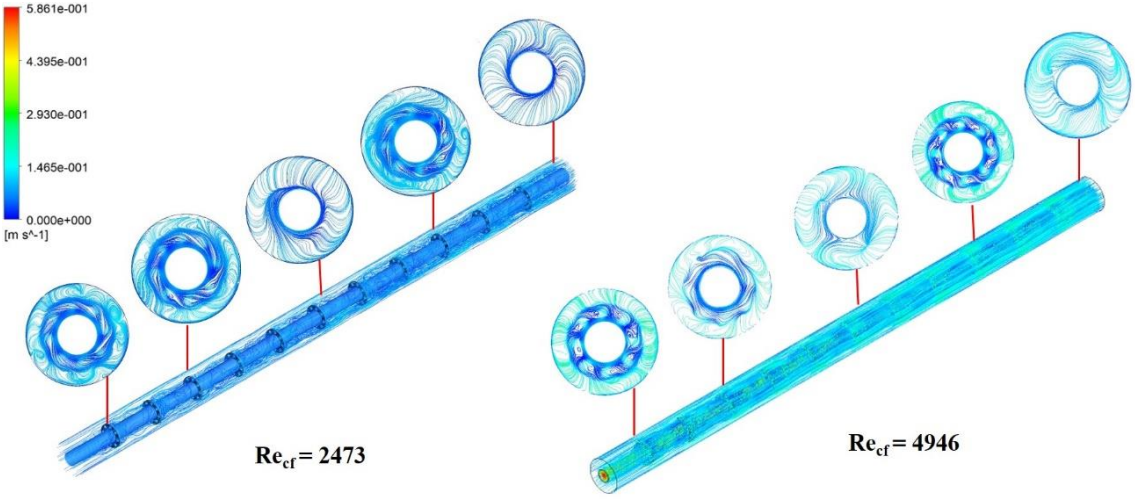

100 rpm **b)**

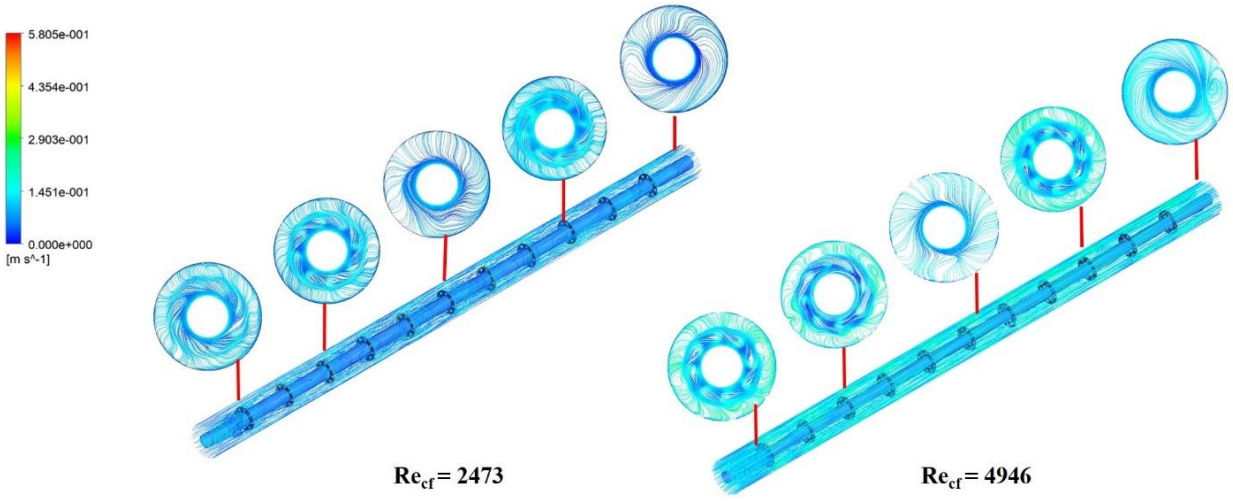

Re_{cf} = 2473 Re_{cf} = 4946

200 rpm **c)**

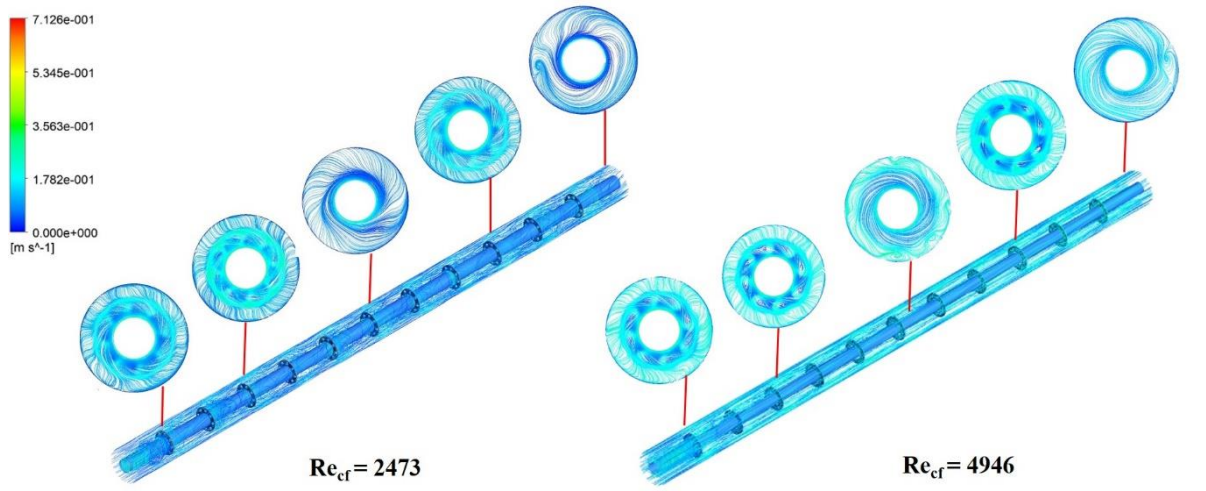

Re_{cf} = 2473 Re_{cf} = 4946

300 rpm **d)**

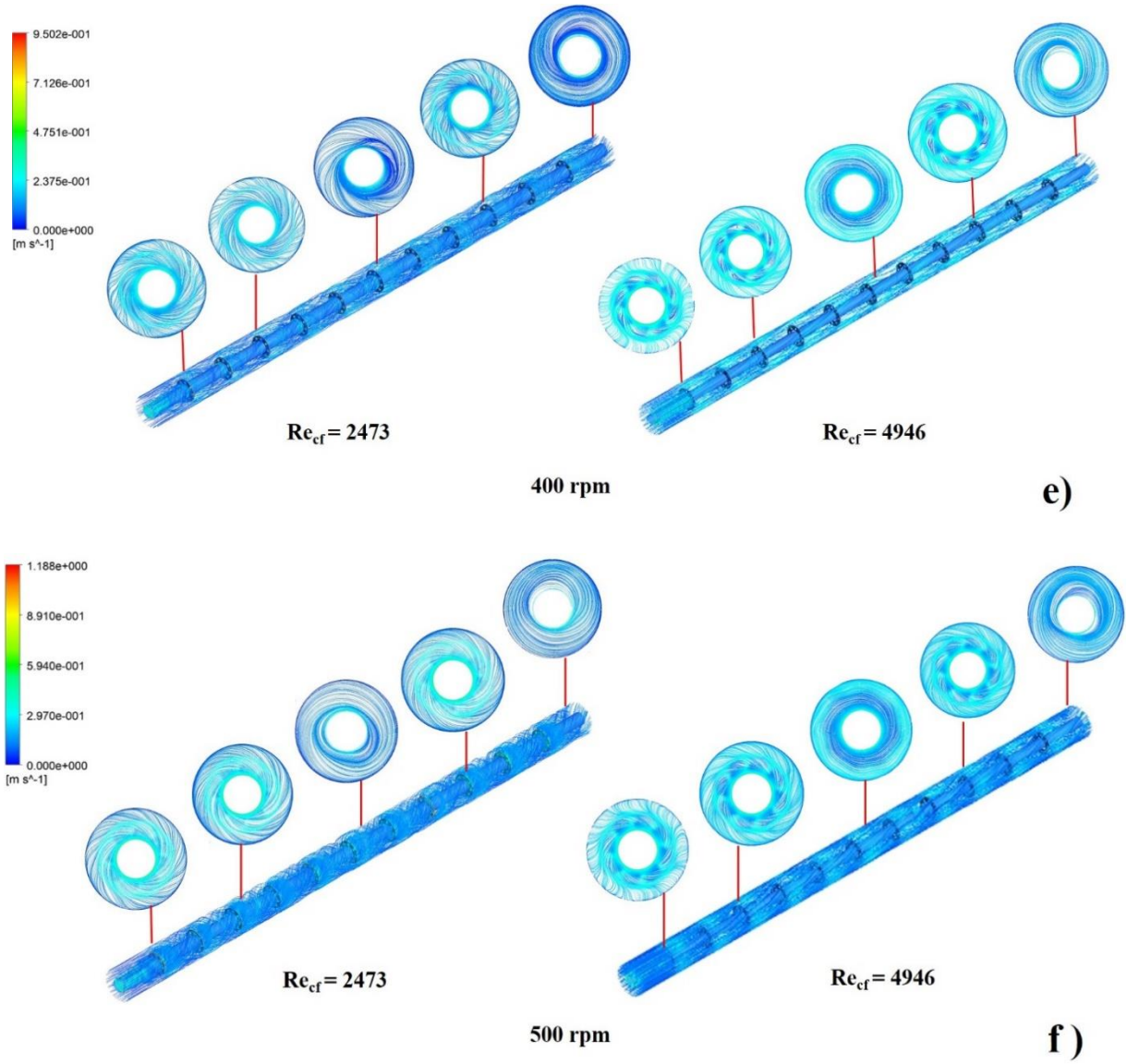

Figure 4.26 3D streamlines in double tube fitted with PCR at different rotational speeds.

4.3.8 Pumping Power

As a result of the increased pressure drop, due to the nanofluids, the rotation of the inner tube and the fitted PCRs, the heat exchanger may require higher pumping power. The pumping power required by the heat exchanger has been calculated and is depicted in Figure 4.27 as a function of the nanofluid volume concentration and inner tube rotational speed for all the studied nanofluids. It may be appreciated that an increase in volume concentration leads to an increase in the pumping power, due to the increase in fluid density and viscosity. At the same time, increasing the rotational

speed of the inner tube fitted with PCR leads to an increase in the pumping power as well. At 3% nanoparticle concentration, Re_{cf} = 4,946 and 500 rpm, the pumping power increases to 24.47 % (Al_2O_3) compared to 0 rpm and 1% volume concentration, as shown in Figure 4.27. For Al_2O_3-Cu, the increase is of 27.35 %, whereas for Cu, it is of 27.46%.

Figure 4.28 depicts the ratio of average heat transfer to pumping power, as performed with the plain tube numerical model, to provide a better understanding of the heat transfer enhancement with respect to the pumping cost. The Cu-water nanofluid has the highest values among the tested nanofluids, resulting in higher heat transfer values per unit of pumping power. As the concentration of nanoparticles increases, so does the ratio of heat transfer to pumping power. Increasing rotational speed, on the other hand, only increases this ratio at low rotational speeds, hinting at the fact that speeds over 500 rpm could not be beneficial for operation of this heat exchanger.

Finally, it must be considered that the maximum pumping power required is 0.12W, so the benefits of the heat exchanger optimization in terms of heat transfer are much more relevant that the small increase in the pumping power.

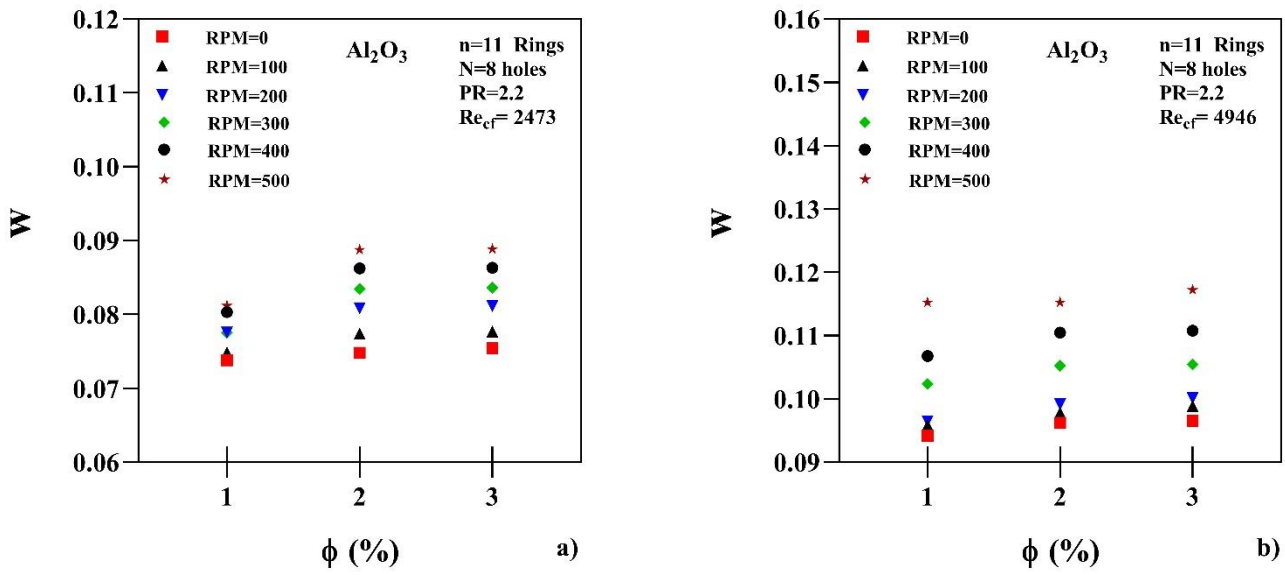

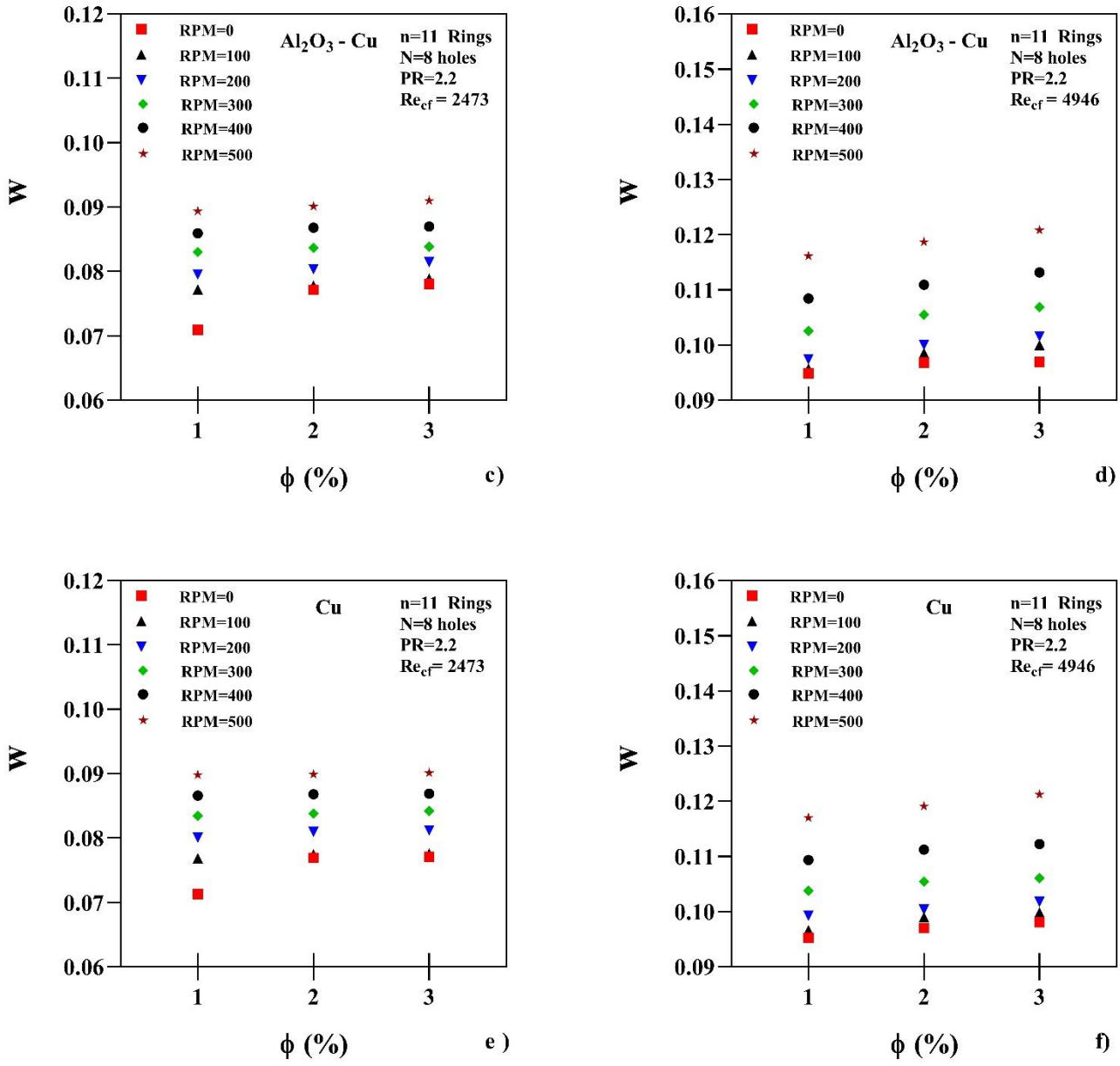

Figure 4.27 Effect of rotational speed, concentration and PCR on pumping power.

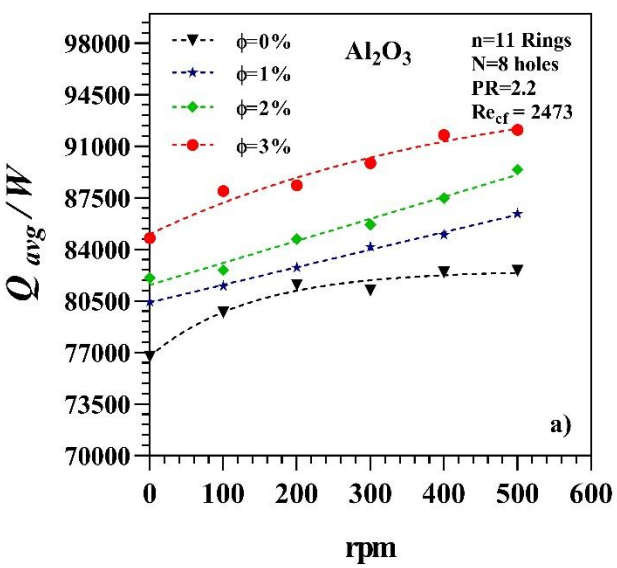
ϕ=0%
ϕ=1%
ϕ=2%
ϕ=3%
Al2O3
n=11 Rings
N=8 holes
PR=2.2
Recf = 2473
a)
Q avg / W
rpm

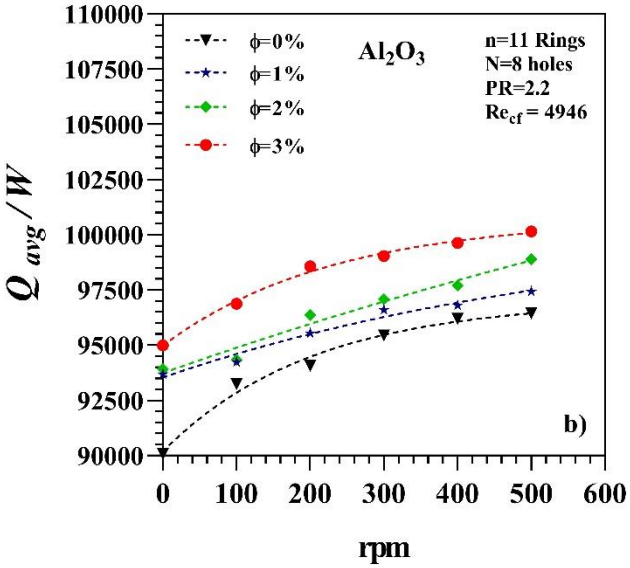
ϕ=0%
ϕ=1%
ϕ=2%
ϕ=3%
Al2O3
n=11 Rings
N=8 holes
PR=2.2
Recf = 4946
b)
Q avg / W
rpm

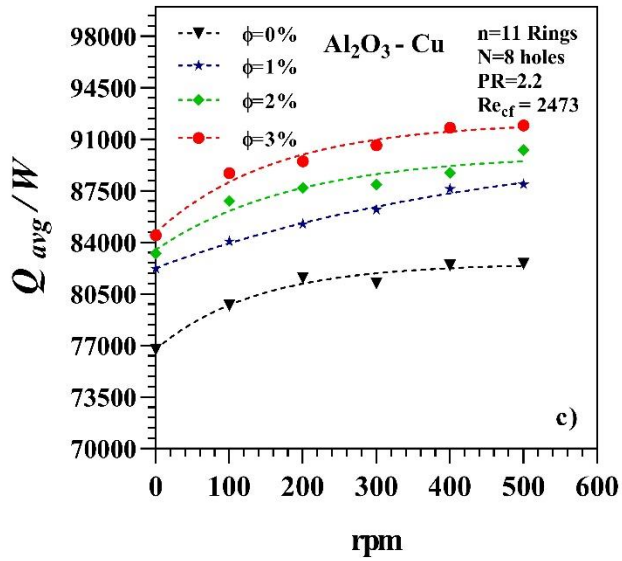
ϕ=0%
ϕ=1%
ϕ=2%
ϕ=3%
Al2O3 - Cu
n=11 Rings
N=8 holes
PR=2.2
Recf = 2473
c)
Q avg / W
rpm

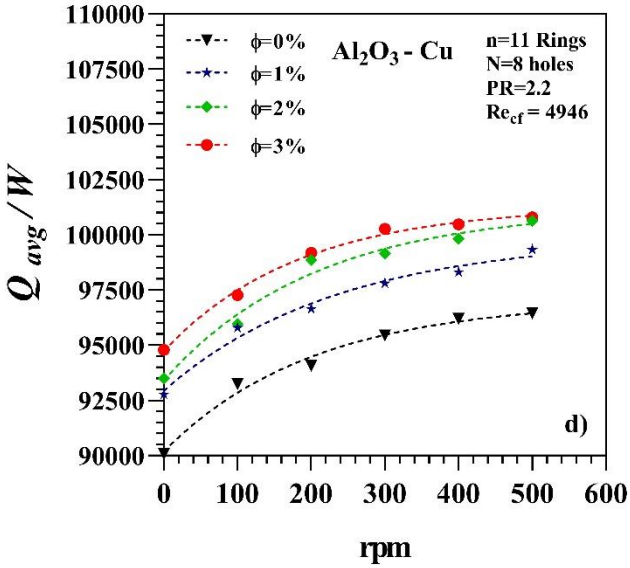
ϕ=0%
ϕ=1%
ϕ=2%
ϕ=3%
Al2O3 - Cu
n=11 Rings
N=8 holes
PR=2.2
Recf = 4946
d)
Q avg / W
rpm

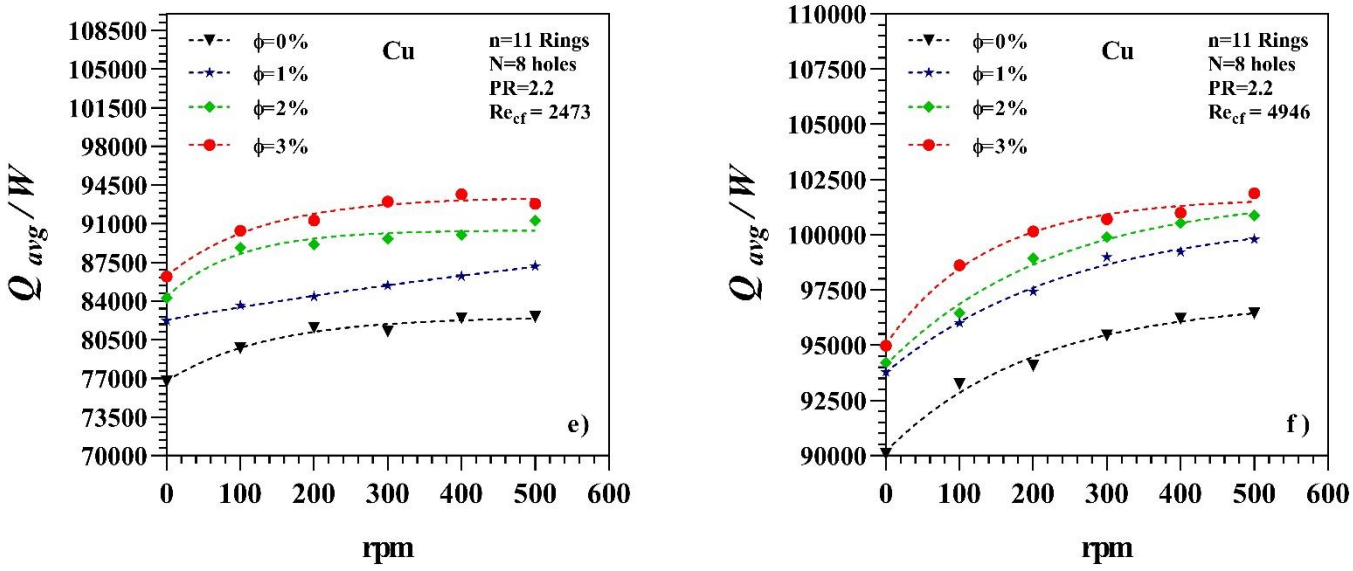

Figure 4.28 Ratio of average heat transfer and pumping power with rotational speed at PR 2.2.

4.4 Conclusion

In this chapter, the steps followed to develop three different numerical models of increasing complexity have been described. Firstly, a 2D axisymmetric model and a 3D model were developed to understand the behavior of the original heat exchanger. The 2D model was able to give the main performance characteristics of the heat exchanger and to study the possibility of adding nanoparticles to the working fluid, but the 3D model allowed a deeper insight of the flow structure and mechanisms that arise during the operation of the heat exchanger, as well as to account for the introduction of rotation in the heat exchanger inner tube. Finally, geometrical modifications of the exchanger were proposed by the introduction of fitter rings and perforated rings on the outer surface of the inner tube, and a 3D model was used to predict the performance of such design.

Heat transfer was found to improve with the addition of nanoparticles of Al_2O_3,Al_2O_3-Cu and Cu into pure water with different volume concentrations from 0 to 3%, with the Cu-water nanofluid exhibiting the best behavior. Additionally, the rotation of the

inner tube up to 500 rpm was found to be beneficial to increase the efficiency of the exchanger, as well as the proposed geometrical modification of adding perforated circular rings to the outer surface of the inner tube of the exchanger. Meanwhile, the pressure drop increased due to the different modifications performed (nanoparticles, rotational speed and circular rings).

Nevertheless, the results of this study may be used to recommend using perforated circular rings fitted in a rotating inner tube to improve the performance of a tubular heat echanger, as well as the incorporation of Cu nanoparticles, as they have provided the best improvements with respect to the other nanoparticles. In any case, the maximum pumping power required was found to be 0.12 W, so the benefits of this propsal exceed the drawbacks of the small pressure drop increase.

CHAPTER FIVE

CONCLUSIONS AND FUTURE WORK

Chapter Five – Conclusions and future work

5.1 Conclusion

Following a comprehensive review of concentric double tube heat exchangers, the methods for improving their performance and the main experimental, numerical and analytical techniques used for their design and evaluation, numerical models based on the Computational Fluid Dynamics (CFD) approach have been implemented to characterize an existing heat exchanger and propose modifications to improve its performance.

A 2D axisymmetric model was implemented to understand the behavior of the original heat exchanger and obtain its main performance variables. The effect of adding nanoparticles to the working fluid was assessed as well. Then, a 3D model allowed the evaluation of the flow structure developed inside the exchanger, as well as getting insight into the effect of rotating the inner tube of the exchanger in its performance. Both models were validated with previous experimental results, finding good agreement between them.

The effect of varying the inner tube rotational speed from 0 to 500 rpm and nanoparticle concentration for Al_2O_3, Cu, and hybrid Cu-Al_2O_3 at (0,1,2, and 3) % on heat exchanger performance and heat transfer characteristics was studied. The most beneficial fluid was found to be the Cu-water nanofluid at its highest concentration, 3%, combined with a rotational speed of 500 rpm for the exchanger inner tube.

Once the original heat exchanger was characterized, a geometrical modification based on the addition of fitted perforated circular rings to the outer surface of the inner tube of the exchanger was proposed and analyzed with a 3D model. A configuration with 11 rings with a pitch ratio of 2.2 and 8 perforated holes was found to be the optimal one in terms of heat transfer performance and pressure drop.

In this sense, it is possible to claim that all of the research objectives proposed in this thesis have been successfully achieved. The main findings are summarized below:

- Increasing the concentration of nanoparticles in the working fluid from 0 to 3% leads to higher heat transfer values.
- The thermal performance of the Al_2O_3-water nanofluid was better than pure water, but less than the Al_2O_3-Cu hybrid nanofluid. The Cu-water nanofluid exhibited the best performance.
- Higher cold fluid Reynolds numbers lead to higher heat transfer rates, due to convective heat.
- Rotation of the heat exchanger inner tube up to 500 rpm increases heat transfer rate and enhances the performance of the heat exchanger.
- The increased pressure drop and friction caused by higher rotational speeds, as well as the density and viscosity increase in the nanofluids led to an increase in pumping power.
- Inserts of typical circular rings (TCR) improve heat transfer rate and effectiveness of heat exchangers, due to the increase of turbulence. An optimal number of 11 TCR for the studied heat exchanger was found.
- The pressure drop increases with the number of typical circular rings (TCR), the Reynolds number and the inner tube rotational speed, but using perforated rings decreases it.
- The increased pressure drop led to higher pumping power values required to operate the heat exchanger; however, the value of pumping power remained low, so normal pump operation should not be strongly affected.

5.2 Recommendations for future work

The following items have been recognized as possible future research ideas, based on the findings of this study.

- A user defined function (UDF) could be developed to simulate nanoparticles in the CFD simulation.

- The volume concentration of nanofluids could be increased to values higher than than 3 %. Different hybrid nanofluids could be studied as well.
- The geometry of the perforated circular ring could be modified by altering the hole shape (triangular and/or hexagonal).

Capítulo Cinco– Conclusiones y trabajos futuros

5.1 Conclusiones

Tras realizar una revisión biliográfica exhaustiva sobre los intercambiadores de calor de doble tubo, los métodos para mejorar sus prestaciones y las principales técnicas experimentales, numéricas y analíticas utilizadas para su diseño y evaluación, se implementaron modelos numéricos basados en la Dinámica de Fluidos Computacional (CFD) para caracterizar un intercambiador de calor existente y proponer modificaciones para mejorar sus prestaciones.

Se implementó un modelo 2D axisimétrico para comprender el comportamiento del intercambiador de calor original y obtener sus principales variables de funcionamiento. También se analizó el efecto de la adición de nanopartículas al fluido de trabajo. Después, un modelo 3D permitió evaluar la estructura del flujo desarrollado dentro del intercambiador, así como conocer el efecto de rotar el tubo interior del intercambiador en sus prestaciones. Ambos modelos se validaron con resultados experimentales previos, encontrando una buena correspondencia entre ellos.

Se estudió el efecto de la variación de la velocidad de rotación del tubo interior de 0 a 500 rpm y la concentración de nanopartículas de Al_2O_3, Cu, y Cu-Al_2O_3 al 0,1,2, y 3 % en las prestaciones del intercambiador y la transferencia de calor. El fluido más adecuado resultó ser el basado en Cu a su mayor concentración, 3%, con una velocidad de rotación del tubo interior del intercambiador de 500 rpm.

Tras caracterizar el intercambiador de calor original, se propuso la modificación de su geometría a través de la adición de anillos circulares perforados en la superficie exterior del tubo interior del intercambiador. Dicha modificación se analizó con un modelo 3D, encontrando que la configuración óptima para la mejor transferencia de calor y caída de presión tenía 11 anillos con una relación de paso de 2,2 y 8 agujeros en cada anillo.

En este sentido, se puede afirmar que todos los objetivos de la investigación propuesta en esta tesis se han conseguido satisfactoriamente. Los principales resultados se resumen a continuación:

- El aumento de la concentración de nanopartículas en el fluido de trabajo de 0 a 3% conlleva valores mayores de transferencia de calor.
- Las características térmicas del nanofluido Al_2O_3-agua mejoraron respecto al agua pura, pero eran peores que las del fluido híbrido Al_2O_3-Cu. El nanofluido Cu-agua mostró las mejores propiedades.
- Números de Reynolds más altos supusieron mejoras en la transferencia de calor, debido a la transferencia de calor por convección.
- La rotación del tubo interior del intercambiador de calor a velocidades de hasta 500 rpm aumenta la velocidad de transferencia de calor y aumenta las prestaciones del intercambiador de calor.
- El aumento de la caída de presión y de la fricción causada por las mayores velocidades de rotación, así como el aumento de la densidad y viscosidad en los nanofluidos conllevó un aumento en la potencia de bombeo necesaria.
- La inserción de anillos circulares mejoró la transferencia de calor y la efectividad de los intercambiadores, debido al aumento de la turbulencia. Se encontró que el número óptimo de anillos era 11.
- La caída de presión aumentó con el número de anillos circualres, el número de Reynolds y la velocidad de rotación del tubo interior del intercambiador, pero la perforación de los anillos contribuyó a disminuirla.
- El aumento de la caída de presión supuso la necesidad de mayores potencias de bombeo para la operación del intercambiador; sin embargo, el valor de dicha potencia se mantuvo en niveles bajos, así que la operación normal de las bombas no debería verse fuertemente afectada.

5.2 Posibles trabajos futuros

A partir de los resultados de este estudio, se han encontrado las siguientes ideas como posibles trabajos de investigación futuros.

- Se podría desarrollar una función definida por el usuario (UDF) para simular las nanopartículas en la simulación CFD.

- La concentración de nanofluidos podría aumentarse por encima del 3%. Podrían estudiarse, además, otros nanofluidos diferentes.
- La geometría de los anillos circulares perforados podría modificarse cambiando la forma de los agujeros (triangular y/o hexagonal).

REFERENCES

[1] Y.A. Cengel, Heat Transfer: A Practical Approach. 2nd Edition, McGraw-Hill, New York (2002).

[2] R. K. Shah, D. P. Sekulic, fundamentals of heat exchanger design, JOHN WILEY & SONS, INC (2003).

[3] S. Kakaç, H. Liu, A. Pramuanjaroenkij, Heat Exchangers Selection, Rating, and Thermal Design. Fourth Edition, Taylor & Francis Group, LLC (2020).

[4] M. Bezaatpour, M. Goharkhah, Convective heat transfer enhancement in a double pipe mini heat Exchanger by magnetic field induced swirling flow, Applied Thermal Engineering 167 (2020) 114801.

[5] P. Forooghi , M. Flory , D. Bertsche, T. Wetzel, B. Frohnapfel, Heat transfer enhancement on the liquid side of an industrially designed flat-tube heat exchanger with passive inserts – Numerical investigation, Applied Thermal Engineering 123 (2017) 573–583.

[6] A. Gomaa , M.A. Halim , A.M. Elsaid, Experimental and numerical investigations of a triple concentric-tube heat exchanger, Applied Thermal Engineering 99 (2016) 1303–1315.

[7] N. Sinaga , S. khorasani , K. S. Nisar , A. Kaood , Second law efficiency analysis of air injection into inner tube of double tube heat exchanger, Alexandria Engineering Journal (2021) 60, 1465–1476.

[8] M. Kumar, V. K. Yadav, Bhawna Verma, K. K. Srivastava, Experimental study of friction factor during convective heat transfer in miniature double tube Hair-pin heat exchanger, Procedia Technology 24 (2016) 669 – 676.

[9] M. Sheikholeslami, M. Hatami ,M. Jafaryar, ,F. Farkhadni, D. D. Ganjia, M. G. Bandpy, Thermal management of double-pipe air to water heat exchanger. Energy and Buildings 88 (2015) 361–366.

[10] P. Liu, N. Zheng, F. Shan, Z. Liu, W. Liu, An experimental and numerical study on the laminar heat transfer and flow characteristics of a circular tube fitted with multiple conical strips inserts, International Journal of Heat and Mass Transfer 117 (2018) 691–709.

[11] T.N. Verma, P. Nashine, D. V. Singh, T.S. Singh, D. Panwar, ANN:

Prediction of an Experimental heat transfer analysis of concentric tube heat exchanger with corrugated inner tubes, Applied Thermal. Engineering,120 (2017) 219–227.

[12] Thejaraju R , Girisha KB , S.H. Manjunath , B.S. Dayananda ,Experimental investigation of turbulent flow behavior in an air to air double pipe heat exchanger using novel para winglet tape, Case Studies in Thermal Engineering 22 (2020) 100791.

[13] S. Chokphoemphun, M. Pimsarn, C. Thianpong, P. Promvonge, Heat transfer augmentation in a circular tube with winglet vortex generators, Chinese Journal of Chemical Engineering 23 (2015) 605–614.

[14] M.M.K. Bhuiya, A.S.M. Sayema, M. Islam, M.S.U. Chowdhury, M. Shahabuddin, Performance assessment in a heat exchanger tube fitted with Double counter twisted tape inserts, International Communications in Heat and Mass Transfer 50 (2014) 25–33.

[15] A. Vaisia, R. Moosavib, M. Lashkaric, M. M. Soltanid, Experimental investigation of perforated twisted tapes turbulator on thermal performance in double pipe heat exchangers, Chemical Engineering & Processing: Process Intensification 154 (2020) 108028.

[16] H. Moria , Compound usage of twisted tape turbulator and air injection for heat transfer augmentation in a vertical straight tube with upward stream, Case Studies in Thermal Engineering 25 (2021) 100854.

[17] S.W. Chang , C.H. Kang, C.L. Lee, C.H. Yu, Effect of pitching and rolling motion on hydrothermal performance of rectangular channel flow enhanced by twisted-tape pin–fin array, Applied Thermal Engineering 192 (2021) 116971.

[18] T. Dagdevir, V. Ozceyhan, An experimental study on heat transfer enhancement and flow characteristics of a tube with plain, perforated and dimpled twisted tape inserts, International Journal of Thermal Sciences 159 (2021) 106564.

[19] S. Pourahmad, S.M. Pesteei , H. Ravaeei , S. Khorasani, Experimental study of heat transfer and pressure drop analysis of the air/ water two-phase flow in a double tube heat exchanger equipped with dual twisted tape turbulator:

Simultaneous usage of active and passive methods, Journal of Energy Storage 44 (2021) 103408.

[20] Y. Ding, W. Zhang, B. Deng, Y. Gu, Q. Liao, Z. Long, X. Zhu, Experimental and numerical investigation on natural convection heat transfer characteristics of vertical 3-D externally finned tubes, Energy 239 (2022) 122050.

[21] K. Yakut, B. Sahin, Flow-induced vibration analysis of conical rings used for heat transfer enhancement in heat exchangers, Applied Energy 78 (2004) 273–288.

[22] P. Promvonge ,S. Eiamsa-ard, Heat transfer behaviors in a tube with combined conical-ring and twisted-tape insert, International Communications in Heat and Mass Transfer 34 (2007) 849–859.

[23] P. Promvonge, Heat transfer behaviors in round tube with conical ring inserts, Energy Conversion and Management 49 (2008) 8–15.

[24] V. Kongkaitpaiboon, K. Nanan, S. Eiamsa-ard, Experimental investigation of convective heat transfer and pressure loss in a round tube fitted with circular-ring turbulators, International Communications in Heat and Mass Transfer 37 (2010) 568–574.

[25] P. Promvonge, N. Koolnapadol, M. Pimsarn, C. Thianpong, Thermal performance enhancement in a heat exchanger tube fitted with inclined vortex rings, Applied Thermal Engineering 62 (2014) 285-292.

[26] W.C. Huang, C.A. Chen, C. Shen, J.Y. San, Effects of characteristic parameters on heat transfer enhancement of repeated ring-type ribs in circular tubes, Experimental Thermal and Fluid Science 68 (2015) 371–380.

[27] V. Singh, S. Chamoli, M. Kumar, A. Kumar, Heat transfer and fluid flow characteristics of heat exchanger tube with multiple twisted tapes and solid rings inserts, Chemical Engineering and Processing 102 (2016) 156–168.

[28] M. Sheikholeslami , M. G. Bandpy, D.D. Ganji, Experimental study on turbulent flow and heat transfer in an air to water heat exchanger using perforated circular-ring, Experimental Thermal and Fluid Science 70 (2016) 185–195.

[29] S. Yadav, S. K. Sahu, Heat transfer augmentation in double pipe water to air Counter flow Heat exchanger with helical surface disc turbulators, Chemical

Engineering & Processing: Process Intensification 135 (2019) 120–132.

[30] J. Dirker , J.P. Meyer, R.M. Steyn, Influence of ring type flow turbulators on the local heat transfer coefficients in an annular passage – An experimental and numerical investigation, International Journal of Thermal Sciences 168 (2021) 107052.

[31] W. D. Morris, K. F. R. Abadi , Convective heat transfer in rotating ribbed Tubes, Int. J. Heat Mass transfer ,39(1996) 2253- 2266.

[32] B. Watel, S. Harmand , B. Desmet , Influence of fin spacing and rotational speed on the convective heat exchanges from a rotating finned tube, International Journal of Heat and Fluid Flow 21(2000) 221-227.

[33] W. Duangthongsuk, S.Wongwises, An experimental investigation of the heat transfer and pressure drop characteristics of a circular tube fitted with rotating turbine-type swirl generators, Experimental Thermal and Fluid Science 45 (2013) 8–15.

[34] S. Eiamsa-ard , P. Somkleang , C. Nuntadusit , C. Thianpong, Heat transfer enhancement in tube by inserting uniform/non-uniform twisted-tapes with alternate axes: Effect of rotated-axis length, Applied Thermal Engineering 54 (2013) 289e309.

[35] H.Z. Abou-Ziyan , A.B. Helali , M. Y.E. Selim, Enhancement of forced convection in wide cylindrical annular channel using rotating inner pipe with interrupted helical fins, International Journal of Heat and Mass Transfer 95 (2016) 996–1007.

[36] L. H. K. Goh, Y. M. Hung, G.M. Chen, C.P. Tso, Entropy generation analysis of turbulent convection in a heat exchanger with self-rotating turbulator inserts, International Journal of Thermal Sciences 160 (2021) 106652.

[37] T. Mohapatra, B.N. Padhi, S.S. Sahoo, Experimental investigation of convective heat transfer in an inserted coiled tube type three fluid heat exchanger. Applied Thermal Engineering. 117 (2017) 297–307.

[38] S. S. Sonawane, R.S. Khedkar, K. L. Wasewar, Study on concentric tube heat Exchanger heat transfer performance using Al_2O_3 – water based nanofluids. International Communications in Heat and Mass Transfer 49 (2013) 60–68.

[39] M. S. E. Rao, D. Sreeramulu, C. J. Rao, M. V. Ramana, Experimental Investigation on Forced Convective Heat Transfer Coefficient of a Nanofluid. Materials Today Proceedings 4(2017) 8717–8723.

[40] P.V. D. Prasad, A.V.S.S.K.S. Gupta, K. Deepak, Investigation of Trapezoidal-Cut Twisted Tape Insert in a Double Pipe U-Tube Heat Exchanger using Al_2O_3/Water Nanofluid, Procedia Materials Science 10 (2015) 50 – 63.

[41] W. Duangthongsuk, S. Wongwises, An experimental study on the heat transfer Performance and pressure drop of TiO_2-water nanofluids flowing under a turbulent flow regime. International Journal of Heat and Mass Transfer 53 (2010) 334 –344.

[42] E. E.Bajestan , M.C. Moghadam, H. Niazmand ,W. Daungthongsuk , S.Wongwises, Experimental and numerical investigation of nanofluids heat transfer characteristics for application in solar heat exchangers, International Journal of Heat and Mass Transfer 92 (2016) 1041–1052.

[43] C, Qi, T. Luo, M. Liu, F. Fan, Y. Yan, Experimental study on the flow and heat transfer characteristics of nanofluids in double-tube heat exchangers based on thermal efficiency assessment, Energy Conversion and Management 197 (2019) 111877.

[44] M. Hazbehian, H. Maddah, H. Mohammadiun, M. Alizadeh, Experimental investigation of heat transfer augmentation inside double pipe heat exchanger equipped with reduced width twisted tapes inserts using polymeric nanofluid. Heat Mass Transfer 52 (2016) 2515–2529.

[45] C. Thianpong , K. Wongcharee , H. Safikhani , S. Chokphoemphun , A. Saysroy , S. Skullong , S. Eiamsa-ard , Multi objective optimization of TiO_2/water nanofluid flow within a heat exchanger enhanced with loose-fit delta-wing twisted tape inserts, International Journal of Thermal Sciences 172 (2022) 107318.

[46] J. C. Yang, F. C. Li, H. P. Xu, Y. R. He, Y. M. Huang, B. C. Jiang, heat transfer performance of viscoelastic- fluid-based nanofluid pipe flow at entrance region, Experimental Heat Transfer 28 (2015) 125–138.

[47] W. M. El-Maghlany, A. A. Hanafy, A. A. Hassan, M. A. El-Magid, Experimental study of Cu–water nanofluid heat transfer and pressure drop in

a horizontal double-tube heat exchanger, Experimental Thermal and Fluid Science 78 (2016) 100–111.

[48] M. H. Esfe, S.Saedodin, M. Mahmoodi, Experimental studies on the convective heat transfer performance and thermophysical properties of MgO–water nanofluid under turbulent flow. Experimental Thermal and Fluid Science. 52 (2014) 68–78.

[49] N.T. R. Kumar, P. Bhramara, L. S. Sundar, M. K. Singh, A.C.M. Sousa, Heat transfer, friction factor and effectiveness of Fe_3O_4 nanofluid flow in an inner tube of double pipe U- bend heat exchanger with and without longitudinal strip inserts. Experimental Thermal and Fluid Science, 85 (2017) 331–343.

[50] S.R. Chaurasia, R. M. Sarviya, Thermal performance analysis of CuO/water nanofluid Flow in a pipe with single and double strip helical screw tape. Applied Thermal Engineering 166 (2020) 114631.

[51] S. Halelfadl , P. Estellé, T. Maré, Heat transfer properties of aqueous carbon Nanotubes nanofluids in coaxial heat exchanger under laminar regime, Experimental Thermal and Fluid Science 55 (2014) 174–180.

[52] M. Goodarzi, A.S. Kherbeet, M. Afrand , E. Sadeghinezhadd, M. Mehrali , P. Zahedi , S. Wongwises, M. Dahari, Investigation of heat transfer performance and friction factor of a counter-flow double-pipe heat exchanger using nitrogen-doped, graphene-based nanofluids, International Communications in Heat and Mass Transfer 76 (2016) 16–23.

[53] B. Ilhan, H. Ertürk, Experimental characterization of laminar forced convection of hBN- water nanofluid in circular pipe. International Journal of Heat and Mass Transfer 111 (2017) 500 – 507.

[54] D. Madhesh, R. Parameshwaran, S. Kalaiselvam, Experimental investigation on convective heat transfer and rheological characteristics of Cu–TiO_2 hybrid nanofluids. Experimental Thermal and Fluid Science 52 (2014) 104 – 115.

[55] F. Hormozi, B. ZareNezhad , H.R. Allahyar, An experimental investigation on the effects of surfactants on the thermal performance of hybrid nanofluids in helical coil heat exchangers, International Communications in Heat and Mass Transfer 78 (2016) 271–276.

[56] S. K. Singh, J. Sarkar, Improving hydrothermal performance of hybrid nanofluid in double tube heat exchanger using tapered wire coil turbulator, Advanced Powder Technology 31 (2020) 2092–2100.

[57] S. K. Singh, J. Sarkar, Hydrothermal performance comparison of modified twisted tapes and wire coils in tubular heat exchanger using hybrid nanofluid, International Journal of Thermal Sciences 166 (2021) 106990.

[58] M.M.K. Bhuiya, A.S.M. Sayema, M. Islam, M.S.U. Chowdhury, M. Shahabuddin, Performance assessment in a heat exchanger tube fitted with Double counter twisted tape inserts, International Communications in Heat and Mass Transfer 50 (2014) 25–33.

[59] E. Zanchini, A. Jahanbin, Effects of the temperature distribution on the thermal resistance of double u-tube borehole heat exchangers, Geothermics 71 (2018) 46–54.

[60] H. Shao, M. Zhang, Q. Zhao, Y. Wang, Z. Liang, Study of improvements on flow maldistribution of double tube-passes shelland- tube heat exchanger with rectangular header, Applied Thermal Engineering 144 (2018) 106–116.

[61] N. Zheng, P. Liu, F. Shan, Z. Liu, W. Liu, Turbulent flow and heat transfer enhancement in a heat exchanger tube fitted with novel discrete inclined grooves. International Journal of Thermal Sciences. 111 (2017) 289-300.

[62] A. R. Al-Obaidi, Investigation of fluid field analysis, characteristics of pressure drop and improvement of heat transfer in three-dimensional circular corrugated pipes, Journal of Energy Storage 26 (2019) 101012.

[63] Z. Wu, L. Qiu, C. Wu, D. Zhou, Study on flow and heat performance of thermal-hydrolyzed sludge in a double-pipe heat exchanger with a series of inner corrugated tube, International Journal of Thermal Sciences 170 (2021) 107160.

[64] M. K. Aliabadi, A. Feizabadi, Performance intensification of tubular heat exchangers using compound twisted-tape and twisted-tube, Chemical Engineering & Processing: Process Intensification 148 (2020) 107799.

[65] C. Yu, Y. Cui, H. Zhang, B. Gao, M. Zeng, L. Han, Comparative study on turbulent flow characteristics and heat transfer mechanism of a twisted oval tube with different twisted tapes, International Journal of Thermal Sciences

174 (2022) 107455.

[66] Harish H. V, Manjunath K, Heat and fluid flow behaviors in a laminar tube flow with circular protruded twisted tape inserts, Case Studies in Thermal Engineering 32 (2022) 101880.

[67] M. R. Kalateh , A. Kianifar , M.Sardarabadi, A three-dimensional numerical study of the effects of various twisted tapes on heat transfer characteristics and flow field in a tube: Experimental validation and multi-objective optimization via response surface methodology, Sustainable Energy Technologies and Assessments 50 (2022) 101798.

[68] H. Bucak , F. Yilmaz, Heat transfer augmentation using periodically spherical dimple-protrusion patterned walls of twisted tape, International Journal of Thermal Sciences 171 (2022) 107211.

[69] M. Dastmalchi, G.A. Sheikhzadeh, A. Arefmanesh, Optimization of micro-finned tubes in double pipe heat exchangers using particle swarm algorithm, Applied Thermal Engineering 119 (2017) 1–9.

[70] H. Chen, H. Ayed, R. Marzouki , F. Emami , I. Mahariq , F. Jarad , Thermal, hydraulic, exergitic and economic evaluation of a flat tube heat exchanger equipped with a plain and modified conical turbulator, Case Studies in Thermal Engineering 28 (2021) 101587.

[71] M. A.M. Ali, W. M. El-Maghlany, Y.A. Eldrainy, A. Attia, Heat transfer enhancement of double pipe heat exchanger using rotating of variable eccentricity inner pipe, Alexandria Engineering Journal 57 (2018) 3709–3725.

[72] Y.Q. Song, N. Izadpanahi , M. A. Fazilati , Y.P. Lv , D. Toghraie, Numerical analysis of flow and heat transfer in an elliptical duct fitted with two rotating twisted tapes, International Communications in Heat and Mass Transfer 125 (2021) 105328.

[73] W. Dang, L. B. Wang, Convective heat transfer enhancement mechanisms in circular tube inserted with a type of twined coil, International Journal of Heat and Mass Transfer 169 (2021) 120960.

[74] G. Liang, M.D. Islam, N. Kharoua, R. Simmons, Numerical study of heat transfer and flow behavior in a circular tube fitted with varying arrays of winglet vortex generators, International Journal of Thermal Sciences 134

(2018) 54–65.

[75] S. Skullong , P. Promvonge , C. Thianpong , N. Jayranaiwachira , M. Pimsarn , Thermal performance of heat exchanger tube inserted with curved winglet tapes, Applied Thermal Engineering 129 (2018) 1197–1211.

[76] P. Promvonge , P. Promthaisong , S. Skullong, Experimental and numerical heat transfer study of turbulent tube flow through discrete V-winglets, International Journal of Heat and Mass Transfer 151 (2020) 119351.

[77] A. El Maakoul, M. El Metoui, A. B. Abdellah, S. Saadeddine, M. Meziane, Numerical investigation of thermohydraulic performance of air to water double pipe heat exchanger with helical fins. Applied Thermal Engineering. 127 (2017) 127–139.

[78] S.A. Nada, M.A. Said, Effects of fins geometries, arrangements, dimensions and numbers on natural convection heat transfer characteristics in finned-horizontal annulus, International Journal of Thermal Sciences 137 (2019) 121–137.

[79] A.R. Anvari , K. Javaherdeh , M. Emami-Meibodi , A.M. Rashidi, Numerical and experimental investigation of heat transfer behavior in a round tube with the special conical ring inserts, Energy Conversion and Management 88 (2014) 214–217.

[80] M. Sheikholeslami, D.D. Ganji , M. G. Bandpy, Experimental and numerical analysis for effects of using conical ring on turbulent flow and heat transfer in a double pipe air to water heat exchanger, Applied Thermal Engineering 100 (2016) 805–819.

[81] S. Sripattanapipat, S. Tamna, N. Jayranaiwachira, P. Promvonge, Numerical heat transfer investigation in a heat exchanger tube with hexagonal conical-ring inserts, Energy Procedia 100 (2016) 522 – 525.

[82] M.E. Nakhchi, J.A. Esfahani, Numerical investigation of different geometrical parameters of perforated conical rings on flow structure and heat transfer in heat exchangers, Applied Thermal Engineering 156 (2019) 494–505.

[83] M. M. Ibrahim, M. A. Essa, N. H. Mostafa, A computational study of heat transfer analysis for a circular tube with conical ring turbulators, International

Journal of Thermal Sciences 137 (2019) 138–160.

[84] V. Uniyal , S. K. Joshi , S. Kaushik , N. Kanojia, CFD Investigation of transfer of the heat and turbulent flow in circular copper tube with perforated conical rings of aluminum material, Materials Today: Proceedings 46 (2021) 6719–6725.

[85] A. Bartwala, A. Gautamb, M. Kumara, C. K. Mangrulkarc, S. Chamolia, Thermal performance intensification of a circular heat exchanger tube integrated with compound circular ring–metal wire net inserts, Chemical Engineering & Processing: Process Intensification 124 (2018) 50–70.

[86] S. Chamoli , X. Zhuang , P. K. Pant , P.Yu, Heat transfer in a turbulent flow tube integrated with tori as vortex generator inserts, Applied Thermal Engineering 194 (2021) 117062.

[87] K. M. Shirvan, M. Mamourian , S. Mirzakhanlari, R. Ellahi, Numerical investigation of heat exchanger effectiveness in a double pipe heat exchanger filled with nanofluid: A sensitivity analysis by response Surface methodology. Powder Technology. 313 (2017) 99-111.

[88] A. Albojamal, K. Vafai, Analysis of single phase, discrete and mixture models, In predicting nanofluid transport. International Journal of Heat and Mass Transfer, 114 (2017) 225–237.

[89] M. Siadaty, M. Kazazi, Study of water based nanofluid flows in annular tubes Using numerical simulation and sensitivity analysis. Heat and Mass Transfer, (2018).

[90] M. H. Bahmani , G. Sheikhzadeh , M. Zarringhalam , O. Akbari , A. A.A.A. Alrashed , G. Shabani , M. Goodarzi, Investigation of turbulent heat transfer and nanofluid flow in a double pipe heat exchanger, Advanced Powder Technology 29 (2018) 273–282.

[91] M. A. Mohamed, A. J. G. Trashorras, E. B. Marigorta, Numerical Investigation of Heat Transfer with Nanofluids in Concentric Tube Heat Exchanger under Transitional Flow, Energy Perspectives 1 (2020) 34-56.

[92] A.A. R. Darzi , M.Farhadi , K. Sedighi ,S. Aallahyari , M. A. Delavar, Turbulent heat transfer of Al_2O_3–water nanofluid inside helically corrugated tubes: Numerical study, International Communications in Heat and Mass

Transfer 41 (2013) 68–75.

[93] A. Karimi , A. A.A.A. Al-Rashed , M. Afrand , O. Mahian , S. Wongwises , A. Shahsavar, the effects of tape insert material on the flow and heat transfer in a nanofluid-based double tube heat exchanger: Two-phase mixture model, International Journal of Mechanical Sciences 156 (2019) 397–409.

[94] S. Saedodin, M. Zaboli, S. H. Rostamian , Effect of twisted turbulator and various metal oxide nanofluids on the thermal performance of a straight tube: Numerical study based on experimental data, Chemical Engineering and Processing: Process Intensification 158 (2020) 108106.

[95] H. A. Mohammed, I.A.M. A. Abuobeida, H. B. Vuthalurua, S. Liu, Two-phase forced convection of nanofluids flow in circular tubes using convergent and divergent conical rings inserts, International Communications in Heat and Mass Transfer 101 (2019) 10–20.

[96] M. Karuppasamy, R. Saravanan , M. Chandrasekaran , V. Muthuraman, Numerical exploration of heat transfer in a heat exchanger tube with cone shape inserts and Al_2O_3 and CuO nanofluids, Materials Today: Proceedings 21 (2020) 940–947.

[97] H. Demir, A.S. Dalkilic, N.A. Kürekci, W. Duangthongsuk, S. Wongwises, Numerical investigation on the single phase forced convection heat transfer characteristics of TiO_2 nanofluids in a double-tube counter flow heat exchanger, International Communications in Heat and Mass Transfer 38 (2011) 218–228.

[98] S. E. Ard , K. Kiatkittipong, Heat transfer enhancement by multiple twisted tape inserts and TiO_2/water nanofluid, Applied Thermal Engineering 70 (2014) 896- 924.

[99] P.A. D. Cruz, E.J.E. Yamat, J. P. E. Nuqui, A. N. Soriano, Computational Fluid Dynamics (CFD) Analysis of the Heat Transfer and Fluid Flow of Copper (II) Oxide-Water Nanofluid in a Shell and Tube Heat Exchanger, Digital Chemical Engineering 3 (2022) 100014.

[100] M.E. Nakhchi , J.A. Esfahani, CFD approach for two-phase CuO nanofluid flow through heat exchangers enhanced by double perforated louvered strip insert, Powder Technology 367 (2020) 877–888.

[101] M. Saeedan, A. R. S. Nazar, Y. Abbasi, R. Karimi, CFD Investigation and neutral network modeling of heat transfer and pressure drop of nanofluids in double pipe helically baffled heat exchanger with a 3-D fined tube, Applied Thermal Engineering 100 (2016) 721–729.

[102] M.E. Nakhchi , J.A. Esfahani, Numerical investigation of turbulent Cu-water nanofluid in Heat exchanger tube equipped with perforated conical rings, Advanced Powder Technology 30 (2019) 1338–1347.

[103] H. Moayedi , Investigation of heat transfer enhancement of Cu-water nanofluid by different configurations of double rotating cylinders in a vented cavity with different inlet and outlet ports, International Communications in Heat and Mass Transfer 126 (2021) 105432.

[104] G. Murali , B. Nagendra , J. Jaya, CFD analysis on heat transfer and pressure drop characteristics of turbulent flow in a tube fitted with trapezoidal-cut twisted tape insert using Fe_3O_4 nano fluid, Materials Today: Proceedings 21 (2020) 313–319.

[105] Y. Wang, C. Qi , Z. Ding, J. Tu, R. Zhao, Numerical simulation of flow and heat transfer characteristics of nanofluids in built-in porous twisted tape tube, Powder Technology 392 (2021) 570–586.

[106] P.C. Mukesh Kumar, M. Chandrasekar, CFD analysis on heat and flow characteristics of double helically coiled tube heat exchanger handling MWCNT/water nanofluids, Heliyon 5 (2019) e02030.

[107] M. Bahiraei, N. Mazaheri, M. S. Mohammadi, H. Moayedi, Thermal performance of a new nanofluid containing biologically functionalized graphene nanoplatelets inside tubes equipped with rotating coaxial double-twisted tapes, International Communications in Heat and Mass Transfer 108 (2019) 104305.

[108] M. Bahiraei, N. Mazaheri, A. Rizehvandi, Application of a hybrid nanofluid containing graphene nanoplatelet–platinum composite powder in a triple-tube heat exchanger equipped with inserted ribs. Applied Thermal Engineering,149 (2019) 588 – 601.

[109] A. Fattahi , Numerical simulation of a solar collector equipped with a twisted tape and containing a hybrid nanofluid, Sustainable Energy Technologies and

Assessments 45 (2021)101200.

[110] L. M. Jasim , H. Hamzah , C. Canpolat , B. Sahin, Mixed convection flow of hybrid nanofluid through a vented enclosure with an inner rotating cylinder, International Communications in Heat and Mass Transfer 121 (2021) 105086.

[111] H.T. Chen, W. L. Hsu, Estimation of heat transfer coefficient on the fin of annular-Finned tube heat exchangers in natural convection for various fin spacings, International Journal of Heat and Mass Transfer 50 (2007) 1750–1761.

[112] H. Pfitzer and H. Beer, Heat transfer in an annulus between independently rotating tubes with turbulent axial flow, Int. J. Heat Mass transfer ,35(1992) 623- 633.

[113] Z. Shi, T. Dong, Thermodynamic investigation and optimization of laminar forced convection in a rotating helical tube heat exchanger, Energy Conversion and Management 86 (2014) 399–409.

[114] M. Bahiraei , N. Mazaheri , S. Hosseini, Neural network modeling of thermo-hydraulic attributes and entropy generation of an ecofriendly nanofluid flow inside tubes equipped with novel rotary coaxial double-twisted tape, Powder Technology 369 (2020) 162–175.

[115] R.S. Khedkar, N. Shrivastava, S.S. Sonawane, K.L. Wasewar, Experimental investigations and theoretical determination of thermal conductivity and viscosity of TiO_2–ethylene glycol nanofluid. International Communications in Heat and Mass Transfer 73(2016) 54 – 61.

[116] C. Yang, W. Li, A. Nakayama, Convective heat transfer of nanofluids in a concentric annulus, International Journal of Thermal Sciences 71 (2013) 249-257.

[117] M. C. S. Reddy, V. V. Rao, Experimental investigation of heat transfer coefficient and friction factor of ethylene glycol water based TiO_2 nanofluid in double pipe heat exchanger with and without helical coil inserts, International Communications in Heat and Mass Transfer 50 (2014) 68–76.

[118] J.A. R. Babu, K. K. Kumar, S. S. Rao, State-of-art review on hybrid nanofluids, Renewable and Sustainable Energy Reviews 77 (2017) 551–565.